

# Use of Seakeeping Simulation Capabilities in the Preliminary Phase of the Design of Multihull Vessels

by

Cosimo Malesci

Submitted to the Department of Mechanical Engineering  
in partial fulfillment of the requirements for the degree of

Master of Science in Naval Architecture and Marine Engineering

at the

MASSACHUSETTS INSTITUTE OF TECHNOLOGY

June 2006

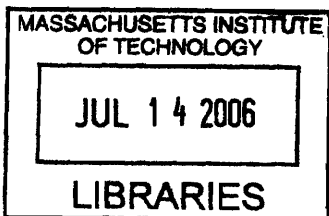
© Massachusetts Institute of Technology 2006. All rights reserved.

Author .....  
Department of Mechanical Engineering  
May 9, 2006

Certified by .....  
Dick K. P. Yue  
Professor of Hydrodynamics and Ocean Engineering  
Thesis Supervisor

Certified by .....  
Timothy J. Mc Coy  
Associate Professor of the Practice of Naval Construction and  
Engineering  
Thesis Supervisor

Accepted by .....  
Lallit Anand  
Chairman, Department Committee on Graduate Students



ARCHIVES



# **Use of Seakeeping Simulation Capabilities in the Preliminary Phase of the Design of Multihull Vessels**

by

Cosimo Malesci

Submitted to the Department of Mechanical Engineering  
on May 9, 2006, in partial fulfillment of the  
requirements for the degree of  
Master of Science in Naval Architecture and Marine Engineering

## **Abstract**

Seakeeping analysis is a fundamental part of the design process of a ship. Due to its complexity, seakeeping analysis is usually completed in a late stage of the design process. Although this approach can be successfully used for monohull vessels, it is not optimal in designing more innovative hull forms, due to the high degree of uncertainty of the seakeeping performances of these vessels. The recent interest in multihull vessels poses a problem to the naval architecture world as little is known about such hull forms and a limited number of design tools is available to analyze them.

These concerns led to the development of the I-Marine Seakeeping Analysis Toolbox that aims to help students and naval architects alike understand the importance of seakeeping analysis and the seakeeping capabilities of multihull vessels. The Toolbox includes five different seakeeping programs suitable for the analysis of multihull vessels and is accessible through a web interface. The integrated nature of I-Marine strongly facilitates the usage of the programs, making it a great educational tool to learn seakeeping analysis without any previous programming knowledge.

This thesis shows that a tool such as I-Marine could be effectively used in calculating the seakeeping capabilities of multihulls and successfully integrated in the preliminary design of a vessel, leading to numerous advantages such as a higher efficiency in the design process, a reduction in the risk of designing multihulls, and an expansion of the design envelope.

Thesis Supervisor: Dick K. P. Yue  
Title: Professor of Hydrodynamics and Ocean Engineering

Thesis Supervisor: Timothy J. Mc Coy  
Title: Associate Professor of the Practice of Naval Construction and Engineering



## Acknowledgments

I would like to thank Prof. Yue for giving me the opportunity to join his research group and to work on such an exciting topic. Prof. Yue has been a great source of help and encouragement in the development of this work.

I also would like to thank Prof. Mc Coy for being a co-advisor for this thesis. His knowledge has been extremely important for the completion of this project.

Very special thanks go to Dr. Kelli Hendrikson for the enormous amount of help she provided since the very beginning. Kelli played a fundamental role in the development of the I-Marine Seakeeping Analysis Toolbox. Her tenacity and creativity made the impossible, possible.

I would like to thank Prof. Scлавounos for allowing me to use NIIRID and providing important insights regarding seakeeping theory.

I would like to thank Steve Malley and Leslie Regan for answering all my questions regarding the Institute's regulations and helping me sort out all my registration problems.

Special thanks go to Claudio Cairoli for revealing me the secrets of Fortran coding and for keeping me updated on the latest trends in yacht design. I also would like to thank my friends Roberto, Marco, Luigi, Omar, Edo, and Michele for making my time in Boston so special and for reminding me what life is all about.

Special thanks go to my friends and co-workers, Andrea and Torquato, for being so accommodating with me. Finally, I want to thank Alexis and Umberto for all the great moral support they provided during the development of this thesis. We made it! Thank you for bearing with me.

Last but not least, I would like to thank my parents for being so supportive during my studies and for giving me life, food, and a roof over my head.



# Contents

<b>1</b>	<b>Introduction</b>	<b>25</b>
<b>2</b>	<b>The Seakeeping Problem</b>	<b>31</b>
2.1	Introduction . . . . .	31
2.2	Motion in Regular Waves for Six Degrees of Freedom . . . . .	32
2.3	Rigid Bodies in Waves . . . . .	35
2.3.1	The Hydrodynamic Forces . . . . .	36
2.3.2	The Hydrostatic Forces . . . . .	40
2.4	Equations of Motion . . . . .	41
2.5	The Strip Theory Method . . . . .	42
2.5.1	Theoretical Explanation . . . . .	43
2.5.2	The Exciting Forces and Moments . . . . .	49
2.6	The Sectional Hydrodynamic Coefficients and Forces . . . . .	49
2.6.1	MIT5D . . . . .	50
2.6.2	NIIRID . . . . .	52
2.6.3	CAT-5 . . . . .	53
2.6.4	CROSSFLOW . . . . .	55
2.7	Resonance Frequencies . . . . .	59
2.8	Vessel Motion . . . . .	60

<b>3</b>	<b>The I-Marine Seakeeping Analysis Toolbox</b>	<b>63</b>
3.1	Introduction . . . . .	63
3.2	Program Chart . . . . .	64
3.3	Vessel Input Geometry (I-Build) . . . . .	66
3.4	Seakeeping Analysis (I-Simulate) . . . . .	69
<b>4</b>	<b>Validation of the I-Marine Seakeeping Analysis Toolbox</b>	<b>73</b>
4.1	Introduction . . . . .	73
4.2	Validation of the Sectional Hydrodynamic Coefficients . . . . .	74
4.2.1	Heave Motion . . . . .	74
4.2.2	Sway Motion . . . . .	76
4.2.3	Roll Motion . . . . .	78
4.2.4	Coupled Sway-Roll Motion . . . . .	80
4.3	NPL Series Tests . . . . .	81
4.3.1	CROSSFLOW Drag Coefficient and Lift Gradient Assessment	82
4.3.2	Head Seas . . . . .	83
4.3.3	Oblique Seas . . . . .	91
4.4	LAMP Comparison . . . . .	93
4.4.1	Catamaran Testing . . . . .	93
4.4.2	Trimaran Testing . . . . .	95
4.5	Summary . . . . .	96
<b>5</b>	<b>Case Study</b>	<b>97</b>
5.1	Introduction . . . . .	97
5.2	High Speed Connector Design Project . . . . .	98
5.2.1	Design Scope . . . . .	98
5.2.2	Design Process . . . . .	98
5.2.3	Actual HSC Design Process . . . . .	101



5.3	The Preliminary Design Process Revisited . . . . .	108
5.3.1	Limitations of the HSC Design Process . . . . .	109
5.3.2	The I-Marine Design Process . . . . .	109
5.3.3	Performance-specific Analysis Using the I-Marine Seakeeping Analysis Toolbox . . . . .	113
5.4	Overall Advantages of the Revisited Design Process . . . . .	127
5.5	Summary . . . . .	131
<b>6</b>	<b>Conclusions</b>	<b>135</b>
6.1	Future Work . . . . .	136
<b>A</b>	<b>CROSSFLOW Drag Coefficient and Lift Gradient Validation</b>	<b>139</b>
<b>B</b>	<b>LAMP-NIIRID Comparison</b>	<b>143</b>
B.1	Catamaran Testing . . . . .	144
B.2	Trimaran Testing . . . . .	155
<b>C</b>	<b>Case Study Results</b>	<b>167</b>
C.1	Catamarans . . . . .	168
C.2	Trimarans . . . . .	179



# List of Figures

3-1	My Daise Page. The menu on the left is dedicated to the Seakeeping Analysis Toolbox. The menu on the right allows the user to access other parts of the I-Marine website. . . . .	65
3-2	I-Marine Seakeeping Analysis Toolbox Program Chart. The platform can be divided in three main blocks: GEOMETRYCREATOR, the programs to calculate the sectional hydrodynamic coefficients, and STRIP-SOLVER. . . . .	67
3-3	Geometry Input Page. Using the scroll down menus, the user can select the shape of the hull sections and the number of hulls. This page is also used to input the overall dimensions of the vessel. . . . .	68
3-4	MyGeometry List Page. This page contains all the geometries previously created. By clicking on the geometry name, the user can look at the geometry files and display a 3D rendering of the geometry. . . . .	69
3-5	Geometry Graphic Interface. The user can have a 360 degrees view of the vessel created using the commands of the interface. The graphical interface is very useful for a quick check of the characteristics of the vessel under analysis. . . . .	70
3-6	NIIRID Input Page. The scroll-down menu allows the user to select a geometry. This page is also used to input the details of the simulation such as vessel speed, wave heading, and incident wave frequencies. . .	71

3-7	My Simulations List. This page contains all the simulations previously completed. By clicking on the name of a simulation, the user can access the output files. . . . .	72
3-8	My Simulation Output. Each simulation generates six output files. Most of these output files are for debugging purposes. In addition, the input file used for each simulation is stored as well. . . . .	72
4-1	Sectional Added Mass of Twin-Cylinder Configuration in Heave ( $b/a = 3.0$ ) . . . . .	76
4-2	Sectional Damping Coefficient of Twin-Cylinder Configuration in Heave ( $b/a = 3.0$ ) . . . . .	77
4-3	Sectional Added Mass of Twin-Cylinder Configuration in Sway ( $b/a = 1.5$ ) . . . . .	78
4-4	Sectional Added Mass of Twin-Cylinder Configuration in Sway ( $b/a = 3.0$ ) . . . . .	79
4-5	Sectional Damping Coefficient of Twin-Cylinder Configuration in Sway ( $b/a = 1.5$ ) . . . . .	80
4-6	Sectional Damping Coefficient of Twin-Cylinder Configuration in Sway ( $b/a = 3.0$ ) . . . . .	81
4-7	Sectional Added Mass of Twin-Cylinder Configuration in Roll ( $b/a = 2.0$ )	82
4-8	Sectional Damping Coefficient of Twin-Cylinder Configuration in Roll ( $b/a = 2.0$ ) . . . . .	83
4-9	Sectional Added Mass of Twin-Cylinder Configuration in Coupled Sway-Roll Motion ( $b/a = 2.0$ ) . . . . .	84
4-10	Sectional Damping Coefficient of Twin-Cylinder Configuration in Coupled Sway-Roll Motion ( $b/a = 2.0$ ) . . . . .	85
4-11	Heave RAO for NPL Model 5b at $Fn = 0.2$ and $\mu = 180^\circ$ . . . . .	86
4-12	Pitch RAO for NPL Model 5b at $Fn = 0.2$ and $\mu = 180^\circ$ . . . . .	86

4-13	Heave RAO for NPL Model 5b at $F_n = 0.5$ and $\mu = 180^\circ$ . . . . .	87
4-14	Pitch RAO for NPL Model 5b at $F_n = 0.5$ and $\mu = 180^\circ$ . . . . .	87
4-15	Heave RAO for NPL Model 5b at $F_n = 0.67$ and $\mu = 180^\circ$ . . . . .	89
4-16	Pitch RAO for NPL Model 5b at $F_n = 0.67$ and $\mu = 180^\circ$ . . . . .	89
4-17	Heave RAO for NPL Model 5b at $F_n = 0.8$ and $\mu = 180^\circ$ . . . . .	90
4-18	Pitch RAO for NPL Model 5b at $F_n = 0.8$ and $\mu = 180^\circ$ . . . . .	90
4-19	Heave RAO for NPL Model 5b at $F_n = 0.67$ and $\mu = 150^\circ$ . . . . .	91
4-20	Heave RAO for NPL Model 5b at $F_n = 0.67$ and $\mu = 120^\circ$ . . . . .	92
4-21	Pitch RAO for NPL Model 5b at $F_n = 0.67$ and $\mu = 150^\circ$ . . . . .	92
4-22	Pitch RAO for NPL Model 5b at $F_n = 0.67$ and $\mu = 120^\circ$ . . . . .	93
4-23	Roll RAO for NPL Model 5b at $F_n = 0.67$ and $\mu = 150^\circ$ . . . . .	94
4-24	Roll RAO for NPL Model 5b at $F_n = 0.67$ and $\mu = 120^\circ$ . . . . .	94
5-1	HSC Preliminary Design Process Flow Chart. Zouridakis and Wang [31]	99
5-2	Ranking Scheme Used in the Qualitative Layer of the Analysis. Zouridakis and Wang [31] . . . . .	101
5-3	Transport Factor vs. Life Cycle Cost. Zouridakis and Wang [31] . . .	103
5-4	Transport Factor vs. Acquisition Cost. Zouridakis and Wang [31] . .	104
5-5	Carrying Capacity vs. Life Cycle Cost. Zouridakis and Wang [31] . .	105
5-6	Rating Summary. Zouridakis and Wang [31] . . . . .	106
5-7	Basic Categories Scores. Zouridakis and Wang [31] . . . . .	107
5-8	Risk Analysis Results. Zouridakis and Wang [31] . . . . .	108
5-9	Modified Design Process Chart . . . . .	111
5-10	Performance-Specific Analysis Chart for Seakeeping . . . . .	114
5-11	Vertical RMS Acceleration for Catamarans . . . . .	121
5-12	Vertical RMS Acceleration for Trimarans . . . . .	122

5-13	Sum of the RMS Vertical Accelerations for the Four Angles of Wave Incidence Calculated. The results have been normalized by the gravitational acceleration, $g$ . . . . .	124
5-14	Heave RAO Comparison for Catamaran 1 and Trimaran 1 at $F_n = 0.0$ and $\mu = 150^\circ$ . . . . .	126
5-15	Roll RAO Comparison for Catamaran 1 and Trimaran 1 at $F_n = 0.0$ and $\mu = 150^\circ$ . . . . .	127
5-16	Roll RAO at $F_n = 0.0$ and $\mu = 150^\circ$ for the Catamaran Configurations Considered in the Case Study . . . . .	128
A-1	CROSSFLOW: Heave RAO at $F_n = 0.2$ and $\mu = 180^\circ$ . . . . .	140
A-2	CROSSFLOW: Pitch RAO at $F_n = 0.2$ and $\mu = 180^\circ$ . . . . .	140
A-3	CROSSFLOW: Heave RAO at $F_n = 0.5$ and $\mu = 180^\circ$ . . . . .	141
A-4	CROSSFLOW: Pitch RAO at $F_n = 0.5$ and $\mu = 180^\circ$ . . . . .	141
A-5	CROSSFLOW: Heave RAO at $F_n = 0.8$ and $\mu = 180^\circ$ . . . . .	142
A-6	CROSSFLOW: Pitch RAO at $F_n = 0.8$ and $\mu = 180^\circ$ . . . . .	142
B-1	LAMP-NIIRID Comparison for Catamaran 1: Heave RAO at $F_n = 0.0$ and $\mu = 180^\circ$ . . . . .	144
B-2	LAMP-NIIRID Comparison for Catamaran 1: Pitch RAO at $F_n = 0.0$ and $\mu = 180^\circ$ . . . . .	144
B-3	LAMP-NIIRID Comparison for Catamaran 1: Heave RAO at $F_n = 0.0$ and $\mu = 150^\circ$ . . . . .	145
B-4	LAMP-NIIRID Comparison for Catamaran 1: Pitch RAO at $F_n = 0.0$ and $\mu = 150^\circ$ . . . . .	145
B-5	LAMP-NIIRID Comparison for Catamaran 1: Roll RAO at $F_n = 0.0$ and $\mu = 150^\circ$ . . . . .	146

B-6	LAMP-NIIRID Comparison for Catamaran 1: Heave RAO at $F_n = 0.0$ and $\mu = 120^\circ$ . . . . .	146
B-7	LAMP-NIIRID Comparison for Catamaran 1: Pitch RAO at $F_n = 0.0$ and $\mu = 120^\circ$ . . . . .	147
B-8	LAMP-NIIRID Comparison for Catamaran 1: Roll RAO at $F_n = 0.0$ and $\mu = 120^\circ$ . . . . .	147
B-9	LAMP-NIIRID Comparison for Catamaran 1: Heave RAO at $F_n = 0.0$ and $\mu = 45^\circ$ . . . . .	148
B-10	LAMP-NIIRID Comparison for Catamaran 1: Pitch RAO at $F_n = 0.0$ and $\mu = 45^\circ$ . . . . .	148
B-11	LAMP-NIIRID Comparison for Catamaran 1: Roll RAO at $F_n = 0.0$ and $\mu = 45^\circ$ . . . . .	149
B-12	LAMP-NIIRID Comparison for Catamaran 1: Heave RAO at $F_n = 0.4$ and $\mu = 180^\circ$ . . . . .	149
B-13	LAMP-NIIRID Comparison for Catamaran 1: Pitch RAO at $F_n = 0.4$ and $\mu = 180^\circ$ . . . . .	150
B-14	LAMP-NIIRID Comparison for Catamaran 1: Heave RAO at $F_n = 0.4$ and $\mu = 150^\circ$ . . . . .	150
B-15	LAMP-NIIRID Comparison for Catamaran 1: Pitch RAO at $F_n = 0.4$ and $\mu = 150^\circ$ . . . . .	151
B-16	LAMP-NIIRID Comparison for Catamaran 1: Roll RAO at $F_n = 0.4$ and $\mu = 150^\circ$ . . . . .	151
B-17	LAMP-NIIRID Comparison for Catamaran 1: Heave RAO at $F_n = 0.4$ and $\mu = 120^\circ$ . . . . .	152
B-18	LAMP-NIIRID Comparison for Catamaran 1: Pitch RAO at $F_n = 0.4$ and $\mu = 120^\circ$ . . . . .	152

B-19 LAMP-NIIRID Comparison for Catamaran 1: Roll RAO at $F_n = 0.4$ and $\mu = 120^\circ$ . . . . .	153
B-20 LAMP-NIIRID Comparison for Catamaran 1: Heave RAO at $F_n = 0.4$ and $\mu = 45^\circ$ . . . . .	153
B-21 LAMP-NIIRID Comparison for Catamaran 1: Pitch RAO at $F_n = 0.4$ and $\mu = 45^\circ$ . . . . .	154
B-22 LAMP-NIIRID Comparison for Catamaran 1: Roll RAO at $F_n = 0.4$ and $\mu = 45^\circ$ . . . . .	154
B-23 LAMP-NIIRID Comparison for Trimarans: Heave RAO at $F_n = 0.0$ and $\mu = 180^\circ$ . . . . .	155
B-24 LAMP-NIIRID Comparison for Trimarans: Pitch RAO at $F_n = 0.0$ and $\mu = 180^\circ$ . . . . .	155
B-25 LAMP-NIIRID Comparison for Trimarans: Heave RAO at $F_n = 0.0$ and $\mu = 150^\circ$ . . . . .	156
B-26 LAMP-NIIRID Comparison for Trimarans: Pitch RAO at $F_n = 0.0$ and $\mu = 150^\circ$ . . . . .	156
B-27 LAMP-NIIRID Comparison for Trimarans: Roll RAO at $F_n = 0.0$ and $\mu = 150^\circ$ . . . . .	157
B-28 LAMP-NIIRID Comparison for Trimarans: Heave RAO at $F_n = 0.0$ and $\mu = 120^\circ$ . . . . .	157
B-29 LAMP-NIIRID Comparison for Trimarans: Pitch RAO at $F_n = 0.0$ and $\mu = 120^\circ$ . . . . .	158
B-30 LAMP-NIIRID Comparison for Trimarans: Roll RAO at $F_n = 0.0$ and $\mu = 120^\circ$ . . . . .	158
B-31 LAMP-NIIRID Comparison for Trimarans: Heave RAO at $F_n = 0.0$ and $\mu = 45^\circ$ . . . . .	159



B-32 LAMP-NIIRID Comparison for Trimarans: Pitch RAO at $F_n = 0.0$ and $\mu = 45^\circ$ . . . . .	159
B-33 LAMP-NIIRID Comparison for Trimarans: Roll RAO at $F_n = 0.0$ and $\mu = 45^\circ$ . . . . .	160
B-34 LAMP-NIIRID Comparison for Trimarans: Heave RAO at $F_n = 0.4$ and $\mu = 180^\circ$ . . . . .	160
B-35 LAMP-NIIRID Comparison for Trimarans: Pitch RAO at $F_n = 0.4$ and $\mu = 180^\circ$ . . . . .	161
B-36 LAMP-NIIRID Comparison for Trimarans: Heave RAO at $F_n = 0.4$ and $\mu = 150^\circ$ . . . . .	161
B-37 LAMP-NIIRID Comparison for Trimarans: Pitch RAO at $F_n = 0.4$ and $\mu = 150^\circ$ . . . . .	162
B-38 LAMP-NIIRID Comparison for Trimarans: Roll RAO at $F_n = 0.4$ and $\mu = 150^\circ$ . . . . .	162
B-39 LAMP-NIIRID Comparison for Trimarans: Heave RAO at $F_n = 0.4$ and $\mu = 120^\circ$ . . . . .	163
B-40 LAMP-NIIRID Comparison for Trimarans: Pitch RAO at $F_n = 0.4$ and $\mu = 120^\circ$ . . . . .	163
B-41 LAMP-NIIRID Comparison for Trimarans: Roll RAO at $F_n = 0.4$ and $\mu = 120^\circ$ . . . . .	164
B-42 LAMP-NIIRID Comparison for Trimarans: Heave RAO at $F_n = 0.4$ and $\mu = 45^\circ$ . . . . .	164
B-43 LAMP-NIIRID Comparison for Trimarans: Pitch RAO at $F_n = 0.4$ and $\mu = 45^\circ$ . . . . .	165
B-44 LAMP-NIIRID Comparison for Trimarans: Roll RAO at $F_n = 0.4$ and $\mu = 45^\circ$ . . . . .	165

C-1	Case Study Analysis of Catamaran Geometries: Heave RAO at $F_n = 0$ and $\mu = 180^\circ$ . . . . .	168
C-2	Case Study Analysis of Catamaran Geometries: Pitch RAO at $F_n = 0$ and $\mu = 180^\circ$ . . . . .	168
C-3	Case Study Analysis of Catamaran Geometries: Heave RAO at $F_n =$ $0.4$ and $\mu = 180^\circ$ . . . . .	169
C-4	Case Study Analysis of Catamaran Geometries: Heave RAO at $F_n =$ $0.4$ and $\mu = 180^\circ$ . . . . .	169
C-5	Case Study Analysis of Catamaran Geometries: Heave RAO at $F_n = 0$ and $\mu = 150^\circ$ . . . . .	170
C-6	Case Study Analysis of Catamaran Geometries: Pitch RAO at $F_n = 0$ and $\mu = 150^\circ$ . . . . .	170
C-7	Case Study Analysis of Catamaran Geometries: Roll RAO at $F_n = 0$ and $\mu = 150^\circ$ . . . . .	171
C-8	Case Study Analysis of Catamaran Geometries: Heave RAO at $F_n =$ $0.4$ and $\mu = 150^\circ$ . . . . .	171
C-9	Case Study Analysis of Catamaran Geometries: Pitch RAO at $F_n =$ $0.4$ and $\mu = 150^\circ$ . . . . .	172
C-10	Case Study Analysis of Catamaran Geometries: Roll RAO at $F_n = 0.4$ and $\mu = 150^\circ$ . . . . .	172
C-11	Case Study Analysis of Catamaran Geometries: Heave RAO at $F_n = 0$ and $\mu = 120^\circ$ . . . . .	173
C-12	Case Study Analysis of Catamaran Geometries: Pitch RAO at $F_n = 0$ and $\mu = 120^\circ$ . . . . .	173
C-13	Case Study Analysis of Catamaran Geometries: Roll RAO at $F_n = 0$ and $\mu = 120^\circ$ . . . . .	174

C-14 Case Study Analysis of Catamaran Geometries: Heave RAO at $F_n = 0.4$ and $\mu = 120^\circ$ . . . . .	174
C-15 Case Study Analysis of Catamaran Geometries: Pitch RAO at $F_n = 0.4$ and $\mu = 120^\circ$ . . . . .	175
C-16 Case Study Analysis of Catamaran Geometries: Roll RAO at $F_n = 0.4$ and $\mu = 120^\circ$ . . . . .	175
C-17 Case Study Analysis of Catamaran Geometries: Heave RAO at $F_n = 0$ and $\mu = 45^\circ$ . . . . .	176
C-18 Case Study Analysis of Catamaran Geometries: Pitch RAO at $F_n = 0$ and $\mu = 45^\circ$ . . . . .	176
C-19 Case Study Analysis of Catamaran Geometries: Roll RAO at $F_n = 0$ and $\mu = 45^\circ$ . . . . .	177
C-20 Case Study Analysis of Catamaran Geometries: Heave RAO at $F_n = 0.4$ and $\mu = 45^\circ$ . . . . .	177
C-21 Case Study Analysis of Catamaran Geometries: Pitch RAO at $F_n = 0.4$ and $\mu = 45^\circ$ . . . . .	178
C-22 Case Study Analysis of Catamaran Geometries: Roll RAO at $F_n = 0.4$ and $\mu = 45^\circ$ . . . . .	178
C-23 Case Study Analysis of Trimaran Geometries: Heave RAO at $F_n = 0$ and $\mu = 180^\circ$ . . . . .	179
C-24 Case Study Analysis of Trimaran Geometries: Pitch RAO at $F_n = 0$ and $\mu = 180^\circ$ . . . . .	179
C-25 Case Study Analysis of Trimaran Geometries: Heave RAO at $F_n = 0.4$ and $\mu = 180^\circ$ . . . . .	180
C-26 Case Study Analysis of Trimaran Geometries: Heave RAO at $F_n = 0.4$ and $\mu = 180^\circ$ . . . . .	180

C-27 Case Study Analysis of Trimaran Geometries: Heave RAO at $F_n = 0$ and $\mu = 150^\circ$ . . . . .	181
C-28 Case Study Analysis of Trimaran Geometries: Pitch RAO at $F_n = 0$ and $\mu = 150^\circ$ . . . . .	181
C-29 Case Study Analysis of Trimaran Geometries: Roll RAO at $F_n = 0$ and $\mu = 150^\circ$ . . . . .	182
C-30 Case Study Analysis of Trimaran Geometries: Heave RAO at $F_n = 0.4$ and $\mu = 150^\circ$ . . . . .	182
C-31 Case Study Analysis of Trimaran Geometries: Pitch RAO at $F_n = 0.4$ and $\mu = 150^\circ$ . . . . .	183
C-32 Case Study Analysis of Trimaran Geometries: Roll RAO at $F_n = 0.4$ and $\mu = 150^\circ$ . . . . .	183
C-33 Case Study Analysis of Trimaran Geometries: Heave RAO at $F_n = 0$ and $\mu = 120^\circ$ . . . . .	184
C-34 Case Study Analysis of Trimaran Geometries: Pitch RAO at $F_n = 0$ and $\mu = 120^\circ$ . . . . .	184
C-35 Case Study Analysis of Trimaran Geometries: Roll RAO at $F_n = 0$ and $\mu = 120^\circ$ . . . . .	185
C-36 Case Study Analysis of Trimaran Geometries: Heave RAO at $F_n = 0.4$ and $\mu = 120^\circ$ . . . . .	185
C-37 Case Study Analysis of Trimaran Geometries: Pitch RAO at $F_n = 0.4$ and $\mu = 120^\circ$ . . . . .	186
C-38 Case Study Analysis of Trimaran Geometries: Roll RAO at $F_n = 0.4$ and $\mu = 120^\circ$ . . . . .	186
C-39 Case Study Analysis of Trimaran Geometries: Heave RAO at $F_n = 0$ and $\mu = 45^\circ$ . . . . .	187

C-40 Case Study Analysis of Trimaran Geometries: Pitch RAO at $F_n = 0$ and $\mu = 45^\circ$ . . . . .	187
C-41 Case Study Analysis of Trimaran Geometries: Roll RAO at $F_n = 0$ and $\mu = 45^\circ$ . . . . .	188
C-42 Case Study Analysis of Trimaran Geometries: Heave RAO at $F_n = 0.4$ and $\mu = 45^\circ$ . . . . .	188
C-43 Case Study Analysis of Trimaran Geometries: Pitch RAO at $F_n = 0.4$ and $\mu = 45^\circ$ . . . . .	189
C-44 Case Study Analysis of Trimaran Geometries: Roll RAO at $F_n = 0.4$ and $\mu = 45^\circ$ . . . . .	189



# List of Tables

4.1	NPL Model 5b General Characteristics . . . . .	88
4.2	Values of the Drag Coefficient $C_D$ and the Lift Gradient $a$ as a Function of Froude Number Used for the NPL Analysis in Head and Oblique Seas	88
4.3	Overall Dimensions of the Catamaran Used for LAMP-NIIRID Com- parison . . . . .	95
4.4	Overall Dimensions of the Trimarans Used for LAMP-NIIRID Com- parison . . . . .	95
5.1	Design Categories and Relative Weight Factor . . . . .	106
5.2	Threshold and Goal Values for the HSC Design Project . . . . .	106
5.3	Design Constraints for the HSC Design Project . . . . .	107
5.4	Catamaran Designs . . . . .	115
5.5	Trimaran Designs . . . . .	115
5.6	Catamaran Variants. [ft] . . . . .	116
5.7	Trimaran Variants . . . . .	117
5.8	Estimated Resonance Frequencies for Catamaran and Trimaran Con- figurations Analyzed in the Case Study . . . . .	118
5.9	Summary of the objectives achieved in the case study analysis . . . . .	133





# Chapter 1

## Introduction

Seakeeping is the study of the response of a ship to waves. Analyzing the seakeeping performances of a vessel is important in order to determine the range of sea-state conditions in which a ship can be safely operated. Nowadays seakeeping analysis is carried out using seakeeping prediction programs that allow the naval architect to predict the response of a vessel and the loads caused by such motion without requiring any experimental measurement. Seakeeping analysis, once carried out only in a small number of projects due to its complexity, has become a key step in the design process of every vessel. Factors such as stricter requirements imposed by regulatory bodies together with passengers' comfort and maximum cargo capacity have made seakeeping analysis critical not only for safety reasons but also from a business prospective, inducing ship owners to be very demanding regarding the seakeeping capabilities of their vessels.

Seakeeping analysis entails three different steps: estimation of the environmental conditions that the vessel will encounter, prediction of the response in those conditions, and evaluation of the seakeeping performances based on the computed response [4]. The analysis is carried out for a range of sea-state values and the resulting motion is computed. The results are then used to calculate the limiting environmental

conditions for operability and the motion criteria.

The basic theory behind modern seakeeping analysis was developed in the mid 20th Century by Ursell [28, 29], and St Denis and Pierson [27]. The first numerical method to calculate the response of a vessel in heave and pitch was developed by Korvin-Kroukovsky and Jacobs [13]. In their method, called strip theory, the vessel is divided into a number of thin transverse sections and the hydrodynamic properties of each section are computed assuming two dimensional inviscid flow. The results are then integrated over the whole length of the body to calculate the overall response of the ship. Strip theory was then developed and modified by many researchers such as Salvsen, Tuck and Faltinsen [23] who were the first to develop a numerical method to predict a vessel response in six degrees of freedom. Due to its relative simplicity, strip theory is the most widely used method to compute the hydrodynamic forces acting on a ship in a seaway.

More recently, three-dimensional seakeeping analysis methods have been developed. The first three dimensional methods were proposed by Chang [25] and Inglis and Price [11] which solved the three-dimensional linear problem for a vessel in waves at forward speed. Liapis and Beck [16] and King *et al.* [12] brought the analysis a step forward by solving the problem directly in the time domain. In recent years some of the three-dimensional methods have been used to develop commercial seakeeping analysis programs such as LAMP, SWAN, or SPLASH. Although these programs show a higher accuracy compared to two-dimensional methods, they haven't gained wide acceptance due to their complexity and the long computation time required.

It must be pointed out that the large majority of the research done on seakeeping prediction methods is for monohulls. The new interest in multihull vessels poses a new challenge to the seakeeping analysis. A great stability, a large deck area, and the possibility to achieve high speeds are only some of the factors that have induced many companies to include multihulls in their design efforts. Specifically where passengers'

comfort and speed are a priority, multihulls are found to be the most effective solution. In analyzing the response of a multihull in a seaway, new factors not relevant in the monohull analysis need to be included such as the interaction between the demihulls or the viscous damping. Due to this reason, multihull specific methods for seakeeping analysis were developed. The research on seakeeping prediction methods for multihulls started in the early Seventies with the papers of Wang and Wahab [30] and Ohkusu [20] on the motion of twin-cylinders in waves. A more advanced two-dimensional method that takes into account some of the viscous effects using a crossflow approach was proposed by Rathje and Schelling [22] and by Centeno *et al.* [2]. In the last decade, a  $2D+t$  time-domain strip theory for multihull vessels was proposed by Davis and Holloway [5] and other authors. Although these methods proved to be successful and reliable, due to the limited interest in multihull vessels, very few of these programs were developed into a commercial-grade seakeeping prediction software. As a consequence, very little information about the seakeeping performances of multihull vessels are easily available.

The limited knowledge about the seakeeping capabilities of multihull vessels together with the lack of appropriate analysis tools strongly limits the development of these innovative hull forms. This phenomenon strongly affects the naval architecture world, forcing designers to limit the level of innovation in their projects due to the unacceptable high level of risk in developing innovative hull forms. These limitations are also reflected in the academic world, where students don't have the possibility to explore the capabilities of multihull vessels due to the lack of proper tools. With these problems in mind, the I-Marine Seakeeping Analysis Toolbox was created.

The I-Marine Seakeeping Analysis Toolbox contains different seakeeping programs which are able to analyze multihulls. The Toolbox has been developed integrating the different programs together to facilitate its usage. By doing so, I-Marine makes seakeeping analysis programs available to everyone independently of any previous

programming experience. The Toolbox is accessible through a web interface where the user can create different hull geometries and test their seakeeping capabilities. Such a platform has been designed to be effectively used in an educational environment to help students understand the importance of seakeeping analysis and to develop a better knowledge of the performances of multihulls.

The goal of this thesis is to investigate the advantages of using an integrated analysis tool such as the I-Marine Seakeeping Analysis Toolbox in the design of multihull vessels. Being able to easily obtain quantitative information about the seakeeping performances of multihull vessels would allow designers to explore more innovative hull forms, decreasing the risk in developing such vessels. Additionally, using an integrated platform would strongly facilitate the analysis allowing the assessment of seakeeping capabilities also in the preliminary design process. The benefits of using this approach will be analyzed.

In addition, this thesis investigates the use of strip theory to calculate the response of multihulls in waves. Although strip theory has been extensively validated for monohulls, such a validation has not been completed for catamarans and trimarans. If proven accurate and reliable, strip theory could provide important information regarding the seakeeping of multihull vessels and be used in numerous scenarios.

Finally, this thesis addresses the use of the I-Marine integrated analysis platform in an educational environment. Such a platform strongly facilitates the use of seakeeping programs because no programming knowledge is required. As a consequence, students would be able to focus on seakeeping analysis instead of spending time to learn programming and debugging. By doing so, seakeeping could be covered in great detail and students would be able to understand the differences between the various seakeeping programs and develop experience in analyzing the results.

In Chapter 2, the theoretical principles behind seakeeping analysis and strip theory will be reviewed. In addition, the different conformal mapping methods used by each

of the programs included in the I-Marine Seakeeping Analysis Toolbox will be covered in detail. In Chapter 3, the overall structure of the I-Marine Seakeeping Analysis Toolbox will be explained together with its web interface. In Chapter 4, the results of a series of tests to validate the I-Marine Seakeeping Analysis Toolbox will be presented. In Chapter 5, a case study analysis will be completed. The goal of the case study is to show how a tool like I-Marine can be integrated in a traditional design process. A revisited preliminary design process based on [31] will be presented highlighting its advantages in term of efficiency and quality of the results. Chapter 6 covers what conclusions can be drawn from this research and possible future developments.



# Chapter 2

## The Seakeeping Problem

### 2.1 Introduction

Computing the response of a vessel advancing in waves is a non-linear phenomenon which involves the vessel dynamics and hydrodynamic forces. Although a nonlinear analysis has been presented by different authors [26], for many applications the order of the nonlinearities is small enough that a linear theory provides accurate results. Experimental and theoretical results have shown that linear theory gives accurate results over a wide range of scenarios [8, 10, 9]. As a consequence, the linear theory of ship motion is the most widely used and will be presented in this chapter. The following theoretical explanation has been derived from [15].

A ship advancing at a constant speed with a given heading in a train of regular waves will move in six degrees of freedom. The motion can be decomposed into three translational components, called surge, sway, and heave, and three rotational components, called roll, pitch, and yaw. For a general ship geometry, this leads to a system of six non-linear equations of motion. For the relatively common case of a ship with port-starboard symmetry, the system of six non-linear equations is reduced to two systems of three linear equations. With this assumption, the motions on the

longitudinal plane (surge, heave, and pitch) and the motions on the transverse plane (sway, roll, and yaw) are decoupled.

## 2.2 Motion in Regular Waves for Six Degrees of Freedom

The equations of motion for a ship advancing at a constant forward speed and heading in a train of regular sinusoidal waves is presented. Three different coordinate systems will be used in the analysis. The right-hand coordinate system  $(x_o, y_o, z_o)$  is fixed at a given position on the surface of the Earth and will be used to define the incident wave system. The  $z_o$ -axis is positive upwards and the  $x_o - y_o$  plane coincides with the calm water level, with  $x_o$  pointing in the direction where the ship is moving. The second coordinate system,  $(x, y, z)$ , which represents the translation of the ship in  $(x_o, y_o, z_o)$ , is set with the origin  $O$  on the calm water level. The  $x$ -axis is coincident with  $x_o$  and the  $z$ -axis is positive upwards. The  $(x, y, z)$  coordinate system moves with velocity  $U_o$  in the positive  $x_o$  direction. The transformation from  $(x, y, z)$  to  $(x_o, y_o, z_o)$  can be computed as follows:

$$\begin{aligned} x_o &= x + U_o t \\ y_o &= y \\ z_o &= z \end{aligned} \tag{2.1}$$

The third coordinate system,  $(\bar{x}, \bar{y}, \bar{z})$ , is fixed to the ship with  $\bar{z}$ -axis positive upwards, the  $\bar{x}$ -axis positive forward, and the  $\bar{x} - \bar{y}$  plane coincident with the calm waterplane of the ship. In this analysis, the ship is assumed to have port - starboard symmetry and the  $\bar{x} - \bar{z}$  plane is considered the plane of symmetry. As a consequence, the origin will be at the intersection of the calm waterplane of the ship and the plane of symmetry. The  $x$ -coordinate of the origin will be placed at amidship for convenience.

The response of the vessel will be computed by calculating the relative motion of



$(\bar{x}, \bar{y}, \bar{z})$  with respect to  $(x, y, z)$ , The motion  $\eta$  will be uniquely defined by a total of six components: three translational and three rotational. It is common to assign a number to each motion. More specifically,  $\eta_1$  indicates a translation along the x-axis and is called surge,  $\eta_2$  a translation along the y-axis, called sway, and  $\eta_3$  a translation along the z-axis, called heave. For rotations the notation is:  $\eta_4$  indicates a rotation around the x-axis, called roll,  $\eta_5$  indicates a rotation around the y-axis, called pitch, and  $\eta_6$  indicates a rotation around the z-axis, called yaw. Counterclockwise rotations are considered positive.

The regular waves encountered by the vessel are considered to be linear, deepwater, Airy waves. For a wave amplitude  $\zeta_A$ , wave number  $k$ , and frequency  $\omega$ , the wave elevation  $\zeta$  is defined as a wave travelling from left to right:

$$\zeta = \zeta_A \cos(kx_o - \omega t) \quad (2.2)$$

The fact that the ship and the waves are moving with different velocities leads to a shift in the frequency at which the vessel will encounter the waves. Due to the linearity of the system the frequency of the response is also affected. This frequency is called encounter frequency,  $\omega_e$ , and for a vessel travelling with forward speed  $U_o$ , is given by:

$$\omega_e = \omega - kU_o \cos \mu \quad (2.3)$$

where  $\mu$  is the angle between the direction of propagation of the wave train and the direction of the vessel. When the vessel is travelling in head seas with  $\mu = 180^\circ$ , the frequency of encounter will be higher than the incident wave frequency. When the vessel is travelling in beam seas with a speed less than the incident wave speed, the frequency of encounter will be lower than the incident wave frequency. The encounter frequency can also become negative when the ship is travelling in beam seas with a forward velocity higher than the velocity of propagation of the wave crests.

Because the system is assumed linear, the resulting vessel motion in the  $(x, y, z)$  coordinate system will have a form similar to the incident waves and respond at the encounter frequency. The motion of the ship can be expressed as follows:

$$\eta_i = \eta_{a_i} \cos(\omega_e t + \epsilon_i) \quad \text{with } i = 1, \dots, 6 \quad (2.4)$$

where  $\eta_{a_i}$  is the amplitude of the response,  $\epsilon_i$  is the phase shift, and  $i = 1, \dots, 6$  refers to the direction of motion, as previously defined.

The harmonic velocities and accelerations in the  $(x, y, z)$  coordinate system are calculated by taking the first and second derivative of the displacements leading to:

$$\dot{\eta}_i = \eta_{a_i} \omega_e \sin(\omega_e t + \epsilon_i) \quad \text{with } i=1, \dots, 6 \quad (2.5)$$

$$\ddot{\eta}_i = -\omega_e^2 \eta_{a_i} \cos(\omega_e t + \epsilon_i) \quad \text{with } i=1, \dots, 6 \quad (2.6)$$

$$\ddot{\eta}_i = -\omega_e^2 \eta_{a_i} \cos(\omega_e t + \epsilon_i) \quad \text{with } i=1, \dots, 6 \quad (2.7)$$

The general form of the linearized equations of motion in six degrees of freedom in the  $(\bar{x}, \bar{y}, \bar{z})$  coordinate system is:

$$\sum_{k=1}^6 \Delta_{jk} \ddot{\eta}_k(t) = F_{H_j}(t) \quad \text{with } j=1, \dots, 6 \quad (2.8)$$

where  $\Delta_{jk}$  indicates the components of the mass matrix,  $\ddot{\eta}_k$  is the acceleration in mode  $k$  as computed in Equation (2.7), and  $F_{H_j}$  is the force or moment in direction  $j$ . For a vessel with port-starboard symmetry, linearization leads to a simplification

of the system of equations as follows:

$$\begin{aligned}
\Delta(\ddot{\eta}_1 + \bar{z}_c \ddot{\eta}_5) &= F_{H_1} \\
\Delta(\ddot{\eta}_2 - \bar{z}_c \ddot{\eta}_4 + \bar{x}_c \ddot{\eta}_6) &= F_{H_2} \\
\Delta(\ddot{\eta}_3 + \bar{x}_c \ddot{\eta}_5) &= F_{H_3} \\
I_{44} \ddot{\eta}_4 - I_{46} \ddot{\eta}_6 - \Delta \bar{z}_c \ddot{\eta}_2 &= F_{H_4}
\end{aligned} \tag{2.9}$$

Consequently, the mass matrix is reduced to:

$$\Delta_{jk} = \begin{pmatrix} \Delta & 0 & 0 & 0 & +\Delta \bar{z}_c & 0 \\ 0 & \Delta & 0 & -\Delta \bar{z}_c & 0 & \Delta \bar{x}_c \\ 0 & 0 & \Delta & 0 & -\Delta \bar{x}_c & 0 \\ 0 & -\Delta \bar{z}_c & 0 & I_{44} & 0 & -I_{46} \\ +\Delta \bar{z}_c & 0 & -\Delta \bar{x}_c & 0 & I_{55} & 0 \\ 0 & \Delta \bar{x}_c & 0 & -I_{46} & 0 & I_{66} \end{pmatrix} \tag{2.10}$$

where  $\Delta$  is the vessel displacement,  $I_{ij}$  are the products of inertia around the  $\bar{x}$ ,  $\bar{y}$ ,  $\bar{z}$  axis, and  $(\bar{x}_c, 0, \bar{z}_c)$  are the coordinates for the center of gravity of the ship in the  $(\bar{x}, \bar{y}, \bar{z})$  coordinate system. This matrix depends only on the geometry of the vessel and is straight forward to calculate.

## 2.3 Rigid Bodies in Waves

Equation (2.8) and Equation (2.9) cannot be solved without knowing the hydrodynamic forcing on the body. The force  $F_{H_j}$  which acts on the vessel can be obtained by integrating the fluid pressure along the wetted area of the hull, namely:

$$F_{H_j} = \iint_S P n_j ds \quad \text{for } j=1, \dots, 6 \tag{2.11}$$

where  $n_j$  is the generalized normal to the surface of the hull pointing into the hull,  $P$  is the fluid pressure, and  $S$  is the wetted area of the hull.

By assuming that the flow is inviscid and irrotational, the pressure acting on the hull can be found using the unsteady Bernoulli's equation:

$$P = \frac{1}{2}\rho U_o^2 - \rho \frac{\partial \Phi}{\partial t} - \frac{1}{2}\rho (\nabla \Phi \cdot \nabla \Phi) - \rho g z \quad (2.12)$$

where  $\rho$  is the fluid density,  $\nabla \Phi$  is the total velocity vector representing the fluid flow, and  $U_o$  is still the speed of the ship. The first three terms in Equation (2.12) represent the hydrodynamic component of the pressure, and the last term represents the hydrostatic component of the pressure. Consequently, the right hand side of Equation (2.11) can then be divided into the hydrodynamic force  $F_{HD_j}$  and the hydrostatic force  $F_{HS_j}$ , leading to the following equations:

$$F_{H_j} = F_{HS_j} + F_{HD_j} \quad (2.13)$$

$$F_{HS_j} = -\rho g \iint_S z n_j ds \quad (2.14)$$

$$F_{HD_j} = \rho \iint_S \left( \frac{1}{2}U_o^2 - \frac{\partial \Phi}{\partial t} - \frac{1}{2}\nabla \Phi \cdot \nabla \Phi \right) n_j ds \quad (2.15)$$

### 2.3.1 The Hydrodynamic Forces

In order to calculate the hydrodynamic forces acting on the vessel using Equation (2.15), the total velocity potential  $\Phi(x, y, z, t)$  must be known. To analytically determine the exact velocity potential is generally not possible. As a consequence, some assumptions are required.

The velocity potential is assumed to be composed by a steady part and by an unsteady part:

$$\Phi(x, y, z, t) = \Phi_S + \Phi_T \quad (2.16)$$

where  $\Phi_S$  and  $\Phi_T$  are called the steady and unsteady perturbation potentials, respectively. By separating the time dependence, the potentials can be expressed as follows:

$$\Phi_S = -U_0x + \phi_S(x, y, z) \quad (2.17)$$

$$\Phi_T = \phi_T e^{i\omega_e t} \quad (2.18)$$

where  $\phi_S$  and  $\phi_T$  are the time-independent part of the perturbation potentials. The steady part of the potential  $\Phi_S$  is caused by the vessel moving at forward speed. The term  $-U_0x$  represents the free stream velocity and  $\phi_S$  is the steady perturbation potential due to the presence of the hull of the ship. The unsteady part of the velocity potential has a sinusoidal time dependence with a frequency equal to the frequency of encounter  $\omega_e$ . In order for the unsteady velocity potential to be valid, the following requirements and boundary conditions need to be applied:

Continuity Condition:

$$\nabla^2 \Phi = 0 \quad (2.19)$$

Seabed Boundary Condition:

$$\frac{\partial \Phi}{\partial z} = 0 \quad \text{for } z=-h \quad (2.20)$$

Dynamic Boundary Condition at the Free Surface:

$$\frac{\partial^2 \Phi}{\partial t^2} + g \frac{\partial \Phi}{\partial z} = 0 \quad \text{for } z=0 \quad (2.21)$$

Kinematic Boundary Condition on the Oscillating Body Surface:

$$\frac{\partial \Phi}{\partial n} = v_n(x, y, z, t) \quad (2.22)$$

Radiation Condition:

$$\lim_{R \rightarrow \infty} \Phi = 0 \quad (2.23)$$

Symmetric or Anti-symmetric Condition:

$$\Phi(-x, y) = -\Phi(x, y) \quad (2.24)$$

As the waves are also considered linear, the unsteady perturbation potential  $\phi_T$  is divided into three components:

$$\phi_T = \phi_I + \phi_D + \sum_{j=1}^6 \phi_{R_j} \bar{\eta}_j \quad (2.25)$$

where  $\phi_I$  is the incident wave potential,  $\phi_D$  is the diffracted wave potential,  $\phi_{R_j}$  is the radiation potential due to unit motion in the  $j^{th}$  direction, and  $\bar{\eta}_j$  is the amplitude of the complex response in the  $j^{th}$  direction. The incident wave potential  $\phi_I$  is known. The diffraction potential  $\phi_D$  can be obtained by solving the diffraction problem where incident waves strikes the floating body in its equilibrium position leading to diffracted waves scattered from the body. The radiation potential  $\phi_{R_j}$  can be found by solving the radiation problem where the vessel undergoes oscillatory motion in calm water.

The  $\nabla\Phi \cdot \nabla\Phi$  term present in Equation (2.12) is considered nonlinear and dropped leading to the following simplified version of the unsteady Bernoulli equation:

$$P \approx -\rho \left[ i\omega_e - U_o \frac{\partial}{\partial x} \right] \phi_T e^{i\omega_e t} \quad (2.26)$$

Using Equation (2.15) and Equation (2.26), the unsteady part of the hydrodynamic force can be calculated as follows:

$$F_{HD_j} \approx -\rho \iint_S n_j \left[ i\omega_e - U_o \frac{\partial}{\partial x} \right] \phi_T e^{i\omega_e t} ds \quad (2.27)$$

The total hydrodynamic force acting on the body in the six degrees of freedom can be decomposed in three components:

$$F_{HD_j} = F_{EX_j} + F_{R_j} \quad \text{for } j=1, \dots, 6 \quad (2.28)$$

with

$$F_{EX_j} = (F_j^I + F_j^D) e^{i\omega_e t} \quad (2.29)$$

where  $F_j^I$  is the Froude-Krylov force,  $F_j^D$  is the diffraction force, and  $F_R$  is the force caused by the forced oscillation of the body in calm water.

The Froude-Krylov force is caused by the incident waves acting on the vessel and can be calculated integrating the pressure over the underwater part of the hull. Referring to Equation (2.26), the amplitude of the Froude-Krylov force can be expressed as follows:

$$F_j^I = -\rho \iint_S n_j \left( i\omega_e - U_o \frac{\partial}{\partial x} \right) \phi_I ds \quad (2.30)$$

The diffraction force is caused by the diffraction of the incident waves due to the presence of the vessel floating on the surface. Using the Haskind Relations, the diffraction force  $F_j^D$  can be found without having to calculate the diffraction potential  $\phi_D$ . The equation to calculate the amplitude of the diffraction force in the six degrees of freedom is the following:

$$F_j^D = -\rho \iint n_j \left( i\omega_e - U_o \frac{\partial}{\partial x} \right) \phi_D ds \quad (2.31)$$

The third component of the unsteady hydrodynamic force is the radiation force,  $F_j^R$  that results from forced oscillations of the body in calm water in six degrees of freedom. The forces caused by the oscillatory motion of the body in calm water involves the calculation of the added mass and damping coefficients,  $A_{ij}$  and  $B_{ij}$ , in the six degrees of freedom. In order to calculate the radiation forces, the following

equation can be used:

$$F_{R_j} = -\rho \iint_S n_j \left( i\omega_e - U_o \frac{\partial}{\partial x} \right) \left( \sum_{k=1}^6 \phi_R \bar{\eta}_k e^{i\omega_e t} \right) ds = \sum_{k=1}^6 \left[ -\rho \iint_S n_j \left( i\omega_e - U_o \frac{\partial}{\partial x} \right) \phi_R ds \right] \bar{\eta}_k e^{i\omega_e t} \quad (2.32)$$

Usually the notation is changed as follows:

$$F_{R_j} = \sum_{k=1}^6 T_{jk} \bar{\eta}_k e^{i\omega_e t} \quad (2.33)$$

The real and imaginary part of  $T_{jk}$  are usually separated as:

$$T_{jk} = \omega_e^2 A_{jk} - i\omega_e B_{jk} \quad (2.34)$$

where  $A_{jk}$  is the added mass in the  $j^{th}$  direction due to a unit motion in the  $k^{th}$  direction, and  $B_{jk}$  is the damping coefficient in the  $j^{th}$  direction due to a unit motion in the  $k^{th}$  direction. It should be kept in mind that the terms added mass and damping coefficient are related to how each component of the force behaves. As it will be shown in the equation of motion of the ship, the real part of the radiation force is in phase with the acceleration, and for this reason called added mass, and the imaginary part of the diffraction force is in phase with the velocity, therefore acting as a damper. In addition, both the added mass and the damping coefficients strictly depend on the frequency of oscillation.

### 2.3.2 The Hydrostatic Forces

To find the hydrostatic forces acting on a floating body, the integral in Equation (2.14) must be solved. The hydrostatic forces are generally expressed in the following notation:

$$F_{HS_j} = - \sum_{k=1}^6 C_{jk} \bar{\eta}_k e^{i\omega_e t} \quad (2.35)$$



where  $C_{jk}$  is called the hydrostatic restoring coefficient in the  $j$  direction due to a unit motion in the  $k$  direction. The hydrostatic restoring coefficients for a ship depend only on the ship geometry. The equations to calculate the restoring coefficients of a ship are:

$$C_{33} = \rho g \int B(x) dx \quad (2.36)$$

$$C_{35} = -\rho g \int x B(x) dx \quad (2.37)$$

$$C_{53} = C_{35} \quad (2.38)$$

$$C_{55} = \rho g \int x^2 B(x) dx \quad (2.39)$$

$$C_{44} = \rho g \nabla \overline{GM}_T \quad (2.40)$$

where  $\rho$  is the water density,  $g$  is the acceleration of gravity,  $B(x)$  is the local maximum beam of the vessel,  $\nabla$  is the displacement, and  $\overline{GM}_T$  is the transverse metacentric height.

## 2.4 Equations of Motion

Substituting the components of the force acting on the vessel into Equation (2.8) yields the following equation of motion:

$$\sum_{k=1}^6 -\omega_e^2 \Delta_{jk} \bar{\eta}_k e^{i\omega_e t} = -\sum_{k=1}^6 C_{jk} \bar{\eta}_k e^{i\omega_e t} + F_j^I e^{i\omega_e t} + F_j^D e^{i\omega_e t} + \sum_{k=1}^6 (\omega_e^2 A_{jk} - i\omega_e B_{jk}) \bar{\eta}_k e^{i\omega_e t} \quad (2.41)$$

Using Equation (2.30) and Equation (2.35), and bringing the added mass, damping coefficient and the restoring force to the left of the equation leads to the equation of motion for a ship in waves in six degrees of freedom:

$$\sum_{k=1}^6 \left[ -\omega_e^2 (\Delta_{jk} + A_{jk}) + i\omega_e B_{jk} + C_{jk} \right] \bar{\eta}_k = F_j^I + F_j^D \quad \text{with } j=1, \dots, 6 \quad (2.42)$$

Equation (2.42) is very similar to the equation of a spring-mass-damper system with six degrees of freedom under forced motion. However, the added mass and the damping coefficients for a ship are strongly dependent on the frequency of oscillation.

At this point  $\Delta_{jk}$ ,  $F_j^I$ , and  $F_j^D$  are the quantities known. The added mass  $A_{jk}$  and the damping coefficient  $B_{jk}$  are strongly dependent on the encounter frequency  $\omega_e$  and require the solution of  $\phi_R$  to completely describe the equation of motion.

## 2.5 The Strip Theory Method

In order to be able to compute the response of a ship in waves using the equations of motion presented in Chapter 2.4, the added mass and damping coefficients need to be calculated together with the Froude-Krylov and diffraction forces acting on the vessel. In general this requires the solution of the Laplace equation with complex boundary conditions. Strip theory reduces the three dimensional problem of a ship moving in waves to a succession of two-dimensional problems. The assumptions made limit the use of this theory: factors such as a high vessel speed, a low frequency of oscillation, and a low length-to-beam ratio violate this assumption leading to erroneous results. Although more advanced methods have been developed, strip theory remains the most used method due to its simplicity.

The theoretical principles behind strip theory are explained in the following section. Although slightly different strip theory methods exist, the one proposed by Salvseen, Tuck and Faltinsen [23] is the most widely used and will be presented here. The theoretical explanation will be composed by two parts. The first part will go over the calculation of the hydrodynamic coefficients,  $A_{ij}$  and  $B_{ij}$ , based on the sectional added mass and damping coefficients,  $a_{ij}$  and  $b_{ij}$ . The second part will go over the calculation of the Froude-Krylov and diffraction forces and moments based on the sectional excitation forces  $f_i$  and  $h_i$ .

## 2.5.1 Theoretical Explanation

### Hydrodynamic Coefficients

Recall that the hydrodynamic coefficients expressed in Equation (2.33) are a function of the radiation potential  $\phi_R$  integrated over the hull surface. In order to reduce these expressions to an integral of the hydrodynamic coefficients along the length of the body, Stokes' theorem is needed:

$$\iint_S (\vec{n} \times \nabla) \times \vec{q} ds = \int_C \vec{dl} \times \vec{q} \quad (2.43)$$

where  $C$  is the closed curve around the surface  $S$ , and  $q$  is any vector function. For this application, the curve is defined as the underwater surface of the hull and by setting:

$$\begin{aligned} q &= \phi U \hat{i} & \text{for } j = 1,2,3 \\ q &= \phi U \hat{i} \times \hat{r} & \text{for } j = 4,5,6 \end{aligned} \quad (2.44)$$

where  $\phi$  is a differentiable scalar function, we have:

$$\iint_S n_j U \frac{\partial}{\partial x} \phi ds = U \iint_S m_j \phi ds - U \int_{C_x} n_j \phi dl \quad (2.45)$$

where  $C_x$  is a cross section of the hull,  $S$  is the portion of hull surface forward of the cross section  $C_x$ ,  $n_j$  is the generalized unit vector normal to the surface, and  $m_j$  is the generalized vector involving the gradient of the forward speed potential. Applying Equation (2.45) to Equation (2.33) we have:

$$T_{jk} = -\rho i \omega \iint_S n_j \phi_R ds + U \rho \iint_S m_j \phi_R ds - U \rho \int_{C_a} n_j \phi_R dl \quad (2.46)$$

where  $C_a$  is the aftermost section of the vessel. Recalling that the oscillatory potential can be divided in a time dependent and time-independent part:

$$\phi_j = \phi_j^0 + \frac{U}{i\omega} \phi_j^U \quad (2.47)$$

we can express the speed-independent part of  $T_{jk}$  as:

$$T_{jk}^0 = -\rho i \omega \iint_S n_j \phi_R^0 ds \quad (2.48)$$

and the speed-independent part of the line integral at any cross section  $C_x$  as:

$$t_{jk} = -\rho i \omega \int_{C_x} n_j \phi_R^0 dl \quad (2.49)$$

As a consequence, the added mass and damping coefficients can be now expressed as shown below:

$$T_{jk} = T_{jk}^0 + \frac{U}{i\omega} t_{jk}^A \quad \text{for } j = 5, 6 \text{ and } k = 1, 2, 3, 4 \quad (2.50)$$

$$T_{5k} = T_{5k}^0 - \frac{U}{i\omega} T_{3k}^0 + \frac{U}{i\omega} t_{5k}^A \quad \text{for } j = 5, 6 \text{ and } k = 1, 2, 3, 4 \quad (2.51)$$

$$T_{6k} = T_{6k}^0 - \frac{U}{i\omega} T_{2k}^0 + \frac{U}{i\omega} t_{6k}^A \quad \text{for } j = 5, 6 \text{ and } k = 1, 2, 3, 4 \quad (2.52)$$

$$T_{j5} = T_{j5}^0 - \frac{U}{i\omega} T_{j3}^0 + \frac{U}{i\omega} t_{j5}^A - \frac{U^2}{\omega^2} t_{j3}^A \quad \text{for } j = 1, 2, 3, 4 \text{ and } k = 5, 6 \quad (2.53)$$

$$T_{j6} = T_{j6}^0 - \frac{U}{i\omega} T_{j2}^0 + \frac{U}{i\omega} t_{j6}^A - \frac{U^2}{\omega^2} t_{j2}^A \quad \text{for } j = 1, 2, 3, 4 \text{ and } k = 5, 6 \quad (2.54)$$

$$T_{55} = T_{55}^0 - \frac{U}{i\omega} T_{33}^0 + \frac{U}{i\omega} t_{55}^A - \frac{U^2}{\omega^2} t_{33}^A \quad \text{for } j = k = 5, 6 \quad (2.55)$$

$$T_{66} = T_{66}^0 - \frac{U}{i\omega} T_{22}^0 + \frac{U}{i\omega} t_{66}^A - \frac{U^2}{\omega^2} t_{62}^A \quad \text{for } j = k = 5, 6 \quad (2.56)$$

Assuming that the length of the ship is much larger than the draft and the beam, we can state that  $ds = d\xi dl$  where  $d\xi$  is along the x-axis and  $dl$  is an element of arc along the cross section  $C_x$ . Consequently, Equation (2.48) is reduced to:

$$T_{jk}^0 = -\rho i \omega \int_L \int_{C_x} n_j \phi_R^0 dl d\xi = \int_L t_{jk} d\xi \quad (2.57)$$

where  $L$  is the length of the ship. The radiation potential  $\phi_R^0$  satisfies the Continuity Equation (2.19) and the Boundary Conditions (2.21-2.23). Assuming that the hull is slender, we can replace the three components of the three dimensional normal vector  $n_j$  ( $j = 2, 3, 4$ ) with the two dimensional generalized normal vector  $N_J$  ( $J = 2, 3, 4$ ) and obtain the following expression:

$$\begin{aligned} n_5 &= -x N_3 \\ n_6 &= x N_2 \end{aligned} \quad (2.58)$$

Finally, in order to simplify the dynamic boundary condition at the free surface (2.21), a high frequency of encounter  $\omega_e$  will be assumed. With these assumptions in place, the problem can be reduced to an infinitely long cylinder with cross section  $C_x$  oscillating on the free surface. Defining  $\psi_k$  as the two-dimensional potential, at a given cross section we have:

$$\phi_k^0 = \psi_k \quad \text{for } k = 2, 3, 4 \quad (2.59)$$

and

$$\begin{aligned} \phi_5^0 &= -x \psi_3 \\ \phi_6^0 &= -x \psi_2 \end{aligned} \quad (2.60)$$

As a consequence, we can state that:

$$t_{jj} = -\rho i \omega \int_{C_x} N_j \psi_j dl = \omega^2 a_{jj} - i \omega b_{jj} \quad \text{for } j = 2, 3, 4 \quad (2.61)$$

where  $a_{jj}$  and  $b_{jj}$  are the two dimensional added mass and damping coefficients. Similarly, for the sway-roll coupled motion, we have:

$$t_{24} = -\rho i \omega \int_{C_x} N_2 \psi_4 dl = \omega^2 a_{24} - i \omega b_{24} \quad (2.62)$$

It follows that the speed-independent part of  $T_{jk}$  can be expressed in terms of the sectional values  $t_{22}$ ,  $t_{33}$ ,  $t_{44}$ , and  $t_{24}$  as follows:

$$\begin{aligned} T_{22}^0 &= \int t_{22} d\xi \\ T_{26}^0 &= T_{62}^0 = \int \xi t_{22} d\xi \\ T_{66}^0 &= \int \xi^2 t_{22} d\xi \\ T_{33}^0 &= \int t_{33} d\xi \\ T_{35}^0 &= T_{53}^0 = -\int \xi t_{33} d\xi \\ T_{55}^0 &= \int \xi^2 t_{33} d\xi \\ T_{44}^0 &= \int t_{44} d\xi \\ T_{24}^0 &= T_{42}^0 = \int t_{24} d\xi \\ T_{46}^0 &= T_{64}^0 = \int \xi t_{24} d\xi \end{aligned} \quad (2.63)$$

Now recalling Equation (2.34), we obtain the equation for the total added mass and damping coefficients in the six degrees of freedom using the sectional values of  $a_{ij}$  and  $b_{ij}$ .

The equations for vertical motion are:

$$\begin{aligned}
A_{11} &= \int a_{11} dx \\
A_{13} &= \int a_{13} dx \\
A_{31} &= A_{13} \\
B_{11} &= \int b_{11} dx \\
B_{13} &= \int b_{13} dx \\
B_{31} &= B_{13} \\
A_{15} &= -\int x a_{13} dx - \frac{U_o}{\omega_e^2} B_{13} \\
B_{15} &= -\int x b_{13} dx - U_o A_{13} \\
A_{51} &= -\int x a_{13} dx - \frac{U_o}{\omega_e^2} B_{31} \\
B_{51} &= -\int x b_{31} dx - U_o A_{13} \\
A_{33} &= \int a_{33} dx - \frac{U}{\omega_e^2} b_{33}^A \\
B_{33} &= \int b_{33} dx + U a_{33}^A \\
A_{35} &= -\int x a_{33} dx - \frac{U_o}{\omega_e^2} B_{33} + \frac{U}{\omega_e^2} x_A b_{33}^A - \frac{U^2}{\omega_e^2} a_{33}^A \\
B_{35} &= -\int x b_{33} dx + U_o A_{33} - U x_a a_{33}^A - \frac{U^2}{\omega_e^2} b_{33}^A \\
A_{53} &= -\int x a_{33} dx - \frac{U_o}{\omega_e^2} B_{33} + \frac{U}{\omega_e^2} x_A b_{33}^A \\
B_{53} &= -\int x b_{33} dx - U_o A_{33} - U x_A a_{33}^A \\
A_{55} &= \int x^2 a_{33} dx - \frac{U_o^2}{\omega_e^2} A_{33} - \frac{U}{\omega_e^2} x_A^2 b_{33}^A + \frac{U^2}{\omega_e^2} x_A a_{33}^A \\
B_{55} &= \int x^2 a_{33} dx - \frac{U_o^2}{\omega_e^2} B_{33} + U x_A^2 a_{33}^A + \frac{U^2}{\omega_e^2} x_A b_{33}^A
\end{aligned} \tag{2.64}$$

The equations for horizontal motion are:

$$\begin{aligned}
A_{22} &= \int a_{22} dx - \frac{U}{\omega_e^2} b_{22}^A \\
A_{24} &= \int a_{24} dx - \frac{U}{\omega_e^2} b_{24}^A \\
A_{42} &= A_{24} \\
B_{22} &= \int b_{22} dx + U a_{22}^A \\
B_{24} &= \int b_{24} dx + U a_{24}^A \\
B_{42} &= B_{24} \\
A_{26} &= \int x a_{22} dx - \frac{U_o}{\omega_e^2} B_{22} - \frac{U}{\omega_e^2} x_A b_{22}^A + \frac{U^2}{\omega_e^2} a_{22}^A \\
A_{46} &= \int x a_{24} dx + \frac{U_o}{\omega_e^2} B_{24} - \frac{U}{\omega_e^2} x_A b_{24}^A + \frac{U^2}{\omega_e^2} a_{24}^A \\
B_{26} &= \int x b_{22} dx - U_o A_{22} + U x_A a_{22}^A + \frac{U^2}{\omega_e^2} b_{22}^A \\
A_{44} &= \int a_{44} dx - \frac{U}{\omega_e^2} b_{44}^A \\
B_{46} &= \int x b_{24} dx - U_o B_{24} + U x_A a_{24}^A + \frac{U^2}{\omega_e^2} b_{24}^A \\
A_{62} &= \int x a_{22} dx - \frac{U_o}{\omega_e^2} B_{22} - \frac{U}{\omega_e^2} x_A b_{22}^A \\
B_{62} &= - \int x b_{22} dx + U_o A_{22} + U x_A a_{22}^A \\
A_{64} &= \int x a_{24} dx - \frac{U_o}{\omega_e^2} B_{24} - \frac{U}{\omega_e^2} x_A b_{24}^A \\
B_{64} &= \int x b_{24} dx - U_o A_{24} + U x_A a_{24}^A \\
A_{66} &= \int x^2 a_{22} dx + \frac{U_o^2}{\omega_e^2} A_{22} - \frac{U}{\omega_e^2} x_A^2 b_{22}^A + \frac{U^2}{\omega_e^2} x_A a_{22}^A \\
B_{66} &= \int x^2 b_{22} dx + \frac{U_o^2}{\omega_e^2} B_{22} U x_A^2 a_{22}^A + \frac{U^2}{\omega_e^2} x_A b_{22}^A
\end{aligned} \tag{2.65}$$



## 2.5.2 The Exciting Forces and Moments

By using the relationships presented in Equation (2.58) and Equation (2.59), the total exciting forces can be obtained integrating the sectional Froude-Krylov and diffraction forces along the length of the vessel. Defining the sectional Froude-Krylov force as:

$$f_j(x) = g e^{-ikx \cos \mu} \int_{C_x} N_j e^{iky \sin \mu} e^{kz} dl \quad \text{for } j = 2, 3, 4 \quad (2.66)$$

and the sectional diffraction force as:

$$h_j(x) = \omega_o e^{-ikx \cos \mu} \int_{C_x} (iN_3 - N_2 \sin \mu) e^{iky \sin \mu} e^{kz} \psi_j dl \quad \text{for } j = 2, 3, 4 \quad (2.67)$$

the total excitation force can be calculated as follows:

$$F_{HD_j} = \rho \zeta_A \int_L (f_i + h_i) d\xi + \rho \zeta_A \frac{U}{i\omega} h_j^A \quad \text{for } j = 2, 3, 4 \quad (2.68)$$

$$F_{HD_5} = -\rho \zeta_A \int_L \left[ \xi(f_3 + h_3) + \frac{U}{i\omega} h_3 \right] d\xi - \rho \zeta_A \frac{U}{i\omega} x_A h_2^A \quad \text{for } j = 2, 3, 4 \quad (2.69)$$

$$F_{HD_6} = \rho \zeta_A \int_L \left[ \xi(f_2 + h_2) + \frac{U}{i\omega} h_2 \right] d\xi + \rho \zeta_A \frac{U}{i\omega} x_A h_2^A \quad \text{for } j = 2, 3, 4 \quad (2.70)$$

## 2.6 The Sectional Hydrodynamic Coefficients and Forces

The most important step in calculating the ship response in a seaway using strip theory is computing the sectional added mass and damping coefficients,  $a_{ij}$  and  $b_{ij}$  and excitation forces  $f_j$  and  $h_j$  at each section of the ship. This is the most critical part of the computation because it strongly affects the accuracy of the results. Many different methods of computing the two-dimensional hydrodynamic coefficients and forces have been developed by many authors [28, 29, 7, 30]. Four different methods have been included in the I-Marine Seakeeping Analysis Toolbox. Each method is

related to a specific program that outputs the sectional hydrodynamic coefficients and excitation forces for a given geometry and other input parameters. The four methods to compute the sectional values of the hydrodynamic coefficients and excitation forces are: MIT5D, NIIRID, CAT-5, and CROSSFLOW. MIT5D is based on Lewis bulbous forms, NIIRID and CAT-5 are two-dimensional panel methods, and CROSSFLOW is based on cross-flow aerodynamic theory. A detailed description of each of these programs follows.

### 2.6.1 MIT5D

MIT5D uses a two-parameters Lewis and bulbous forms conformal mapping method to calculate the sectional added mass and damping coefficients and the sectional excitation forces. The advantage of this method is that the velocity potential of the fluid around a ship section of arbitrary shape in a complex plane expressed as  $z = x + iy$  can be mapped using a semicircular section in another complex plane, such as  $\zeta = ie^\alpha e^{-i\Theta}$ . The general transformation formula for any conformal mapping method is:

$$z = M_s \sum \{a_{2n-1} \zeta^{-(2n-1)}\} \quad (2.71)$$

where:

$z$	$= x + iy$	plane of the ship's cross section	
$\zeta$	$= ie^\alpha e^{-i\Theta}$	plane of the unit circle	
$M_s$		scale factor	
$a_{-1}$	$= 1$		(2.72)
$a_{2n-1}$		conformal mapping coefficients (n=1, . . . ,N)	
$N$		maximum parameter index number	

The Lewis conformal mapping method is obtained by setting  $N = 2$ . As a consequence, the Lewis transformation of a cross section is defined as:

$$z = M_s(a_{-1} \zeta + a_1 \zeta^{-1} + a_3 \zeta^{-3}) \quad (2.73)$$

From Equation (2.73), the relationship between the  $z$ -plane and the  $\zeta$ -plane coordinate systems can be obtained analytically. The resulting equations are:

$$\begin{aligned} x &= M_s(e^\alpha \sin \theta + a_1 e^{-\alpha} \sin \theta - a_3 e^{-3\alpha} \sin 3\theta) \\ y &= M_s(e^\alpha \cos \theta - a_1 e^{-\alpha} \cos \theta - a_3 e^{-3\alpha} \cos 3\theta) \end{aligned} \quad (2.74)$$

where  $a_1$  and  $a_3$  are called the Lewis coefficients. The contour of a ship's cross section is obtained by setting  $\alpha = 0$ :

$$\begin{aligned} x &= M_s((1 + a_1) \sin \theta - a_3 \sin 3\theta) \\ y &= M_s((1 - a_1) \cos \theta + a_3 \cos 3\theta) \end{aligned} \quad (2.75)$$

where

$$M_s = \frac{B_s/2}{1 + a_1 + a_3} = \frac{D_s}{1 - a_1 + a_3} \quad (2.76)$$

in which  $B_s$  is the sectional breadth at the waterline and  $D_s$  is the sectional draft. The coefficients  $a_1$  and  $a_3$  and the scale factor  $M_s$  will be calculated to have the breadth, the draft, and the area of the approximated cross section equal to the one of the real cross section of the vessel. Integrating the Lewis form, the sectional area coefficient  $\sigma_s$  can be found to be a function of the cross-sectional area  $A_s$ :

$$\sigma_s = \frac{A_s}{B_s D_s} = \frac{\pi}{4} \frac{1 - a_1^2 - 3a_3^2}{(1 + a_3)^2 - a_1^2} \quad (2.77)$$

In addition, the half-breadth-to-draft ratio can be computed as follows:

$$H_o = \frac{B_s/2}{D_s} = \frac{1 + a_1 + a_3}{1 - a_1 + a_3} \quad (2.78)$$

Solving Equation (2.78) for  $a_1$  and substituting the value obtained in Equation (2.77) results in the following quadratic equation:

$$c_1 a_3^2 + c_2 a_3 + c_3 = 0 \quad (2.79)$$

in which

$$\begin{aligned} c_1 &= 3 + \frac{4\sigma_s}{\pi} + \left(1 - \frac{4\sigma_s}{\pi}\right) \left(\frac{H_o - 1}{H_o + 1}\right)^2 \\ c_2 &= 2c_1 - 6 \\ c_3 &= c_1 - 4 \end{aligned} \quad (2.80)$$

By solving Equation (2.79),  $a_1$  and  $a_3$  can be calculated:

$$\begin{aligned} a_3 &= \frac{-c_1 + 3 + \sqrt{9 - 2c_1}}{c_1} \\ a_1 &= \frac{H_o - 1}{H_o + 1} (a_3 + 1) \end{aligned} \quad (2.81)$$

The values of  $a_1$  and  $a_3$  are then used in Equation (2.75) to calculate the geometry of the ship.

## 2.6.2 NIIRID

As reported in [24], NIIRID solution is based on Green's theorem, which is used to obtain a Fredholm integral equation of the second kind for the velocity potential on the body boundary. The wave source potential is used as the Green's function. The body is approximated by N segments and the velocity potential is assumed constant along each segment. The integral equation is satisfied at the mid-point of each segment. The regular integrals are evaluated by the use of the midpoint rule or by a two-node

Gauss Legendre quadrature. The regular part of the Green's function is evaluated by the algorithm developed by Newman.

### 2.6.3 CAT-5

In CAT-5, the potential theory of Frank [7] is used to determine the sectional hydrodynamic coefficients and excitation forces. The following explanation has been derived from [17]. The velocity potential at a ship cross section is defined as follows:

$$\Phi^{(m)}(y, z, t) = Re \left[ \phi_{(m)}(y, z) e^{-i\omega t} \right] \quad (2.82)$$

where  $\phi^{(m)} = \phi_c^{(m)} + i\phi_s^{(m)}$  and  $m = 2$  is sway,  $m = 3$  is heave, and  $m = 4$  is roll.

Using Green's theorem, the velocity potential is constructed with two dimensional pulsating sources distributed along the cylinder contour. A pulsating source of unit strength has a potential of the form:

$$G_R^{(m)}(w, \zeta, t) = Re[G_R^{(m)}(w, \zeta) e^{-i\omega t}] \quad (2.83)$$

where:

$$G_R^{(m)}(w, \zeta) = G_{RC}^{(m)}(y, z; \zeta, \eta) + iG_{RS}^{(m)}(y, z; \zeta, \eta) \quad (2.84)$$

$$G_{RC}^{(m)} = \frac{1}{2\pi} Re \left\{ \left[ \ln \frac{w - \zeta}{w - \bar{\zeta}} + 2 \int_0^\infty \frac{e^{-ik(w-\bar{\zeta})}}{K - k} dk \right] - \right. \\ \left. (-1)^m \left[ \ln \frac{(w + \bar{\zeta})}{w + \zeta} + 2 \int_0^\infty \frac{e^{-ik(w+\zeta)}}{K - k} dk \right] \right\} \quad (2.85)$$

$$G_{RS}^{(m)} = -Re \{ e^{-ik(w-\zeta)} - (-1)^m e^{-ik(w+\zeta)} \} \quad (2.86)$$

As a consequence, expressing the velocity potential as a contour integral of source

singularities of unknown strength along the contour of the cylinder we have:

$$\phi^{(m)}(y, z) = \int_{C_x} Q(s) G_R^{(m)}(y, z; s) ds \quad (2.87)$$

where the source density  $Q(s)$  is defined as:

$$Q(s) = Q_c + iQ_s \quad (2.88)$$

Applying the linearized kinematic boundary condition on the cylinder wall, the source strength can be determined as follows:

$$\begin{aligned} (\hat{n} \cdot \nabla) \left\{ \int_{C_x} Q_c(s) G_{RC}^{(m)}(y, z; s) ds - \int_{C_x} Q_s(s) G_{RS}^{(m)}(y, z; s) ds \right\} &= A\omega n^{(m)} \\ (\hat{n} \cdot \nabla) \left\{ \int_{C_x} Q_c(s) G_{RS}^{(m)}(y, z; s) ds - \int_{C_x} Q_s(s) G_{RC}^{(m)}(y, z; s) ds \right\} &= 0 \end{aligned} \quad (2.89)$$

The cylinder contour is approximated by  $N$  straight line segments with a source of constant but unknown strength over each segment. The  $N$  unknown complex source strengths can then be determined using the  $2N$  equations obtained using Equation (2.89). The results are:

$$\begin{aligned} \sum_{j=1}^N Q_{cj} I_{ij}^{(m)} - \sum_{j=1}^N Q_{sj} J_{ij}^{(m)} &= A\omega n_i^{(m)} \quad \text{for } i=1,2,\dots,N \\ \sum_{j=1}^N Q_{cj} J_{ij}^{(m)} - \sum_{j=1}^N Q_{sj} I_{ij}^{(m)} &= 0 \quad \text{for } i=1,2,\dots,N \end{aligned} \quad (2.90)$$

with:

$$I_{ij}^{(m)} = (\hat{n} \cdot \nabla) \int_{C_j} G_{RC}^{(m)} ds \quad (2.91)$$

$$J_{ij}^{(m)} = (\hat{n} \cdot \nabla) \int_{C_j} G_{RS}^{(m)} ds \quad (2.92)$$

Once the  $N$  source strengths have been determined, Equation (2.82) can be used to find the total velocity potential which is:

$$\phi^{(m)}(y_i, z_i) = \sum_{j=1}^N \left( Q_{cj} I_j^{(m)} - Q_{sj} J_j^{(m)} \right) + i \sum_{j=1}^N N \left( Q_{cj} J_j^{(m)} + Q_{sj} I_j^{(m)} \right) \quad (2.93)$$

with:

$$I_j^{(m)} = \int_{C_j} G_{RC}^{(m)}(y_i, z_i; s) ds \quad (2.94)$$

$$J_{ij}^{(m)} = \int_{C_j} G_{RS}^{(m)}(y_i, z_i; s) ds \quad (2.95)$$

The total force acting on the cylinders can be determined using the linearized Bernoulli equation:

$$\begin{aligned} F^{(m)} &= -a_{mm} \ddot{I}(t) - b_{mm} \dot{I}(t) = \\ &= \left\{ -2\rho\omega \int_{C_x} \phi_c(y_i, z_i) \hat{n} ds \right\} \sin \omega t + \left\{ 2\rho\omega \int_{C_x} \phi_s(y_i, z_i) \hat{n} ds \right\} \cos \omega t \end{aligned}$$

As a consequence, the added mass and damping coefficients are:

$$a_{mm} = -\frac{2\rho}{A\omega} \int_{C_x} \phi_c \hat{n} ds \quad (2.96)$$

$$b_{mm} = -\frac{2\rho}{A} \int_{C_x} \phi_s \hat{n} ds \quad (2.97)$$

## 2.6.4 CROSSFLOW

The program CROSSFLOW is based on the theory developed by Rathje and Schellin and reported in [22]. The method involves the calculation of lift and drag produced by the demihulls using a cross flow approach, originally developed in airfoil theory. The cross flow theory is based on the fact that the displacement hulls of a catamaran act as slender lifting bodies in an inclined flow.

Considering a ship advancing at a constant forward speed  $U_o$  on the free surface in small amplitude harmonic waves, a right-handed coordinate system  $(x, y, z)$  with the origin  $O$  in the plane of the mean free surface moving with the ship is used for the analysis. The x-axis points in the direction of motion of the ship, parallel to the ship centerline. The z-axis points vertically upward through the ship's center of gravity. The six equations of motions can be written as follows:

$$\sum_{k=1}^6 \left\{ \begin{array}{l} -\omega^2(M_{jk}^R + A_{jk}^I) \quad -i\omega(B_{jk}^I + B_{jk}^R) + (C_{jk}^I + C_{jk}^R) \end{array} \right\} \eta_k e^{-i\omega t} =$$

$$= (F_j^I + F_j^R) e^{-i\omega t} \quad \text{for } j=1,2,\dots,6$$

In the expression above,  $M^R$  represents the generalized mass of the ship's hull.  $A$ ,  $B$ , and  $C$  represent the added mass, damping and restoring matrix respectively. The superscript  $I$  stands for real fluid and the superscript  $R$  stands for viscous flow effects on hull. Index  $j$  and  $k$  indicate respectively the direction of fluid force and the mode of motion of the ship. The force acting on an incremental length of the hull with projected area  $dA_P$  comprises lift  $dL$  and drag  $dD$  resolved normal to and along the relative fluid velocity  $V$ . These force components can be expressed as:

$$dL = 0.5 \rho C_L V^2 dA_P \quad (2.98)$$

$$dD = 0.5 \rho C_D V^2 dA_P \quad (2.99)$$

where  $\rho$  is the density of water, and  $C_L$  and  $C_D$  are the lift and drag coefficients respectively. Setting  $\alpha$  as the angle of incidence of the flow, the force components normal to the body axes are:

$$dL_n = dL \cos \alpha \quad (2.100)$$

$$dD_n = dD \cos \alpha \quad (2.101)$$



As a consequence, the normal components of the lift and drag forces can be computed as follows:

$$dQ = dL_n + dD_n = 0.5 \rho V \sin \alpha (C_L |V \cot \alpha| + C_D |V \sin \alpha|) dA_P \quad (2.102)$$

Integrating over the hull length  $L$  and substituting the viscous lift gradient  $a \approx C_L / \sin \alpha$  yields the viscous damping force  $Q$  on one hull:

$$Q = 0.5 \rho \int_L V \sin \alpha (a |V \cos \alpha| + C_D |V \sin \alpha|) dA_P \quad (2.103)$$

where the first term on the right hand side of the equation accounts for hydrodynamic lift due to vortex shedding around a slender body at steady state translation. The second term on the right hand side arises from boundary layer growth and flow separation.

Since both viscous lift and cross flow drag are non-linear, they cannot be calculated directly into the motion equation. The viscous damping forces are computed calculating the projected area of a hull strip, the vector component of the relative velocity, and the complex amplitude of the relative velocity. These expressions are then used in Equation (2.103) to compute the total viscous damping force on the hulls in the horizontal and vertical directions. The center of action of the vertical viscous forces is assumed to be the hull separation. The center of action of the horizontal hull forces is assumed to be half the hull draft. The resulting viscous forces and moments are separated in viscous damping, viscous restoration, and viscous excitation. Using these values, the viscous damping coefficients  $B_{jk}^R$ , the viscous restoring coefficients  $C_{jk}^R$ , and the complex amplitudes of the viscous exciting forces and moments  $F_j^R$ , are computed. As a consequence, first the  $A$ ,  $B$ ,  $C$ , and  $F$  matrices are calculated together with the vessel motion assuming ideal flow. Once these values are obtained, they are used to compute the  $B^R$ ,  $C^R$ , and  $F^R$  matrices. The values are then added

together and the new vessel motion is calculated. Viscous interactions between strips and between two hulls as well as viscous forces in the longitudinal direction of the hulls are neglected.

Assuming pseudo steady-state conditions, the particle velocity can be computed from the potential of the incident wave  $\phi_I$ . The relative velocities can be computed by summing the particle velocities to the velocity components of the ship at the center of action of the incremental hull length. The vertical and horizontal displacements  $\eta_v$  and  $\eta_h$ , at any point  $(x, y, z)$  in the hull are given by:

$$\eta_v = \eta_3 - x \eta_5 + y \eta_4 \quad (2.104)$$

$$\eta_h = \eta_2 - x \eta_6 + z \eta_4 \quad (2.105)$$

The horizontal and vertical relative velocities of the fluid particles at a section  $x$ , with respect to the port and starboard hulls, are given by:

$$v_{2P}(x) = \dot{\eta}_2 + x \dot{\eta}_6 + d_2(x) \dot{\eta}_4 - \dot{\xi}_h(x, +b(x), -d_2(x)) \quad (2.106)$$

$$v_{2S}(x) = \dot{\eta}_2 + x \dot{\eta}_6 + d_2(x) \dot{\eta}_4 - \dot{\xi}_h(x, -b(x), -d_2(x)) \quad (2.107)$$

$$v_{3P}(x) = \dot{\eta}_3 - x \dot{\eta}_5 + b(x) \dot{\eta}_4 - \dot{\xi}_v(x, +b(x), -d_3(x)) \quad (2.108)$$

$$v_{3S}(x) = \dot{\eta}_3 - x \dot{\eta}_5 - b(x) \dot{\eta}_4 - \dot{\xi}_v(x, -b(x), -d_3(x)) \quad (2.109)$$

where  $\dot{\xi}_v$  and  $\dot{\xi}_h$  are respectively the vertical and horizontal velocity of the fluid particles induced by the incident wave and  $\dot{\eta}_k$  is the ship velocity in the  $k^{th}$  mode of motion. The distance  $d_2$  is the half draft at a cross section at  $x$ ,  $d_3$  is the depth of

the maximum breadth point of the submerged cross section at  $x$ , and  $b(x)$  is the half distance between the axis of the demihulls.

## 2.7 Resonance Frequencies

In order to fully understand the results calculated by the above programs, it is necessary to point out that a multihull oscillating in waves is subject to a series of resonance phenomena. These phenomena are usually observed when the motion of the fluid between the hulls is strongly excited by the oscillations of the vessel at  $x$ .

As reported by Wang and Wahab in [30], the resonance frequencies are a function of the spacing between the demihulls and are caused by the energy trapped between the hulls. Looking at a twin cylinder configuration oscillating in heave, the energy reaches a particularly high value when the waves generated in between the demihulls have a length equal to  $\frac{H}{n}$ , where  $H$  is the inner distance between the hulls, and  $n$  is any multiple of one. As a consequence, the resonance frequencies for a catamaran in heave can be calculated using the following equation:

$$\omega_{R_n} = \sqrt{\frac{2\pi gn}{H}} \quad \text{for } n=1,2,3,\dots \quad (2.110)$$

As reported in [30], this function is similar to the natural modes of motion of a fluid between two vertical walls of  $H$  distance apart, with no energy dissipation. Due to the multihull configuration, part of the energy leaks from the bottom of the demihulls and transmits to infinity. As a consequence, the characteristic frequencies are not exactly in coincidence with the characteristic frequencies calculated with Equation (2.110).

The same concept applies for the resonance frequencies in sway and roll which can

be calculated as follows:

$$\omega_{R_2} = \sqrt{\frac{(2n+1)\pi g}{H}} \quad \text{for } n=0,1,2,3,\dots \quad (2.111)$$

The reasons behind such resonance phenomena are not limited to catamarans but are valid for any multihull vessels with port-starboard symmetry.

Although resonance is a physical phenomenon, factors such as the ship velocity, a constant change in the ship cross section, and the viscosity of water, dampen the resonance effects on the ship motion. These factors cannot be taken into account with a two dimensional method and can lead to wrong results. Particular attention needs to be given when calculating the sectional hydrodynamic coefficients around a resonance frequency. Using a large number of panels along the body limits these effects [30].

## 2.8 Vessel Motion

The vessel motion  $\eta_j$  is strictly related to four independent variables which are: the amplitude of the incident waves  $\zeta_A$ , the incident wave frequency  $\omega$ , the ship speed  $U_o$ , and the angle of wave incidence  $\mu$ . Assuming that the vessel behaves as a linear system, the amplitude of the vessel motion is proportional to the amplitude of the exciting incident waves. As a consequence, the response of a ship in waves is usually expressed as a ratio between the amplitude of the ship response  $\bar{\eta}_j$  and the amplitude of the incident waves  $\zeta_A$  as a function of  $\omega_e$ , also known as the transfer function. The modulus of the transfer function is called the Response Amplitude Operator (RAO) and is used to evaluate the motion of a vessel in six degrees of freedom.

The RAO for the six degrees of motion are uniquely defined as the ratio of the amplitude of vessel motion  $\bar{\eta}_j$  in the  $j^{th}$  direction over the wave amplitude  $\zeta_A$  as follows:

- $SwayRAO = \frac{\overline{\eta_2}}{\zeta_A}$
- $HeaveRAO = \frac{\overline{\eta_3}}{\zeta_A}$
- $RollRAO = \frac{\overline{\eta_4}}{\zeta_A} \cdot \frac{g}{\omega^2}$
- $PitchRAO = \frac{\overline{\eta_5}}{\zeta_A} \cdot \frac{g}{\omega^2}$
- $YawRAO = \frac{\overline{\eta_6}}{\zeta_A} \cdot \frac{g}{\omega^2}$

All the data expressed in this report will follow this notation.



## Chapter 3

# The I-Marine Seakeeping Analysis Toolbox

### 3.1 Introduction

The I-Marine Seakeeping Analysis Toolbox was designed to give students the opportunity to interactively learn and understand all the factors involved in the seakeeping analysis of a vessel. More specifically, the I-Marine platform was developed to solve most of the challenges of using an advanced analysis tool, such as seakeeping prediction programs, in an educational framework. Using a traditional seakeeping analysis program in class is a difficult task due to the large number of hours required to familiarize the students with the program. With I-Marine, this difficulty is removed because of the integrated framework inside I-Marine that allows the focus of the lectures to shift from programming and debugging to seakeeping analysis. The integrated structure of I-Marine also allows students to build a hull-geometry and test it with different seakeeping analysis programs. In doing so, students can compare the results obtained and understand the strengths and weaknesses of the different methods used for the computation. This fact is particularly remarkable considering that

each program has different input files and different settings. Specifically, students will be able to learn what seakeeping analysis program to apply for a given scenario and how to critically analyze the results produced.

Another great advantage of the I-Marine Seakeeping Analysis Toolbox is its capability to analyze advanced hull forms. Particular attention was given to seakeeping programs for multihull vessels due to the little amount of information available about these hull forms. Being able to analyze the seakeeping of multihull vessels is a great advantage to students and designers in general, providing important information about the capabilities of such vessels.

The Seakeeping Analysis Toolbox is part of the I-Marine website. A graphical interface has been developed to facilitate using the different seakeeping analysis programs without requiring any knowledge in programming. The Toolbox is accessible from the main page of the I-Marine website by clicking on "My Daise". The access to My Daise is user restricted and a username and password are required to log in. Each user has a data-locker where all the results from previous experiments and all the created geometries are stored. The My Daise page is shown in Figure 3-1. The page has two menus, one on the right and one on the left of the page. The menu on the right is used to leave the My Daise page and access other parts of the I-Marine website. The menu on the left allows the user to create a new geometry, to run a seakeeping simulation, or to look at the data stored in the locker.

## **3.2 Program Chart**

The I-Marine Seakeeping Analysis Toolbox can be divided in three main blocks: the first block is called I-Build and is used to build the vessel geometry, the second block is used to compute the sectional hydrodynamic coefficients and forces of a given geometry, and the third is used to calculate the vessel response. The second and the



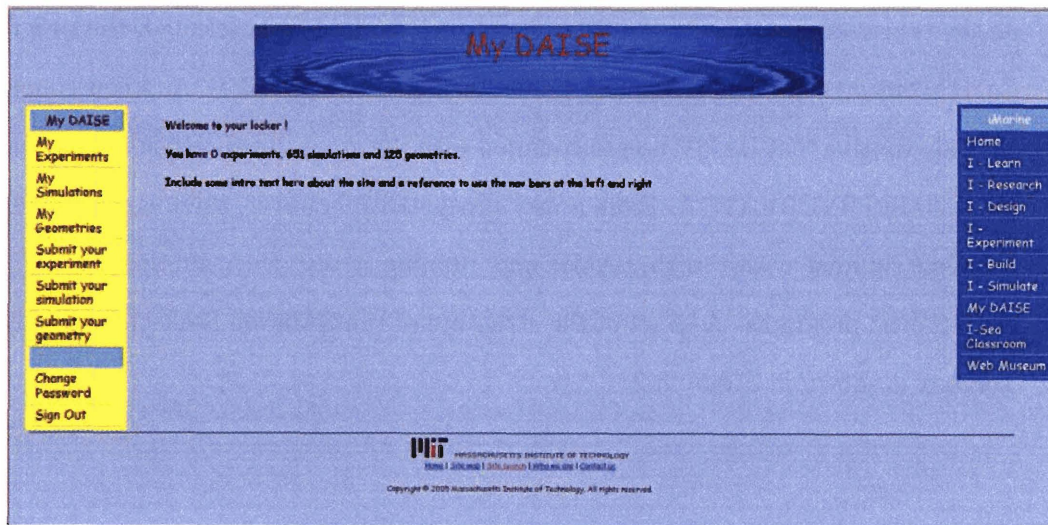


Figure 3-1: My Daise Page. The menu on the left is dedicated to the Seakeeping Analysis Toolbox. The menu on the right allows the user to access other parts of the I-Marine website.

third blocks together are called I-Simulate. The hull geometry is designed in I-Build using a program called GEOMETRYCREATOR that gives the user the possibility to specify the main characteristics of the vessel. Once the geometry has been created, the user can select with which program the added mass and damping coefficients have to be computed. Four different two-dimensional programs have been included, each using a different method to compute the sectional hydrodynamic coefficients and forces. These programs are: MIT5D, NIIRID, CAT-5, and CROSSFLOW. In addition, the I-Marine Seakeeping Analysis Toolbox includes a fifth program called Large Amplitude Motion Program (LAMP). LAMP is a fully three-dimensional seakeeping program that allows both linear and non-linear computation of the forces acting on a vessel in waves.

In case one of the two-dimensional programs is used, the sectional values of the added mass, damping coefficients, and forces calculated are used by STRIPSOLVER to compute the total vessel response using strip theory. The program outputs the RAOs in the six degrees of freedom together with the vessel velocity and acceleration

at the center of gravity. On the other hand, in case LAMP is selected, the program directly outputs the vessel response without using STRIPSOLVER. As a consequence, the only routine that LAMP uses in common with the other two-dimensional programs is GEOMETRYCREATOR. From a user prospective, however, there is no difference between running a test with LAMP and running a test with another one of the strip theory programs. A chart of the structure of the I-Marine Seakeeping Analysis Toolbox is shown in Figure 3-2.

### 3.3 Vessel Input Geometry (I-Build)

The routine I-Build is based on the program GEOMETRYCREATOR that has been developed to create different types of vessel of any given dimensions. The program is able to create monohulls, catamarans, and trimarans, using four different hull shapes which are: circular cylinder, elliptical cylinder, Wigley hull, and NPL Series hull. The user is asked to input the number of hulls, the hull type, and the overall vessel dimensions. This information is used by GEOMETRYCREATOR to build the geometry file which will then be used to calculate the sectional hydrodynamic coefficients and forces.

The program CREATEGEOMETRY works in combination with a series of geometry translators that are used to convert the output geometry file created using GEOMETRYCREATOR into a format that is compatible with each of the seakeeping analysis programs included in I-Marine.

By specifying a series of input parameters and by clicking on "Submit your geometry", the user can create a new hull. A snapshot of the "Submit your geometry" page is shown in Figure 3-3. The page has a menu where the user can select what hull shape to use. The options are: Circle, Ellipse, Wigley, and NPL Series. In addition, there is a second menu that allows the user to specify the number of hulls. The

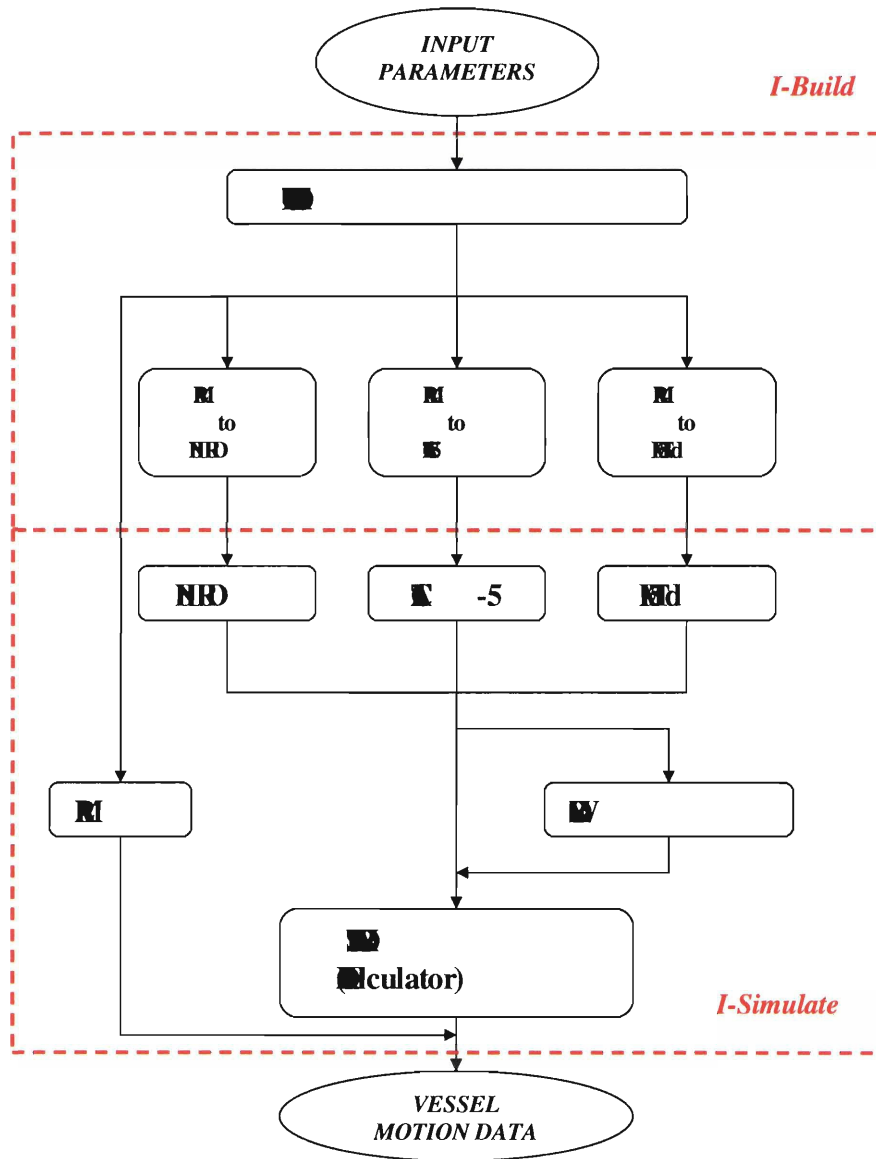


Figure 3-2: I-Marine Seakeeping Analysis Toolbox Program Chart. The platform can be divided in three main blocks: GEOMETRYCREATOR, the programs to calculate the sectional hydrodynamic coefficients, and STRIPSOLVER.

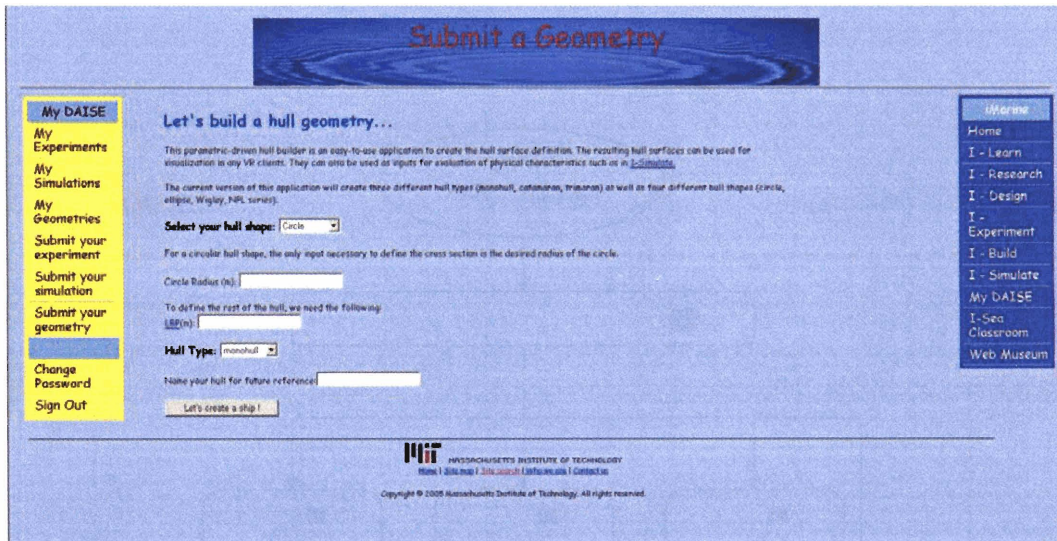


Figure 3-3: Geometry Input Page. Using the scroll down menus, the user can select the shape of the hull sections and the number of hulls. This page is also used to input the overall dimensions of the vessel.

options are: monohull, catamaran, and trimaran. Once both the sectional hull shape and the number of hulls have been selected, the user is asked to input the main dimensions of the vessel. Depending on the sectional shape and on the number of hulls, the required input parameters change. Once all the geometry parameters have been inserted, clicking on the "Let's create a ship !" button will run the GEOMETRYCREATOR program and create the new geometry. The user will then be redirected on the "My Geometries" page where a list of the previously created geometries together with the new geometry is present. The "My Geometry" page is shown in Figure 3-4.

By clicking on one of the geometry names, the user is able to view and download the input file used to create the geometry and the output files produced. In addition, the website also has a graphical interface that allows to see a 3D model of the geometries created. A snapshot of the viewer is shown in Figure 3-5.

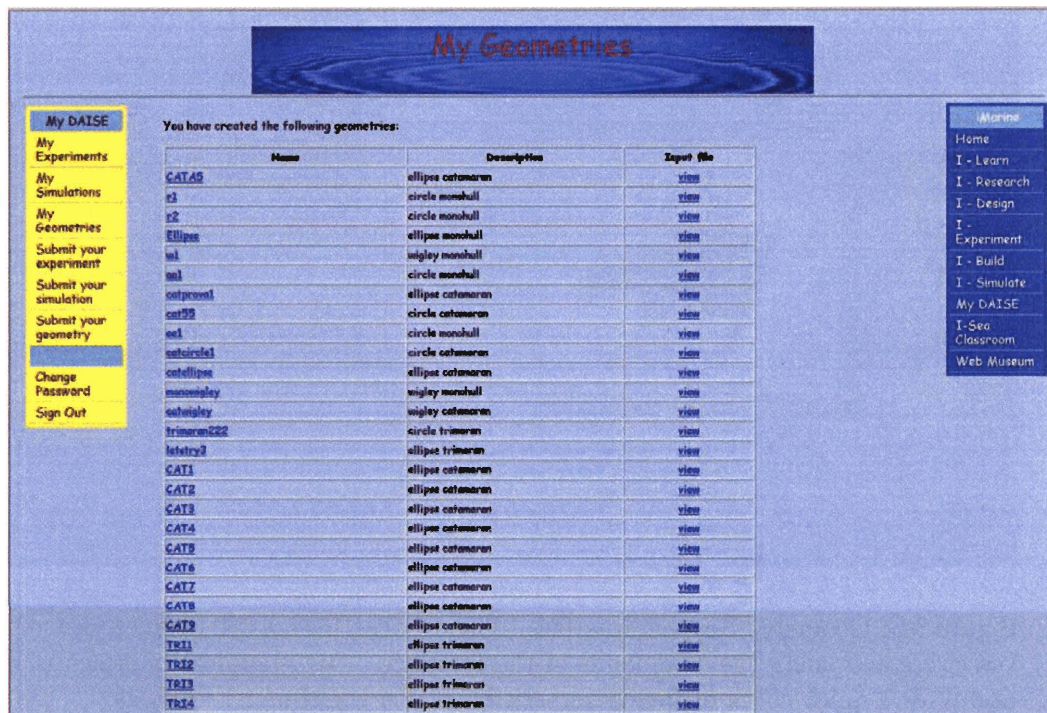


Figure 3-4: MyGeometry List Page. This page contains all the geometries previously created. By clicking on the geometry name, the user can look at the geometry files and display a 3D rendering of the geometry.

### 3.4 Seakeeping Analysis (I-Simulate)

Once the sectional added mass, damping coefficients, and forces have been calculated, the total vessel response is computed using STRIPSOLVER. This program is based on strip theory and can be used with monohulls, catamarans, and trimarans. In addition, the program is able to calculate the velocity and acceleration of the center of gravity of the vessel or of any other specified point along the vessel.

Once the geometry has been created, by clicking on "Submit your simulation", the user has the ability to run the seakeeping analysis. A snapshot of the "Submit your simulation" page is shown in Figure 3-6. The user can select which program to use to run the simulation. Once the program has been selected, the user is asked to select the geometry to analyze, to specify the name of the simulation, the speed, and the



Figure 3-5: Geometry Graphic Interface. The user can have a 360 degrees view of the vessel created using the commands of the interface. The graphical interface is very useful for a quick check of the characteristics of the vessel under analysis.

heading of the vessel. The user is also asked to specify the incidence wave frequencies at which the response should be calculated. Once all the input parameters have been specified, the simulation can be run by clicking on the "Run" button. When the simulation is completed, the user is redirected to the "My Simulations" page where a list of all the simulations that have been run is present. A snapshot of the "My Simulation" page is shown in Figure 3-7. By clicking on one of the simulations, the user is able to view and download both the input and output files of that specific simulation. Clicking on one of the simulation names leads to the the page shown in Figure 3-8. The user can then select which input or output file to download.

**Submit a Simulation**

**My DAISE**

- My Experiments
- My Simulations
- My Geometries
- Submit your experiment
- Submit your simulation
- Submit your geometry

Change Password  
Sign Out

Please Select your simulation type: **NIIRID**

### Simulate with NIIRID

A description of NIIRID here.

This implementation runs NIIRID and then RAO. A description of RAO here.

**Input:**

To run NIIRID you need to have built a geometry under [I-build](#).

**Output:**

NIIRID/RAO output generates a text output files which will be available on [My Data](#). When the simulation is done, you will be redirected to [My Simulations](#) which will enable you to view or download your output.

**Input parameters:**

Simulation Name:

Choose a hull: **CAT48**

Ship Speed (m/s):

Ship Heading (deg):

**Regular Wave:**

# of Frag	Input Frag (1/3)
<input type="text"/>	<input type="text" value="w1,w2,w3..."/>

\*in ascending order.

NIIRID Algorithm:

Allpoint-Rate Quadrature  Two-node Gauss-Logarithm Quadrature

Simulation Description:

**Run NIIRID+RAO**

**Home**

- I - Learn
- I - Research
- I - Design
- I - Experiment
- I - Build
- I - Simulate
- My DAISE
- I-Sea Classroom
- Web Museum

Figure 3-6: NIIRID Input Page. The scroll-down menu allows the user to select a geometry. This page is also used to input the details of the simulation such as vessel speed, wave heading, and incident wave frequencies.

**My Simulations**

You have submitted the following simulations:  
**LAMP: multi-level three-dimensional time-domain computational system**

**NIIRID: Strip theory panel method coupled to iMarine RAO solver**

Simulation Name	Simulation Description	Simulation Output
<a href="#">NIIRIDprevail</a>	test 15 Dec 2005	<a href="#">View</a>
<a href="#">s2</a>	test2	<a href="#">View</a>
<a href="#">d1</a>	333	<a href="#">View</a>
<a href="#">wv1</a>	testtest	<a href="#">View</a>
<a href="#">wv2</a>	test stu2	<a href="#">View</a>
<a href="#">tr1yyy</a>	tr-traron test	<a href="#">View</a>
<a href="#">CAT1180</a>	CAT1 180 deg	<a href="#">View</a>
<a href="#">CAT1_test1</a>	test of zero speed for CAT1	<a href="#">View</a>
<a href="#">CAT1_test2</a>	10 knots	<a href="#">View</a>
<a href="#">CAT1_180S</a>	15 knots	<a href="#">View</a>
<a href="#">CAT1_180</a>	150 degree, speed = 3.2 kts	<a href="#">View</a>
<a href="#">CAT2_180</a>	NII simulation with CAT2 on Tue, 20 Dec 2005 10:23:21 -0500	<a href="#">View</a>
<a href="#">CAT2_180</a>	angle 180, 3.2 kts	<a href="#">View</a>
<a href="#">CAT3_180</a>	angle 180 speed 3.2	<a href="#">View</a>
<a href="#">CAT3_180</a>	NII simulation with CAT3 on Tue, 20 Dec 2005 10:53:26 -0500	<a href="#">View</a>
<a href="#">TR11_180</a>	NII simulation with TR11 on Tue, 20 Dec 2005 11:05:14 -0500	<a href="#">View</a>
<a href="#">TR11_FND</a>	zero speed	<a href="#">View</a>
<a href="#">TR11_lowfreq</a>	NII simulation with TR11 on Tue, 20 Dec 2005 11:22:01 -0500	<a href="#">View</a>
<a href="#">TR11_slfrsq</a>	NII simulation with TR11 on Tue, 20 Dec 2005 11:26:14 -0500	<a href="#">View</a>
<a href="#">TR11_180</a>	NII simulation with TR11 on Tue, 20 Dec 2005 11:31:13 -0500	<a href="#">View</a>
<a href="#">TR11_180b</a>	NII simulation with TR11 on Tue, 20 Dec 2005 11:34:17 -0500	<a href="#">View</a>
<a href="#">TR12_180</a>	NII simulation with TR12 on Tue, 20 Dec 2005 11:49:20 -0500	<a href="#">View</a>

Figure 3-7: My Simulations List. This page contains all the simulations previously completed. By clicking on the name of a simulation, the user can access the output files.

**My Simulations**

Simulation Name: **TR11A6\_150\_FND4**

[Input File](#) [View](#) [Download](#)

You have 6 outputs available for this simulation

<a href="#">txt file</a>	<a href="#">View</a>	<a href="#">Download</a>
<a href="#">txt file</a>	<a href="#">View</a>	<a href="#">Download</a>
<a href="#">txt file</a>	<a href="#">View</a>	<a href="#">Download</a>
<a href="#">txt file</a>	<a href="#">View</a>	<a href="#">Download</a>
<a href="#">txt file</a>	<a href="#">View</a>	<a href="#">Download</a>
<a href="#">txt file</a>	<a href="#">View</a>	<a href="#">Download</a>

[Download all files \(zip\)](#)

Figure 3-8: My Simulation Output. Each simulation generates six output files. Most of these output files are for debugging purposes. In addition, the input file used for each simulation is stored as well.



## Chapter 4

# Validation of the I-Marine Seakeeping Analysis Toolbox

### 4.1 Introduction

A series of tests has been conducted to validate the I-Marine Seakeeping Analysis Toolbox. Both analytical and experimental data were used in this validation process. The validation was carried out in two steps. First, the sectional hydrodynamic coefficients as calculated by NIIRID, CAT5, and MIT5D were considered. Three different twin-cylinder configurations were compared to analytical and experimental data provided in [14, 20, 19]. Second, the strip theory program STRIPSOLVER was validated by a series of tests for catamarans and trimarans in different conditions. For catamaran vessels, the experimental results provided by Wellicome *et al.* for NPL catamarans [18] were used for comparison. As a second source, the results were compared to the response provided by the RAO calculator included in CAT-5. Tests were run both for head and oblique seas at different Froude numbers. On the other hand, for trimaran vessels, due to the lack of experimental results available, the program LAMP was used for comparison. Three different trimaran vessels were tested at zero and

forward speed for different heading angles. To have a better comparison between the two programs, LAMP was also run for a catamaran for the same conditions used in testing the trimarans.

## 4.2 Validation of the Sectional Hydrodynamic Coefficients

Validating the different programs included in I-Marine to calculate the sectional added mass and damping coefficients was considered a fundamental step in the development of the project. An extensive amount of tests was completed both to assess the programs in different scenarios and to understand the limitations of the methods.

Twin-cylinder configurations with different hull spacings were used for the tests. These configurations were selected due to the large quantity of available experimental and analytical data. Tests were run in heave, sway, and roll. The experimental data for two twin-cylinders configurations heaving on the free surface was based on the results reported by Lee *et al.* in [14]. The added mass and damping coefficients in sway and roll for a twin-cylinder configuration oscillating on the free surface were compared to the analytical values reported by Okhusu in [20], and by Nordenstrom *et al.* in [19]. The author is not aware of any experimental data in this area that can be used for comparison.

### 4.2.1 Heave Motion

The added mass and damping sectional coefficients in heave,  $a_{33}$  and  $b_{33}$ , were computed for a twin-cylinder configuration with a spacing ratio  $b/a = 3.0$ , where  $b$  is the half-distance between the axis of the cylinders and  $a$  is the radius of the cylinder.

The programs used to calculate the sectional hydrodynamic coefficients were NI-IRID, MIT5D, and CAT5. Figure 4-1 shows the results of the computed added mass in

heave  $a_{22}$  for two twin-cylinder configurations with a spacing ratio  $b/a = 3.0$  together with the experimental results reported in [14]. The values calculated with NIIRID and CAT-5 are almost identical and show a good agreement with the experimental data. On the other hand, the values calculated by MIT5D are inaccurate. The reason for such a large difference in results is due to the way the sectional hydrodynamic coefficients are computed by each program. Both NIIRID and CAT-5 calculate the sectional added mass and damping coefficients using a potential function which includes both hulls. As a consequence, some of the interaction effects between the two hulls are taken into account. On the other hand, MIT5D computes the added mass of a single hull and then multiplies it by a factor of two to obtain the total added mass for a catamaran. Although the approach used by MIT5D is much simpler to implement, it does not provide accurate results where hull-hull interactions play an important role in the vessel motion. As it can be seen in Figure 4-1, the method used by MIT5D is accurate only at very low frequencies, where hull-hull interactions are very limited. In addition, since the vessel is analyzed as two separate hulls, MIT5D does not present the resonance phenomenon shown by NIIRID and CAT-5.

Figure 4-2 shows the results of the damping coefficient in heave  $b_{33}$  for a twin-cylinder configuration with a spacing ratio  $b/a = 3.0$ . The sectional damping coefficient in heave computed by NIIRID and CAT-5 shows a good agreement with the experimental values across all the range of frequencies at which the programs were tested. As for the added mass case, the values computed with MIT5D shows little agreement with the experimental data.

Using Equation (2.110), the first two resonance frequencies for  $a_{33}$  and  $b_{33}$  for a twin-cylinder configuration with a spacing ratio  $a/b = 3.0$  are  $Ka = 1.57$  and  $Ka = 3.14$ . Given the range of frequencies at which the coefficients were calculated, only the first resonance peak can be observed in Figure 4-1 and Figure 4-2.

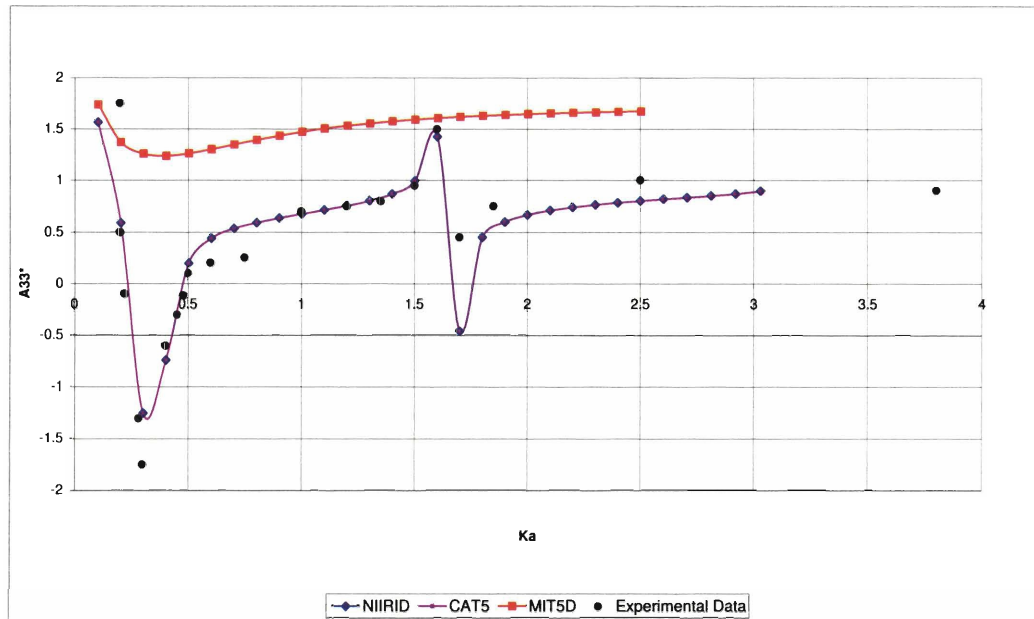


Figure 4-1: Sectional Added Mass of Twin-Cylinder Configuration in Heave ( $b/a = 3.0$ )

#### 4.2.2 Sway Motion

The added mass and damping coefficients in sway,  $a_{22}$  and  $b_{22}$ , were computed for two twin-cylinder configurations with a spacing ratio  $b/a = 1.5$  and  $b/a = 3.0$ . The programs NIIRID, CAT-5, and MIT5D were used for the calculations. The results obtained were compared with the analytical data reported by Okhusu in [20]. Figure 4-3 and Figure 4-4 show the added mass in sway for a twin-cylinder configuration with spacing ratio  $b/a = 1.5$  and  $b/a = 3.0$ . Both the results computed with NIIRID and the results calculated with CAT-5 show an overall very good agreement with the analytical data reported in [20]. On the other hand, the results calculated with MIT5D are not accurate. It must be kept in mind that MIT5D does not take into account the spacing between the demihulls and the results are computed as if the demihulls were infinitely far apart. As a consequence,  $a_{22}$  and  $b_{22}$  are equal for the two catamaran configurations,  $b/a = 1.5$  and  $b/a = 3.0$ . As it can be seen from Figure 4-3

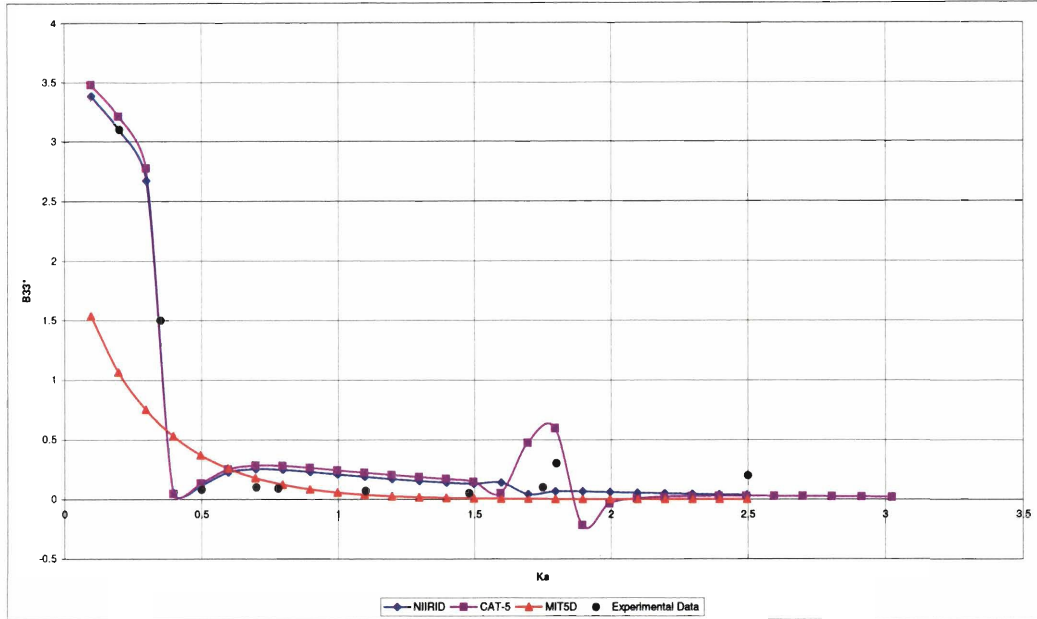


Figure 4-2: Sectional Damping Coefficient of Twin-Cylinder Configuration in Heave ( $b/a = 3.0$ )

and Figure 4-4, this approach is not accurate. For a spacing ratio  $a/b = 1.5$ , MIT5D tends to over-predict the added mass at very low frequencies and to under-predict its value at high frequencies. For a spacing ratio  $a/b = 3.0$ , the results are more accurate than for the  $a/b = 1.5$  case because the demihull spacing is larger.

Figure 4-5 and Figure 4-6 show the values of the damping coefficient in sway  $b_{22}$  calculated with NIIRID and CAT-5 for a spacing ratio  $b/a = 1.5$  and  $b/a = 3.0$ . Due to the different method used to compute the sectional hydrodynamic coefficients, the two programs show different resonance phenomena. Overall, however, NIIRID and CAT-5 show good agreement. On the contrary, MIT5D highly over-predicts the damping coefficients, particularly in the low frequency range. The values calculated by MIT5D tend to asymptotically reach the results of NIIRID and CAT-5 at very high frequencies. Once again, the reason behind the inaccuracy of MIT5D is the hull-hull interactions that are not taken into account. In this case, the two hulls seem to produce a cancellation effect in the low frequency range not taken into account by

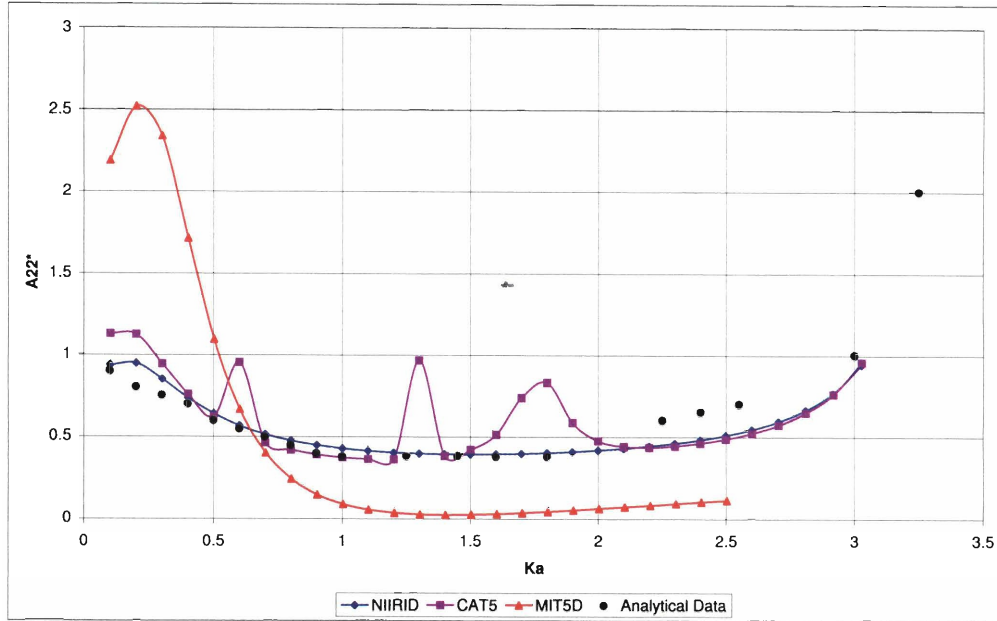


Figure 4-3: Sectional Added Mass of Twin-Cylinder Configuration in Sway ( $b/a = 1.5$ )

MIT5D leading to an over-prediction of  $b_{22}$ . On the other hand, at higher frequencies, the hull-hull interactions are less relevant and the results computed with MIT5D meet the results calculated by NIIRID and CAT-5. Unfortunately, no experimental or theoretical data was available for comparison.

Using Equation (2.111), the first two resonance frequencies for  $a_{22}$  and  $b_{22}$  for a spacing ratio  $a/b = 1.5$  and  $a/b = 3.0$  are  $Ka = 4.49, 7.78$  and  $Ka = 0.785, 2.35$ . In the range of frequencies at which the coefficients were calculated, the resonance peaks can only be observed in Figure 4-4 and Figure 4-6.

### 4.2.3 Roll Motion

The sectional added mass and damping coefficients in roll were computed for a twin-cylinder configuration oscillating on the free surface with a spacing ratio  $b/a = 2.0$ . The values obtained were compared with the analytical data provided by Nordenstrom *et al.* in [19]. Unfortunately, no experimental results were found.

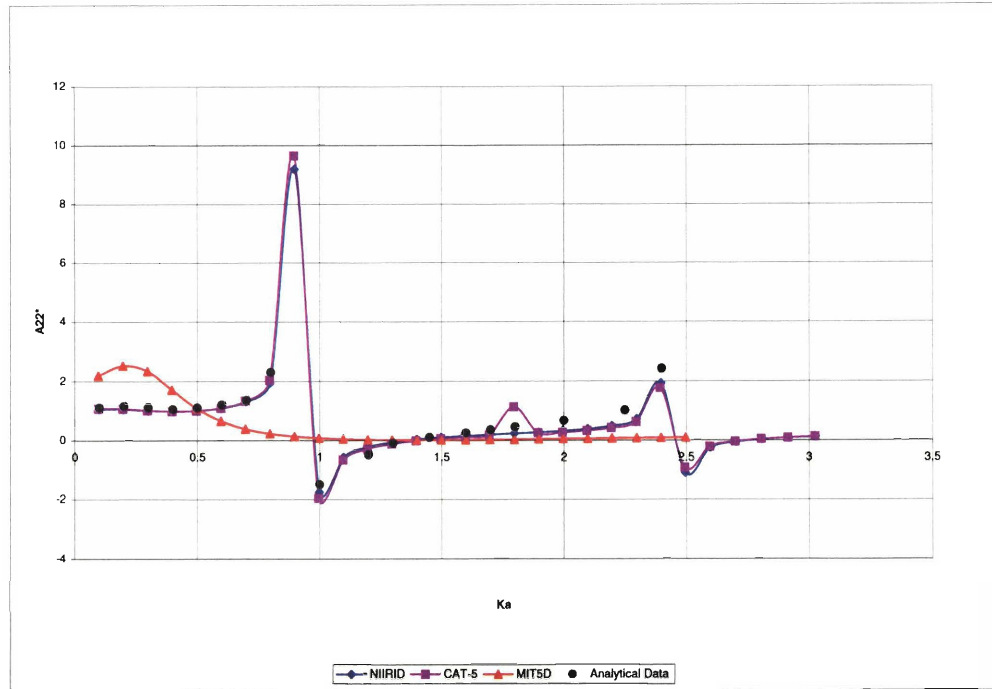


Figure 4-4: Sectional Added Mass of Twin-Cylinder Configuration in Sway ( $b/a = 3.0$ )

Figure 4-7 and Figure 4-8 show the added mass and damping coefficient in roll,  $a_{44}$  and  $b_{44}$ , computed with NIIRID and CAT-5. The results calculated by NIIRID agree very well with the analytical data both for  $a_{44}$  and  $b_{44}$ . The results calculated by CAT-5 are less accurate and constantly under-predict the hydrodynamic coefficients in roll across the whole frequency range. The added mass computed by MIT5D shows a good agreement with the analytical data considering that no hull-hull interaction has been taken into account. On the other hand, the damping coefficient is highly inaccurate particularly in the low frequency range.

The resonance frequency for the added mass and damping coefficients in roll for a twin-cylinder configuration with a spacing ratio  $b/a = 2.0$  equals  $Ka = 1.57$  and  $Ka = 4.70$  as it can be confirmed looking at Figure 4-7 and Figure 4-8.

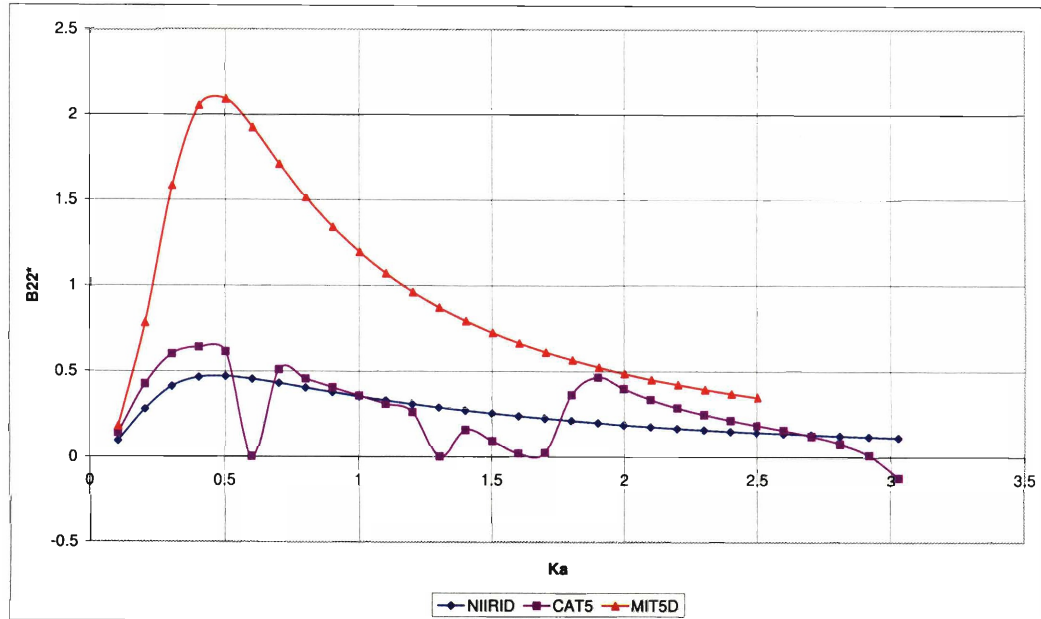


Figure 4-5: Sectional Damping Coefficient of Twin-Cylinder Configuration in Sway ( $b/a = 1.5$ )

#### 4.2.4 Coupled Sway-Roll Motion

The added mass and damping coefficients in coupled sway-roll motion,  $a_{24}$  and  $b_{24}$ , for a twin-cylinder configuration with a spacing ratio of  $b/a = 2.0$  were calculated using NIIRID, CAT-5 and MIT5D. The results obtained were compared with the analytical data provided by Nordenstrom *et al.* in [19].

Figure 4-9 and Figure 4-10 show the calculated values of the added mass and damping coefficients in roll. NIIRID and CAT-5 show very good agreement with the analytical results. On the other hand, MIT5D did not accurately predict  $a_{24}$  and  $b_{24}$ . MIT5D over-predicts the added mass values in the low frequency range due to not taking hull-hull interactions into account. For the same reason, MIT5D largely over-predicts the values of  $b_{24}$  at the low frequency range. In the high frequency range, MIT5D tends to asymptotically meet the values calculated by NIIRID and CAT-5 due to little interaction effects between the hulls.



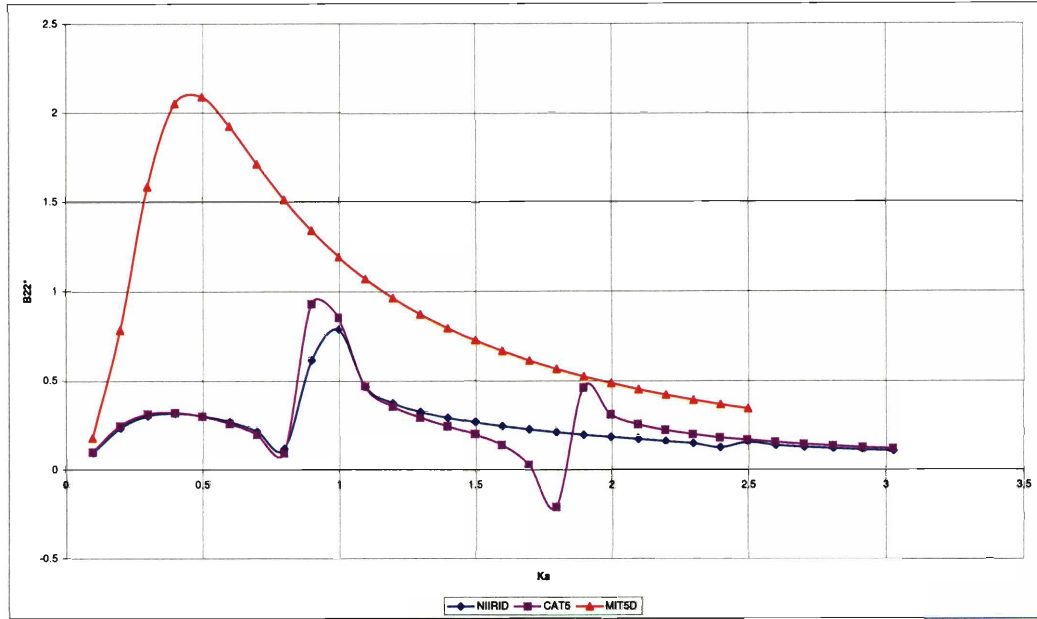


Figure 4-6: Sectional Damping Coefficient of Twin-Cylinder Configuration in Sway ( $b/a = 3.0$ )

The resonance frequencies for  $a_{24}$  and  $b_{24}$  for a twin-cylinder configuration with a spacing ratio  $b/a = 2.0$  equals  $Ka = 1.57, 4.70$  as it can be confirmed by looking at Figure 4-9 and Figure 4-10.

### 4.3 NPL Series Tests

In order to be able to assess the performance of the program STIPSOLVER, a large number of tests was completed. The scope of these tests was both to validate STRIP-SOLVER and to understand the limits of strip theory in predicting the response of multihull vessels in waves.

The data provided in [18] was used in assessing the performances of STRIP-SOLVER. NPL Model 5b with a demihull spacing  $S/L = 0.4$  was used for the validation. The hull offsets were obtained from [1]. The general dimensions of NPL Model 5b are shown in the Table 4.1. Tests were run in head seas at a Froude number

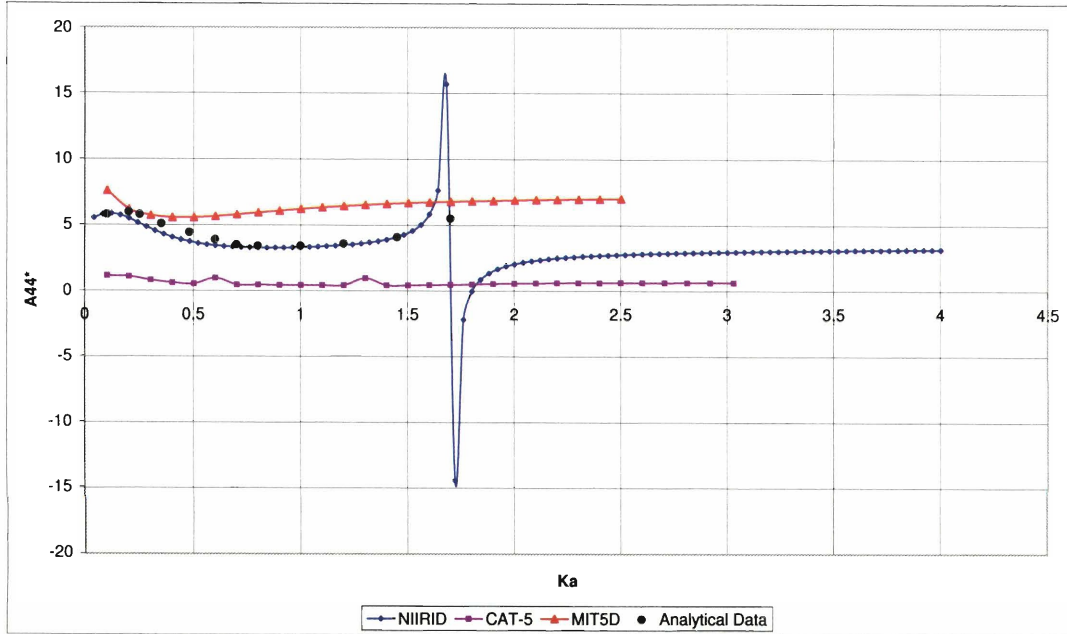


Figure 4-7: Sectional Added Mass of Twin-Cylinder Configuration in Roll ( $b/a = 2.0$ )

$F_n = 0.2, 0.5,$  and  $0.8$ . In addition, tests were run at a Froude number  $F_n = 0.67$  in head seas and in oblique seas at 150 and 120 degrees. NIIRID, CROSSFLOW, and MIT5D were used to compute the sectional added mass and damping coefficients for the vessel. The response was calculated with STRIPSOLVER. In addition, the same tests were run using CAT-5 and the response computed with the RAO calculator of CAT-5.

#### 4.3.1 CROSSFLOW Drag Coefficient and Lift Gradient Assessment

In order to effectively use CROSSFLOW, a series of tests was completed to determine what values of drag coefficient  $C_D$  and lift gradient  $a$  were the most accurate for the NPL Model 5b. The values proposed by Chan in [3] for an ASR catamaran travelling at a Froude number  $F_n = 0.124$  were taken as a reference. The analysis was carried out in head sea at a Froude number  $F_n = 0.2, 0.5,$  and  $0.8$  using three different

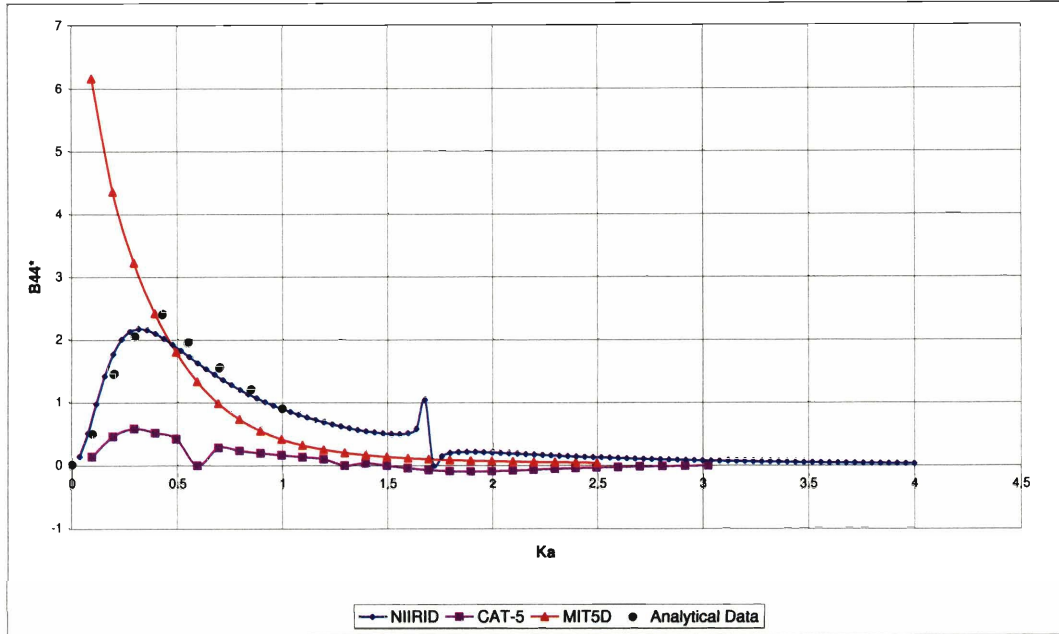


Figure 4-8: Sectional Damping Coefficient of Twin-Cylinder Configuration in Roll ( $b/a = 2.0$ )

values for the drag coefficient  $C_D = 0.4, 0.2,$  and  $0.05$ . The lift gradient  $a$  was left unchanged and equal to  $a = 0.0024$  due to the little effect it has on the calculations. The response calculated with CROSSFLOW was compared to the experimental data provided in [18]. The plot of the results are shown in Appendix A. By looking at the data, it was observed that the best results were obtained by linearly scaling the drag coefficient  $C_D$  with the Froude number. Using this approach, the values of  $C_D$  to use with NPL Model 5b were calculated. The same values were used for both the head seas and oblique seas tests. The results are shown in Table 4.2.

### 4.3.2 Head Seas

Figure 4-11 and Figure 4-12 show the heave and pitch response in head seas at a Froude number  $F_n = 0.2$ . Overall both STRIPSOLVER and CAT-5 performed in a similar fashion showing a good agreement with the experimental data. Both pro-

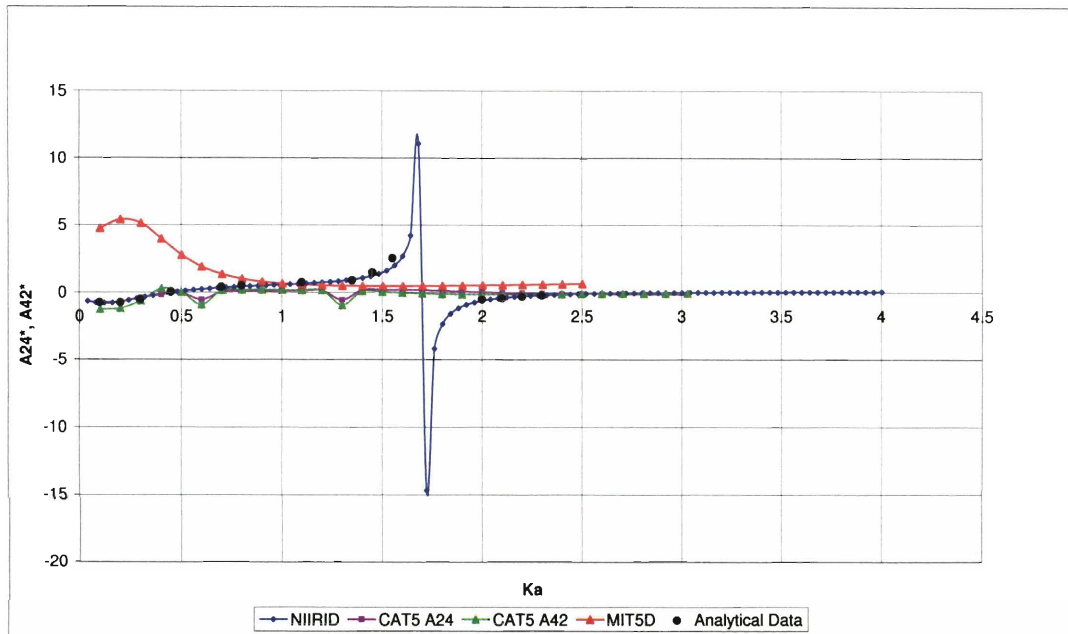


Figure 4-9: Sectional Added Mass of Twin-Cylinder Configuration in Coupled Sway-Roll Motion ( $b/a = 2.0$ )

grams predict peaks in the response for given frequencies which are not present in the experimental results due to the resonance phenomenon explained in Section 2.7. The response calculated with CROSSFLOW shows a substantial improvement compared to NIIRID and CAT-5. By taking into account some of the viscous effects, CROSSFLOW is less sensitive to the internal resonance phenomena leading to a better estimate of the vessel motion in both heave and pitch. In heave, MIT5D shows accurate results both in the very low frequency and in the very high frequency range. However, the results in the mid-frequency range constantly over-predicts the vessel motion. In pitch, MIT5D has similar performances to the other programs showing good agreement with the experimental data all across the frequency range except at very low frequencies, where the pitch response is highly under-predicted. The resonance frequency was calculated to be  $\omega_{R_3} = 4.2$  rad/s.

Figure 4-13 and Figure 4-14 show the heave and pitch response in head seas

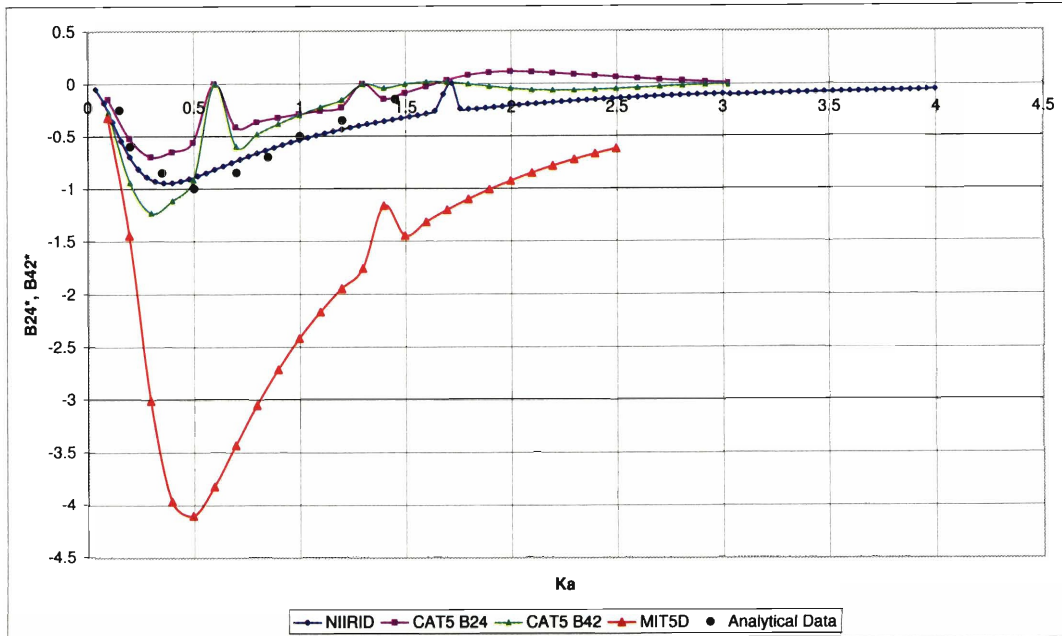


Figure 4-10: Sectional Damping Coefficient of Twin-Cylinder Configuration in Coupled Sway-Roll Motion ( $b/a = 2.0$ )

at a Froude number  $F_n = 0.5$ . The response calculated by STRIPSOLVER and by CAT-5 are quite similar and they agree reasonably well with the experimental data. A decrease in performance is shown around the resonance frequency where both programs largely over-predict the response. CROSSFLOW shows a better agreement with the experimental data than STRIPSOLVER and CAT-5 as it decreases the effects of internal resonance by taking into account some of the viscous effects. Agreement is good in both heave and pitch. MIT5D shows a very good agreement in heave, being the best of the four programs used. On the other hand, the agreement in pitch is the poorest of the four, largely under-predicting the vessel motion. These results show that MIT5D could be effectively used particularly near the resonance frequencies were more advanced panel method programs such as NIIRID and CAT-5 show a peak response which largely affects the accuracy of the results.

Figure 4-15 and Figure 4-16 show the heave and pitch response in head seas at a

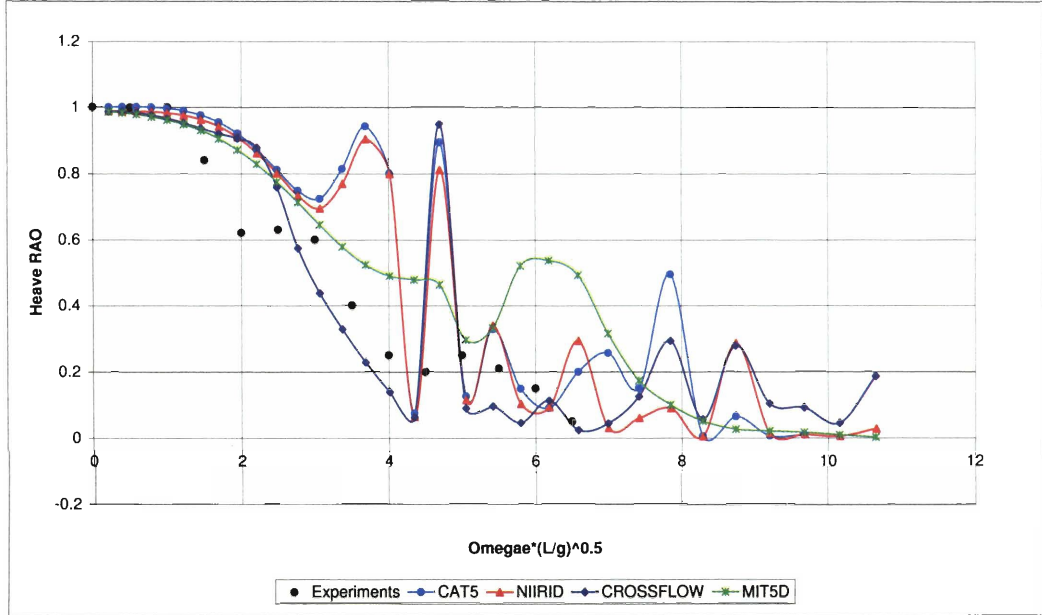


Figure 4-11: Heave RAO for NPL Model 5b at  $F_n = 0.2$  and  $\mu = 180^\circ$

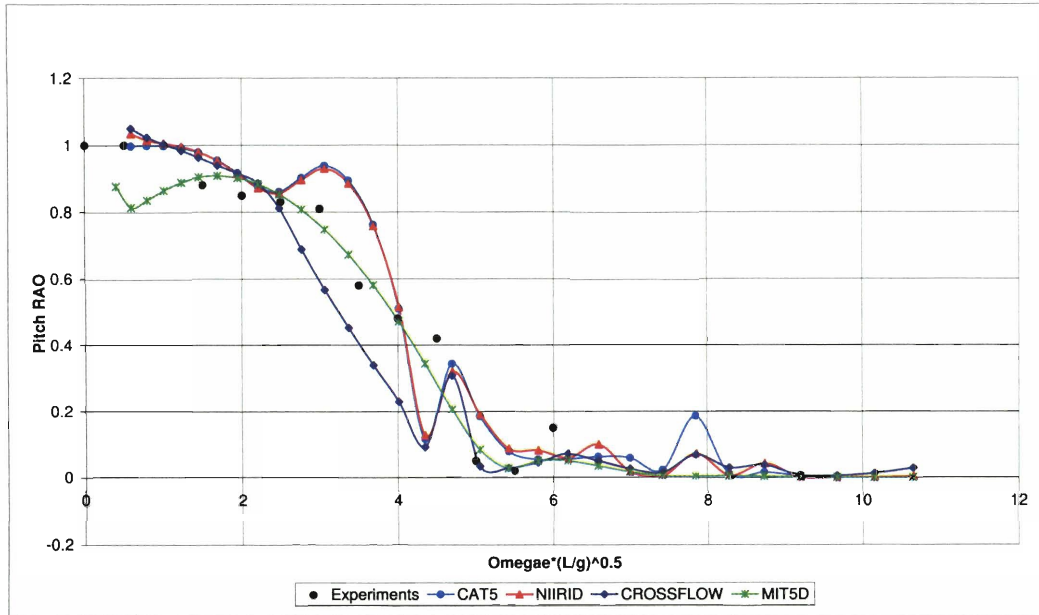


Figure 4-12: Pitch RAO for NPL Model 5b at  $F_n = 0.2$  and  $\mu = 180^\circ$

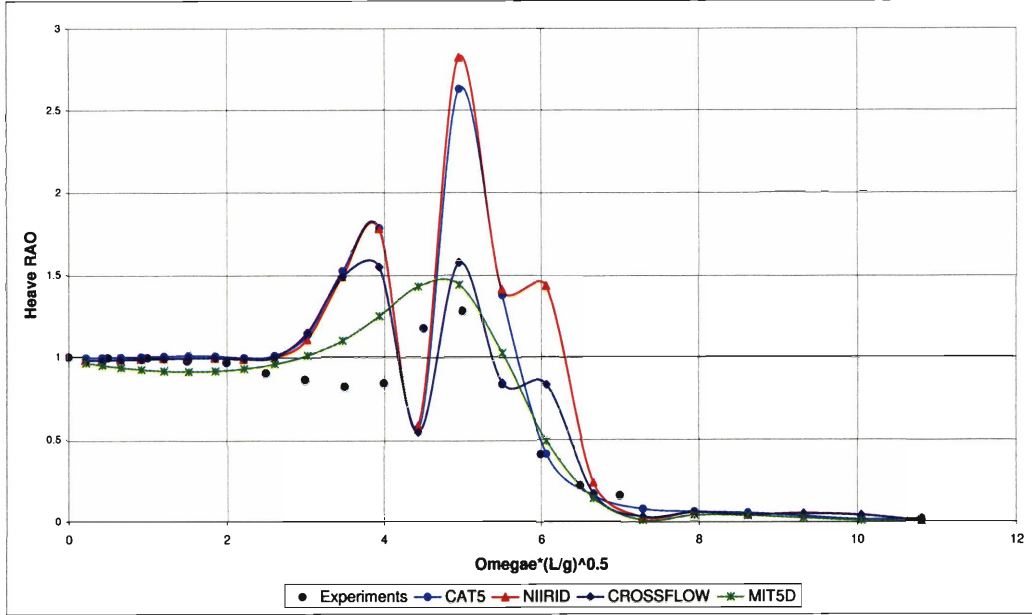


Figure 4-13: Heave RAO for NPL Model 5b at  $F_n = 0.5$  and  $\mu = 180^\circ$

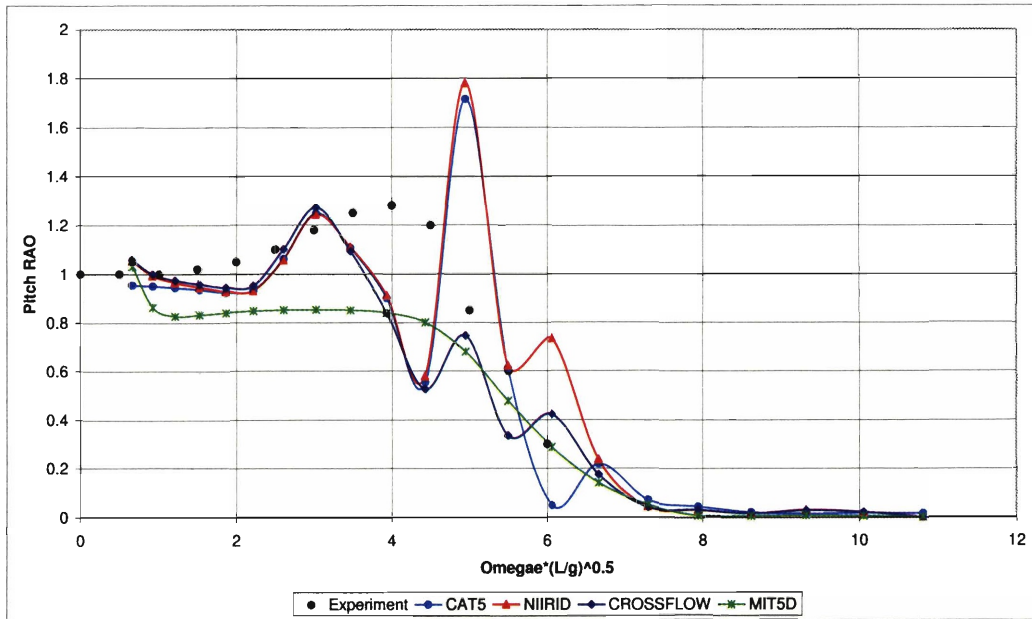


Figure 4-14: Pitch RAO for NPL Model 5b at  $F_n = 0.5$  and  $\mu = 180^\circ$

LOA	5.249 ft
Overall Beam	2.577 ft
Demihull Beam	0.477 ft
Draft	0.238 ft
Volume	0.474 ft <sup>3</sup>
CB	0.1471
LCG	0 ft
VCG	0.1193 ft
RXX	0.577 ft
RYY	1.365 ft
RZZ	1.469 ft

Table 4.1: NPL Model 5b General Characteristics

$F_n$	$C_D$	$a$
0.2	0.4	0.0024
0.5	0.1	0.0024
0.8	0.063	0.0024
0.67	0.075	0.0024

Table 4.2: Values of the Drag Coefficient  $C_D$  and the Lift Gradient  $a$  as a Function of Froude Number Used for the NPL Analysis in Head and Oblique Seas

Froude number of 0.67. As for the previous cases, the agreement in heave and pitch is good.

Figure 4-17 and Figure 4-18 show the heave and pitch response in head seas at a Froude number  $F_n = 0.8$ . Once again, agreement is good. STRIPSOLVER and CAT-5 show a good agreement with the experimental data. Both programs calculate a very similar response in both heave and pitch and largely over-predict the vessel motion around the resonance frequency. CROSSFLOW shows a better agreement with the experimental results than STRIPSOLVER and CAT-5. MIT5D predicts very well the heave response across the whole frequency range being the best of the four programs. In pitch, however, the results of MIT5D are quite inaccurate.



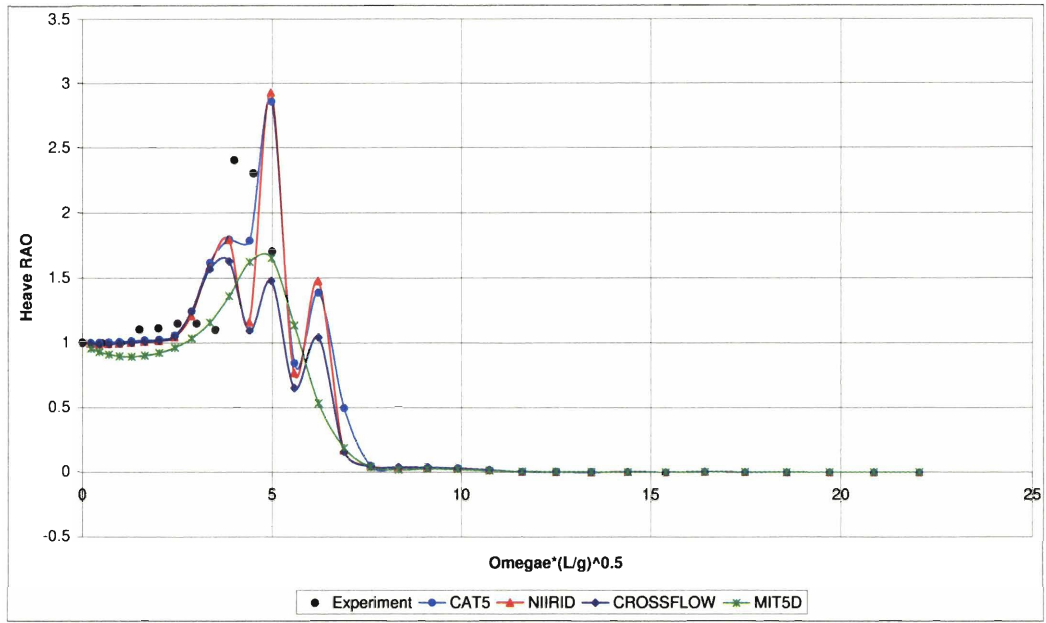


Figure 4-15: Heave RAO for NPL Model 5b at  $F_n = 0.67$  and  $\mu = 180^\circ$

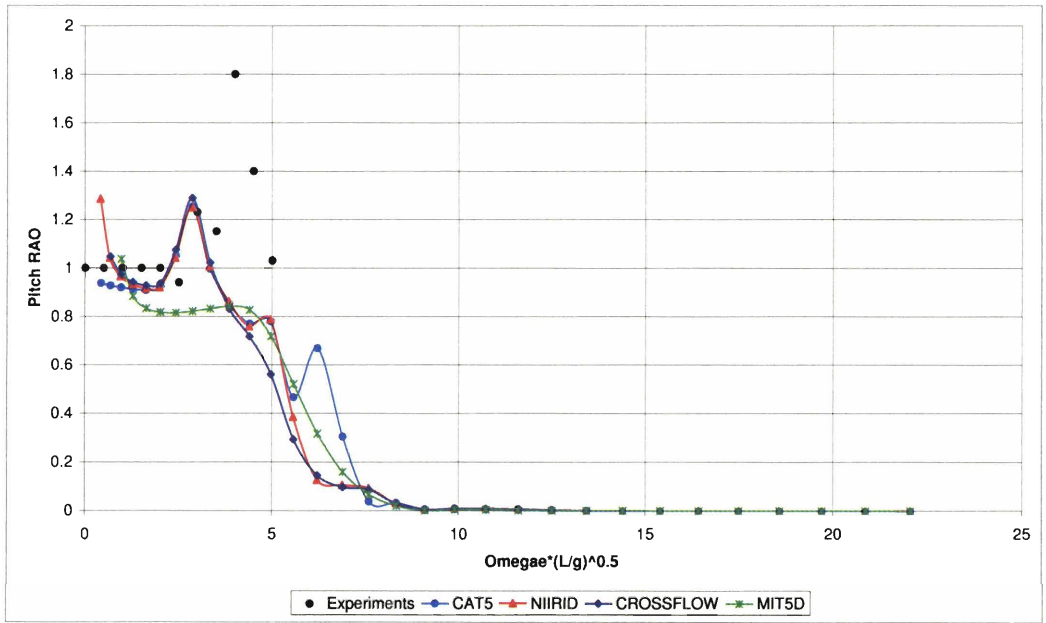


Figure 4-16: Pitch RAO for NPL Model 5b at  $F_n = 0.67$  and  $\mu = 180^\circ$

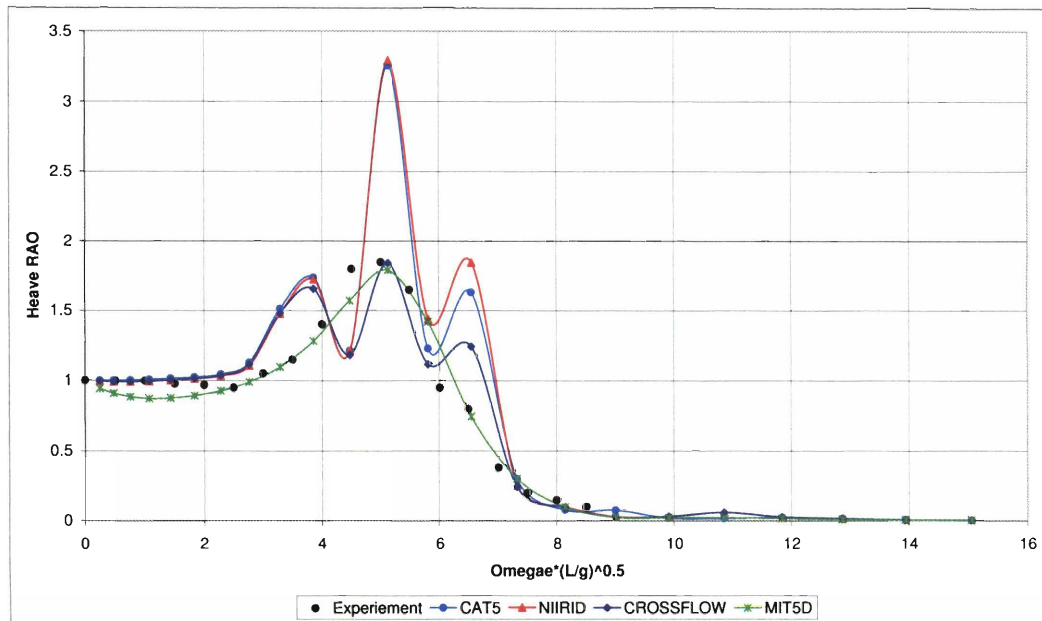


Figure 4-17: Heave RAO for NPL Model 5b at  $F_n = 0.8$  and  $\mu = 180^\circ$

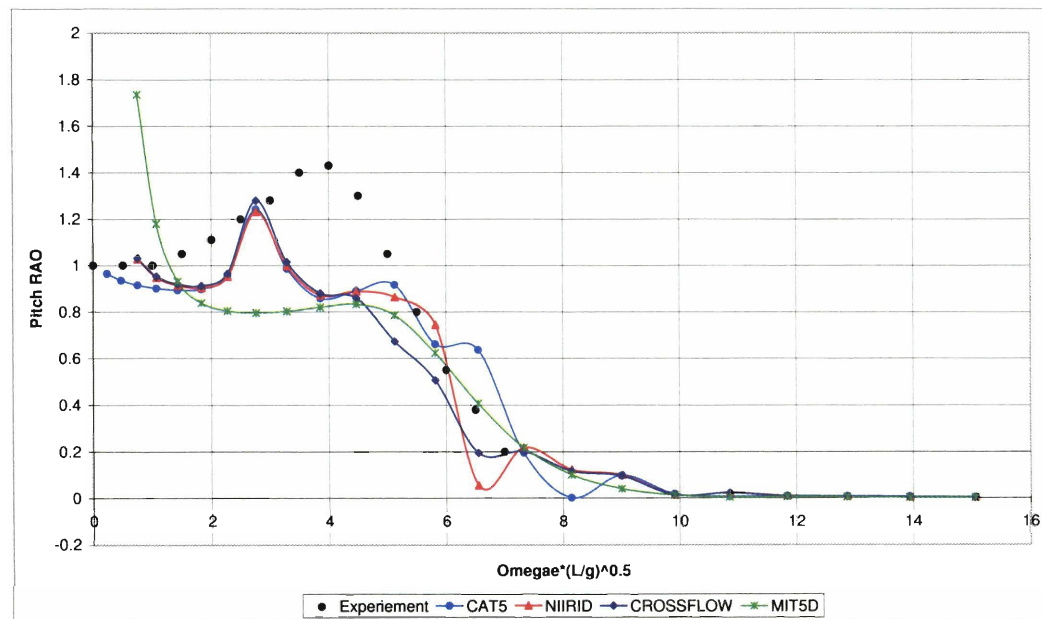


Figure 4-18: Pitch RAO for NPL Model 5b at  $F_n = 0.8$  and  $\mu = 180^\circ$

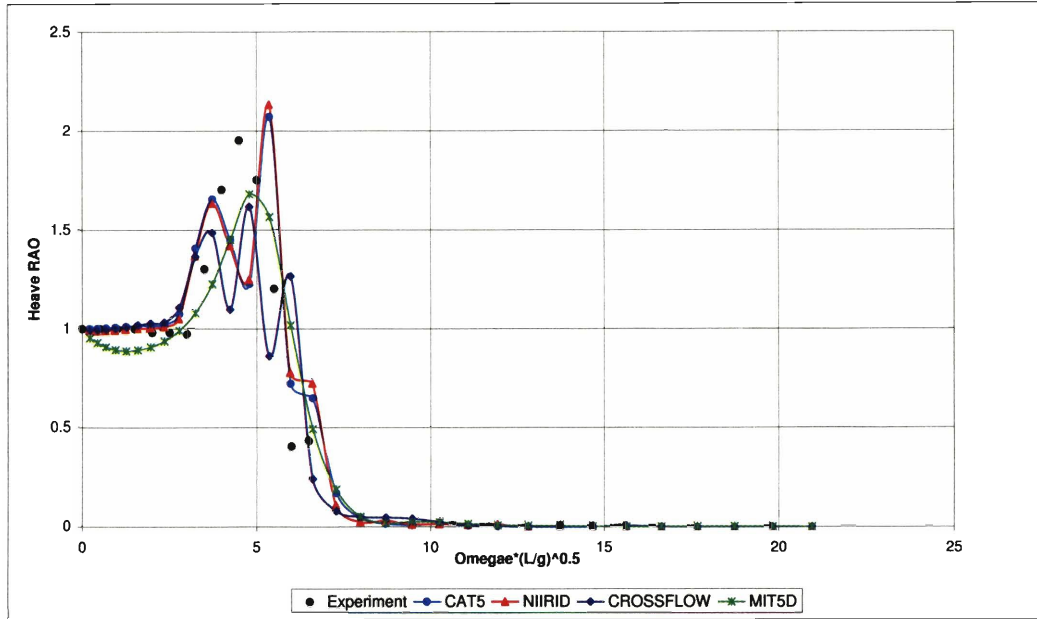


Figure 4-19: Heave RAO for NPL Model 5b at  $F_n = 0.67$  and  $\mu = 150^\circ$

### 4.3.3 Oblique Seas

Figure 4-19 and Figure 4-20 show the heave response in oblique seas at 150 and 120 degrees at a Froude number  $F_n = 0.67$ . As for the head sea case, NIIRID and CAT-5 perform very similarly showing a good agreement with the experimental results. CROSSFLOW overall performances are slightly better than NIIRID. MIT5D shows a surprisingly good agreement with the experimental data for the 150 degrees case and a fair agreement for the 120 degrees case.

Figure 4-21 and Figure 4-22 show the pitch response in oblique seas at 150 and 120 degrees at a Froude number  $F_n = 0.67$ . NIIRID, CAT-5, and CROSSFLOW show a fair agreement with the experimental results. MIT5D shows poor agreement, highly under-predicting the pitch response across the whole frequency range.

Figure 4-23 and Figure 4-24 show the roll response in oblique seas at 150 and 120 degrees at a Froude number  $F_n = 0.67$ . CAT-5 shows good agreement with the experimental results. NIIRID and CROSSFLOW performed in a similar fashion

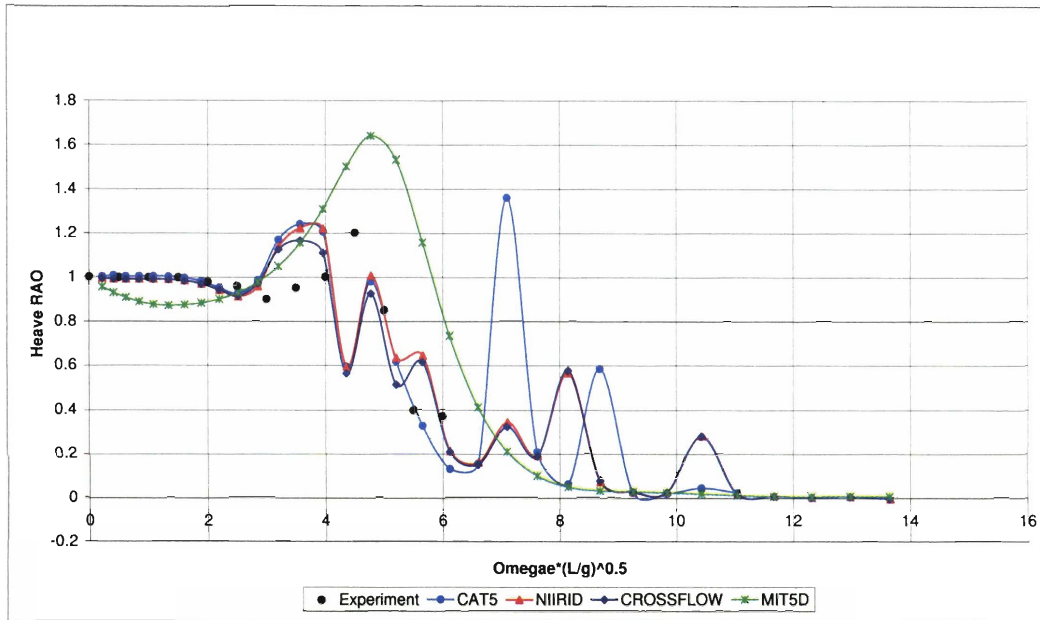


Figure 4-20: Heave RAO for NPL Model 5b at  $F_n = 0.67$  and  $\mu = 120^\circ$

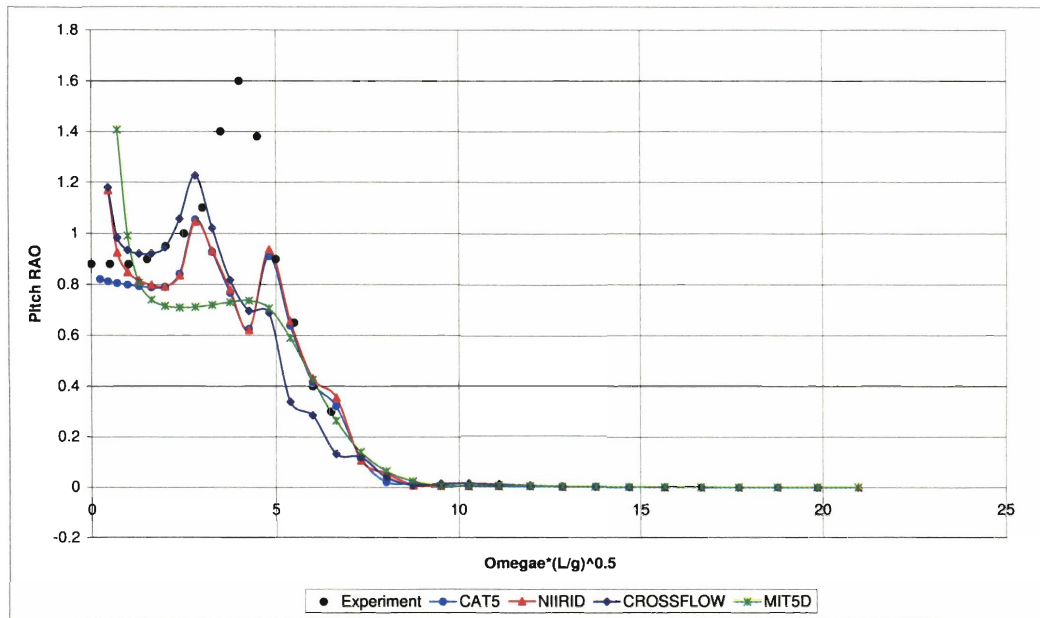


Figure 4-21: Pitch RAO for NPL Model 5b at  $F_n = 0.67$  and  $\mu = 150^\circ$

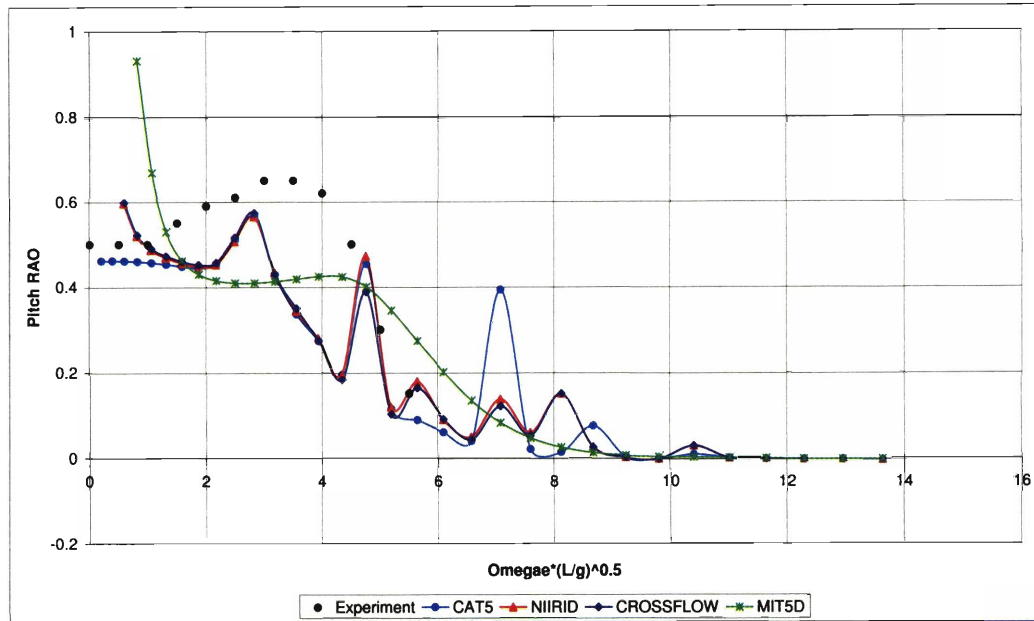


Figure 4-22: Pitch RAO for NPL Model 5b at  $F_n = 0.67$  and  $\mu = 120^\circ$

showing a fair agreement. MIT5D strongly under-predicts the vessel response.

## 4.4 LAMP Comparison

In order to better determine the accuracy of the strip-theory programs included in I-Marine, a series of tests was completed using the Large Amplitude Motion Program (LAMP).

### 4.4.1 Catamaran Testing

LAMP was first run for a catamaran design with elliptical hull sections at  $F_n = 0$  and  $F_n = 0.4$  at an angle of wave incidence of 180, 150, 120, and 45 degrees. The overall dimensions of the catamaran are shown in Table 4.3.

The data calculated with LAMP was compared with the results obtained using NIIRID in I-Marine. The results obtained are shown in Appendix B.1 for the zero

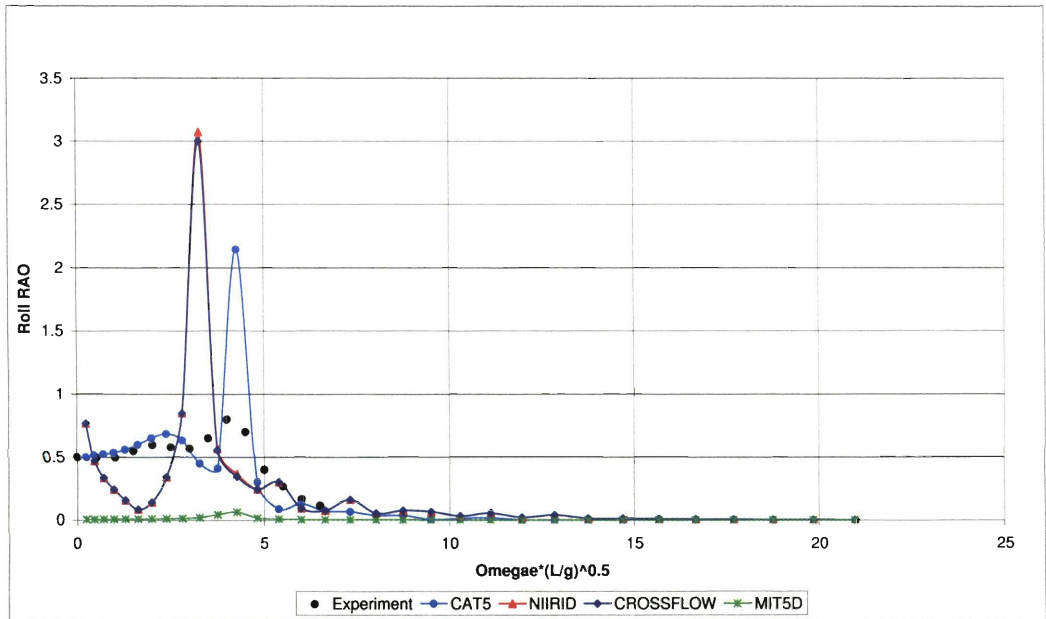


Figure 4-23: Roll RAO for NPL Model 5b at  $Fn = 0.67$  and  $\mu = 150^\circ$

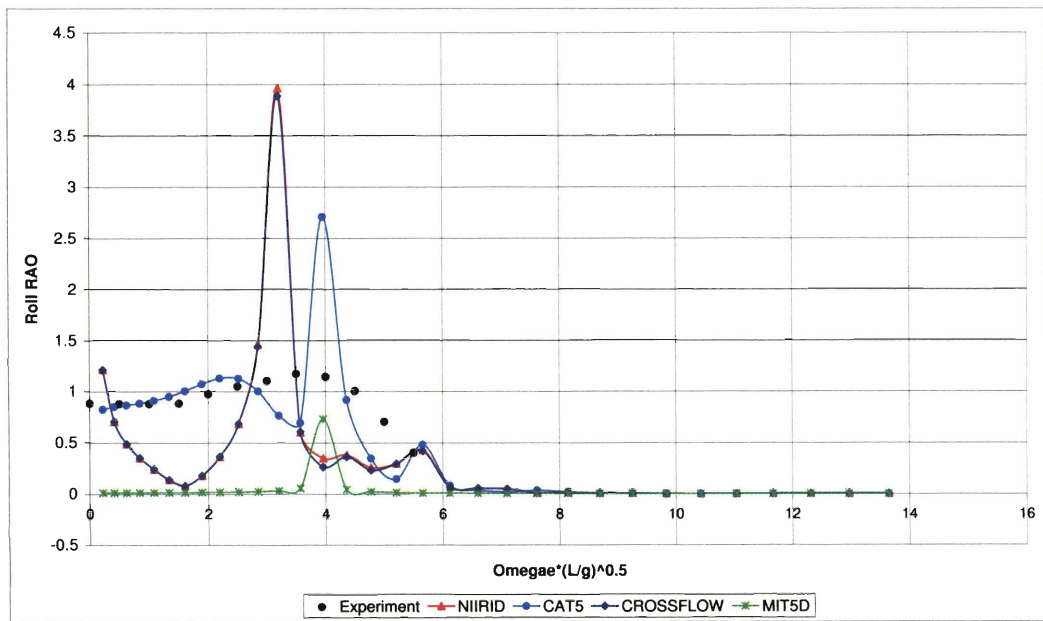


Figure 4-24: Roll RAO for NPL Model 5b at  $Fn = 0.67$  and  $\mu = 120^\circ$

LOA	10.0 ft
Overall Beam	5.0 ft
Draft	0.73 ft
Demihull Beam	0.5 ft

Table 4.3: Overall Dimensions of the Catamaran Used for LAMP-NIIRID Comparison

and the forward speed case. The results show a good agreement between the two programs. The response predicted in heave and pitch at zero forward speed is very similar at any angle of wave incidence. A fair agreement is observed in roll at zero speed due to the internal resonance frequency phenomenon observed in NIIRID.

A very good agreement is recorded also for the forward speed case. In this case however, due to the internal resonance, the results calculated using NIIRID over-predict the vessel response around the resonance frequency. The two programs agree for all the other frequencies.

#### 4.4.2 Trimaran Testing

Three different trimarans were used to compare I-Marine using NIIRID and LAMP. The overall dimensions of the three trimaran geometries are summarized in Table 4.4. These geometries have the same overall length and the same overall beam but

	Trimaran A	Trimaran B	Trimaran C
LOA	10.0 ft	10.0 ft	10.0 ft
Overall Beam	4.0 ft	4.0 ft	4.0 ft
Draft	0.73 ft	0.73 ft	0.73 ft
Center Hull Beam	0.65 ft	0.65 ft	0.64 ft
Demihull Beam	0.25 ft	0.45 ft	0.65 ft

Table 4.4: Overall Dimensions of the Trimarans Used for LAMP-NIIRID Comparison

a different demihull beam. As a consequence, they provide a good test bed to assess the capabilities of I-Marine and NIIRID. The results obtained are shown in Appendix

B.2. The plots show that NIIRID and LAMP predict similar results both at zero and forward speed for any angle of wave incidence. The results provided by I-Marine for the zero speed case in heave and pitch do not contain any resonance peak and agrees well with the results obtained with LAMP. The roll response at zero forward speed is accurate as well, only over-predicting the vessel motion around the resonance frequencies. This agreement was observed at all the angles of wave incidence considered.

The agreement between the NIIRID results and the LAMP results for the forward speed case is good as well. NIIRID tends to over-predict the vessel motion around the resonance frequencies. However, the vessel response computed away from resonance agrees very well with the results calculated with LAMP. This agreement was observed at all the angles of wave incidence considered.

## 4.5 Summary

The overall performance of the I-Marine Seakeeping Analysis Toolbox using NIIRID was good. Good agreement was found for the sectional hydrodynamic coefficients and for the vessel response. Strip theory produced equally good results at Froude number  $F_n = 0.2, 0.5$  and  $0.8$  in head seas. Good results were also obtained for heave, pitch, and roll motion in oblique seas. The largest limitation of using NIIRID was the inaccuracy around the resonance frequencies which reduced the range of frequencies at which the motion can be analyzed.



# Chapter 5

## Case Study

### 5.1 Introduction

In order to show how an advanced seakeeping analysis tool can be effectively used in a real design process, a case study was performed. The report "High Speed Connector Design Project" [31] written by F. Zouridakis and D. Wang in 2005 for the 13.414 class "Projects in New Concept Naval Ship Design" was taken as reference for the case study. The class extends for two terms and focuses on the preliminary design of a naval ship which fulfills a given set of mission requirements. The team is in charge of completing a design plan formulation, a series of system level trade-off studies to achieve a balanced design, and total system integration. The results are presented in a written formal report and an oral presentation at the end of the class. The report written by Zouridakis and Wang was selected because it represents a good example of the standard design process used today both for commercial and military vessels. The report involves the design of a High Speed Connector (HSC) to be used effectively as a functional part of the SeaBase concept. In this chapter, the HSC design process is analyzed in depth and a modified design process which takes into account the analytical capabilities provided by the I-Marine Seakeeping Analysis Toolbox is

proposed.

## 5.2 High Speed Connector Design Project

### 5.2.1 Design Scope

As reported by the Department of Defense of the United States of America [6], "Seabasing is the rapid deployment, assembly, command, projection, reconstitution, and re-employment of joint combat power from the sea, while providing continuous support, sustainment, and force protection to select expeditionary joint forces without reliance on land bases within the Joint Operations Area . These capabilities expand operational maneuver options, and facilitate assured access and entry from the sea."

The High Speed Connector is an integral part of the SeaBase system. Its function is to connect the geographically dispersed nodes that constitute the SeaBase. The main operational mode will be to transport personnel, heavy and oversized equipment, and inter-modal containers between bases. The vessel should be equipped with limited self-defense capabilities and employ advanced modular packaging techniques for improved cargo handling.

### 5.2.2 Design Process

Before starting the preliminary design of the HSC, a set of design priorities was defined by the design team. The goal of this design philosophy is to help the designers in making trade-off decisions. In order of importance, the design priorities are:

1. Loading Interface: navigational agility and cargo handling capabilities at the pier and at sea are the most critical criteria due to the scope of the vessel.
2. Cost Reduction: A relatively low cost of manufacturing is fundamental due to the large number of HSC needed for the SeaBase system.

3. Seakeeping: Good seakeeping performance is considered a key factor as it significantly affects the transportation capabilities of the HSC and the effectiveness of the crew.
4. Signature Reduction: Semi-active and passive defense measures are required due to the high weight sensitivity and the cost constraints. Sophisticated anti-missile systems cannot be implemented on the HSC.

A sketch of the HSC design process is shown in Figure 5-1. The decision making process is based on a risk-benefit analysis using a two-dimensional risk model consisting of consequence and likelihood of occurrence. The software Parametric Assessment of Ship Systems (PASS) developed by CDI Government Systems is used to generate different designs across the whole design space and to determine the cost associated with each variant.

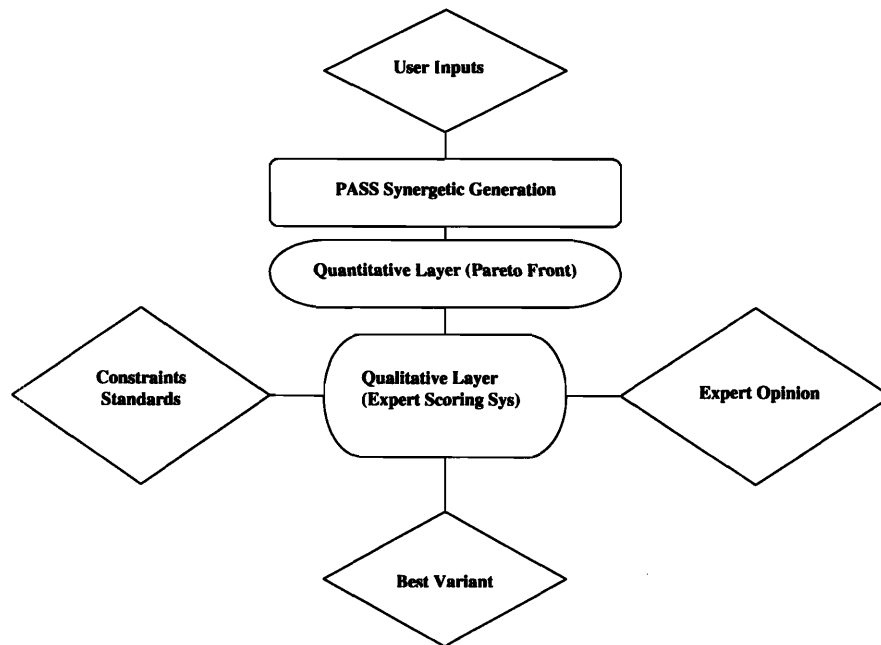


Figure 5-1: HSC Preliminary Design Process Flow Chart. Zouridakis and Wang [31]

The designs generated with PASS are analyzed quantitatively and qualitatively. The quantitative analysis is based on the concept of transport factor (TF) that measures the interaction of some of the fundamental parameters involved such as hull forms, construction materials, and fuel efficiency. The transport factor is a ratio of payload transfer capabilities to shaft horsepower:

$$TF = \frac{K \cdot W \cdot V}{SHP} \quad (5.1)$$

where  $K$  is a dimensionalized constant,  $W$  is payload in long tons,  $V$  is speed in knots, and  $SHP$  is required shaft horse power. A Pareto graph with transport factor on the y-axis and life cycle cost on the x-axis was constructed where each design is represented by a point. The Pareto frontier and the set of non-dominated variants were identified and used to determine the best design configuration.

The qualitative analysis was implemented to analyze the design characteristics not considered by the transport factor. For this analysis, five categories were identified as important characteristics. They are: loading interface, ship survivability, feasibility, seakeeping, and ability to manufacture. A weighting factor was assigned to each of the categories based on the relative importance within the defined design philosophy.

Each variant that was selected from the quantitative analysis was subject to the qualitative analysis where it was scored according to the opinion of experts in the field. In this design, the NSWCCD Carderock's High-Speed Technology Report [21] was used as the primary source of consensus expert opinion. The HSC design team used a modified version of the empirically based five-point ranking system developed by NSWCCD [21] which is listed in Figure 5-2.

Goals and threshold values for payload, speed, range, cost, and crew size are then defined based on requirements and current technological limitations. For the same reason, the upper bound of the design envelope is defined by setting specific design constraints.

Score	When the attribute:	The component or facility:
5	is consistent with platform performance demonstrated at the desired scale, at sea	has demonstrated capacity , capability, or performance at the required scale
4	has been extrapolated from a prototype or a physical model but has not been demonstrated at required scale, at sea	has extrapolated capacity, capability, or performance based on the attributes of a prototype or physical model and is highly compatible with the ship type
3	has been shown to be achievable using physics-based calculations but has not been demonstrated by a physical model or a prototype	has extrapolated capacity, capability, or performance based upon physics-based calculations but has not been demonstrated by a physical model or prototype and can be fitted to the ship type with attention needed during design
2	has been shown to be feasible using semi-empirical methods but the theory and physical basis are not well understood	has extrapolated capacity, capability, or performance based upon semi-empirical calculations but has not been demonstrated by a physical model or prototype and can be fitted to the ship type with considerable effort required.
1	Is believed to be feasible based upon broad parametric data or theory unsupported by experimental data	is believed to have desired capacity, capability , or performance based upon broad parametric data or theory unsupported by experimental data and will require innovation to be fitted to the ship type
0	Incompatible	Incompatible

Figure 5-2: Ranking Scheme Used in the Qualitative Layer of the Analysis. Zouridakis and Wang [31]

### 5.2.3 Actual HSC Design Process

#### Pass Synergetic Generation

All types of existing hull forms were considered for this design. Due to the requirements of speed and payload of the HSC, it was determined that the most viable hull configurations were monohull, catamaran, and trimaran. Surface Effect Ships (SES), Air Cushion Vehicles (ACV) and hydrofoils were excluded due to the high payload requirements of the HSC. Small Waterplane Area Twin Hull Ships (SWATH) were also excluded due to the speed limitations of such vessels.

PASS was used to generate a set of variants which consists of an even distribution of hull forms: 27 monohulls, 26 catamarans, and 28 trimarans. Unfortunately, the information supplied by PASS was not helpful for determining the variant with the highest efficiency and the lowest cost for a given set of operational requirements. As a

consequence, a literature survey of existing and proposed designs was also conducted. This survey revealed design trends and the relationship between the various ship characteristics such as overall length and beam. The survey produced a less balanced distribution of hull forms: 18 fast monohulls, 55 catamarans, and 8 trimarans. The results obtained from the literature survey were used to validate the initial PASS variants.

### **Quantitative Layer (Pareto Frontier)**

The validated PASS results were used for the quantitative layer. An assessment of the transport factor (TF) compared to life cycle cost (LCC) was completed. A copy of this plot is in Figure 5-3. From this analysis, the design team concluded that catamarans demonstrated the best balance between transport factor and life cycle cost.

The design team also compared the acquisition cost of the variants as a function of transport factor. A copy of the plot is shown in Figure 5-4. This analysis showed that trimarans have a much higher acquisition cost than catamarans as they are a new and untested ship technology.

The payload carrying capacity, which is expressed as speed times payload, was considered as a function of life cycle cost. A copy of the plot is shown in Figure 5-5. From this plot, the design team concluded that catamarans are the cheapest solution for a given carrying capacity.

Overall, the quantitative analysis suggests that a catamaran is the most efficient vessel configuration for this design for any combination of speed and payload. In high speed and high payload region, trimarans become comparable to catamarans in terms of transport factor and life cycle cost. However, due to the newness of the trimaran technology, catamarans have a substantially lower acquisition cost than trimarans all across the design space.

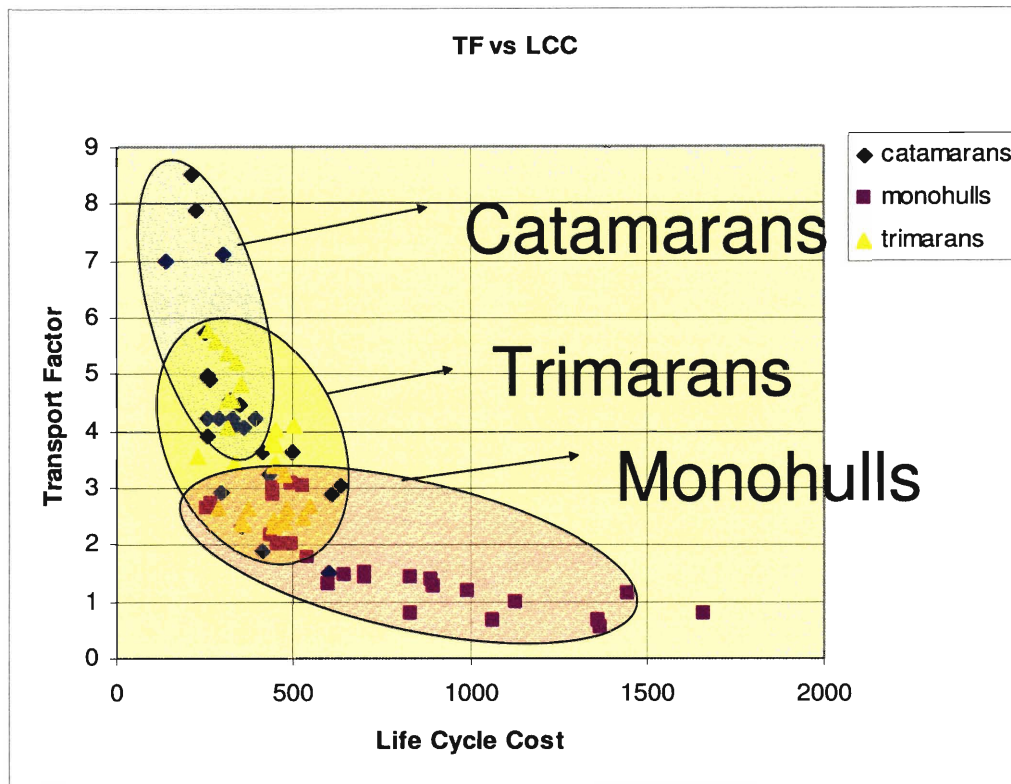


Figure 5-3: Transport Factor vs. Life Cycle Cost. Zouridakis and Wang [31]

### Qualitative Layer (Expert Scoring System)

The qualitative analysis followed the quantitative analysis and provided complementary results. The function of the qualitative analysis is to provide information regarding attributes which were not taken into account in the quantitative analysis such as seakeeping, loading interface, survivability, feasibility, and the ability to manufacture. A summary of the design categories and their relative weighting factor is shown in Table 5.1.

In combination with the qualitative analysis, the PASS variants were assessed within goals and threshold values for payload, speed, range, cost, and crew size. Additionally, the design variants were subject to design constraints based on current

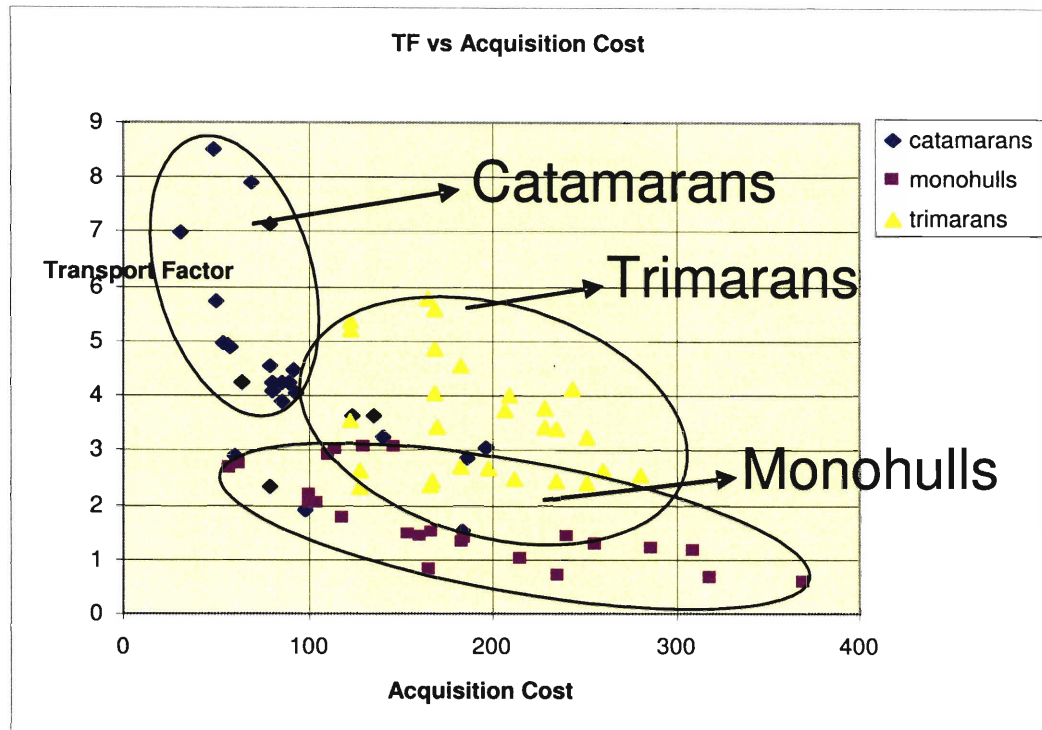


Figure 5-4: Transport Factor vs. Acquisition Cost. Zouridakis and Wang [31]

technological limitations to define an upper bound of the design envelope. The goal and threshold values are described in Table 5.2. The design constraints are summarized in Table 5.3.

The overall results of the qualitative analysis are shown in Figure 5-6. The analysis shows that trimarans constitute the least favorable choice for HSC operation with catamarans performing better and monohulls slightly better than catamarans. Figure 5-7 suggests that monohulls and trimarans have relatively equal seakeeping characteristics and catamarans have the poorest seakeeping due to high accelerations and wet deck slamming in head seas. The risk analysis in Figure 5-8 shows trimarans having the largest number of high risk elements, making them the riskiest design. The second riskiest are catamarans, the least are monohulls.



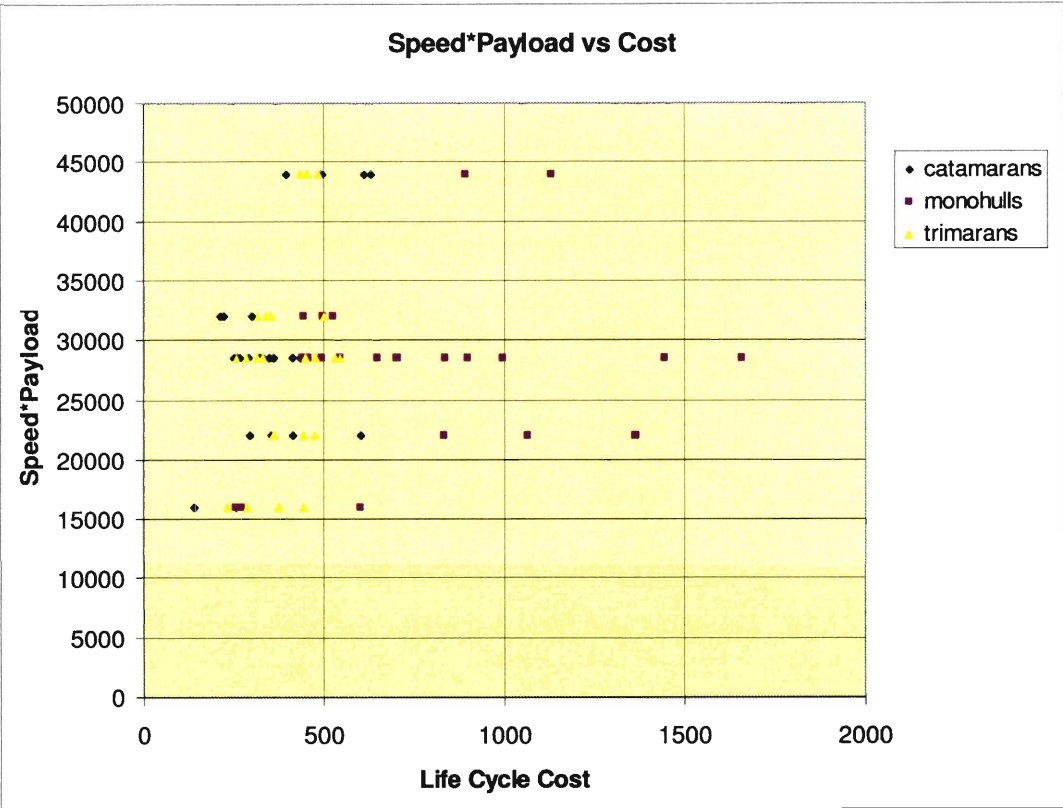


Figure 5-5: Carrying Capacity vs. Life Cycle Cost. Zouridakis and Wang [31]

To sum up, the qualitative analysis suggests monohulls as the best hull forms and catamarans having almost equal characteristics. Trimarans showed the worst performance and risk levels for the attributes under investigation.

**HSC Design Conclusions**

Based on the results of both the quantitative and qualitative analysis, the design team chose the catamaran as the optimal hull form for the HSC design.

With the hull form determined, the hull material and propulsion system were considered using the same quantitative and qualitative approach. This analysis led to the creation of five design variants with different overall dimensions, speed, and

Categories	Weighting Factor
Loading Interface	30
Ship Survivability	15
Feasibility	25
Seakeeping	20
Ability to Manufacture	10

Table 5.1: Design Categories and Relative Weight Factor

Characteristic	Threshold	Goal
Payload	500 LT	1000 LT
Speed	32 Kts	44 Kts
Seakeeping	SS5	SS3
Range	2000 NM	2000 NM
Cost	\$150 M	\$50 M
Crew Size	25	10

Table 5.2: Threshold and Goal Values for the HSC Design Project

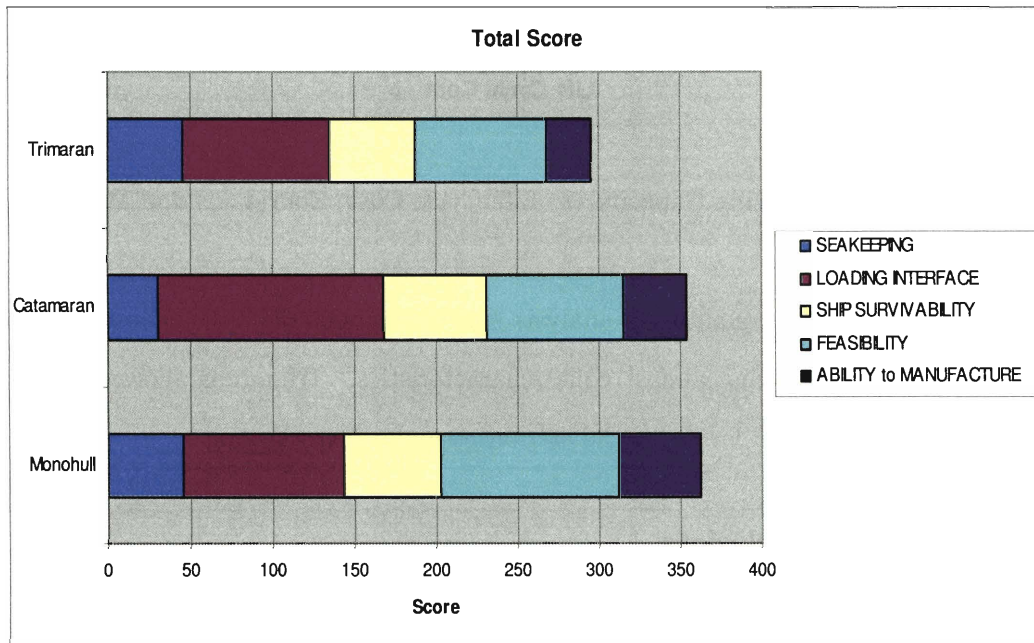


Figure 5-6: Rating Summary. Zouridakis and Wang [31]

Max Draft	25 ft
Max Beam	105.6 ft
Max Displacement	40,000 LT
Max LOA	825 ft

Table 5.3: Design Constraints for the HSC Design Project

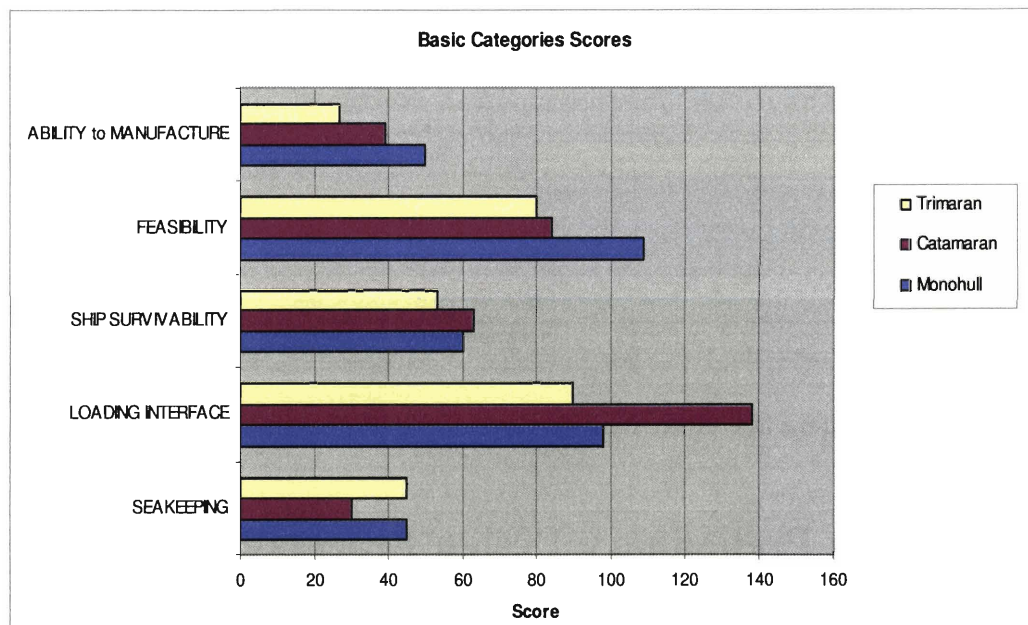


Figure 5-7: Basic Categories Scores. Zouridakis and Wang [31]

payload capabilities. These five design variants were used to analyze the overall performances of the Sea Basing system as a function of the size and capabilities of the HSC fleet. Other parameters taken into account in the analysis of the fleet were: number of HSC vessels, delivery time per ship, fleet life cycle cost, and operational range of each ship. These factors were used in PASS to create a total of 15 fleet variants. Based on the initial prerequisites, the best of the five design variants was selected as the preliminary design of the HSC. This analysis lead to the definition of the ship dimensions, the form coefficients, and the ship speed, range and payload.

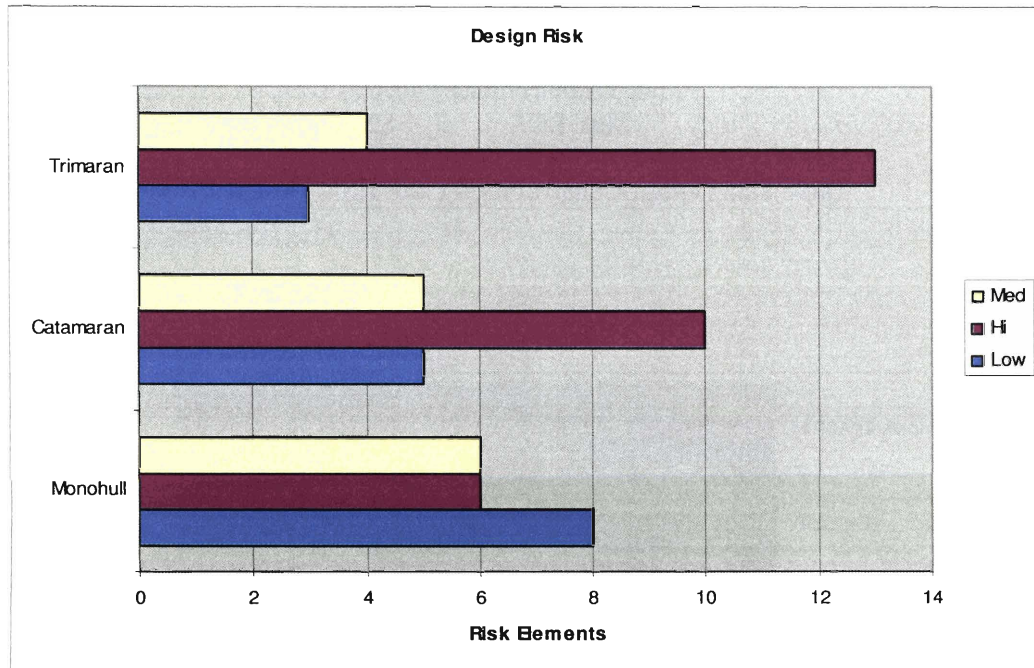


Figure 5-8: Risk Analysis Results. Zouridakis and Wang [31]

### 5.3 The Preliminary Design Process Revisited

By using a seakeeping analysis tool as the one developed in I-Marine, the preliminary design process outlined in Section 5.2 can be significantly improved in terms of efficiency and accuracy. In order to show how this can be accomplished, the analysis computed by the HSC design team is revisited taking advantage of the I-Marine seakeeping analysis tool. The additional information obtained by using the I-Marine platform will be integrated into the analysis computed by the HSC team. This will lead to an updated design process where the results produced using I-Marine will be combined to the results computed with PASS to determine the best overall variant. This is achieved by implementing a second layer in the quantitative analysis where the seakeeping capabilities of each variant are assessed. Being able to have a quantitative measure of the seakeeping performances of the variants under consideration allows the design team to independently analyze each variant instead of using a generalized

analysis. By doing so, the designers will not have to limit the design to well known vessel configurations.

### **5.3.1 Limitations of the HSC Design Process**

While the design process implemented by the HSC design team was successful given the nature of the class project, the qualitative layer weakens the overall effectiveness.

First, the qualitative analysis produces low quality results. For example, the design team was forced to generalize the seakeeping performance of significantly different vessels for a single hull form. Such a generalization can be deceiving. Reducing the number of variants from seventy-seven to three strongly affects the quality of the analysis because of the large number of design parameters that can affect the seakeeping behavior of multihull vessels. The reduction of variants provides information only for a specific geometry and given scenario which might be very different from the design under investigation. For example, the seakeeping capabilities of multihulls are highly affected by the shape of the hull sections and by the distance between the demihulls. Depending on the value of these two parameters, either a catamaran or a trimaran could have the better seakeeping performances.

Secondly, the qualitative analysis imposes limitations on the design envelope and the level of innovation in the design process. The HSC design team based its decision on only existing multihull configurations for which literature existed. For multihull vessels, this approach is particularly inefficient given the large number of design variables and the limited amount of information available regarding their performances.

### **5.3.2 The I-Marine Design Process**

An updated design process which removes part of the qualitative analysis has been developed by integrating seakeeping into the quantitative analysis. Although the modified preliminary design process is based on the HSC report, the approach followed

can be universally applied. A chart of the new design process is shown in Figure 5-9. The design process is composed by three parts: definition of design requirements, generation of variants, and analysis of variants performances.

### **Definition of Vessel Requirements**

The modified design process starts as in the original process by defining the vessel requirements in term of speed, payload, overall dimensions, displacement, etc. Based on these characteristics, the design team determines the goal and threshold values of each of the relevant design parameters, and the design constraints. The vessel requirements also determine the design philosophy. The preliminary design process is based on a set of design priorities which depend on the vessel operational requirements. A different weighting factor is determined for each of these priorities to help the design team making trade-off decisions. For example, for the HSC project, the design priorities in order of importance were: loading interface, cost reduction, seakeeping, and signature reduction.

By defining the vessel requirements and the design philosophy, the design team is able to carry out a concept exploration to determine what vessel configurations could be suitable. In the HSC project, the payload requirements led to the exclusion of hydrofoils, SES, and HCV while the high speed requirements led to the exclusion of SWATH configurations, leaving only monohulls, catamarans, and trimarans as possible candidates.

### **Variants Generation**

Based on the results of the concept exploration, a series of design variants is created and used to assess the most suitable vessel configuration. The process of determining the design variants entails two components: a survey of existing vessels and the generation of the variants using a synergetic generation program like PASS. The survey of

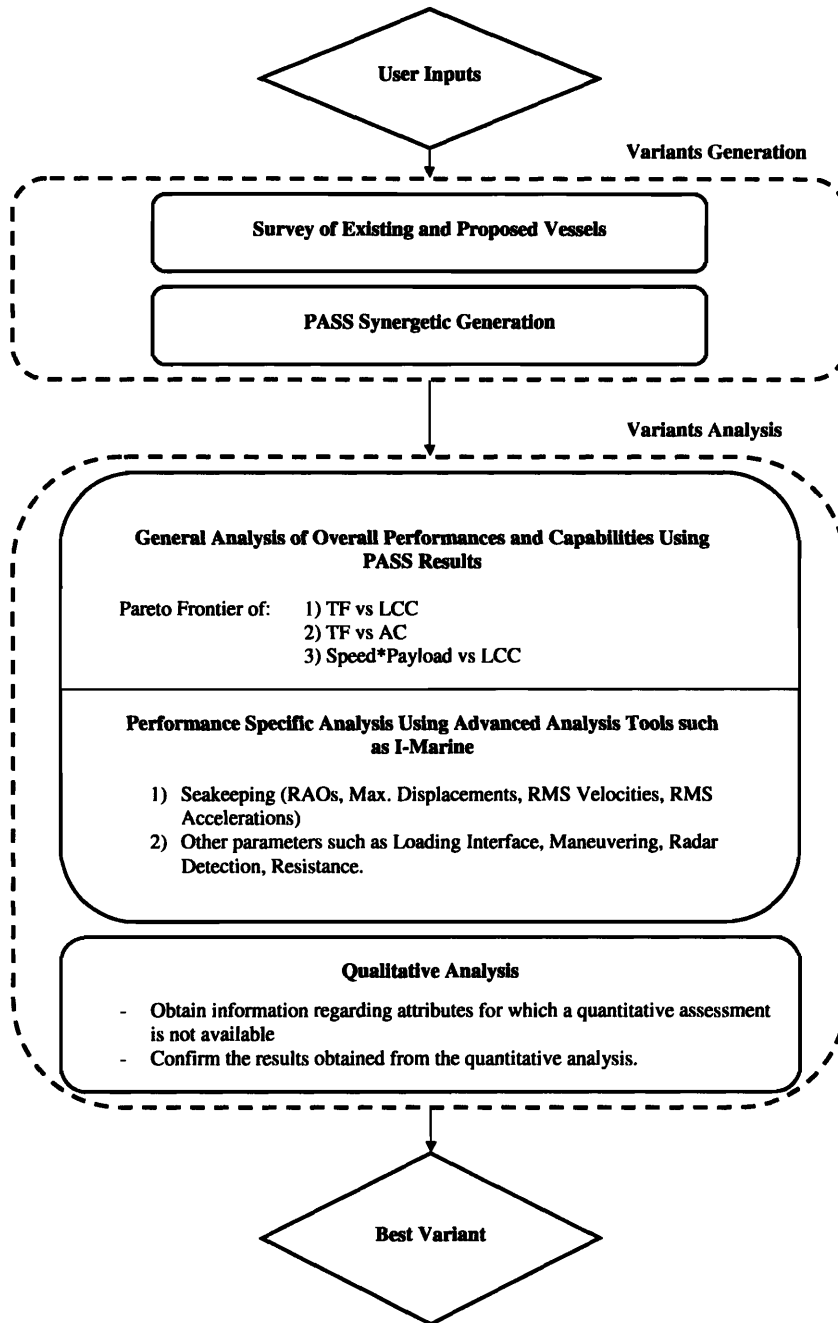


Figure 5-9: Modified Design Process Chart

existing designs contains information such as overall dimensions, displacement, speed, and payload and it includes existing or proposed vessels with one of the configurations selected from the concept exploration. The overall vessel requirements and the information collected from the survey are then used to guide the generation of the design variants using PASS.

### **Variants Analysis**

The variants analysis is composed of a quantitative and of a qualitative layer. The performance of the generated variants are quantitatively assessed carrying out a general analysis and a performance-specific analysis. The general analysis is based on the calculation of transport factor, life cycle cost, acquisition cost, speed, and payload, which are provided by PASS. The strongest configuration can be determined by identifying the vessel with the best combination of these factors. A Pareto frontier analysis, as the one used by the HSC team, is an effective and relatively simple method to identify the most suitable variants.

The performance-specific analysis is carried out using advanced analysis tools such as the I-Marine Seakeeping Analysis Toolbox. The scope of this targeted analysis is to provide quantitative information about vessel characteristics which usually are not assessed in the preliminary phase of the design process. These characteristics could be: seakeeping, loading interface, maneuvering, radar-detection, and vessel resistance. Given the scope of this study, the targeted analysis was carried out only for seakeeping. However, providing tools exist for such an analysis, a similar approach can be used to assess other vessel characteristics.

In order for the performance-specific analysis to be effective, it is necessary to have detailed information regarding the design variants. For example, the hull shape of the variants is needed to determine the seakeeping performance. With this analysis complete, the results can be related to transport factor or life cycle cost. This will



identify the variants with the best overall combination of factors.

The quantitative analysis is followed by a qualitative analysis. The qualitative analysis is required to assess those attributes for which a quantitative analysis is not available. Additionally, such an analysis provides complementary information to the quantitative analysis. As explained in Section 5.3.1, the qualitative analysis only provides a generalized answer which can lead to misleading conclusions. However, in the absence of a tool to obtain quantitative data, it is the only possible approach to obtain an answer. That being said, its results should be weighted accordingly because of the generalizations made in the process.

### **Determining the Best Variant**

The results produced by the quantitative and by the qualitative analysis are used to determine the most suitable variant. This variant will then be used as the basis for designing the vessel.

### **5.3.3 Performance-specific Analysis Using the I-Marine Seakeeping Analysis Toolbox**

The performance-specific analysis for seakeeping was completed using I-Marine. A chart of the seakeeping analysis is shown in Figure 5-10. Given the fact that this analysis was carried out independently from the HSC design, a new set of variants was created to show conceptually how this analysis would be done. These variants include catamaran and trimaran vessels and use the same design space defined by the HSC design team. The dimensions of the PASS variants, as well as of the designs included in the literature survey done by the HSC design team, defined the design envelope. A series of new trimaran designs was added to the list of existing trimarans to have a larger pool of data. All the recorded designs were non-dimensionalized to consider parameters such as length-to-beam ratio and total-beam-to-demihull-beam

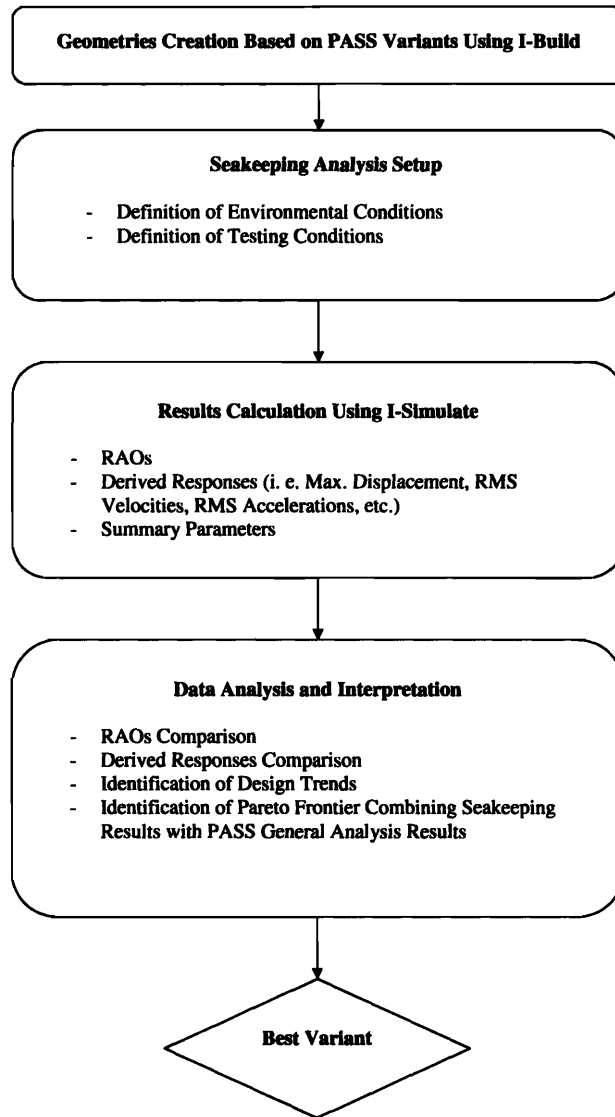


Figure 5-10: Performance-Specific Analysis Chart for Seakeeping

ratio. Two separate design envelopes were defined, one for the catamarans and one for the trimarans. The design envelopes for catamarans and trimarans are shown in Table 5.4 and Table 5.5.

Non-dimensional Parameter	Min. Value	Max. Value
$L/B_{TOT}$	2.32	5.44
$L/T$	13.1	60.25
$B_{TOT}/B_{DH}$	2.66	6.14
Vol/LBT	0.156	0.189

Table 5.4: Catamaran Designs

Non-dimensional Parameter	Min. Value	Max. Value
$L_C/B_{TOT}$	3.83	6.37
$B_{TOT}/B_C$	2.15	3.84
$B_{TOT}/B_{DH}$	7.41	18.51
$L_C/T_C$	11.34	35.9
$L_C/T_{DH}$	33.84	79.04
$L_C/L_{DH}$	2.134	4.13
Vol/LBT	0.055	0.174

Table 5.5: Trimaran Designs

These design envelopes were used to create the variants that were to be tested using I-Marine. The minimum and maximum values of the non-dimensional parameters were used to define the boundaries of the design envelopes. The two series of variants were generated by choosing the minimum, maximum, and midpoint values of each of the non-dimensional parameters which defined the envelopes. These values were then used to create a matrix of geometries and led to the creation of nine catamarans and fifteen trimarans.

Due to the simplified scope of this case study and to the early stage of develop-

ment of I-Build, all vessels were designed with a constant elliptical hull sections and having the same overall length. In addition, the trimaran geometries were simplified having the three hulls of the same length. Given the linearity of the system under analysis, only the non-dimensionalized geometry parameters such as length-to-beam ratio  $\frac{L}{B}$  and length-to-draft-ratio  $\frac{L}{T}$  were considered relevant in the computation. As a consequence, the ship geometry was scaled down and an overall length  $LOA = 10$  ft was used for all the variants. These geometries are identified in Table 5.6 and in Table 5.7. Dimensions are in feet.

While the design simplifications adopted are not very realistic, they do not change the effectiveness of the design method proposed here but only affect the results in absolute value. As a consequence, the results obtained from the seakeeping analysis will have limited value if applied specifically to the HSC design. Since the goal of this study is to consider the design process as a whole, from this prospective, the results still provide valuable information regarding the advantages of obtaining quantitative data about seakeeping in the preliminary design process.

Hull	L [ft]	B [ft]	T [ft]	$B_{DH}$ [ft]	$\frac{L}{B_{TOT}}$	$\frac{L}{T}$	$\frac{B_{TOT}}{B_{DH}}$
1	10.0	5.00	0.730	0.5	2.0	13.70	10.00
2	10.0	5.00	0.416	0.5	2.0	24.04	10.00
3	10.0	5.00	0.286	0.5	2.0	34.97	10.00
4	10.0	2.50	0.730	0.5	4.0	13.70	5.00
5	10.0	2.50	0.416	0.5	4.0	24.04	5.00
6	10.0	2.50	0.286	0.5	4.0	34.97	5.00
7	10.0	1.67	0.730	0.5	6.0	13.70	3.34
8	10.0	1.67	0.416	0.5	6.0	24.04	3.34
9	10.0	1.67	0.286	0.5	6.0	34.97	3.34

Table 5.6: Catamaran Variants. [ft]

Hull	L [ft]	$B_{TOT}$ [ft]	$B_C$ [ft]	T [ft]	$B_{DH}$ [ft]	$\frac{L_C}{B_{TOT}}$	$\frac{B_{TOT}}{B_C}$	$\frac{B_{TOT}}{B_{DH}}$	$\frac{L_C}{T_C}$	$\frac{L_C}{T_{DH}}$
1	10.0	4.00	0.65	0.73	0.25	2.50	6.15	16.00	13.70	13.70
2	10.0	4.00	0.65	0.73	0.45	2.50	6.15	16.00	13.70	13.70
3	10.0	4.00	0.65	0.73	0.65	2.50	6.15	16.00	13.70	13.70
4	10.0	4.00	0.65	0.416	0.25	2.50	6.15	16.00	13.70	13.70
5	10.0	4.00	0.65	0.416	0.45	2.50	6.15	16.00	13.70	13.70
6	10.0	4.00	0.65	0.416	0.65	2.50	6.15	16.00	13.70	13.70
7	10.0	4.00	0.65	0.286	0.25	2.50	6.15	16.00	13.70	13.70
8	10.0	4.00	0.65	0.286	0.45	2.50	6.15	16.00	13.70	13.70
9	10.0	4.00	0.65	0.286	0.65	2.50	6.15	16.00	13.70	13.70
10	10.0	2.75	0.65	0.73	0.25	2.50	6.15	16.00	13.70	13.70
11	10.0	2.75	0.65	0.73	0.45	2.50	6.15	16.00	13.70	13.70
12	10.0	2.75	0.65	0.73	0.65	2.50	6.15	16.00	13.70	13.70
13	10.0	1.50	0.65	0.73	0.25	2.50	6.15	16.00	13.70	13.70
14	10.0	1.50	0.65	0.73	0.45	2.50	6.15	16.00	13.70	13.70
15	10.0	1.50	0.65	0.73	0.65	2.50	6.15	16.00	13.70	13.70

Table 5.7: Trimaran Variants

### Seakeeping Analysis Setup

Each vessel was tested in regular waves at an incident wave angle of 180, 150, 120, and 45 degrees at a Froude number of  $F_n = 0.0$  and  $F_n = 0.4$ . These values were selected to have a complete overall picture of the vessel response both at zero and forward speed. The RAO in heave, pitch, and roll was calculated for each case. NIIRID was used to calculate the sectional hydrodynamic coefficients and forces.

### Results Analysis and Interpretation

The full results from this effort are shown in Appendix C. As explained in Section 2.7, the results produced using NIIRID are subject to resonance phenomena. In order to better understand the data, the resonance frequencies for the catamaran and trimaran configurations analyzed were calculated using Equation (2.110) and Equation (2.111). The results are shown in Table 5.8. It must be kept in mind that due to the multihull configuration, the characteristic frequencies are not exactly in coincidence with the

characteristic frequencies shown in Table 5.8.

Hull	H [ft]	$\omega_{R_3}$ [rad/s]	$\omega_{R_2}$ [rad/s]
Catamaran 1, 2, 3	4.5	6.70, 9.478, ...	4.74, 8.21, ...
Catamaran 4, 5, 6	2.0	10.05, 14.22, ...	7.10, 12.31, ...
Catamaran 7, 8, 9	1.17	13.14, 18.59, ...	9.29, 16.09, ...
Trimaran 1, 4, 7	1.55	11.42, 16.15, ...	8.07, 13.98, ...
Trimaran 2, 5, 8	1.45	11.80, 16.69, ...	8.35, 14.612, ...
Trimaran 3, 6, 9	1.35	12.23, 17.30 ...	8.65, 14.98, ...
Trimaran 10	0.925	14.78, 20.9, ...	10.45, 18.10, ...
Trimaran 11	0.825	15.65, 22.13, ...	11.06, 19.17, ...
Trimaran 12	0.725	16.69, 23.61, ...	11.80, 20.45, ...
Trimaran 13	0.3	25.95, , 36.72, ...	18.3, 31.82, ...
Trimaran 14	0.2	31.82, 44.96, ...	22.48, 38.90, ...
Trimaran 15	0.1	44.96, 63.58, ...	31.79, 55.06, ...

Table 5.8: Estimated Resonance Frequencies for Catamaran and Trimaran Configurations Analyzed in the Case Study

The results obtained from the seakeeping analysis carried out for the HSC design project shown in Appendix C were used to identify how different design parameters affect the seakeeping performances of multihull vessels. The following design trends were observed:

For catamarans:

- An increase in the length-to-beam ratio  $\frac{L}{B_{TOT}}$  leads to an *increase* in the vessel response in both heave and pitch for frequencies lower than the first cancellation frequency. This trend was observed both at  $F_n = 0.0$  and at  $F_n = 0.4$  and for all the angles of wave incidence considered in this study.
- An increase in the length-to-beam ratio  $\frac{L}{B_{TOT}}$  leads to a *decrease* in the vessel response in both heave and pitch for frequencies higher than the first cancella-

tion frequency. This trend was observed both at  $F_n = 0.0$  and at  $F_n = 0.4$  and for all the angles of wave incidence considered in this study.

- At  $F_n = 0.4$ , an increase in the length-to-draft ratio  $\frac{L}{T}$  leads to an overall *decrease* in the amplitude of the response both in heave and pitch. This trend was observed at an angle of incidence of 180, 150, and 120 degrees.
- An increase in the length-to-draft ratio  $\frac{L}{T}$  also leads to a *decrease* in the heave and pitch response at zero forward speed and for all the angles of incidence considered.
- An increase of the length-to-draft ratio  $\frac{L}{T}$  leads to a *decrease* in the response in roll for frequencies lower than the first cancellation frequency and to a shift of the resonance frequency toward higher values. This trend was observed both at  $F_n = 0.0$  and at  $F_n = 0.4$  at an angle of wave incidence of 150, 120, and 45 degrees.
- An increase in the length-to-beam ratio  $\frac{L}{B_{TOT}}$  leads to an *increase* in the response in roll for frequencies lower than the first cancellation frequency and to a shift of the resonance frequency toward lower values.
- The first cancellation frequency in pitch is always higher than the first cancellation frequency in heave. In addition, decreasing the angle of incidence leads to a shift of the cancellation frequencies toward higher values.

For trimarans:

- An increase in the length-to-demihull-beam ratio  $\frac{L}{B_{DH}}$  leads to an *increase* in the vessel response in both heave and pitch across the whole frequency range. This trend was observed both at  $F_n = 0.0$  and at  $F_n = 0.4$  and at all the angles of wave incidence considered in this study.

- An increase in the length-to-beam ratio  $\frac{L}{B_{TOT}}$  leads to a *decrease* in the vessel response in both heave and pitch for frequencies lower than the first cancellation frequency. This trend was observed both at  $F_n = 0.0$  and at  $F_n = 0.4$  and at all the angles of wave incidence considered in this study.
- The first cancellation frequency in pitch is always higher than the first cancellation frequency in heave. In addition, decreasing the angle of incidence leads to a shift of the cancellation frequencies toward higher values.

In order to be able to compare the different vessel configurations, the RMS vertical acceleration at the center of gravity at zero forward speed was computed. As reported in [15], the vertical acceleration of the vessel is strictly related to personnel fatigue and reduced task proficiency. Because crew performance was considered important in this design philosophy, this factor was chosen to compare the variants. In this work, only the vertical RMS acceleration was considered. However, many other parameters such as maximum displacement and maximum velocity in any of the six degrees of freedom could be calculated and used for comparison. The vertical RMS acceleration was calculated for the zero forward speed case for all the angles of wave incidence considered in this study. The results are shown in Figure 5-11 and Figure 5-12. From the data presented in Figure 5-11 and Figure 5-12, the following conclusions were drawn:

For catamarans:

- An increase in the length-to-draft ratio  $\frac{L}{T}$  leads to a *decrease* in the RMS vertical acceleration. This trend was observed for all the angles of wave incidence considered in this study.
- A decrease in the length-to-beam ratio  $\frac{L}{B_{TOT}}$  leads to a *decrease* in the RMS vertical acceleration at an angle of wave incidence of 180 and 120 degrees. On



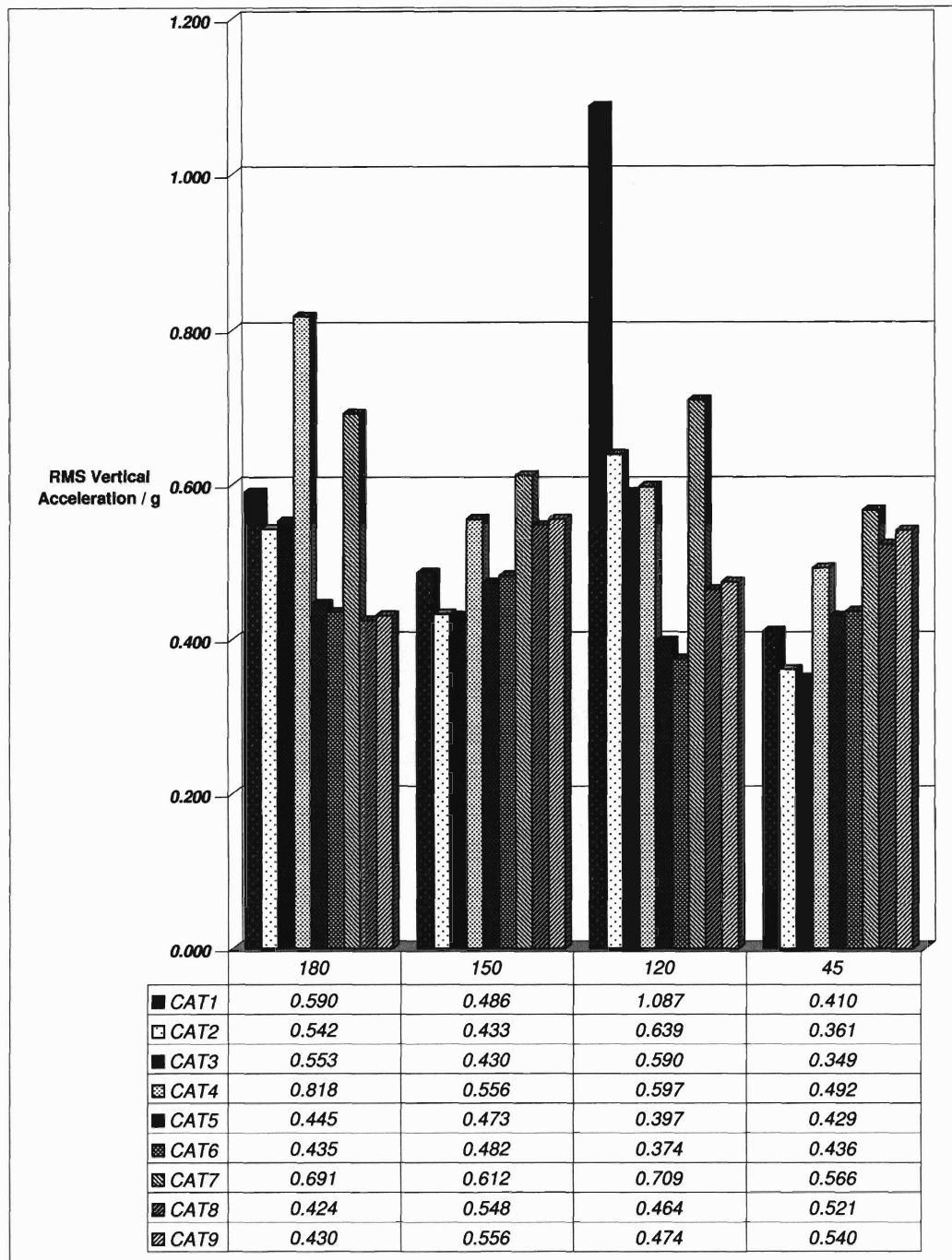


Figure 5-11: Vertical RMS Acceleration for Catamarans

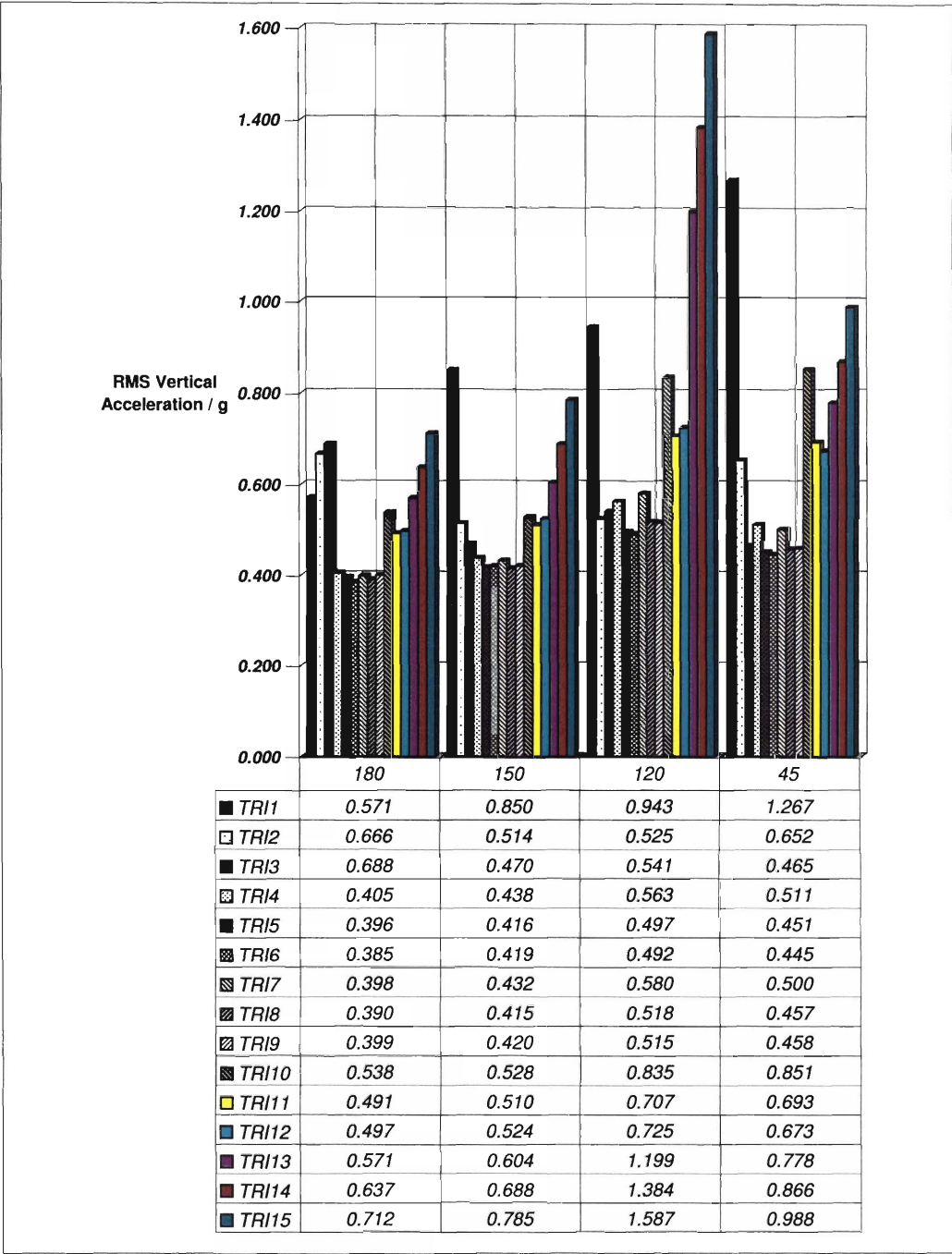


Figure 5-12: Vertical RMS Acceleration for Trimarans

the other hand, it leads to an *increase* in the RMS vertical acceleration for an angle of wave incidence of 150 and 45 degrees.

For trimarans:

- An increase in the length-to-draft ratio  $\frac{L}{T}$  leads to a *decrease* in the RMS vertical acceleration. This trend was observed for all the angles of wave incidence considered in this study.
- A increase in the length-to-beam ratio  $\frac{L}{B_{TOT}}$  leads to a *increase* in the RMS vertical acceleration. This trend was observed for all the angles of wave incidence considered in this study.
- A decrease in the total beam-to-demihull beam ratio  $\frac{B_{TOT}}{B_{DH}}$  leads to an *increase* in the RMS vertical acceleration. This trend was observed for all the angles of wave incidence considered in this study.

Given the profuse amount of data produced by the seakeeping analysis, summarizing the vessel response in a single parameter strongly simplifies the analysis and allows a comparison of different variants. In this study, the sum of the vertical RMS acceleration provided in Figure 5-11 and Figure 5-12 for the four angles of wave incidence considered was used as a parameter to summarize the seakeeping capabilities of each variant. The results are shown in Figure 5-13. Although this parameter only describes the seakeeping performances of the variants in a specific condition, a similar approach could be used to calculate other summary parameters that describe the overall seakeeping performances of a vessel. Ideally, this seakeeping factor would be plotted against other factors such as transport factor or life cycle cost as part of the quantitative analysis. As this was not available for this study, it could not be done.

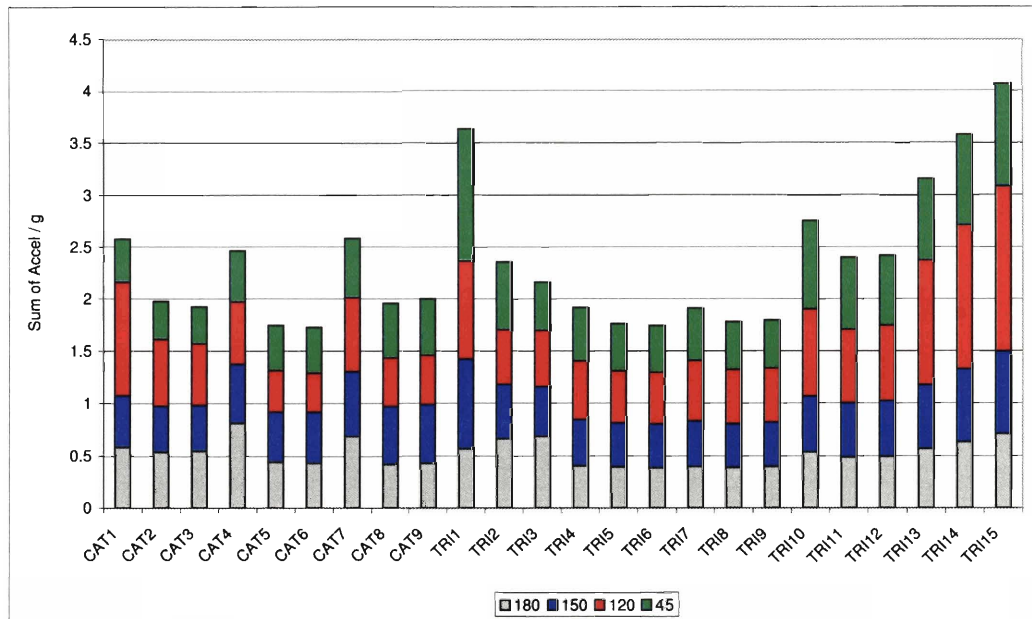


Figure 5-13: Sum of the RMS Vertical Accelerations for the Four Angles of Wave Incidence Calculated. The results have been normalized by the gravitational acceleration, g

### Using the Seakeeping Analysis Results to Determine the Best Variant

Although the geometry of the variants is highly idealized, the results obtained from the seakeeping analysis can still be used to draw conclusions about the advantages of the method proposed here. The results shown in Figure 5-13 confirm that the seakeeping performances of catamarans and trimarans are overlapping and highly affected by the geometry of the vessel. For example, Catamaran 1 overall performances in term of vertical acceleration in heave are worse than Trimaran 7. On the other hand, Trimaran 1 has a much higher vertical acceleration than Catamaran 6. As a consequence, the results presented in Figure 5-13 show that the score assigned to catamarans and trimarans in Figure 5-7 is not always true. This fact confirms that a generalized approach could lead to poor conclusions. In addition, by being able to quantitatively assess the seakeeping performances of each variant, a much higher granularity in the analysis can be achieved. This analysis allows to take into account the overlapping

performances of multihull vessels leading to a better assessment of the best variant.

The results shown in Figure 5-13 can also be used to determine the combinations of parameters that give the best seakeeping performances. Using the sum of the RMS vertical accelerations in heave for comparison, the results shown in Figure 5-13 suggest that Catamaran 5 and 6 together with Trimaran 5, 6, 8, and 9, have the best overall seakeeping performances. This indicates that for catamarans, a length-to-beam ratio  $\frac{L}{B_{TOT}} = 4$  and a length-to-draft ratio  $\frac{L}{T} > 24$  are optimal. For trimarans, a length-to-beam ratio  $\frac{L_C}{B_{TOT}} = 2.5$  and a length-to-draft ratio  $\frac{L_C}{T_C} > 24$  give optimal results. Using the design trends outlined in Section 5.3.3, these results could be used to generate a new set of variants with a length-to-beam ratio  $\frac{L}{B_{TOT}}$  between 4 and 2 for catamarans and between 4 and 2.75 for trimarans. The results obtained from this analysis could provide additional insight to determine the best combination of parameters and the best overall variant.

The results shown in Figure 5-11 and Figure 5-12 could also be used to determine if the accelerations are within specified values to guarantee factors such as crew comfort or helicopter landing. Given the simplifications adopted in this study, this type of assessment cannot be completed. However, in a real design case that included this performance analysis, the information obtained could be used for such a purpose.

The results obtained from the seakeeping analysis can also be used to compare the response of different vessel configurations in a specific scenario. An example of this type of analysis is shown in Figure 5-14 and Figure 5-15 where a catamaran and a trimaran vessel with similar overall dimensions are considered. It can be concluded from Figure 5-14 that the two vessels have similar heave response in the given conditions with the catamaran having a slightly lower response in the low frequency range as well as after the first cancellation frequency. On the other hand, Figure 5-15 shows the two vessels having a distinctly different roll resonance frequency. Although Figure 5-14 and Figure 5-15 provide specific information regarding the response of the

two vessel in heave and roll in a certain operational mode, a similar approach can be used to compare the two vessels in many different seas, headings, speeds, and loading conditions thus creating a full detailed picture of their seakeeping capabilities. The information obtained from such an analysis also allows the optimization of the vessel configuration for a given operating condition. For example, Figure 5-16 shows the optimal spacing of the demihulls which minimizes the roll response at zero forward speed. This information is particularly valuable for loading and unloading operations at the pier and will help the design team decide what is the optimal hull spacing based on the environmental conditions of a given series of locations.

Based on the modified design process shown in Figure 5-10, in order to determine the best overall variant, the seakeeping results should be combined with the other factors taken into account in the quantitative analysis to determine which variant has the best combination of parameters. Since this study was completed independently

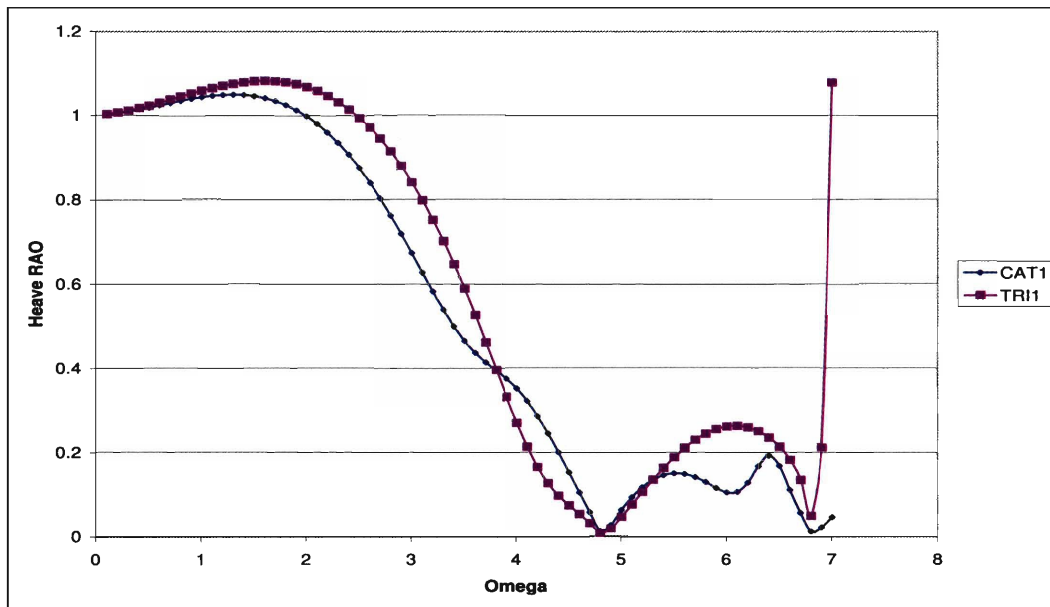


Figure 5-14: Heave RAO Comparison for Catamaran 1 and Trimaran 1 at  $F_n = 0.0$  and  $\mu = 150^\circ$

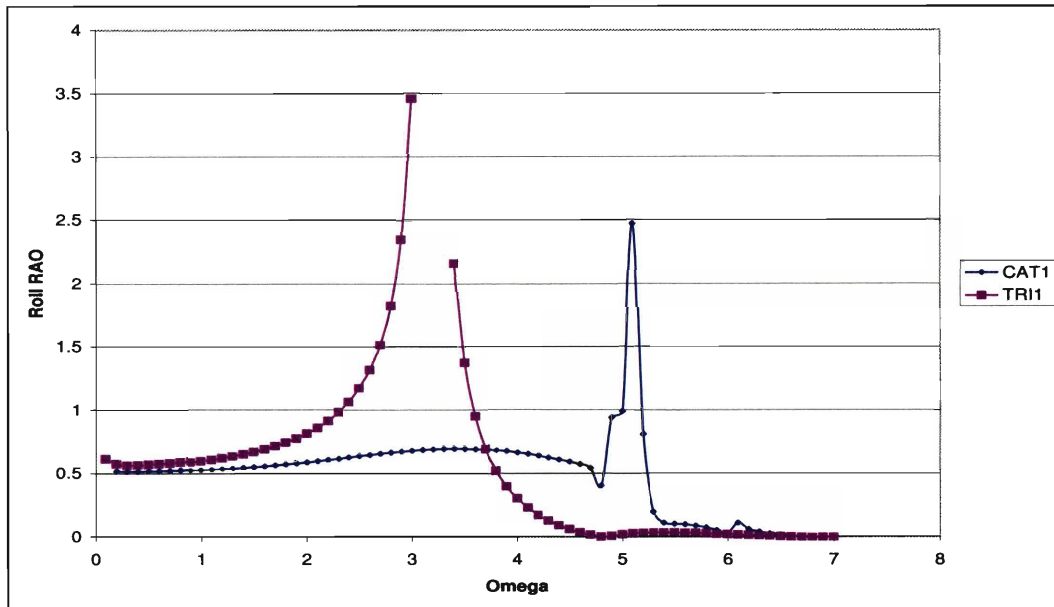


Figure 5-15: Roll RAO Comparison for Catamaran 1 and Trimaran 1 at  $F_n = 0.0$  and  $\mu = 150^\circ$

of the HSC design process, the seakeeping analysis cannot be combined with the results of the quantitative analysis such as transport factor and life cycle costs. As a consequence, this design process cannot be taken to completion at the present time. If these results were available, a Pareto frontier analysis would be used to determine which variant best satisfies the vessel requirements.

## 5.4 Overall Advantages of the Revisited Design Process

The revisited design process described in Section 5.3.2 allows the design team to include the quantitative data obtained from the performance-specific analysis in the preliminary design process. Although the I-Marine Seakeeping Analysis Toolbox at the current stage of development only offers a limited flexibility in terms of hull shapes and analytical capabilities, its effect on the design process is evident. With additional development, I-Marine could be used in a real design process leading to

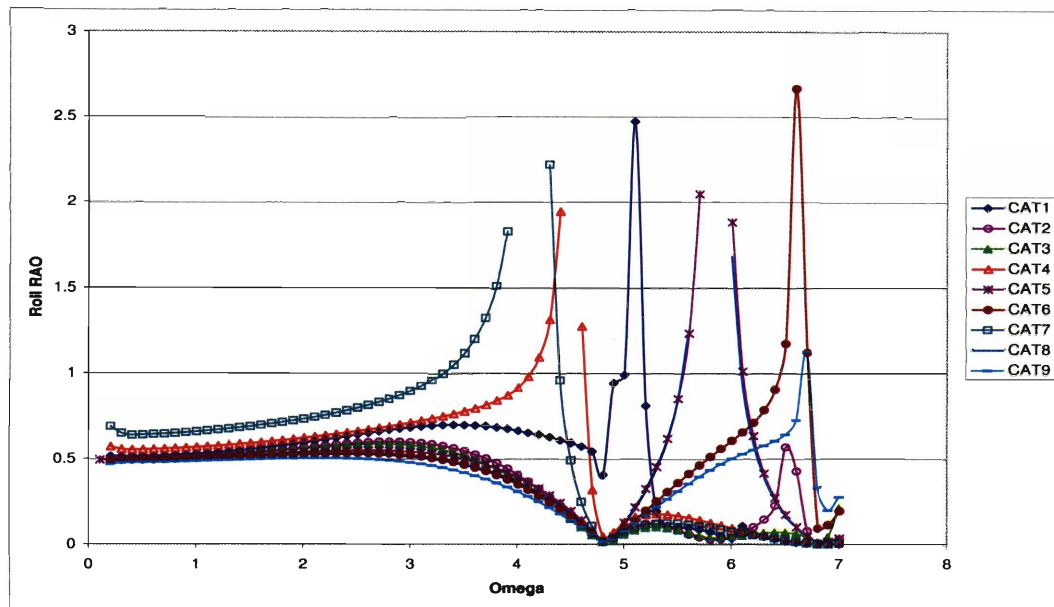


Figure 5-16: Roll RAO at  $F_n = 0.0$  and  $\mu = 150^\circ$  for the Catamaran Configurations Considered in the Case Study

many advantages. In addition, the analytical capabilities of a platform such as I-Marine lead to advantages of much wider breath such as a better understanding of multihull vessels, a decrease in the risk of developing innovative hull forms, and even an improvement in the quality of teaching in an educational framework, which can be beneficial to the naval architecture world in general. The advantages have been divided in four categories.

1. **Quantitative assessment of the seakeeping performances.** Using a platform such as the I-Marine Seakeeping Analysis Toolbox allows the design team to compare different vessel configurations based on quantitative results and not solely rely on the qualitative assessment for a critical component in the design philosophy. An example of this type of analysis is shown in Figure 5-14 and Figure 5-15 where a catamaran and a trimaran vessel with similar overall dimensions are compared. Although the geometries of the two vessels are highly simplified and of limited value



in a real design case, the same approach could be used to create and compare more detailed hull forms. The ease of use and the computational speed of a tool like I-Marine make this operation possible with limited effort and time consumption. With the information obtained from such an analysis, the decision process is strongly improved due to the solidity of the data obtained.

In addition, having detailed quantitative data about the seakeeping response of different multihull configurations allows to compute different performance criteria such as the RMS Vertical Acceleration presented in Section 5.3.3. Such data can help the design team summarize the results of the seakeeping analysis and identify the best vessel configuration for a given set of requirements. In addition, it allows the design team to make a detailed analysis of the performances of each variant without generalizing the answer. This is particularly important as multihull vessels have overlapping seakeeping performances which cannot be taken into account by a generalized analysis.

**2. Capability to predict the seakeeping performances of multihull vessels leading to a higher confidence level in the results, a reduction in the risk of designing such vessels, and an expansion of the design envelope.** Multihull vessels have only been recently considered as a possible option for commercial and military applications. As a consequence very little information is available regarding their performances and capabilities. In addition, most of the information available is proprietary and not available to the public. Actual analysis of innovative vessel configurations is critical to increase the confidence level of designing multihull vessels and expand the design envelope. The designers would be enabled to include more innovative designs in their analysis. In addition, by being able to quantitatively assess the seakeeping performances of innovative hull forms, the risk of designing this type of ships would decrease.

Although the nine catamarans and the fifteen trimarans used in the analysis were

designed keeping in mind existing multihulls, many of them have a combination of parameters such as length-to-beam ratio  $\frac{L_C}{B_{tot}}$  and length-to-draft ratio  $\frac{L_C}{T_C}$  which are not present in any existing design and for which no seakeeping result is available. Once again, although the variants analyzed in the case study are largely simplified, the same approach could be used with more realistic geometries. By being able to predict the seakeeping performance of different vessel configurations in a relatively short time, the design team would also be able to understand how each design parameter, such as length, beam, or draft effect the seakeeping capabilities of a specific type of vessel. This process strongly increases the level of understanding of this type of vessels and helps the designers in determining what combination best fits the needs of the vessel.

**3. Increase in the efficiency of the design process.** Having the capability to easily obtain quantitative results about the seakeeping of different vessels allows a designer to carry on an in-depth seakeeping analysis during the preliminary design of the vessel. By calculating the vessel response in a seaway earlier in the design process, the overall efficiency of the design process increases. This is particularly true with multihull vessels, where the number of design variables is greater than with monohulls. It is important to assess the configuration with the best seakeeping performance during the preliminary design. Having quantitative data would allow the designer to rule out the variants which are not suitable thus reducing the pool of possible designs without having to wait for a more in-depth analysis which generally occurs in a later stage of the design process. Moreover, this approach also reduces the risks of unexpected outcomes which, if noticed at an advance stage of the design process, might require an entire redesign or have significant to the operation of the vessel. This is shown in Figure 5-16 where it is possible to determine the optimal spacing between the demihull in order to minimize the roll response at zero forward speed.

Another example is presented in the summary parameter Figure 5-13, where the

RMS vertical acceleration of all the catamarans and trimarans analyzed during the case study are compared. Having quantitative data would allow the design team to summarize the seakeeping performances of the different variants into a parameter or a series of parameters. The sum of the RMS vertical accelerations for the four angles of wave incidence was chosen as a summary parameter. Although an assessment of the best parameter to summarize the seakeeping performances of a vessel goes beyond the scope of this study, the advantages of such an approach remains valid. Moreover, this method allows the design team to exclude the unsuitable variants during the preliminary design. This analysis leads to a reduction of the number of preliminary designs to include in the successive phases of the design process reducing the number of iterations required to obtain the final design.

**4. More complete educational tool.** The capabilities of the I-Marine Seakeeping Analysis Tool together with its ease of use, make it a great tool for educational purposes. By using the I-Marine platform, students can learn the impact of the seakeeping analysis on the design of a vessel in an integrated environment. Moreover, students are able to explore different vessel configurations like catamarans and trimarans and develop a knowledge in designing and analyzing these type of vessels. By having a fast and easy-to-use seakeeping analysis tool, students would be able to analyze the seakeeping performances of multihull vessels at a much greater depth instead of relying on existing designs or oversimplifying their analysis. This type of educational tool will develop students confidence in the design of innovative hull forms.

## 5.5 Summary

The goal of the case study was to show how an integrated analysis tool such as the I-Marine Seakeeping Analysis Toolbox could be effectively used in a real design process

and what the advantages of using such a platform are. The design process developed by Zouridakis and Wang for the High Speed Connector was analyzed in depth. The analysis revealed some weaknesses in the design process used by the HSC design team which affected the solidity of their conclusions. The design process was modified to take advantage of I-Marine. Using the same design envelope used for the HSC project, twenty-four variants were created and analyzed. Although these geometries were highly simplified, the analysis provided important information regarding the advantages of being able to quantitatively assess the seakeeping capabilities of different vessels in the preliminary design. By expanding the capabilities of the geometry creator I-Build, and including a tool like PASS, I-Marine could be used in a real design process.

The case study shows that by including a seakeeping analysis in the preliminary design process, substantial advantages can be achieved such as a higher granularity in assessing the best variant, a reduction in the risk of designing multihull vessels, and an expansion of the design envelope. Moreover, these capabilities would lead to an overall increase in the efficiency of the design process, helping the design team identify the most suitable vessel configurations in the preliminary phase of the design process.

Finally, the ease of use of a tool such as I-Marine makes it suitable for educational purposes allowing students to understand the importance of seakeeping analysis in the development of a vessel and to develop confidence with different seakeeping programs and vessel configurations. These advantages have been summarized in Table 5.9 together with a reference to the method used to achieve such a goal.

<b>Advantage</b>	<b>Proof</b>
Quantitative assessment of the seakeeping performances	See results in Appendix C and Figure 5-14 and Figure 5-15 in Chapter 5.4.
Possibility to optimize the design for specific requirements and environmental conditions	TRUE. See resonance frequency analysis in Roll shown in Figure 5-14 and Figure 5-15 in Chapter 5.4
High confidence level in innovative designs	See validation tests in Chapter 4 and the case study analysis shown in Appendix C
Capability to obtain information about innovative hull forms	See Chapter 5.4
No restrictions in the design. Do not have to limit the design to well known vessel configurations	See Chapter 5.4
Reduction in the risk of designing unconventional hull forms	See validation tests in Chapter 4
Possibility to estimate vessel performances earlier in the design process	See Chapter 5.3.2 of the case study analysis
Overall reduction in the risk of unexpected outcomes	See Chapter 5.3.2 of the case study analysis
Capability to develop unconventional vessel configurations at an educational level	See results in Appendix C
Fine tuning of vessel performances to satisfy specific requirements. Avoid the "throw a dart in the middle" approach	See design analysis in Chapter 5.3.2

Table 5.9: Summary of the objectives achieved in the case study analysis



# Chapter 6

## Conclusions

This thesis addresses the use of the I-Marine Seakeeping Analysis Toolbox to analyze the seakeeping performances of multihull vessels. The different two-dimensional seakeeping analysis programs included in I-Marine were analyzed starting from the theoretical principles behind them. These programs were then validated comparing the predicted results to experimental and analytical data found in the literature. Finally, a case study was completed to show the benefits of using an integrated tools such as the I-Marine Seakeeping Analysis Toolbox in a real design process.

One of the highlights of I-Marine is the web interface which strongly facilitates the use of its analytical capabilities. The user is able to create various hull geometries and run different seakeeping programs without having to spend significant time understanding how to run each program. This is particularly useful in an educational environment because it allows the students to focus on the seakeeping analysis without worrying about programming and debugging. In this way, students will learn much more quickly what the advantages and limitations of each seakeeping method are and how to interpret the results obtained.

The validation analysis completed in this thesis shows that strip theory programs can be effectively used to obtain important information regarding the seakeeping

response of multihull vessels in waves. Good agreement was observed between simulations and experimental data for all the conditions analyzed in this study. As a consequence, it can be concluded that I-Marine can be used to analyze multihull configurations and obtain information regarding their seakeeping capabilities.

Finally, the case study shows that being able to quantitatively assess the seakeeping capabilities of different preliminary designs leads to great advantages. A revised preliminary design process that effectively integrates this type of analysis has been proposed. Although I-Marine at the moment has limited flexibility in creating hull geometries, the results obtained confirm the effectiveness of using such a platform in the preliminary design process. Using a tool such as I-Marine offers a great advantage for designers because allows to make decisions based on quantitative results. Having quantitative data about the seakeeping capabilities of multihull vessels leads to a better understanding of the parameters involved in the design and an overall reduction in the risk of development. In addition, it allows designers to explore innovative configurations expanding the design envelope. Moreover, the integrated nature of I-Marine largely simplify the analysis allowing to run different seakeeping programs without having to build different input files.

## 6.1 Future Work

The I-Marine Seakeeping Analysis Toolbox is at an early stage of development and many improvements should be made before it is used in a real design process. Overall, the most important upgrade would be expanding the capabilities of the I-Build routine. In order to be able to use I-Marine in a real design process, more advanced geometries need to be created. Although the geometries currently available are useful from an educational point of view, being able to build more detailed hull forms would allow the use of I-Marine in more advanced applications. In addition, it would be



useful to be able to create not only round bilge hulls but also chined hulls. This capability would allow to design an even larger pool of possible variants and a better assessment of the most optimal hull form for a given set of requirements. The I-Build routine should also be expanded to include additional vessel configurations such as pentamarans and SWATH vessels. By doing so, important information about these innovative vessels could be obtained.

Another possible improvement of the I-Marine Seakeeping Analysis Toolbox is regarding the specifications of the input waves. It would be useful from a design stand point to be able to specify not only waves of regular frequencies but also various wave spectrums to have a wider pools of possible scenarios to analyze the seakeeping performances of a vessel.

Finally, a larger validation study should be completed to better understand what are the limits of using strip theory with multihull vessels. Such a study would also help determine the most efficient way to use such a tool in a real design process.



## Appendix A

# CROSSFLOW Drag Coefficient and Lift Gradient Validation

A series of tests was completed to determine what values of drag coefficient and lift gradient are the most accurate for the NPL Model 5b catamaran. The values proposed by Chan [3] for an ASR catamaran travelling at a Froude number  $F_n = 0.124$  were taken as a reference. The analysis was carried out in head seas at a Froude number of  $F_n = 0.2, 0.5, 0.8$  using three different values for the drag coefficient  $C_D = 0.4, 0.2, 0.05$ . The lift gradient  $a$  was set equal to 0.0024. The response calculated with CROSSFLOW was compared to the experimental data provided in [18] and are shown below. The results show that linearly scaling the drag coefficient with the Froude number produces accurate results. The notation used in the figures is as explained in Section 2.8.

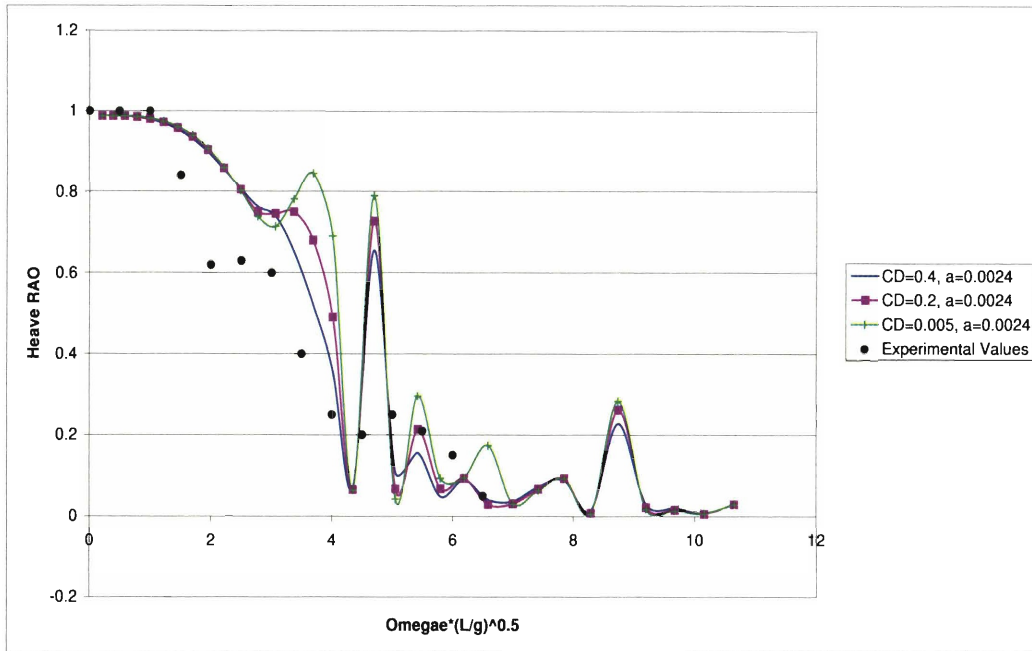


Figure A-1: CROSSFLOW: Heave RAO at  $Fn = 0.2$  and  $\mu = 180^\circ$

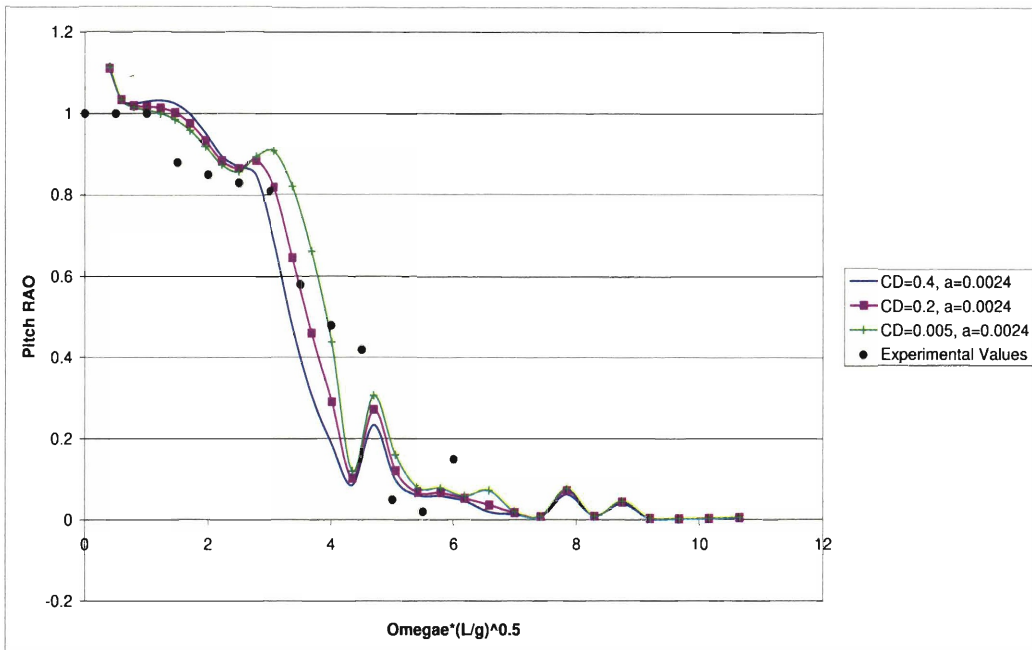


Figure A-2: CROSSFLOW: Pitch RAO at  $Fn = 0.2$  and  $\mu = 180^\circ$

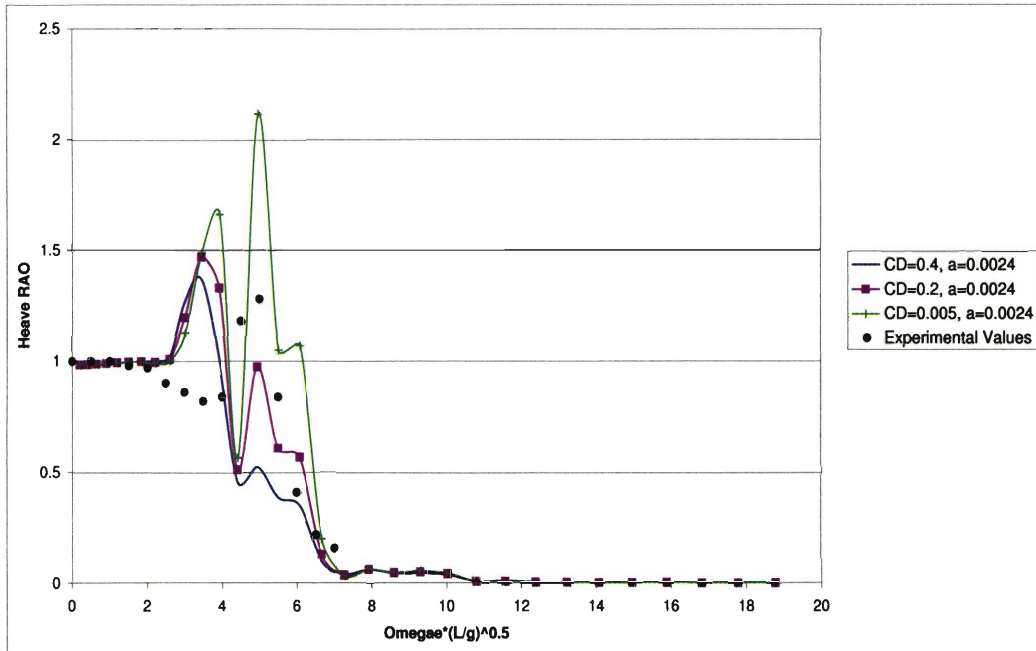


Figure A-3: CROSSFLOW: Heave RAO at  $F_n = 0.5$  and  $\mu = 180^\circ$

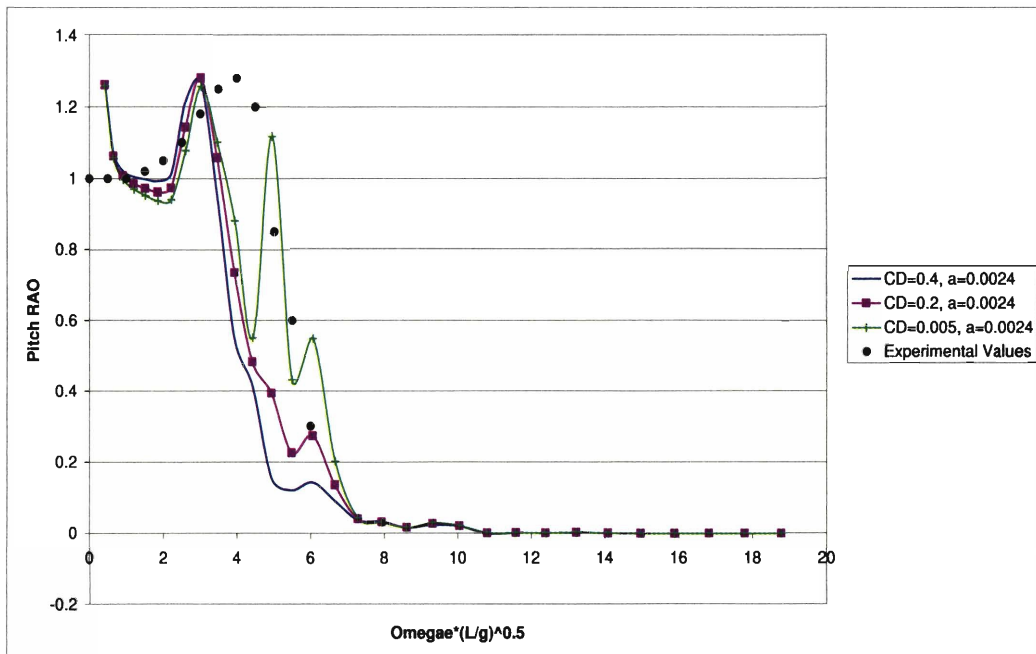


Figure A-4: CROSSFLOW: Pitch RAO at  $F_n = 0.5$  and  $\mu = 180^\circ$

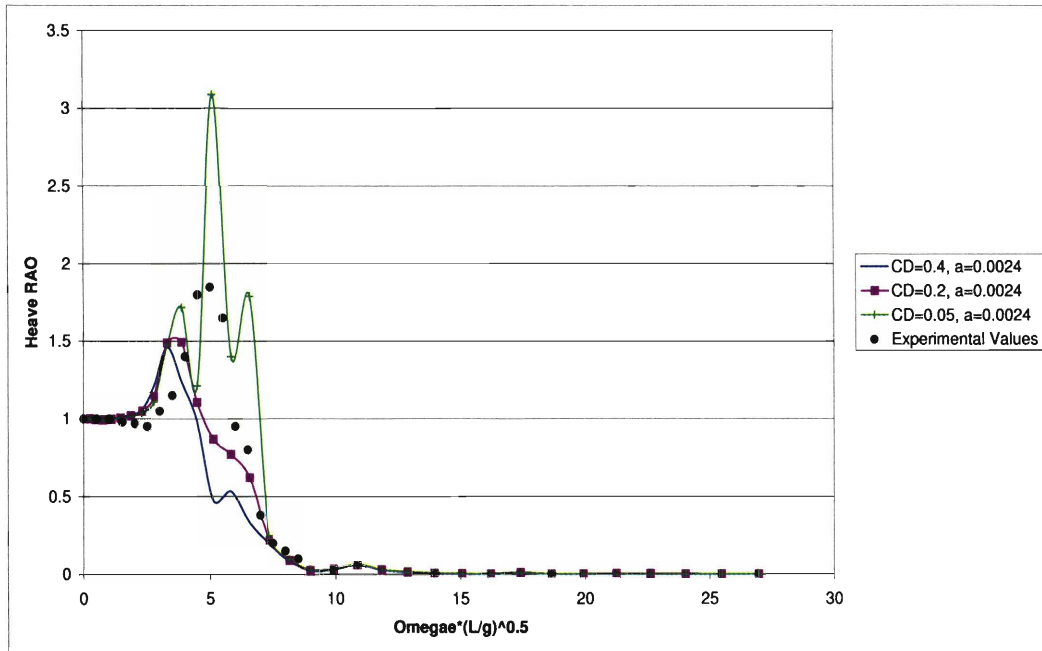


Figure A-5: CROSSFLOW: Heave RAO at  $F_n = 0.8$  and  $\mu = 180^\circ$

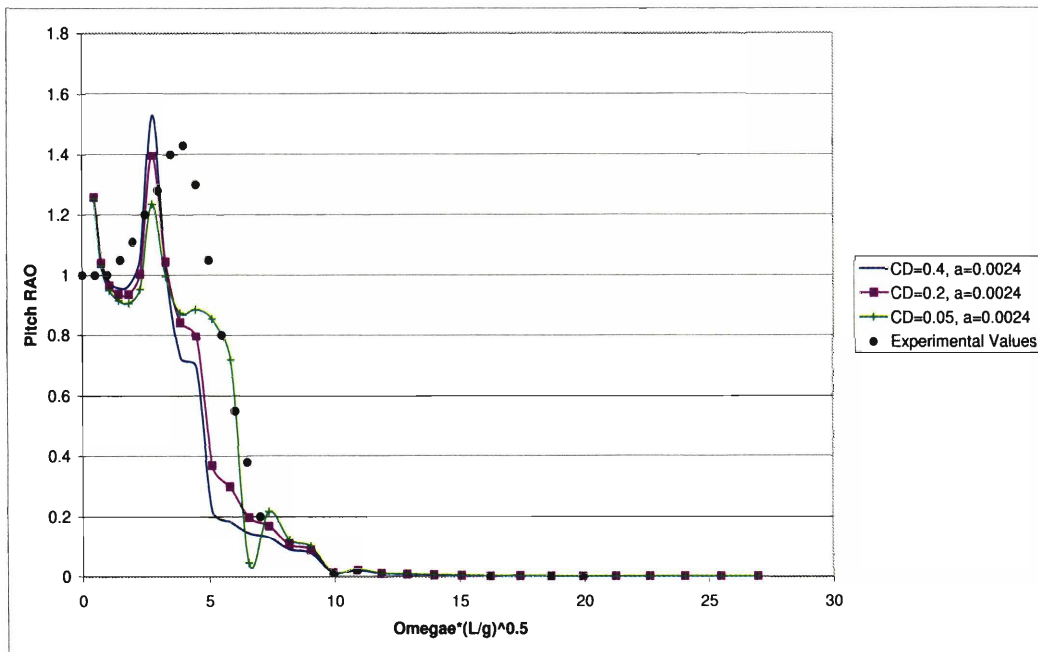


Figure A-6: CROSSFLOW: Pitch RAO at  $F_n = 0.8$  and  $\mu = 180^\circ$

## Appendix B

### LAMP-NIIRID Comparison

A series of tests was completed using the Large Amplitude Motion Program (LAMP) to determine the accuracy of the strip theory programs included in I-Marine. LAMP was run for a catamaran and three trimaran designs with elliptical hull sections at  $F_n = 0$  and  $F_n = 0.4$  at an angle of wave incidence of 180, 150, 120, and 45 degrees. The data calculated with LAMP were then compared with the results obtained using NIIRID in I-Marine. An overall good agreement was found. The notation used in the figures is as explained in Section 2.8.

## B.1 Catamaran Testing

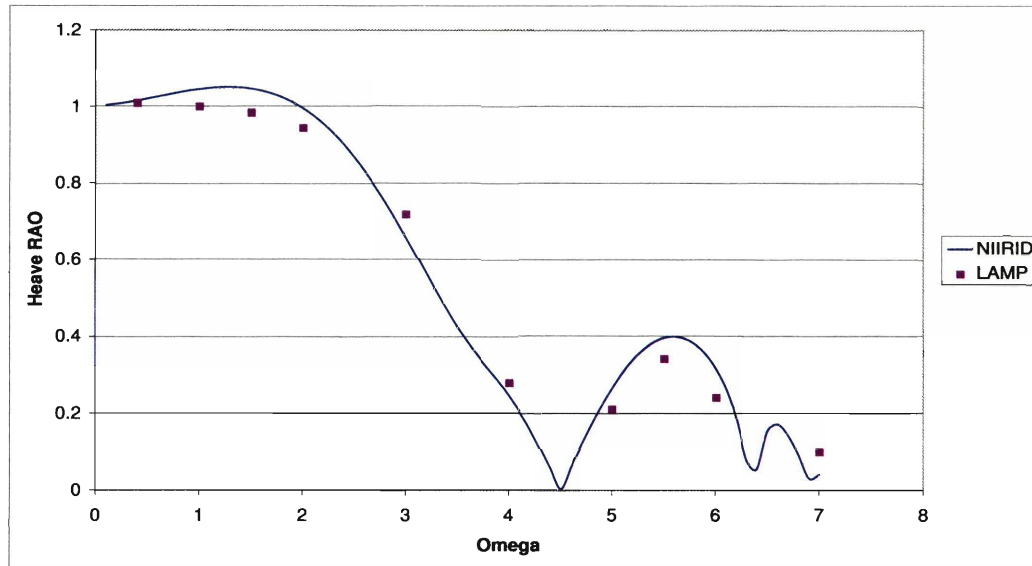


Figure B-1: LAMP-NIIRID Comparison for Catamaran 1: Heave RAO at  $F_n = 0.0$  and  $\mu = 180^\circ$

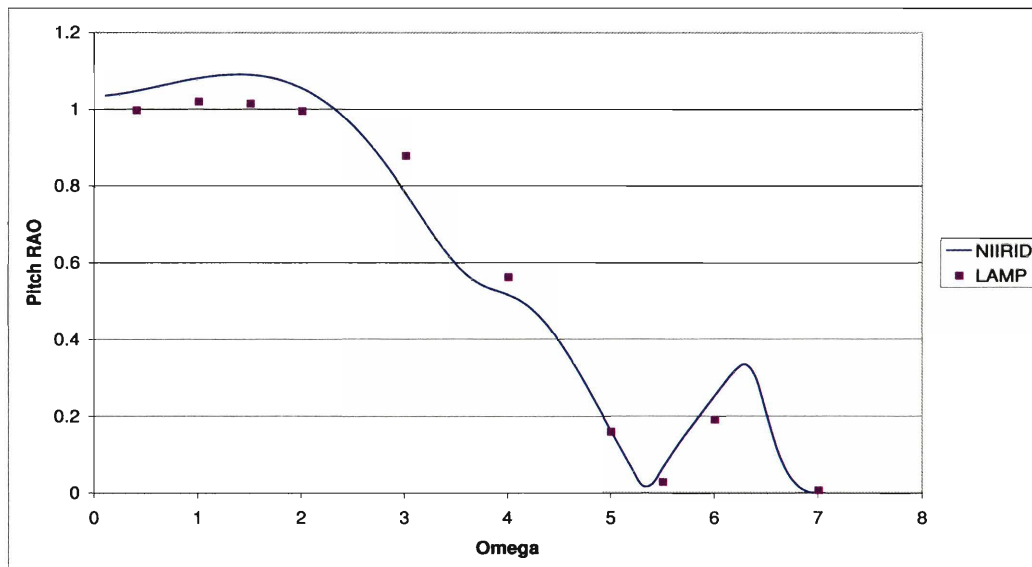


Figure B-2: LAMP-NIIRID Comparison for Catamaran 1: Pitch RAO at  $F_n = 0.0$  and  $\mu = 180^\circ$



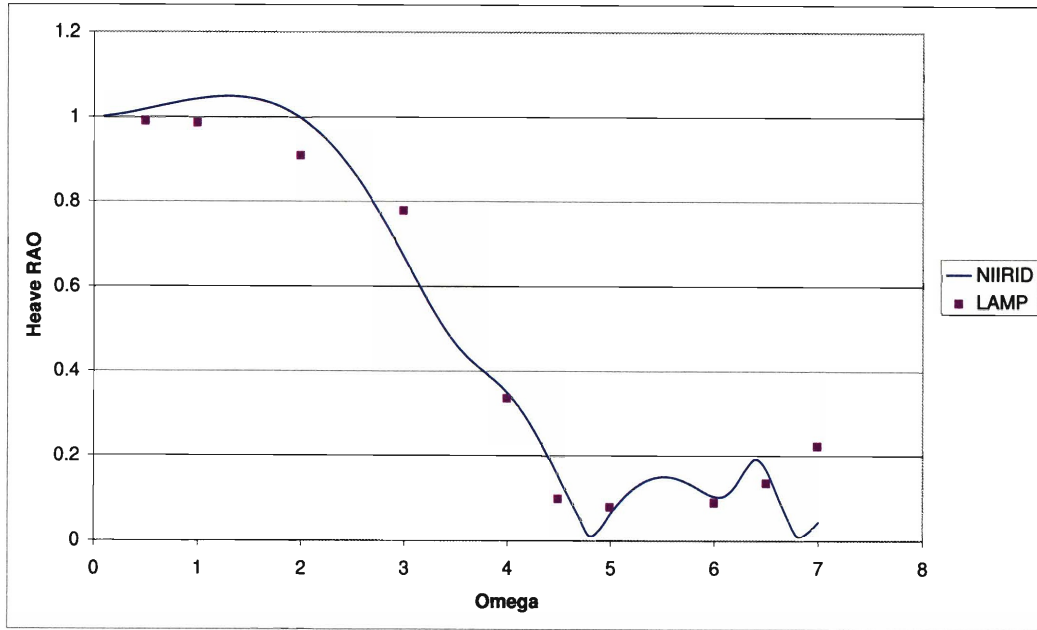


Figure B-3: LAMP-NIIRID Comparison for Catamaran 1: Heave RAO at  $F_n = 0.0$  and  $\mu = 150^\circ$

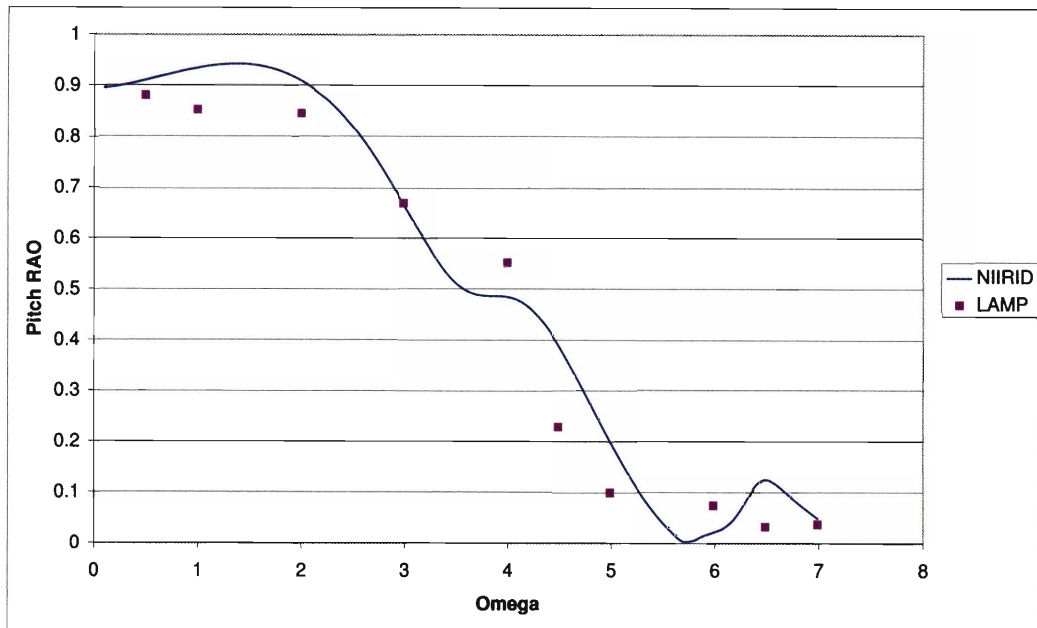


Figure B-4: LAMP-NIIRID Comparison for Catamaran 1: Pitch RAO at  $F_n = 0.0$  and  $\mu = 150^\circ$

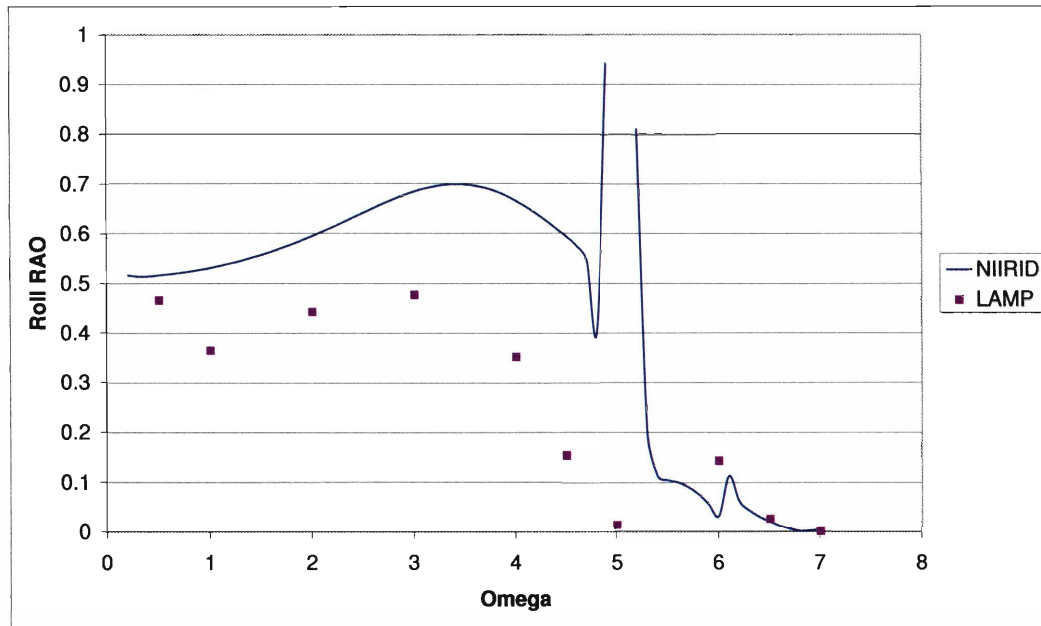


Figure B-5: LAMP-NIIRID Comparison for Catamaran 1: Roll RAO at  $F_n = 0.0$  and  $\mu = 150^\circ$

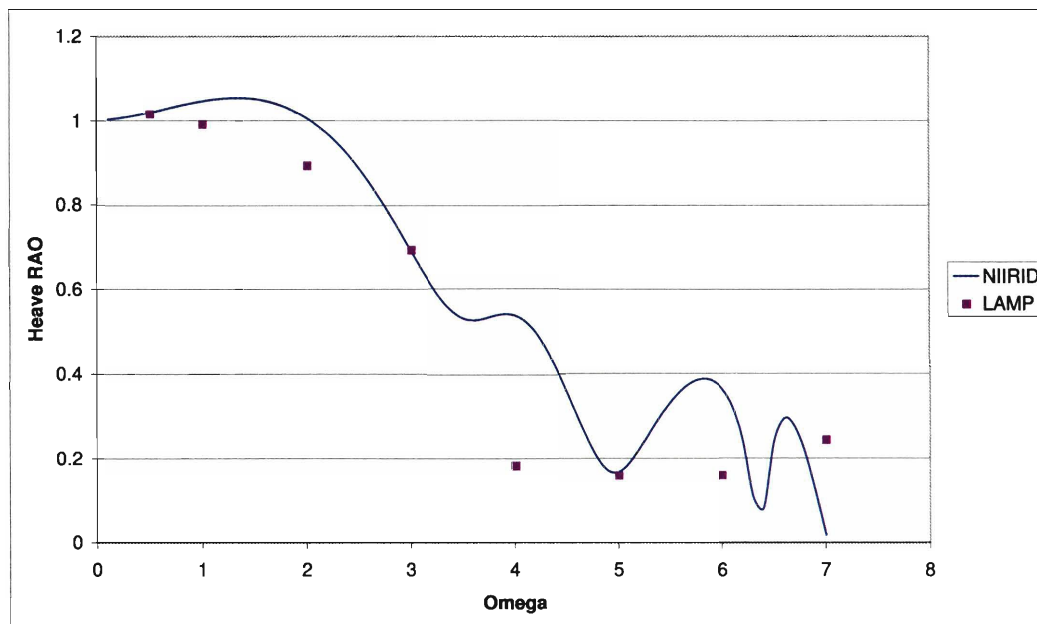


Figure B-6: LAMP-NIIRID Comparison for Catamaran 1: Heave RAO at  $F_n = 0.0$  and  $\mu = 120^\circ$

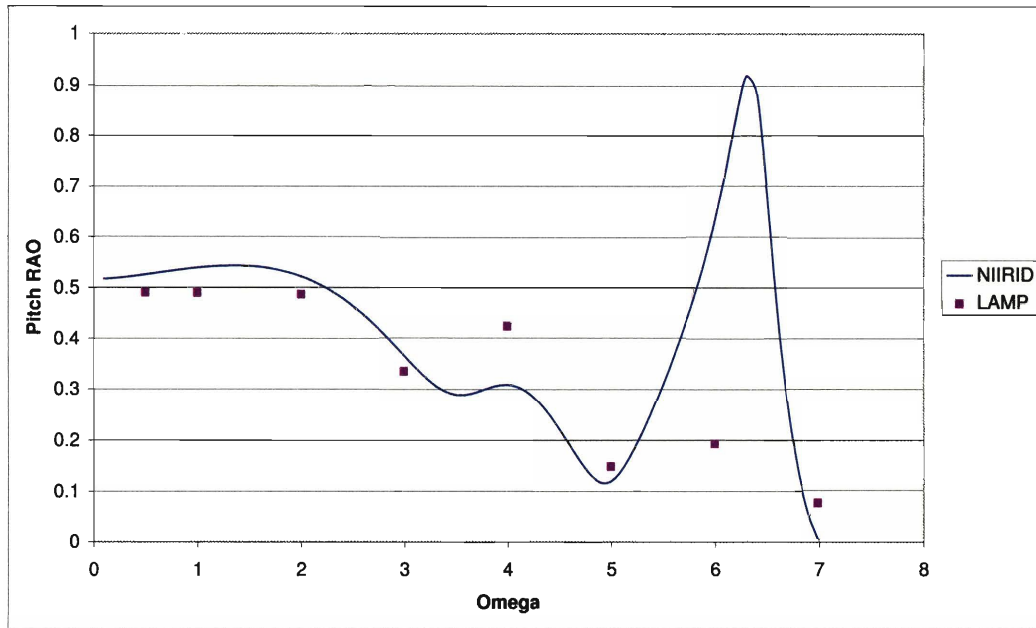


Figure B-7: LAMP-NIIRID Comparison for Catamaran 1: Pitch RAO at  $F_n = 0.0$  and  $\mu = 120^\circ$

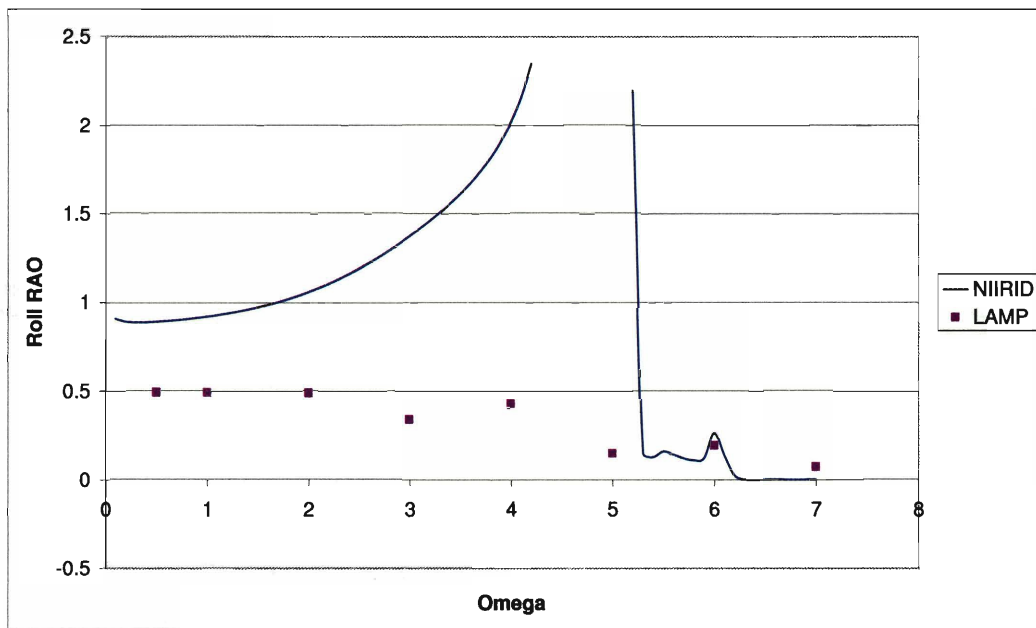


Figure B-8: LAMP-NIIRID Comparison for Catamaran 1: Roll RAO at  $F_n = 0.0$  and  $\mu = 120^\circ$

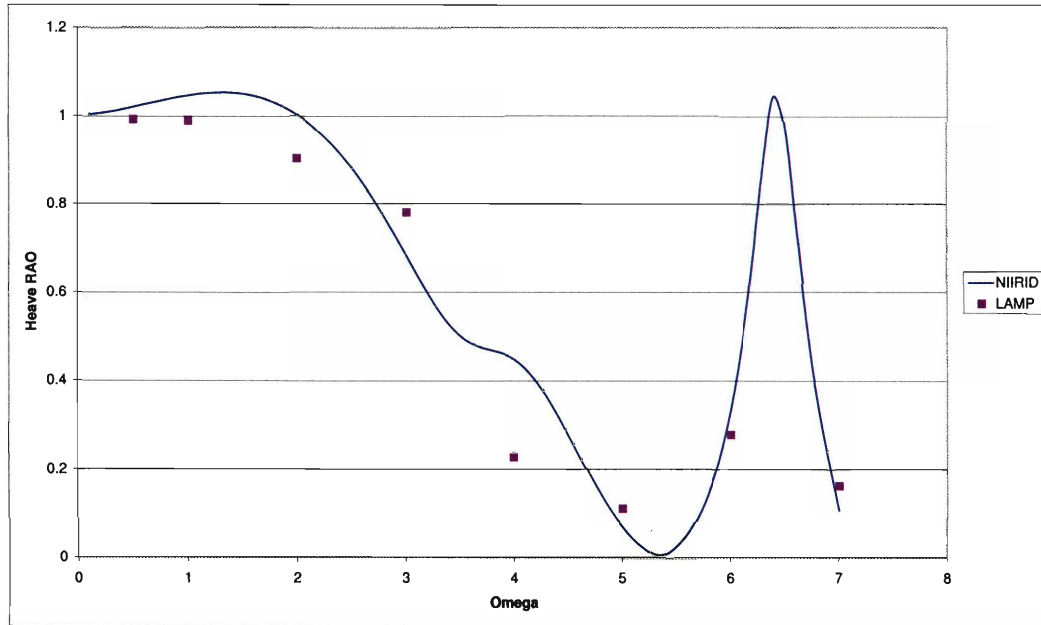


Figure B-9: LAMP-NIIRID Comparison for Catamaran 1: Heave RAO at  $F_n = 0.0$  and  $\mu = 45^\circ$

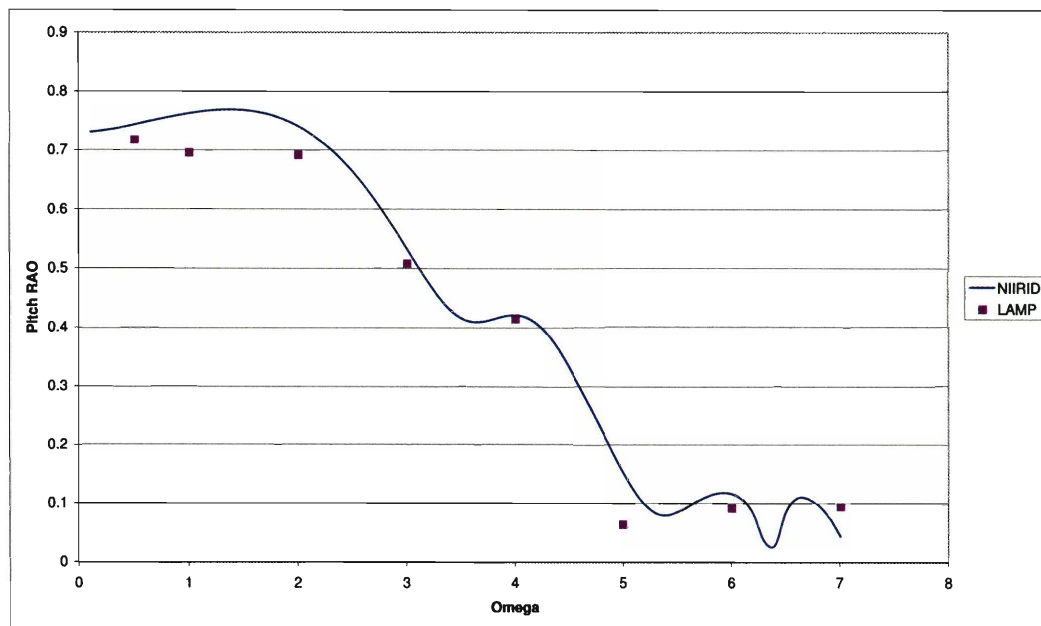


Figure B-10: LAMP-NIIRID Comparison for Catamaran 1: Pitch RAO at  $F_n = 0.0$  and  $\mu = 45^\circ$

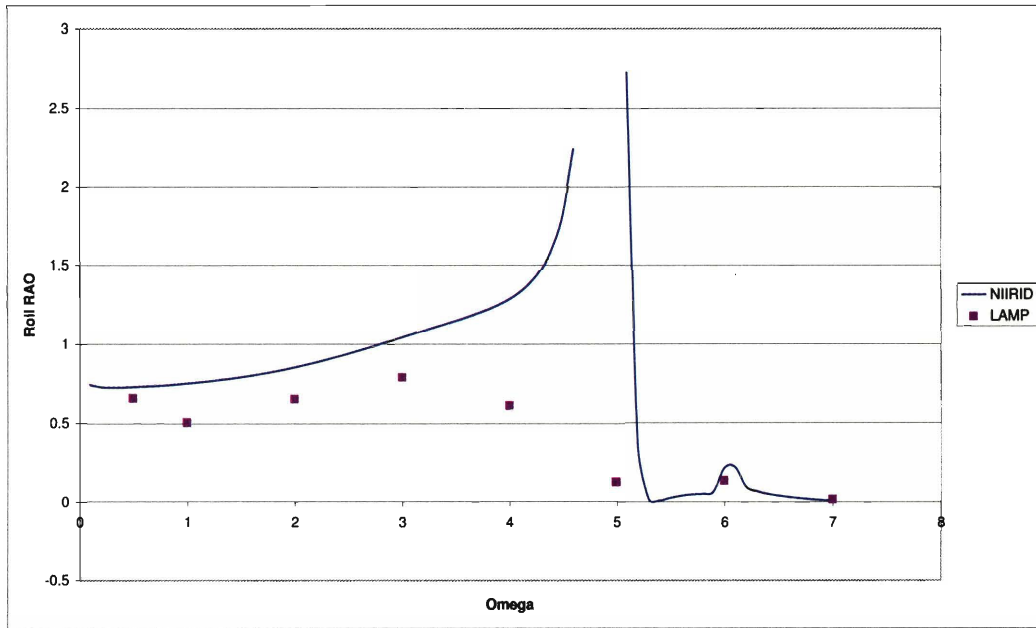


Figure B-11: LAMP-NIIRID Comparison for Catamaran 1: Roll RAO at  $F_n = 0.0$  and  $\mu = 45^\circ$

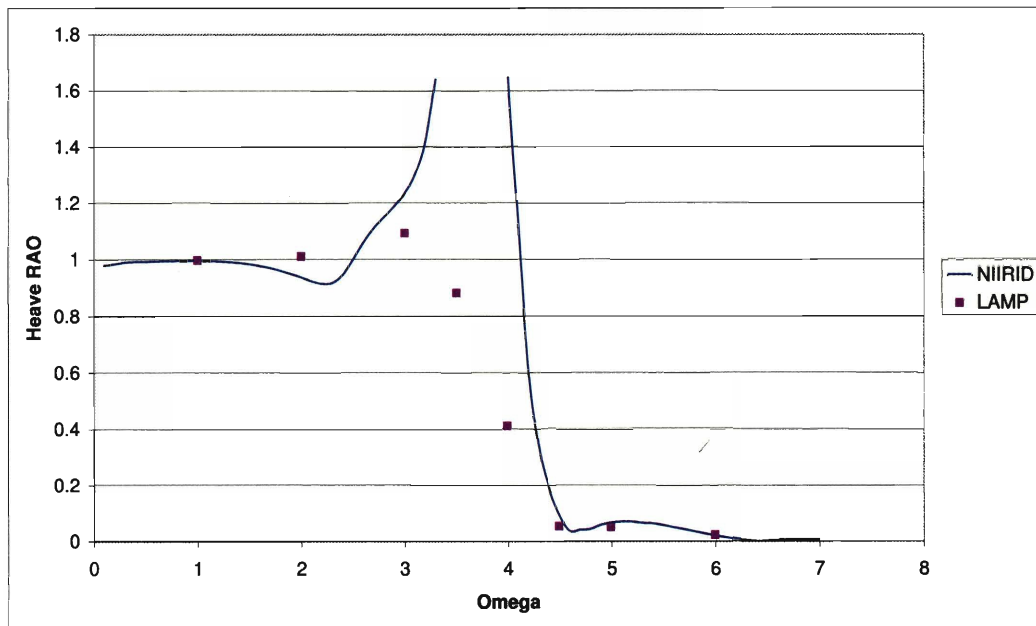


Figure B-12: LAMP-NIIRID Comparison for Catamaran 1: Heave RAO at  $F_n = 0.4$  and  $\mu = 180^\circ$

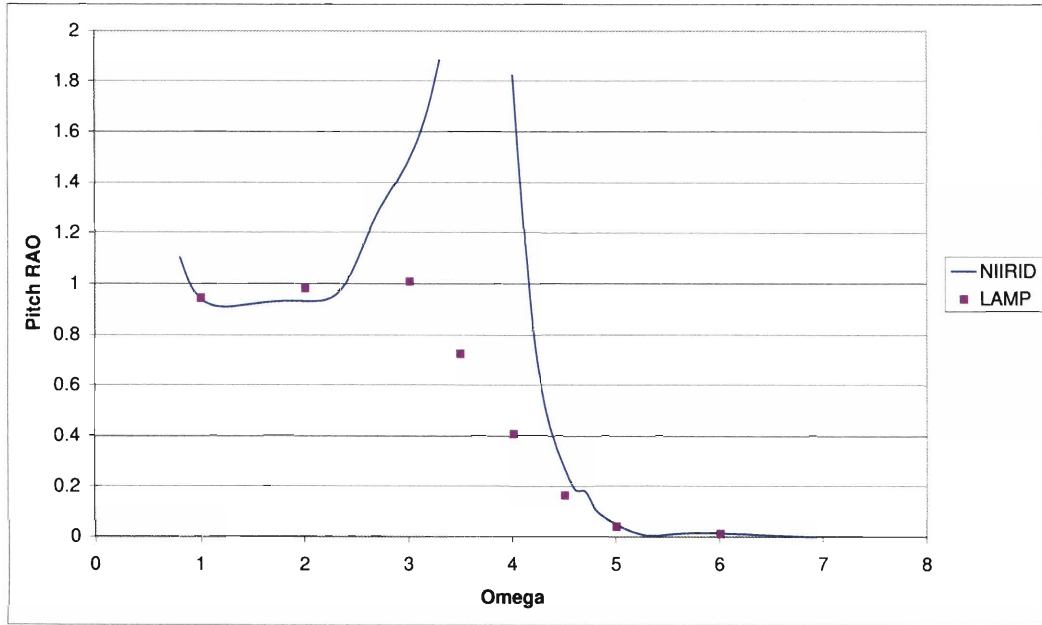


Figure B-13: LAMP-NIIRID Comparison for Catamaran 1: Pitch RAO at  $F_n = 0.4$  and  $\mu = 180^\circ$

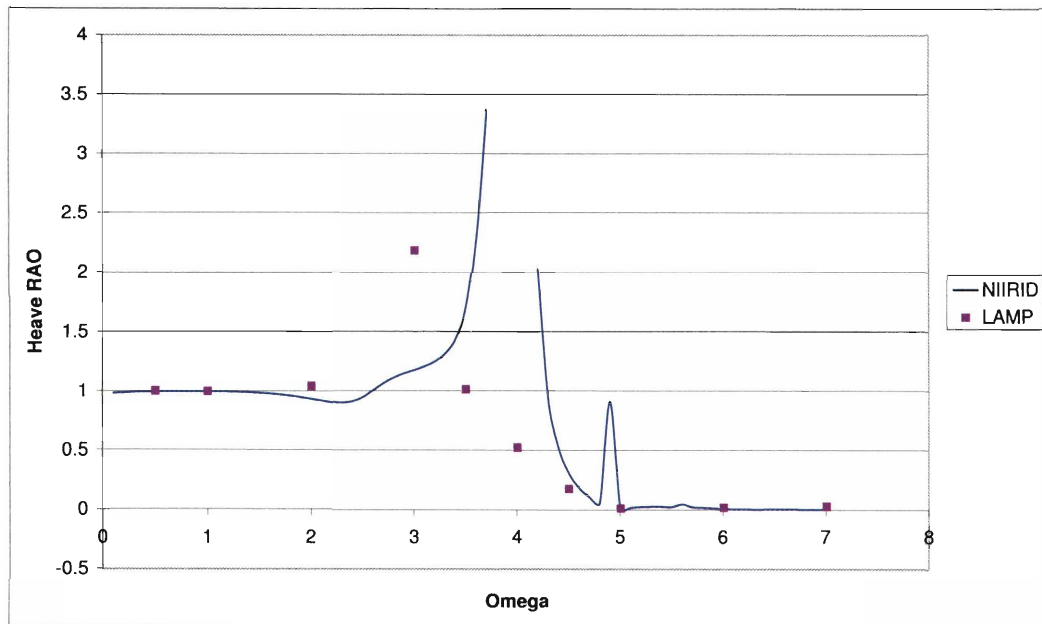


Figure B-14: LAMP-NIIRID Comparison for Catamaran 1: Heave RAO at  $F_n = 0.4$  and  $\mu = 150^\circ$

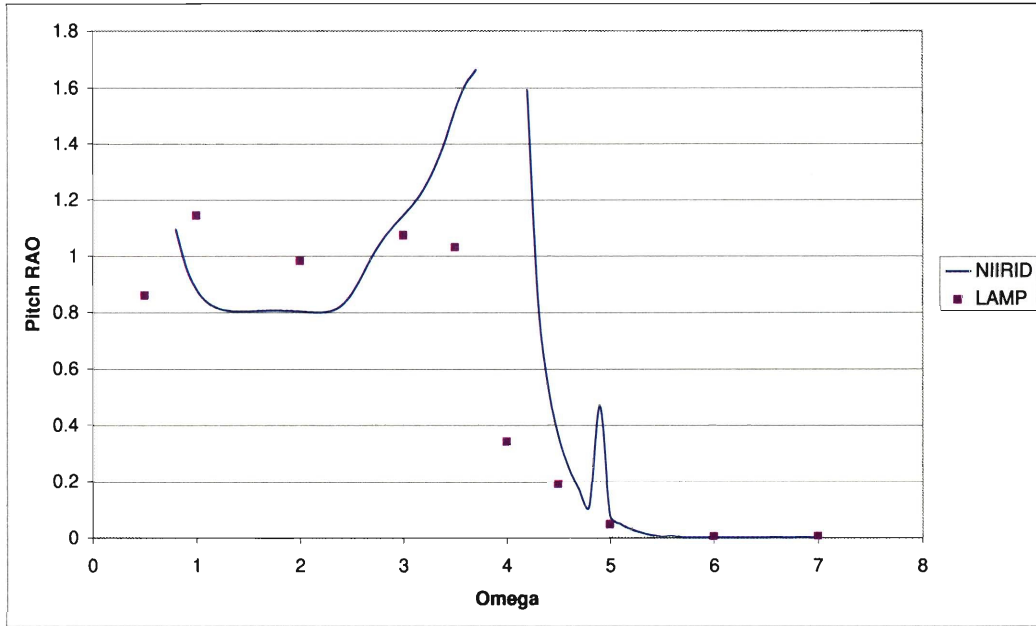


Figure B-15: LAMP-NIIRID Comparison for Catamaran 1: Pitch RAO at  $F_n = 0.4$  and  $\mu = 150^\circ$

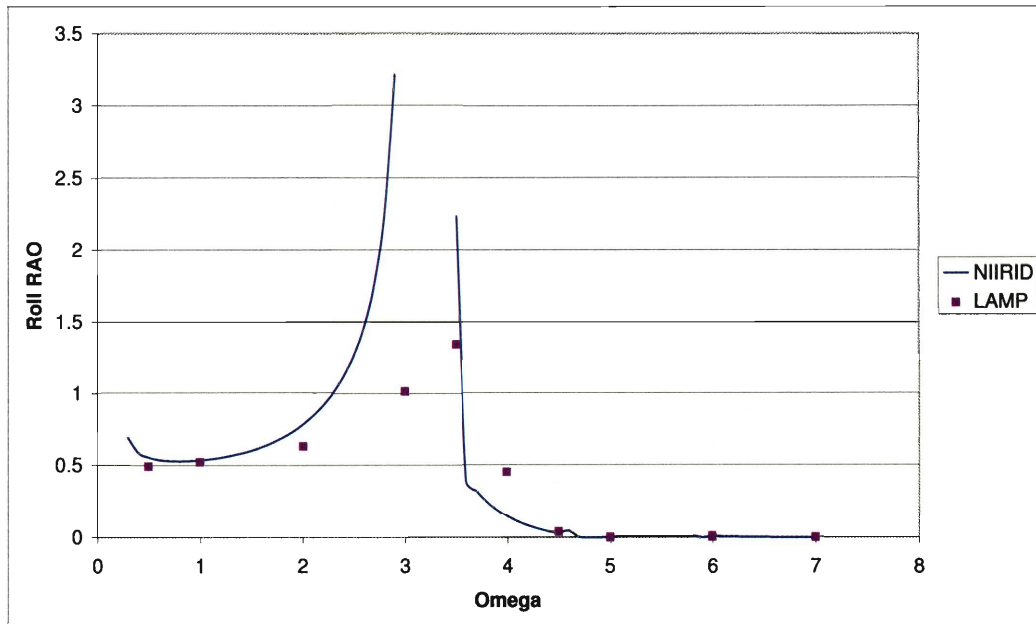


Figure B-16: LAMP-NIIRID Comparison for Catamaran 1: Roll RAO at  $F_n = 0.4$  and  $\mu = 150^\circ$

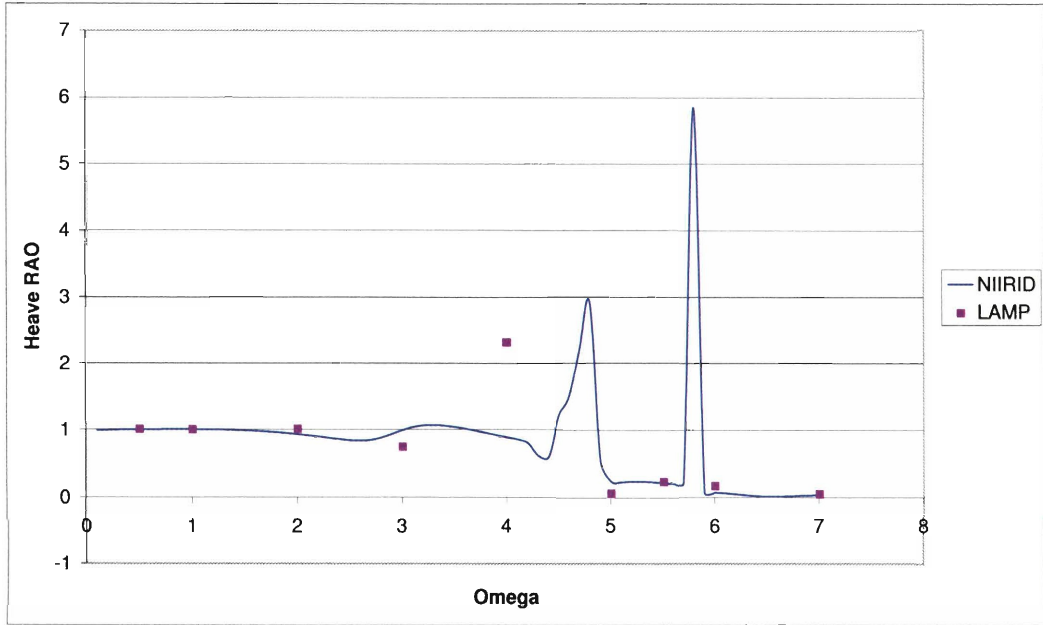


Figure B-17: LAMP-NIIRID Comparison for Catamaran 1: Heave RAO at  $F_n = 0.4$  and  $\mu = 120^\circ$

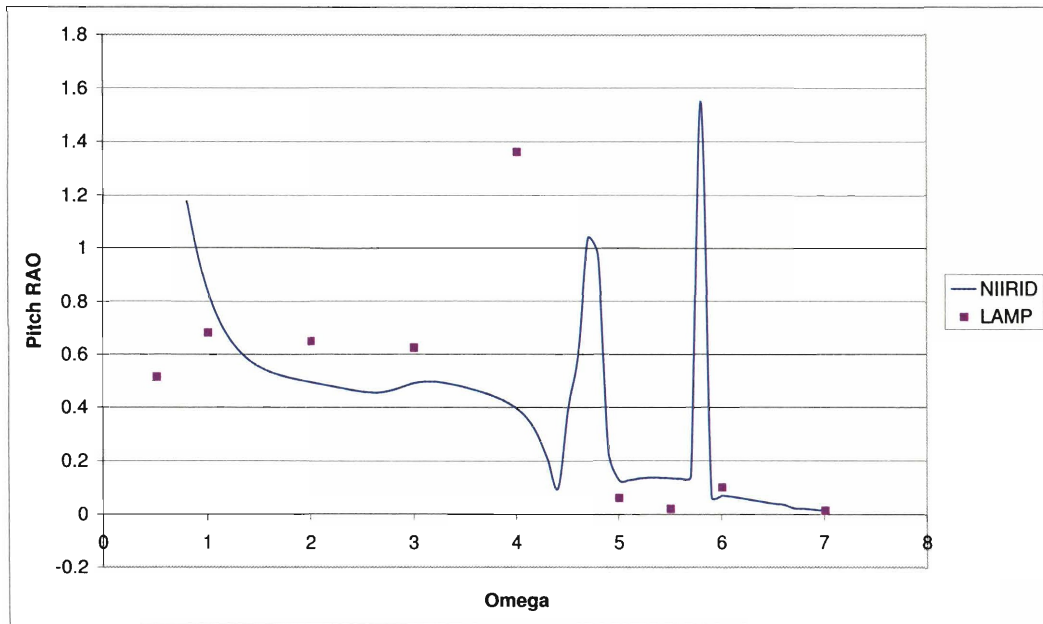


Figure B-18: LAMP-NIIRID Comparison for Catamaran 1: Pitch RAO at  $F_n = 0.4$  and  $\mu = 120^\circ$



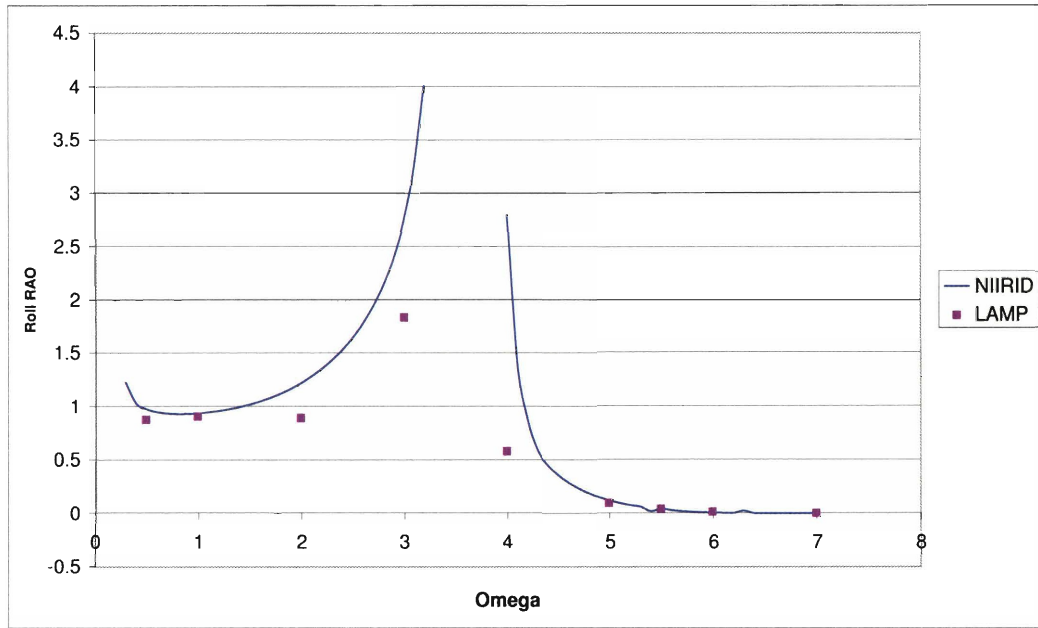


Figure B-19: LAMP-NIIRID Comparison for Catamaran 1: Roll RAO at  $F_n = 0.4$  and  $\mu = 120^\circ$

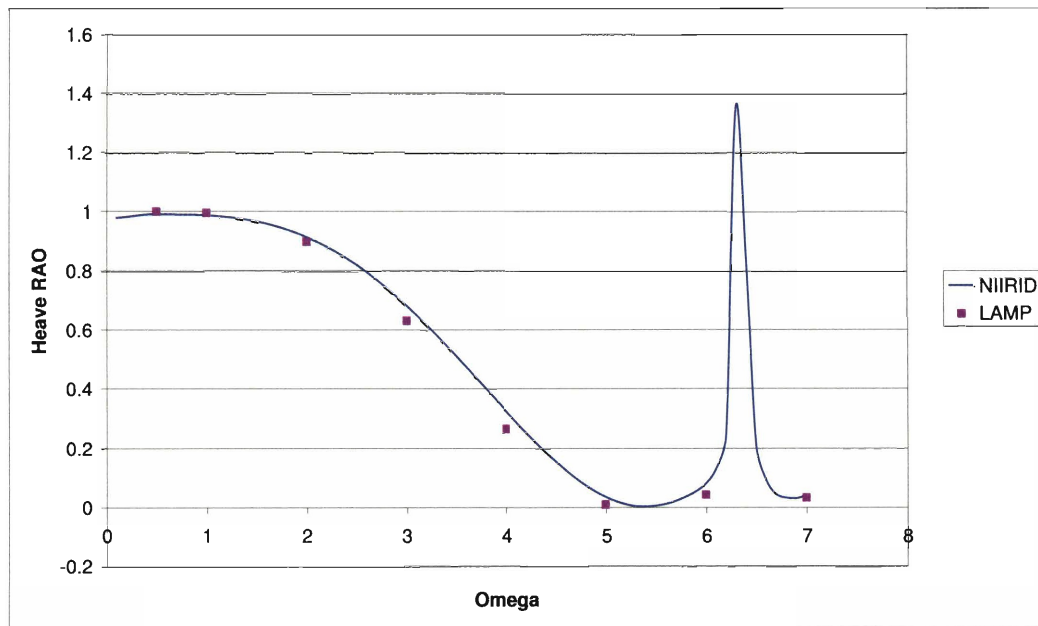


Figure B-20: LAMP-NIIRID Comparison for Catamaran 1: Heave RAO at  $F_n = 0.4$  and  $\mu = 45^\circ$

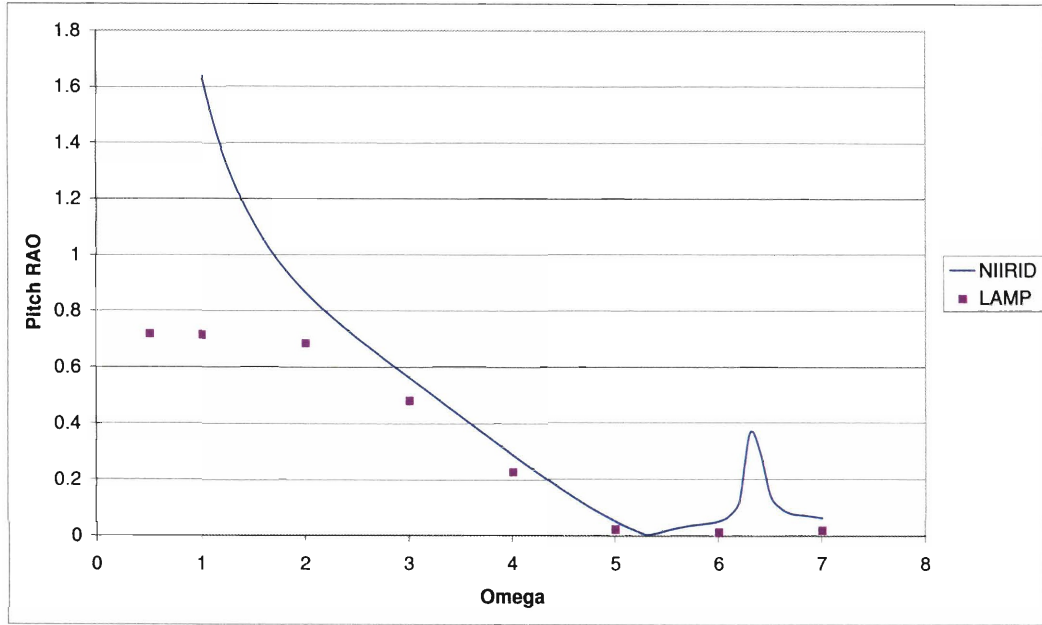


Figure B-21: LAMP-NIIRID Comparison for Catamaran 1: Pitch RAO at  $F_n = 0.4$  and  $\mu = 45^\circ$

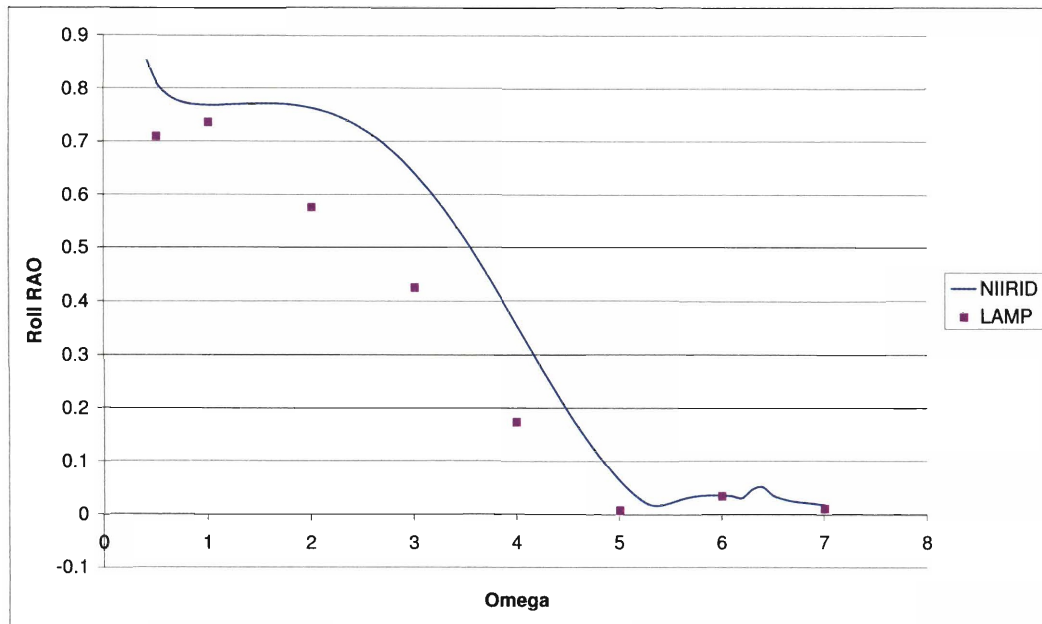


Figure B-22: LAMP-NIIRID Comparison for Catamaran 1: Roll RAO at  $F_n = 0.4$  and  $\mu = 45^\circ$

## B.2 Trimaran Testing

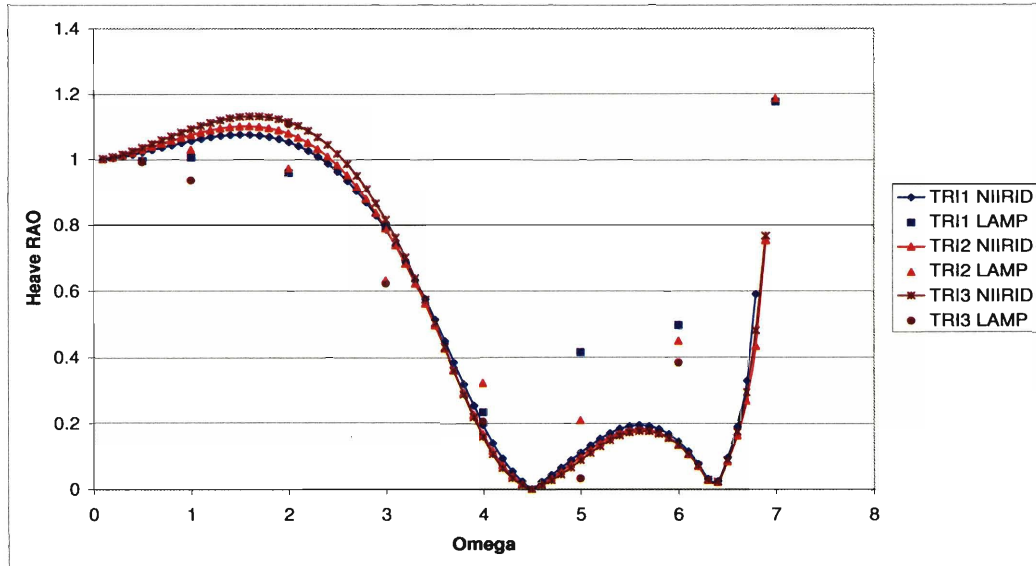


Figure B-23: LAMP-NIIRID Comparison for Trimarans: Heave RAO at  $F_n = 0.0$  and  $\mu = 180^\circ$

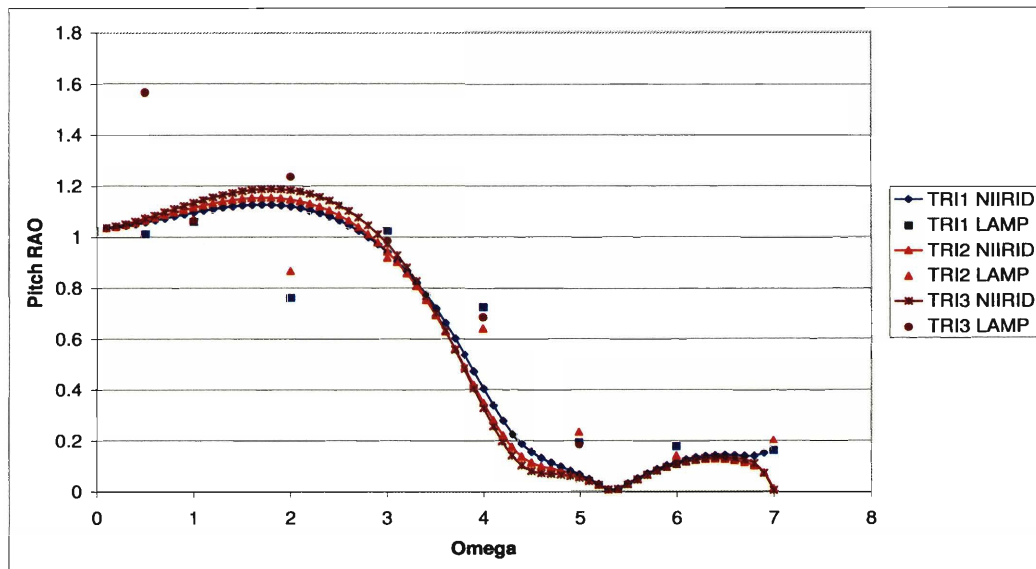


Figure B-24: LAMP-NIIRID Comparison for Trimarans: Pitch RAO at  $F_n = 0.0$  and  $\mu = 180^\circ$

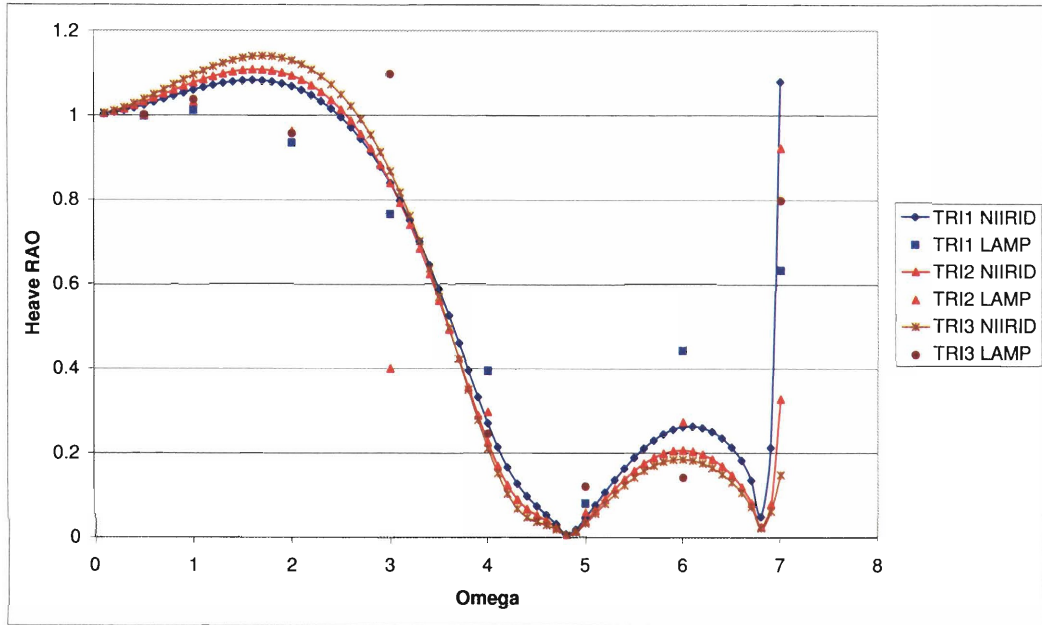


Figure B-25: LAMP-NIIRID Comparison for Trimarans: Heave RAO at  $F_n = 0.0$  and  $\mu = 150^\circ$

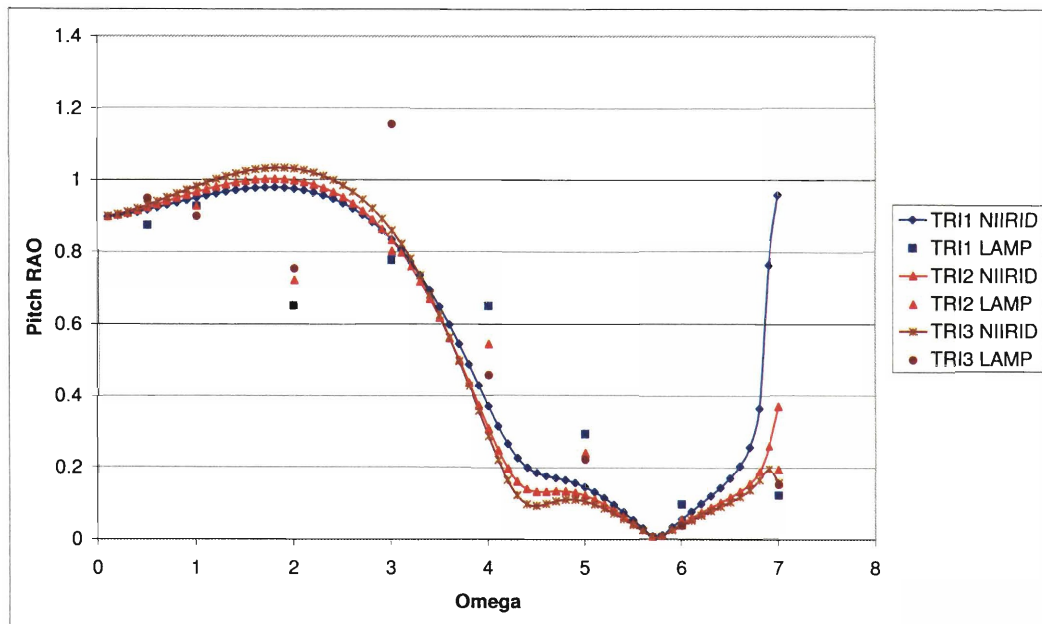


Figure B-26: LAMP-NIIRID Comparison for Trimarans: Pitch RAO at  $F_n = 0.0$  and  $\mu = 150^\circ$

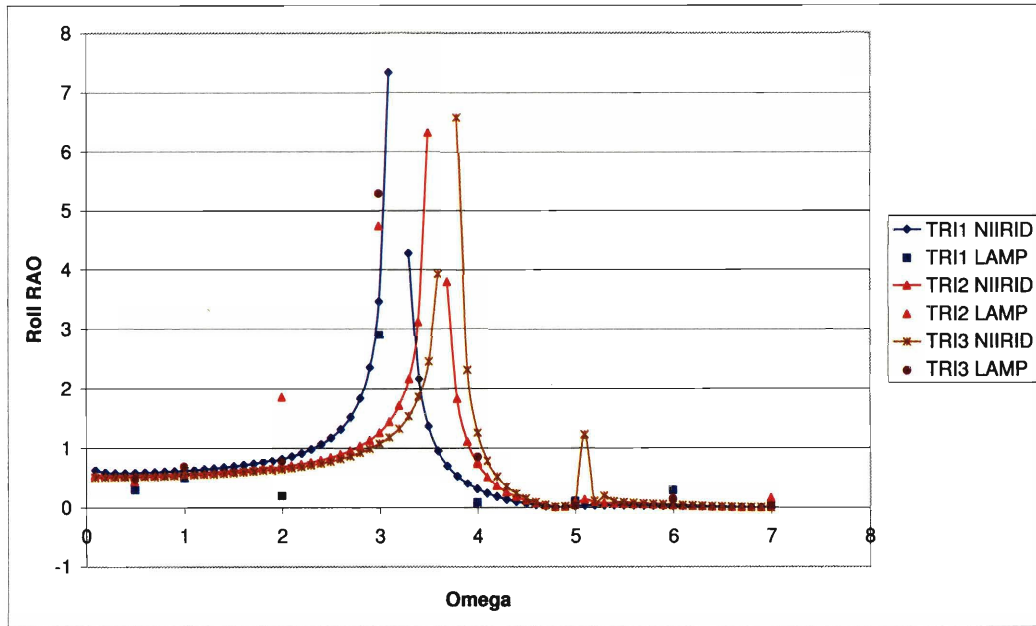


Figure B-27: LAMP-NIIRID Comparison for Trimarans: Roll RAO at  $F_n = 0.0$  and  $\mu = 150^\circ$

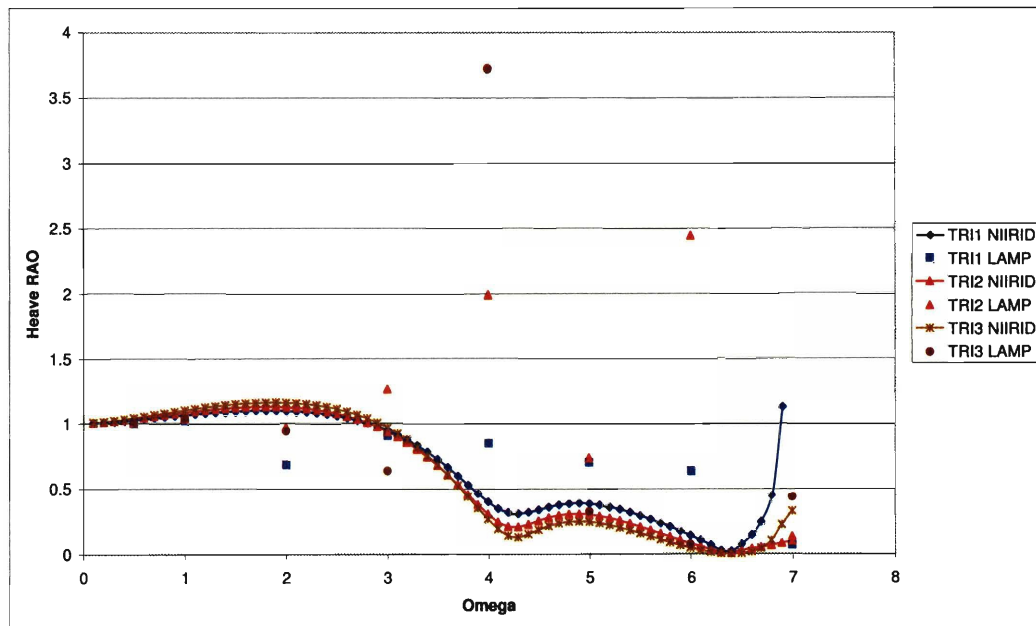


Figure B-28: LAMP-NIIRID Comparison for Trimarans: Heave RAO at  $F_n = 0.0$  and  $\mu = 120^\circ$

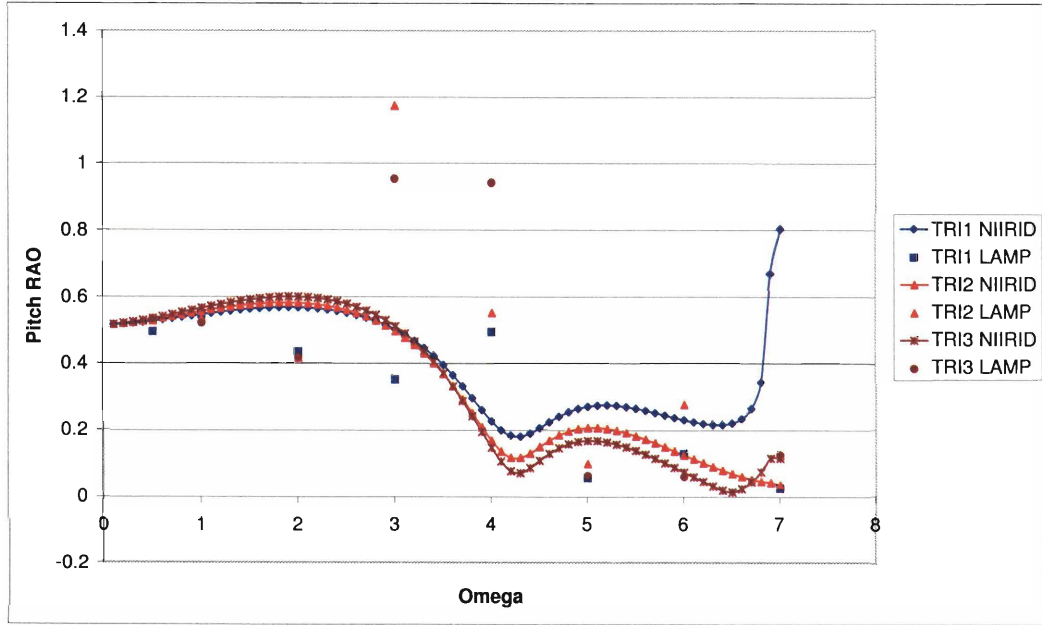


Figure B-29: LAMP-NIIRID Comparison for Trimarans: Pitch RAO at  $F_n = 0.0$  and  $\mu = 120^\circ$

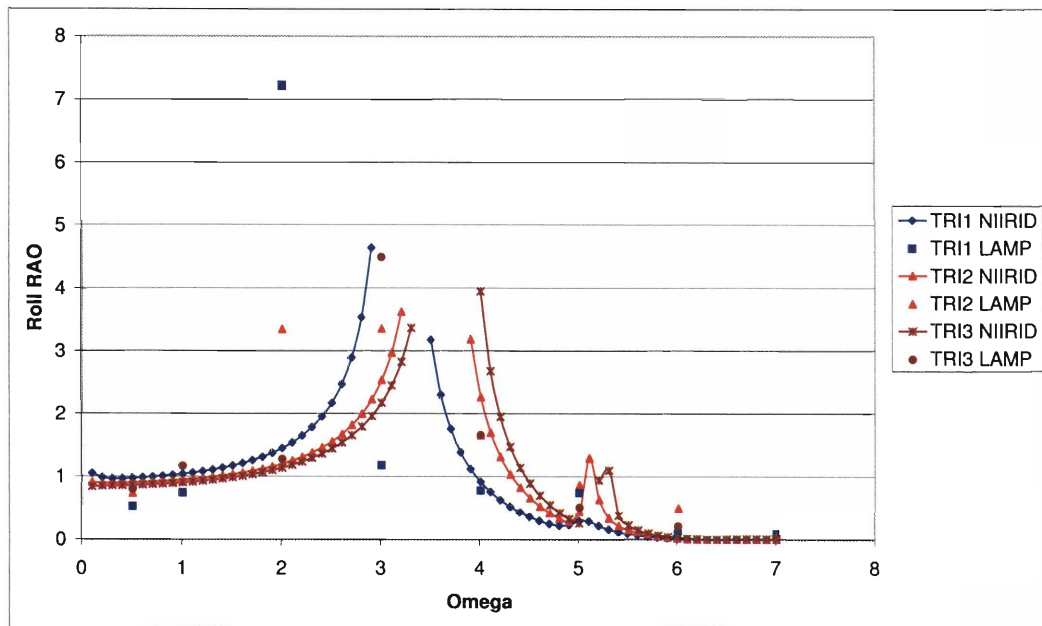


Figure B-30: LAMP-NIIRID Comparison for Trimarans: Roll RAO at  $F_n = 0.0$  and  $\mu = 120^\circ$

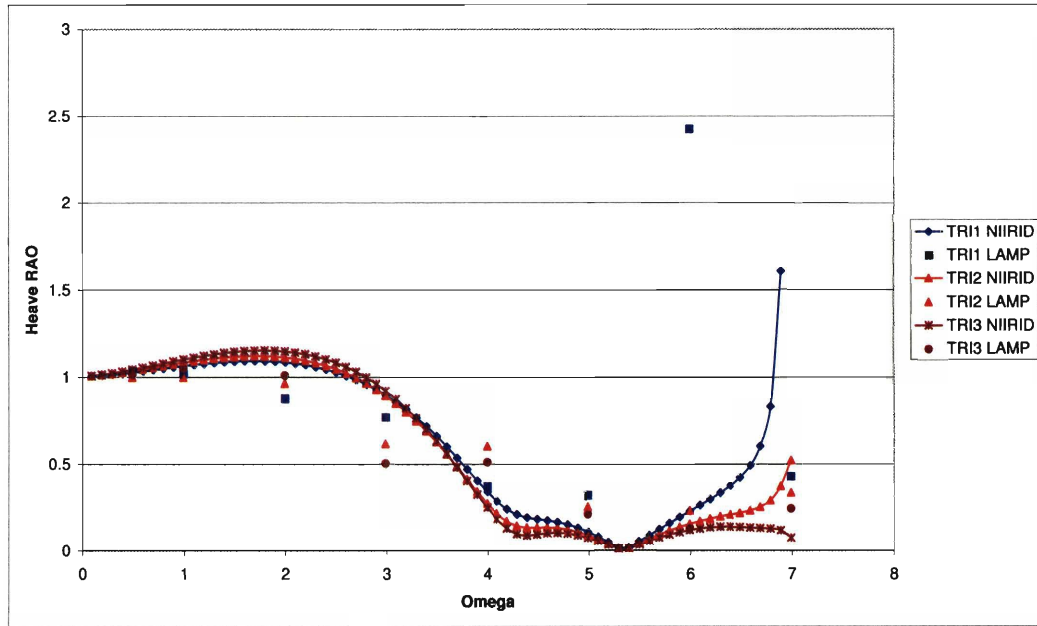


Figure B-31: LAMP-NIIRID Comparison for Trimarans: Heave RAO at  $F_n = 0.0$  and  $\mu = 45^\circ$

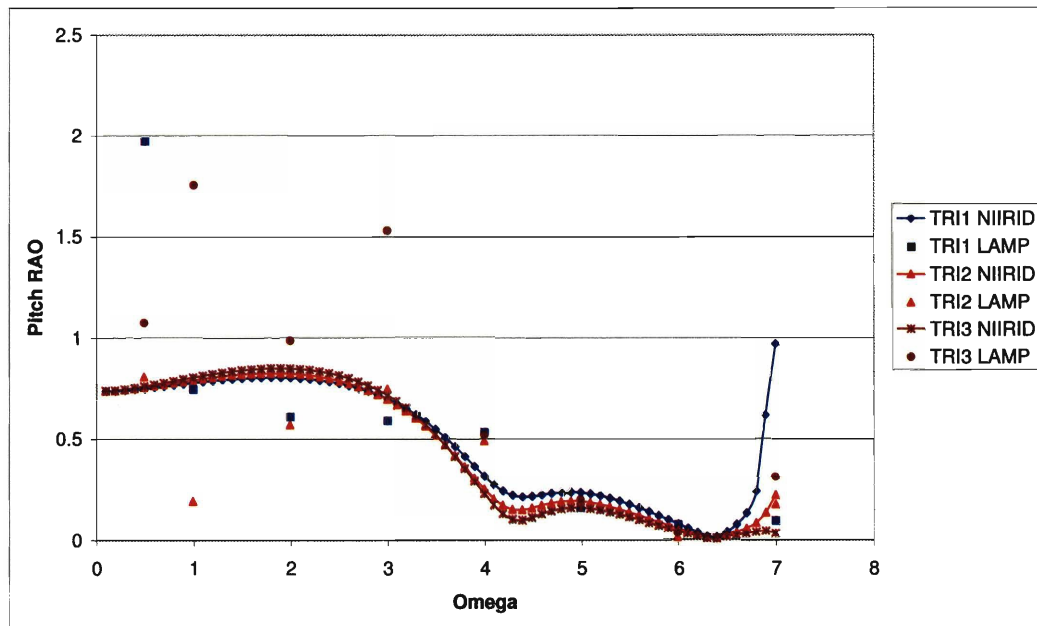


Figure B-32: LAMP-NIIRID Comparison for Trimarans: Pitch RAO at  $F_n = 0.0$  and  $\mu = 45^\circ$

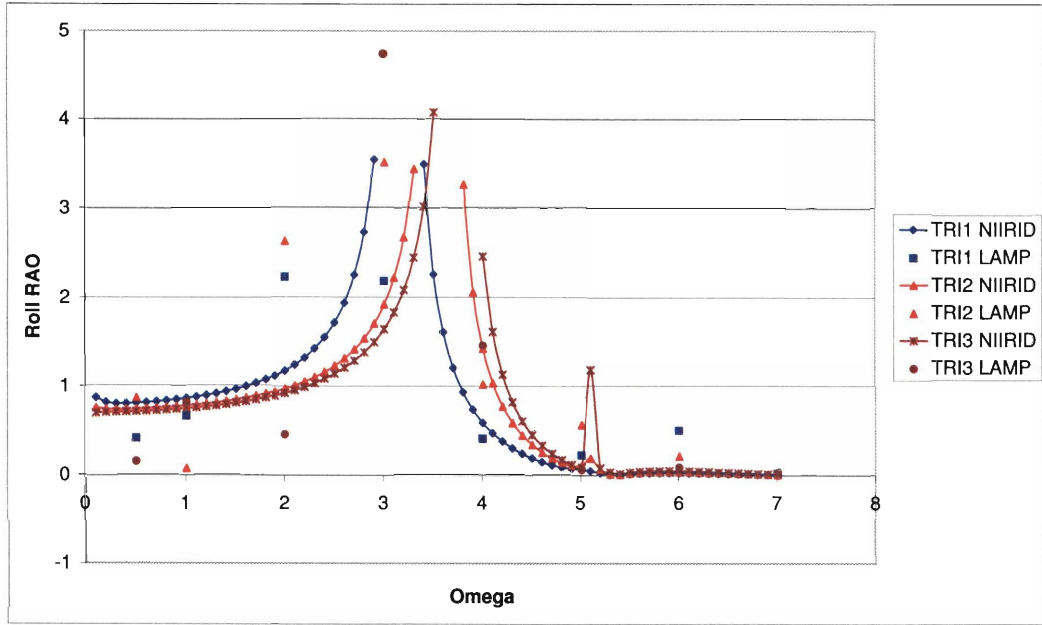


Figure B-33: LAMP-NIIRID Comparison for Trimarans: Roll RAO at  $F_n = 0.0$  and  $\mu = 45^\circ$

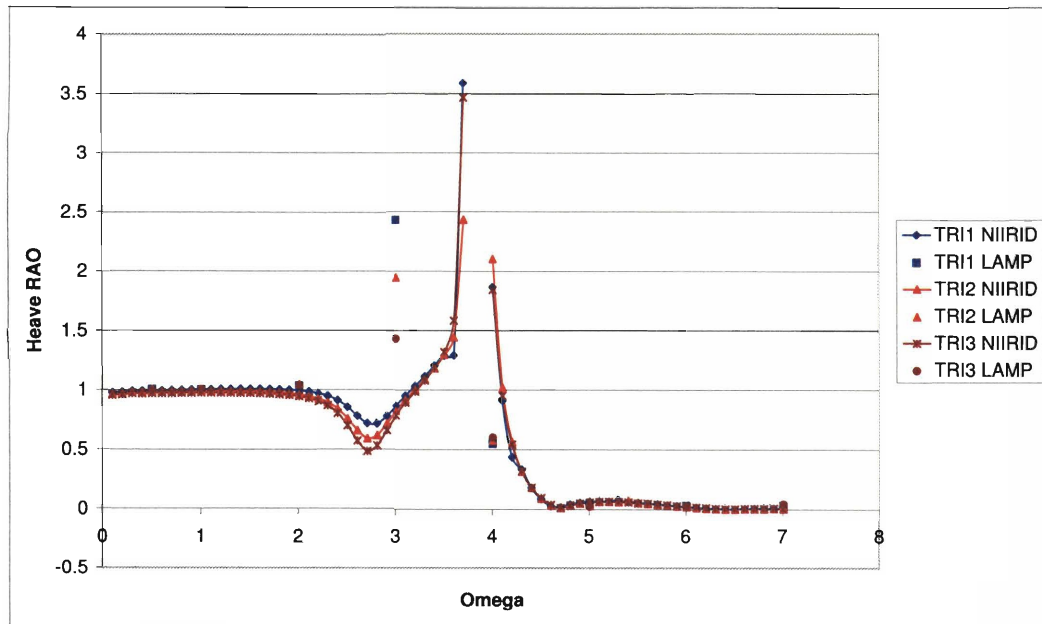


Figure B-34: LAMP-NIIRID Comparison for Trimarans: Heave RAO at  $F_n = 0.4$  and  $\mu = 180^\circ$



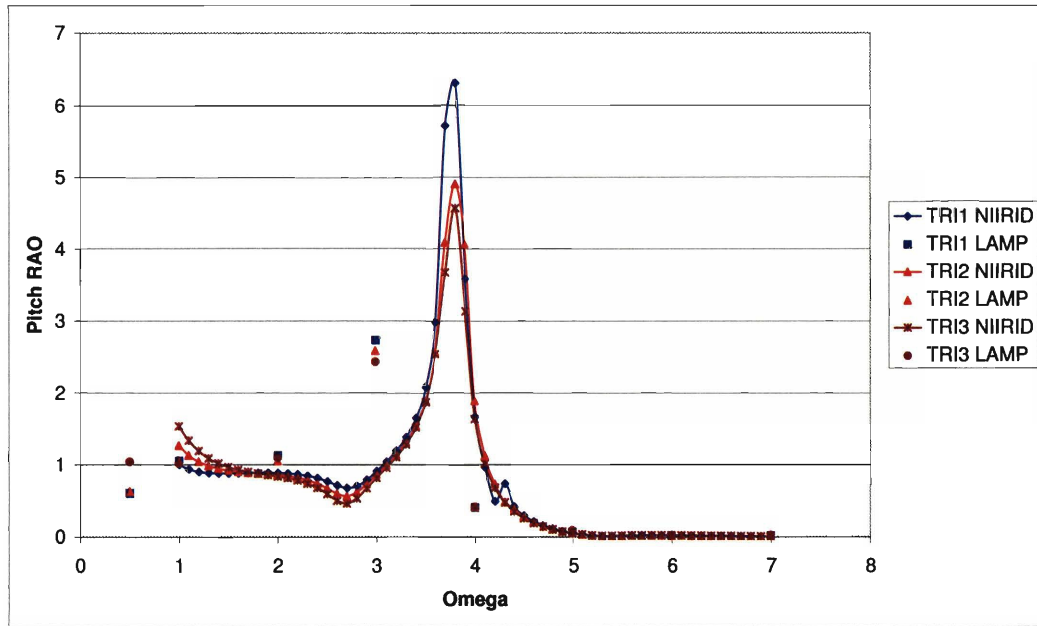


Figure B-35: LAMP-NIIRID Comparison for Trimarans: Pitch RAO at  $F_n = 0.4$  and  $\mu = 180^\circ$

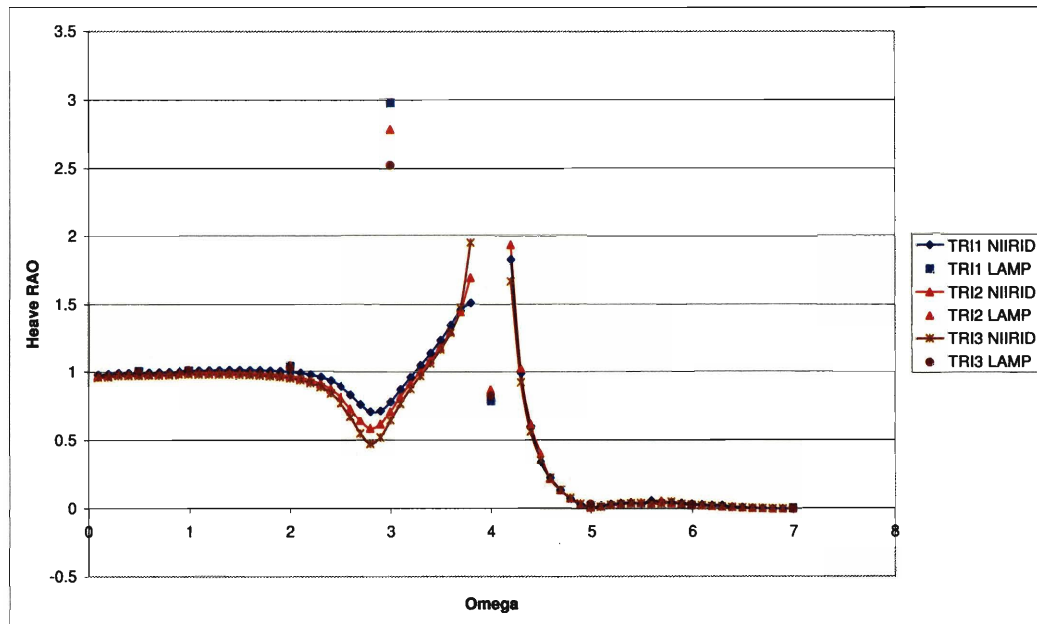


Figure B-36: LAMP-NIIRID Comparison for Trimarans: Heave RAO at  $F_n = 0.4$  and  $\mu = 150^\circ$

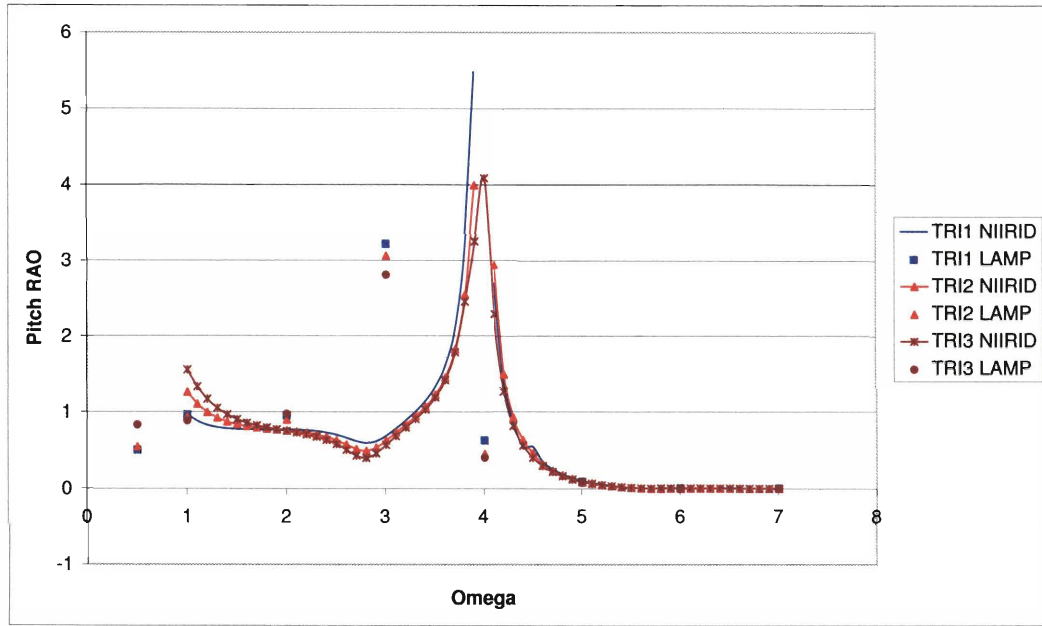


Figure B-37: LAMP-NIIRID Comparison for Trimarans: Pitch RAO at  $F_n = 0.4$  and  $\mu = 150^\circ$

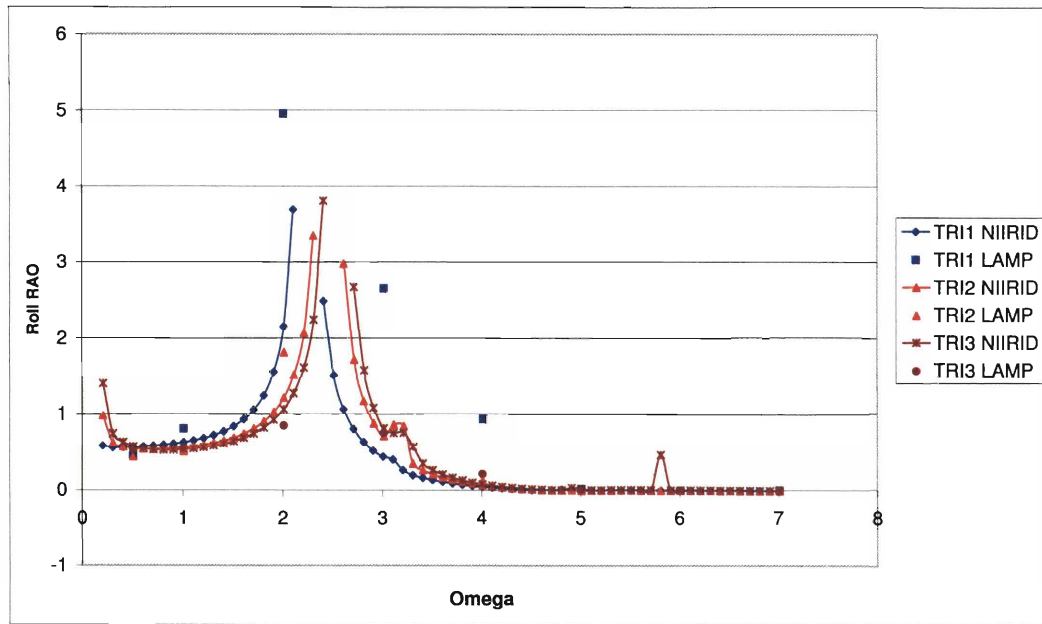


Figure B-38: LAMP-NIIRID Comparison for Trimarans: Roll RAO at  $F_n = 0.4$  and  $\mu = 150^\circ$

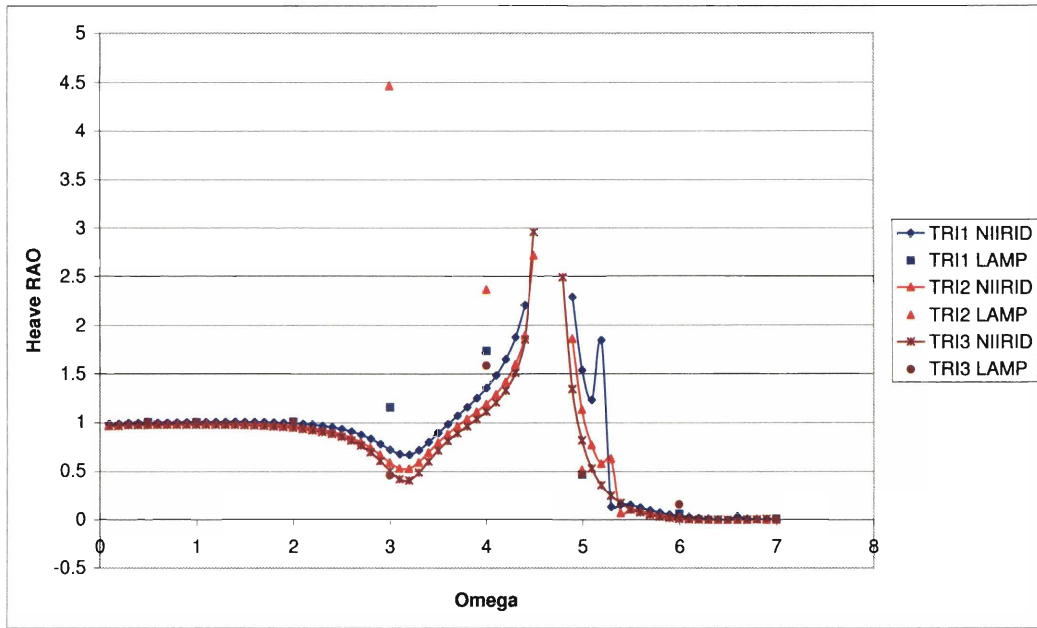


Figure B-39: LAMP-NIIRID Comparison for Trimarans: Heave RAO at  $F_n = 0.4$  and  $\mu = 120^\circ$

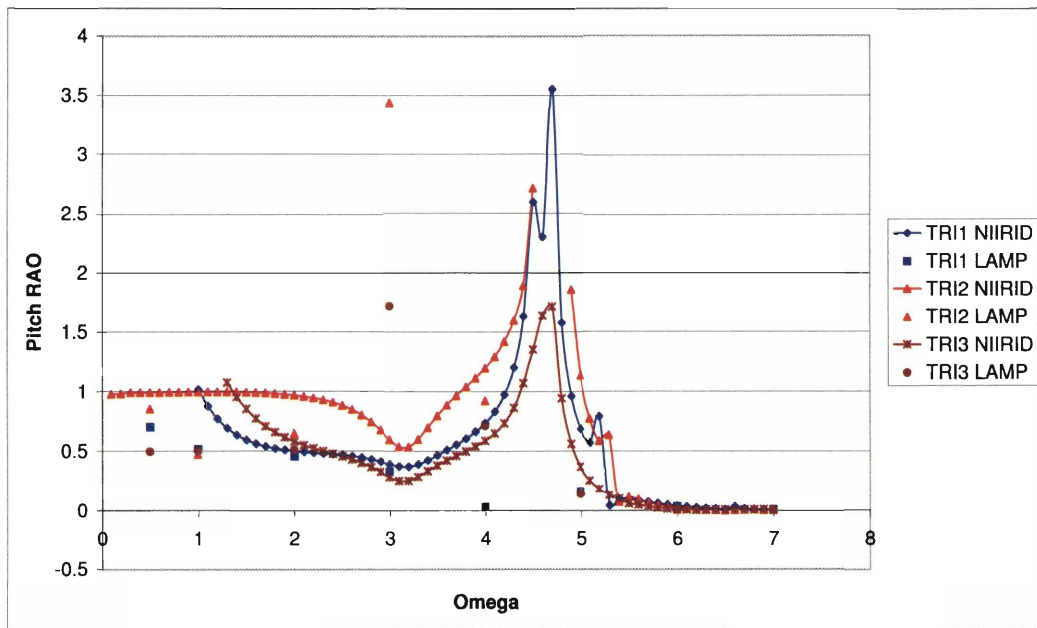


Figure B-40: LAMP-NIIRID Comparison for Trimarans: Pitch RAO at  $F_n = 0.4$  and  $\mu = 120^\circ$

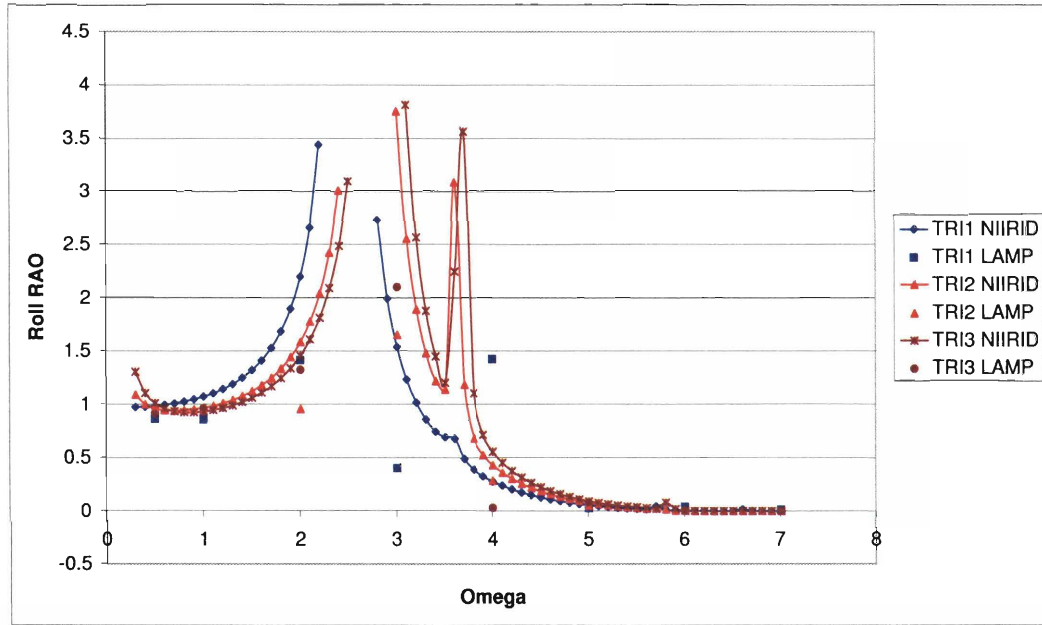


Figure B-41: LAMP-NIIRID Comparison for Trimarans: Roll RAO at  $F_n = 0.4$  and  $\mu = 120^\circ$

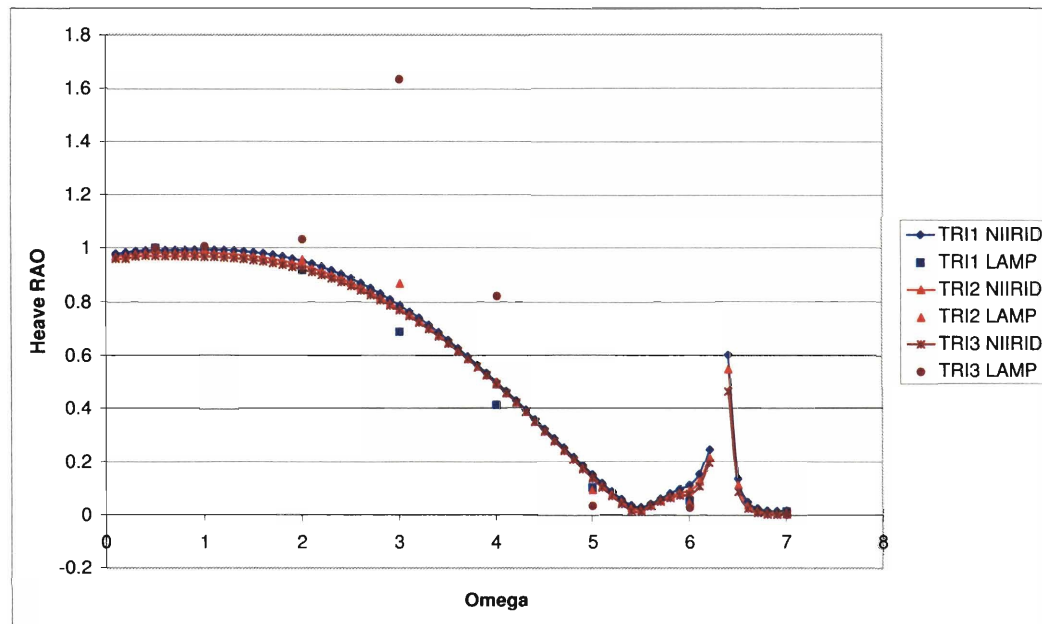


Figure B-42: LAMP-NIIRID Comparison for Trimarans: Heave RAO at  $F_n = 0.4$  and  $\mu = 45^\circ$

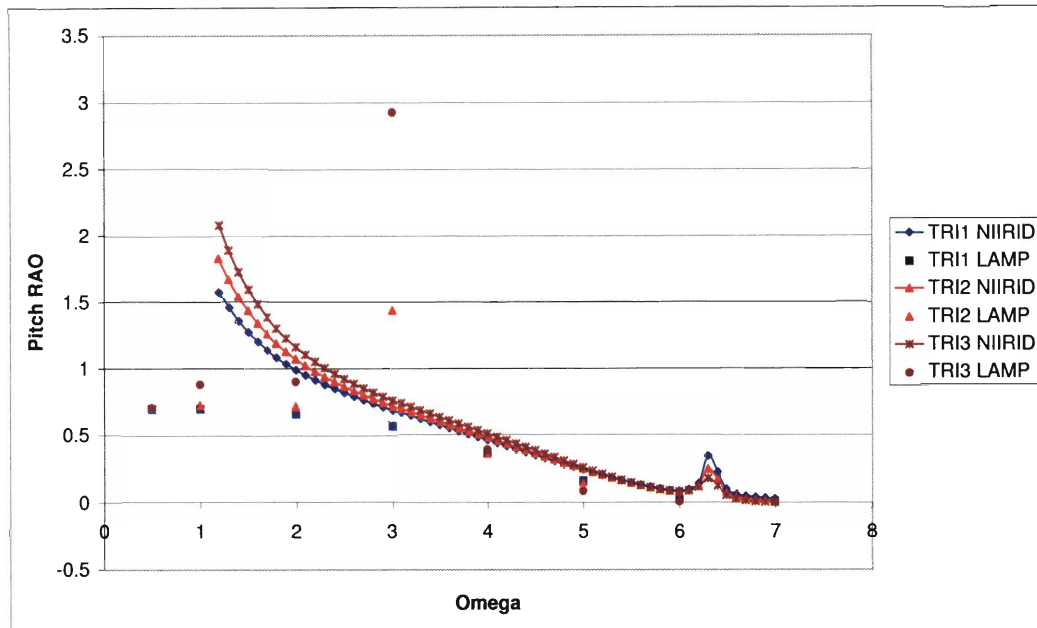


Figure B-43: LAMP-NIIRID Comparison for Trimarans: Pitch RAO at  $F_n = 0.4$  and  $\mu = 45^\circ$

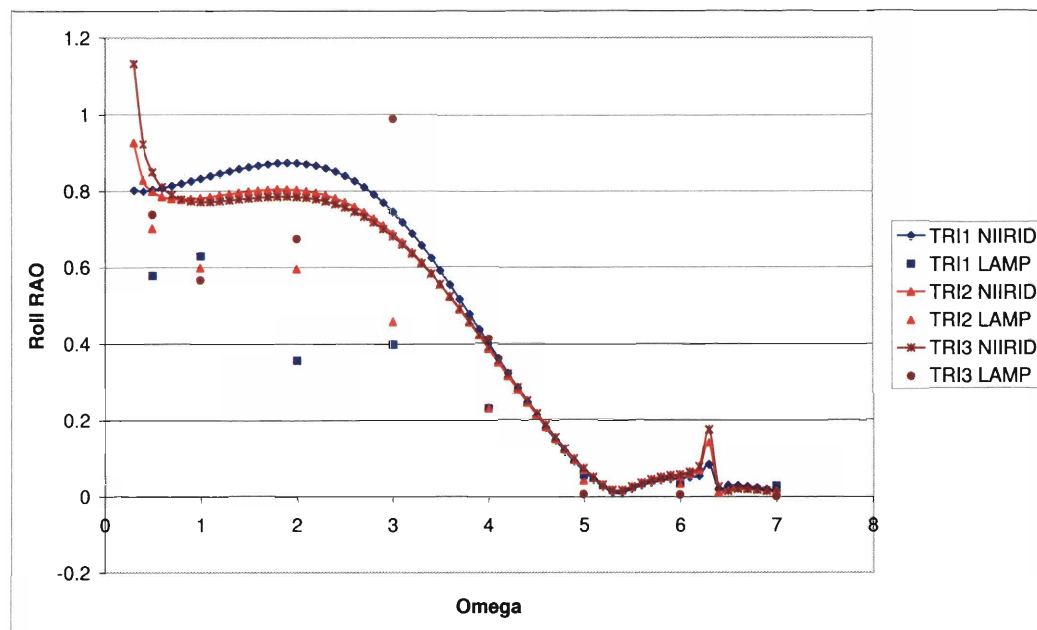


Figure B-44: LAMP-NIIRID Comparison for Trimarans: Roll RAO at  $F_n = 0.4$  and  $\mu = 45^\circ$



# Appendix C

## Case Study Results

A total of nine catamarans and fifteen trimarans were analyzed in the case study. Each vessel was tested in regular waves at an incident wave angle of 180, 150, 120, and 45 degrees at a Froude number  $F_n = 0.0$  and  $F_n = 0.4$ . These values were selected to have a complete overall picture of the vessel response both at zero and forward speed. The RAOs in heave, pitch, and roll were calculated for each case. NIIRID was used to compute the sectional hydrodynamic coefficients and forces. The notation used in the figures is as explained in Section 2.8.

## C.1 Catamarans

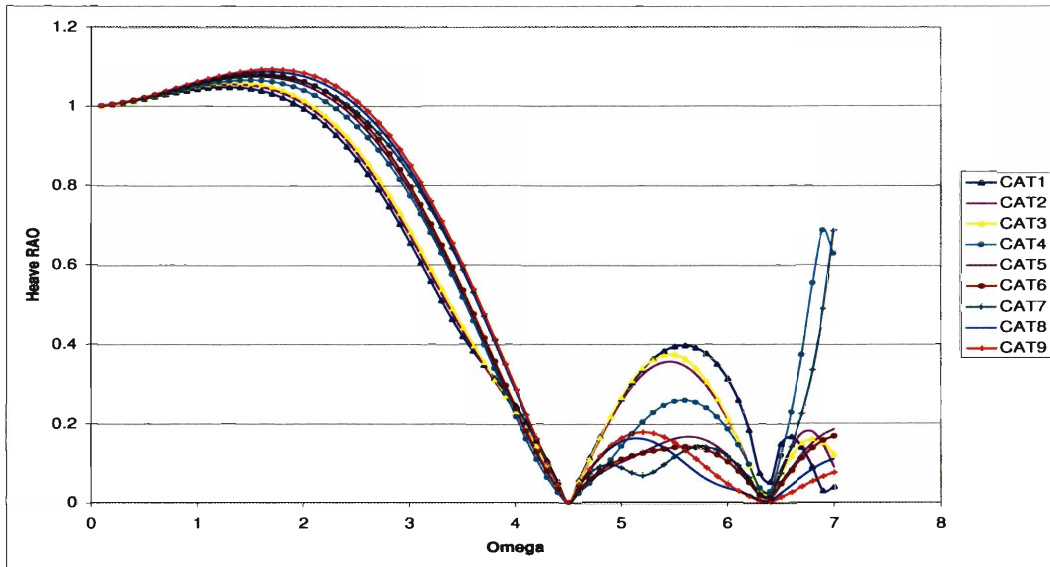


Figure C-1: Case Study Analysis of Catamaran Geometries: Heave RAO at  $F_n = 0$  and  $\mu = 180^\circ$

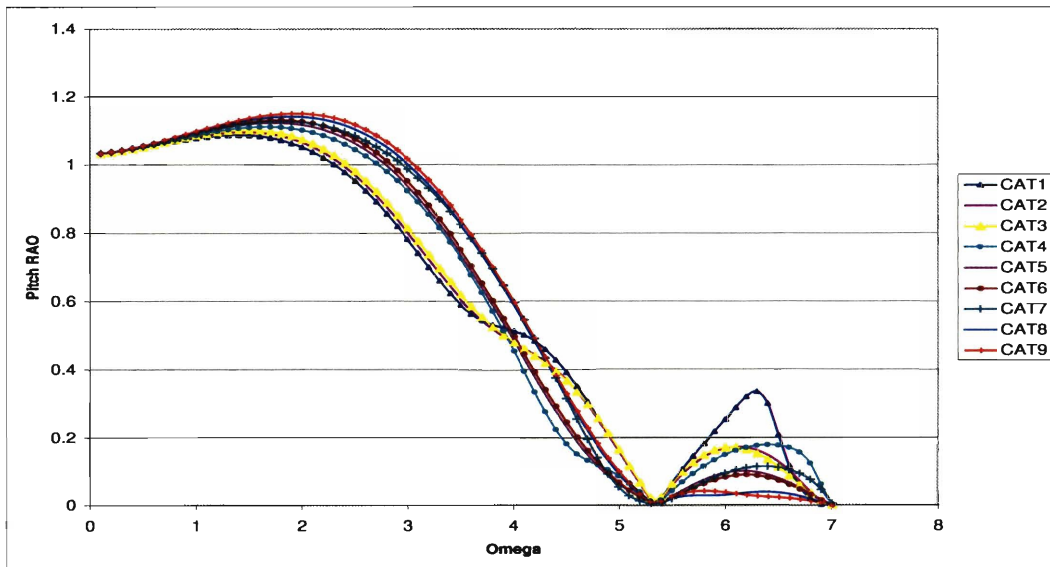


Figure C-2: Case Study Analysis of Catamaran Geometries: Pitch RAO at  $F_n = 0$  and  $\mu = 180^\circ$



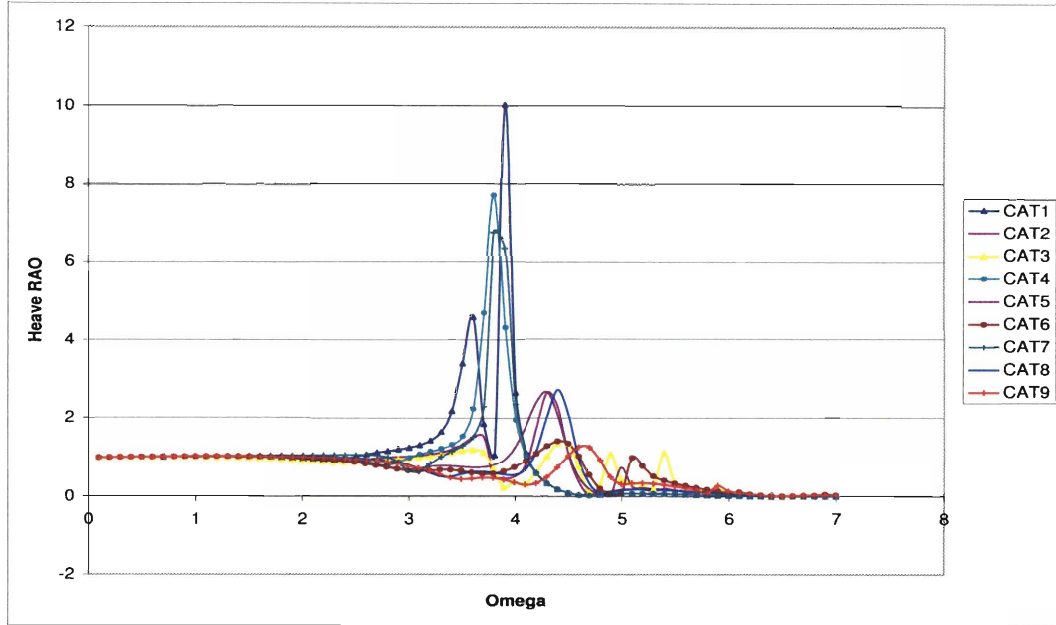


Figure C-3: Case Study Analysis of Catamaran Geometries: Heave RAO at  $F_n = 0.4$  and  $\mu = 180^\circ$

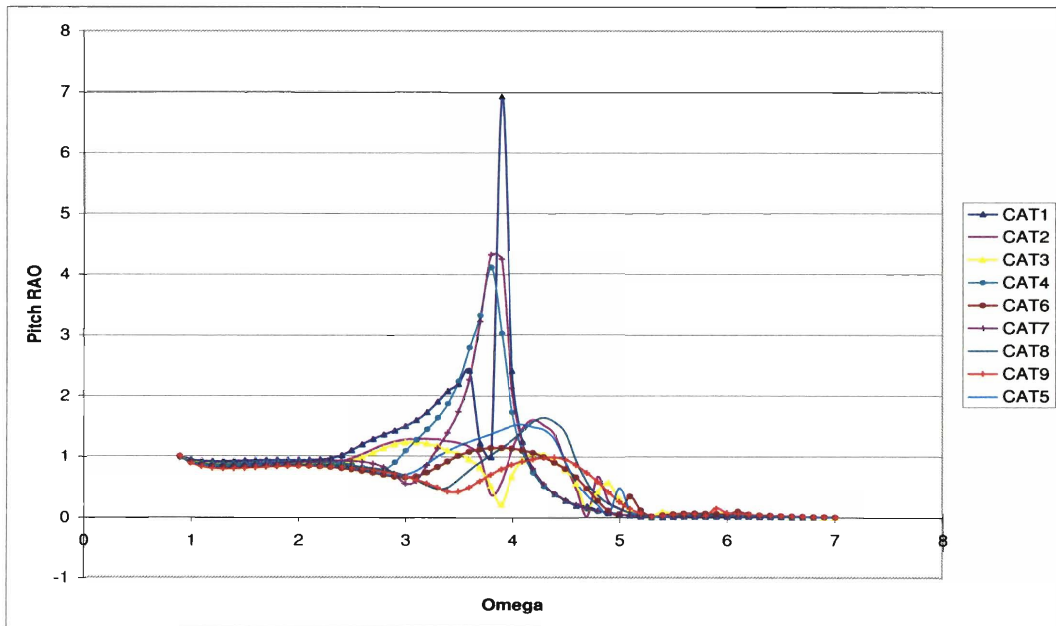


Figure C-4: Case Study Analysis of Catamaran Geometries: Heave RAO at  $F_n = 0.4$  and  $\mu = 180^\circ$

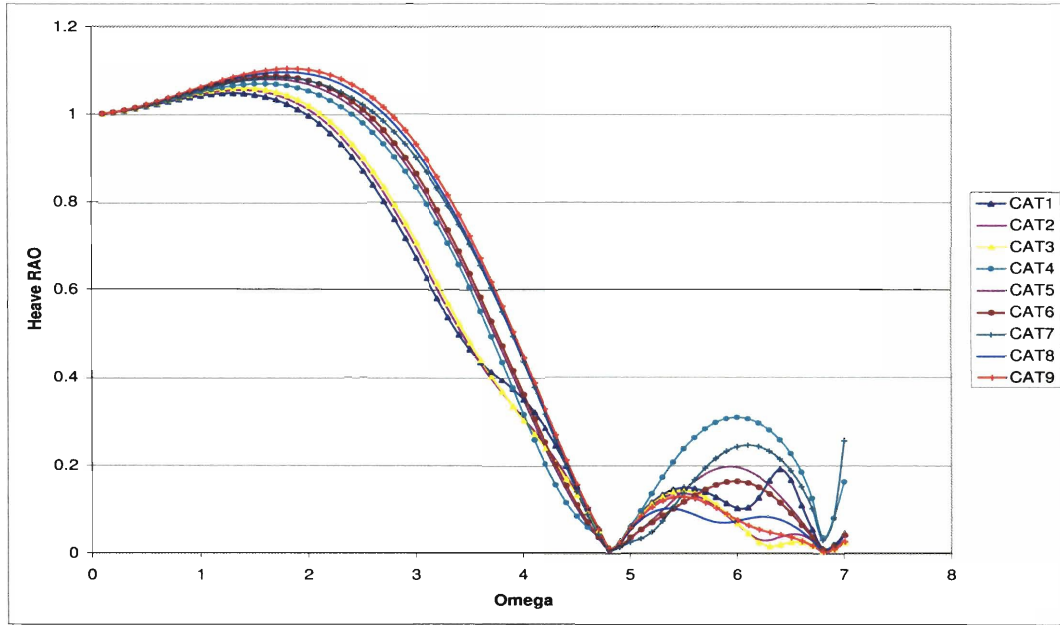


Figure C-5: Case Study Analysis of Catamaran Geometries: Heave RAO at  $F_n = 0$  and  $\mu = 150^\circ$

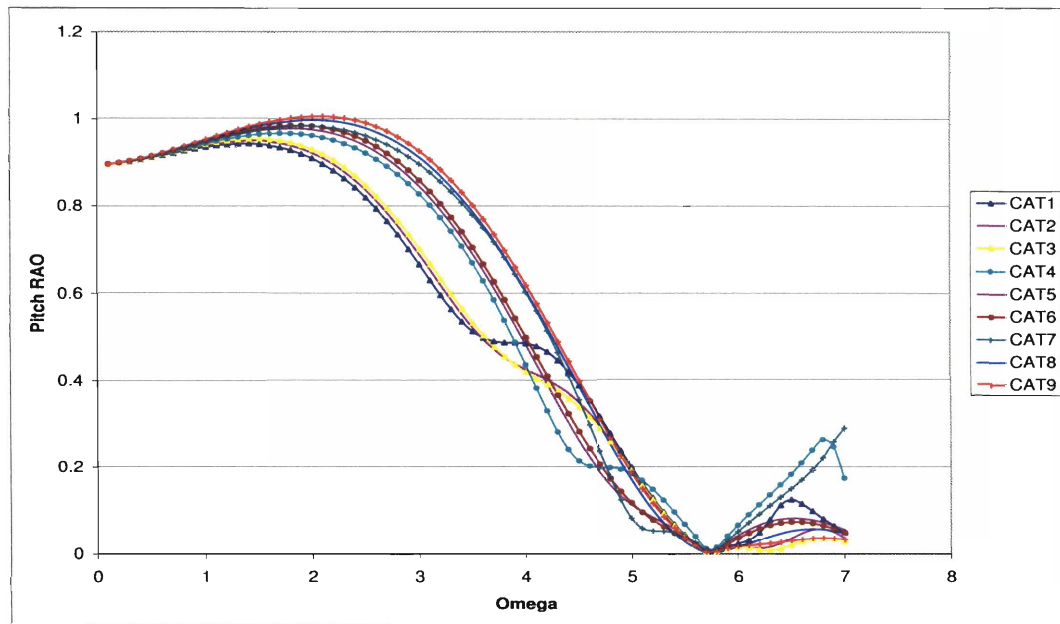


Figure C-6: Case Study Analysis of Catamaran Geometries: Pitch RAO at  $F_n = 0$  and  $\mu = 150^\circ$

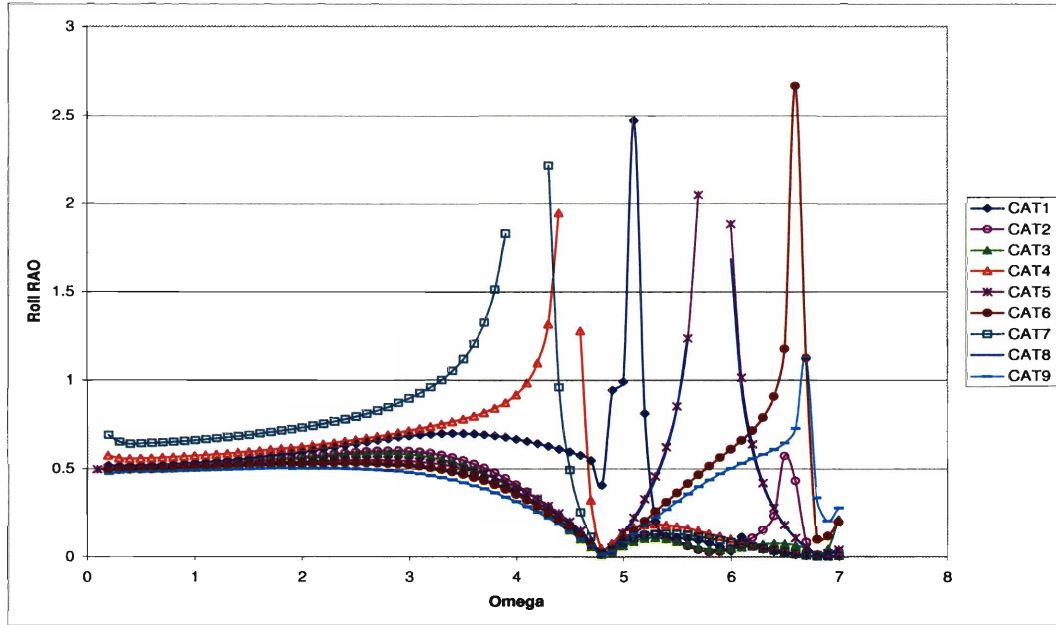


Figure C-7: Case Study Analysis of Catamaran Geometries: Roll RAO at  $F_n = 0$  and  $\mu = 150^\circ$

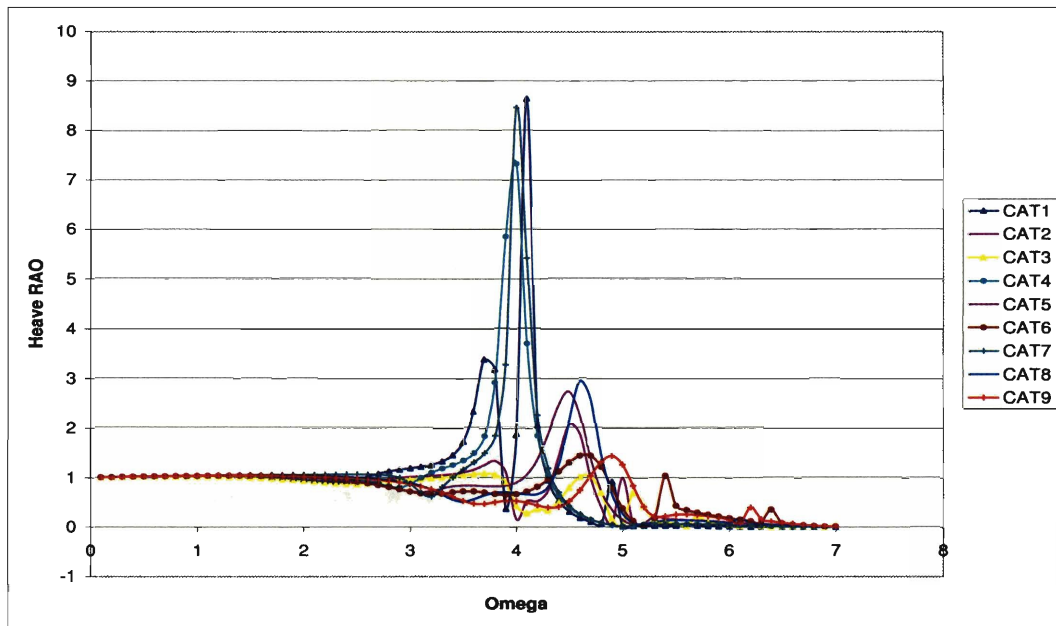


Figure C-8: Case Study Analysis of Catamaran Geometries: Heave RAO at  $F_n = 0.4$  and  $\mu = 150^\circ$

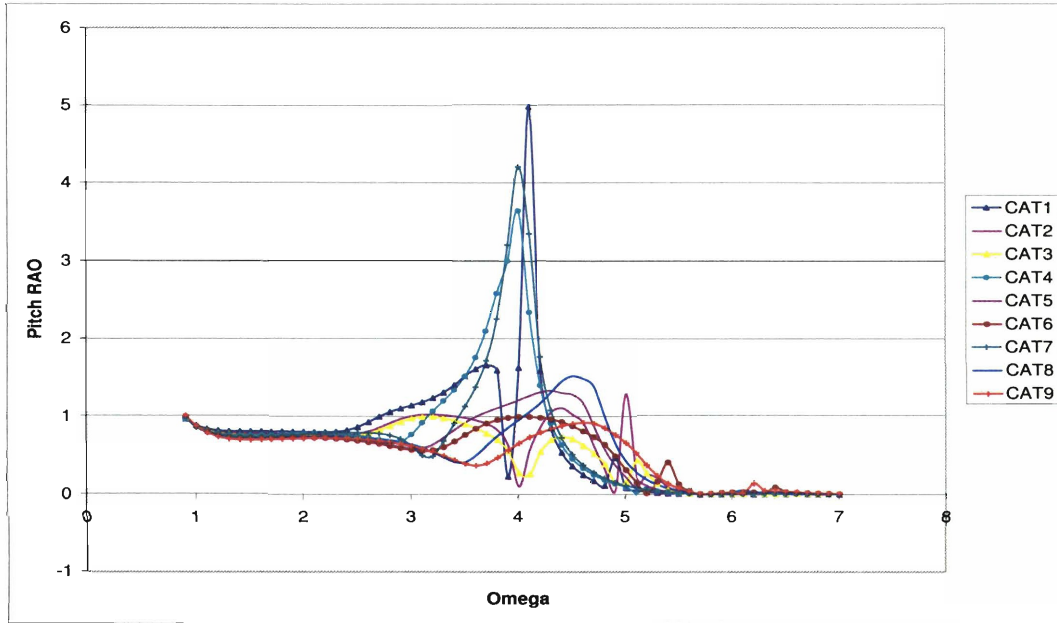


Figure C-9: Case Study Analysis of Catamaran Geometries: Pitch RAO at  $F_n = 0.4$  and  $\mu = 150^\circ$

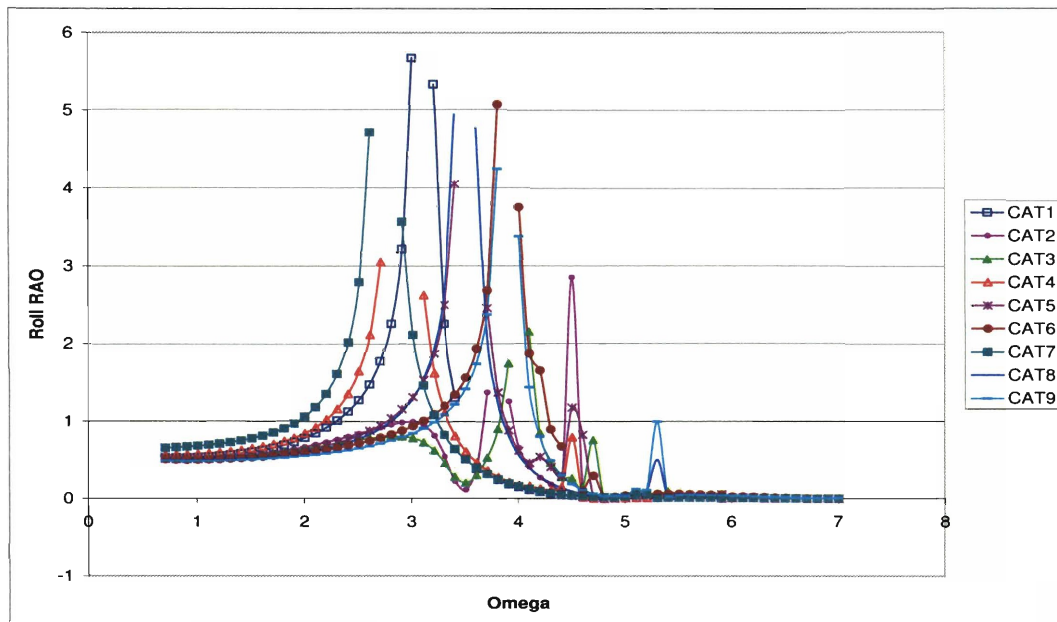


Figure C-10: Case Study Analysis of Catamaran Geometries: Roll RAO at  $F_n = 0.4$  and  $\mu = 150^\circ$

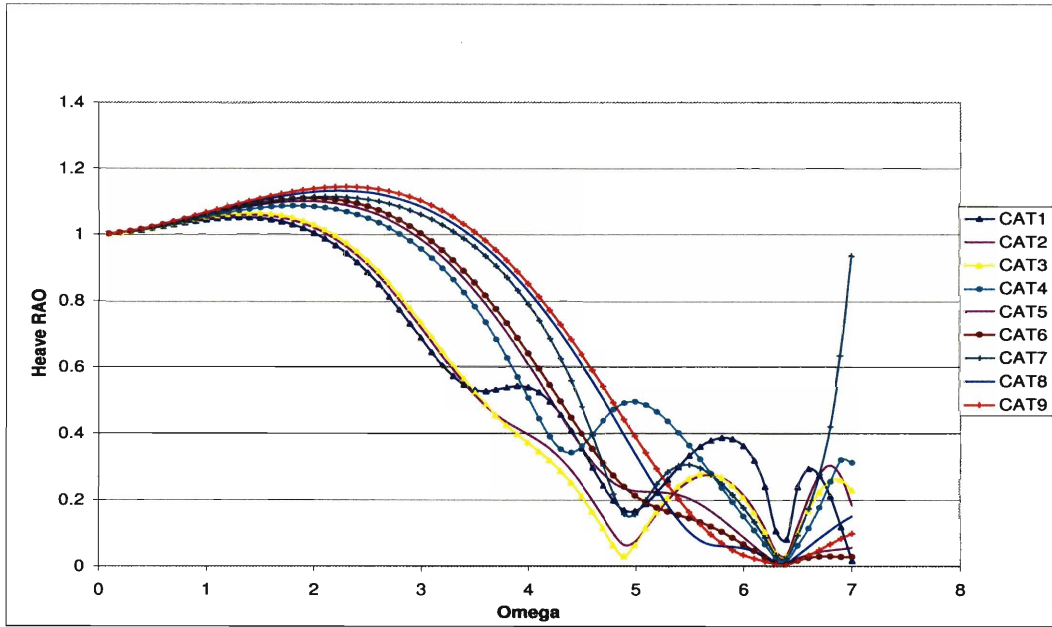


Figure C-11: Case Study Analysis of Catamaran Geometries: Heave RAO at  $F_n = 0$  and  $\mu = 120^\circ$

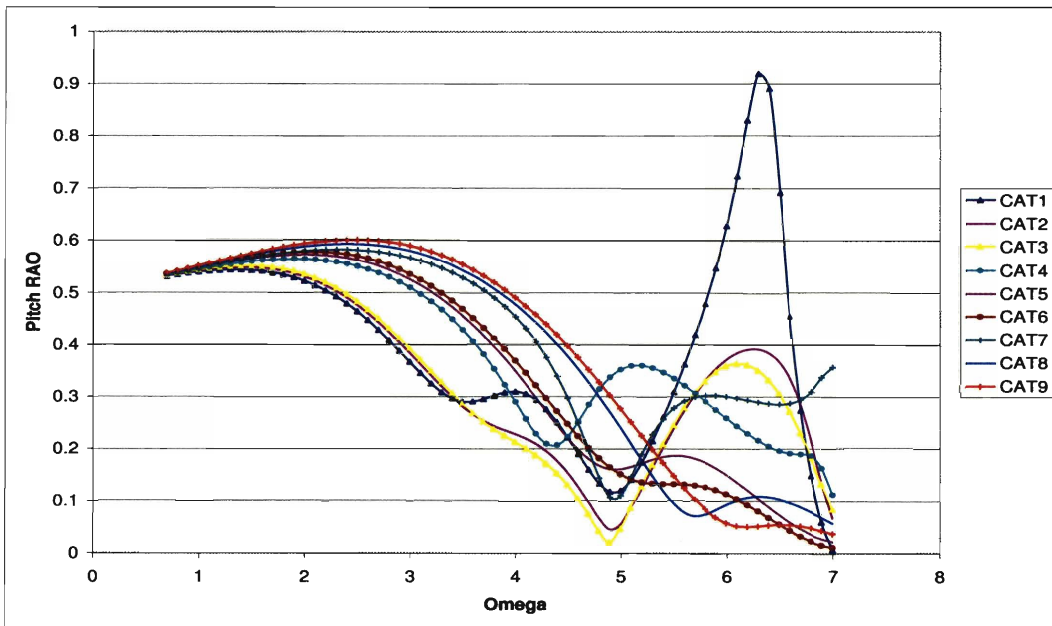


Figure C-12: Case Study Analysis of Catamaran Geometries: Pitch RAO at  $F_n = 0$  and  $\mu = 120^\circ$

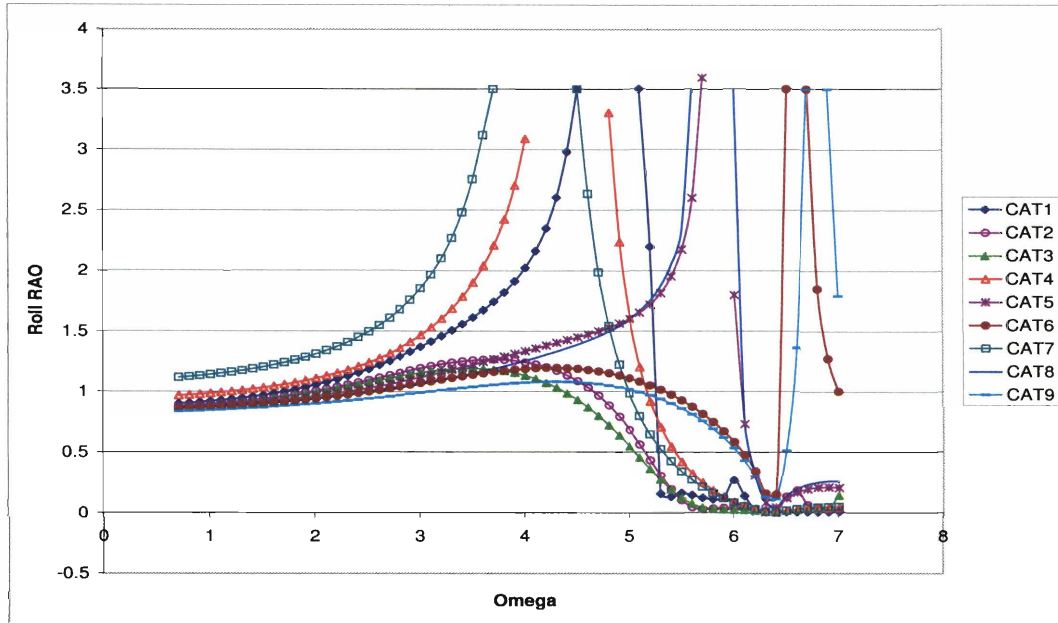


Figure C-13: Case Study Analysis of Catamaran Geometries: Roll RAO at  $F_n = 0$  and  $\mu = 120^\circ$

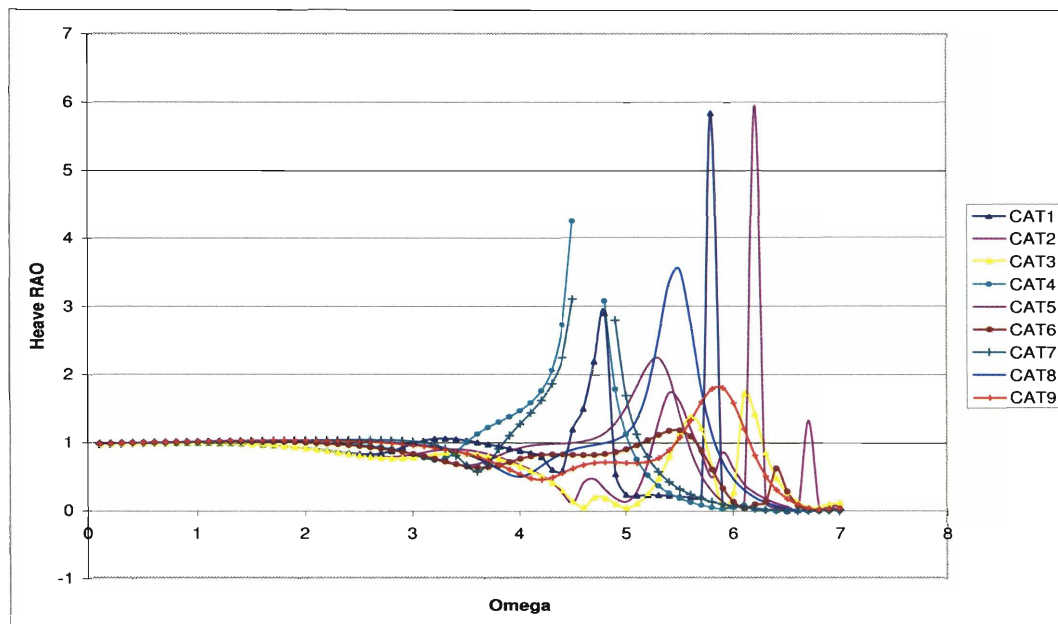


Figure C-14: Case Study Analysis of Catamaran Geometries: Heave RAO at  $F_n = 0.4$  and  $\mu = 120^\circ$

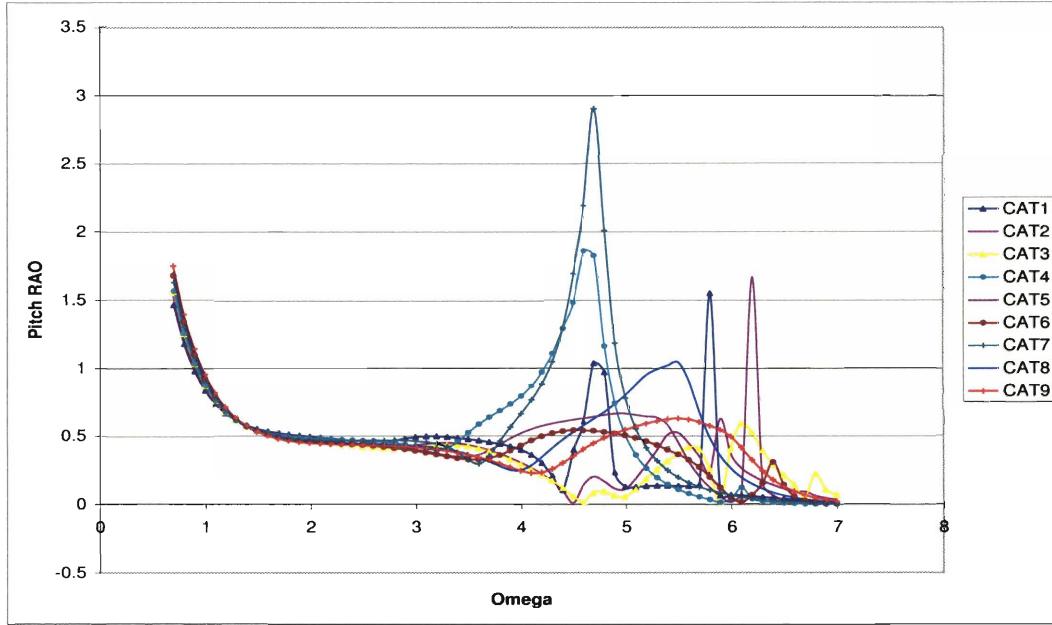


Figure C-15: Case Study Analysis of Catamaran Geometries: Pitch RAO at  $F_n = 0.4$  and  $\mu = 120^\circ$

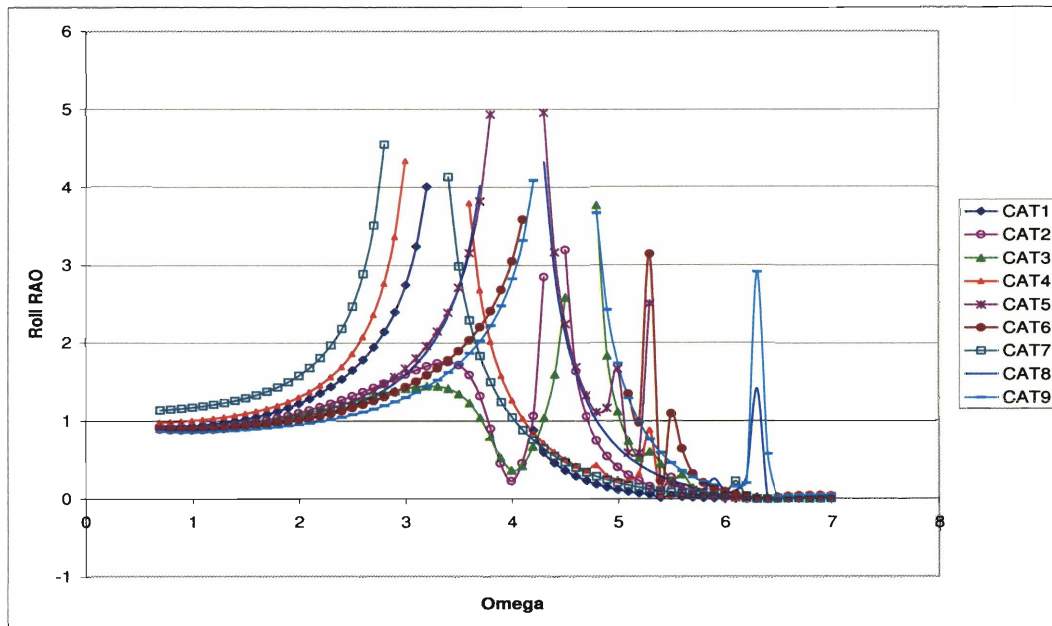


Figure C-16: Case Study Analysis of Catamaran Geometries: Roll RAO at  $F_n = 0.4$  and  $\mu = 120^\circ$

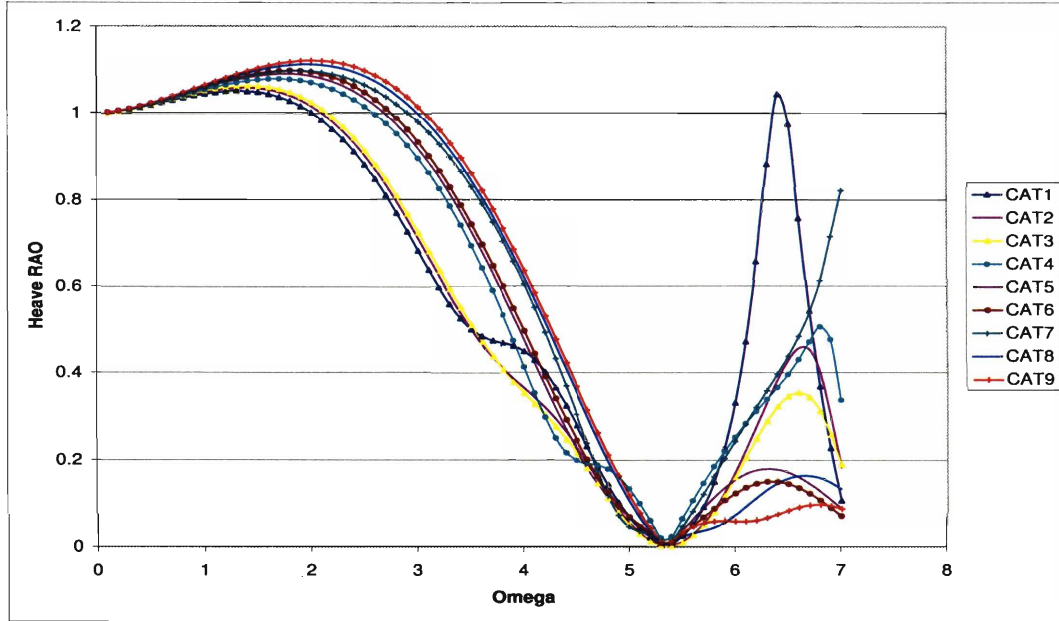


Figure C-17: Case Study Analysis of Catamaran Geometries: Heave RAO at  $F_n = 0$  and  $\mu = 45^\circ$

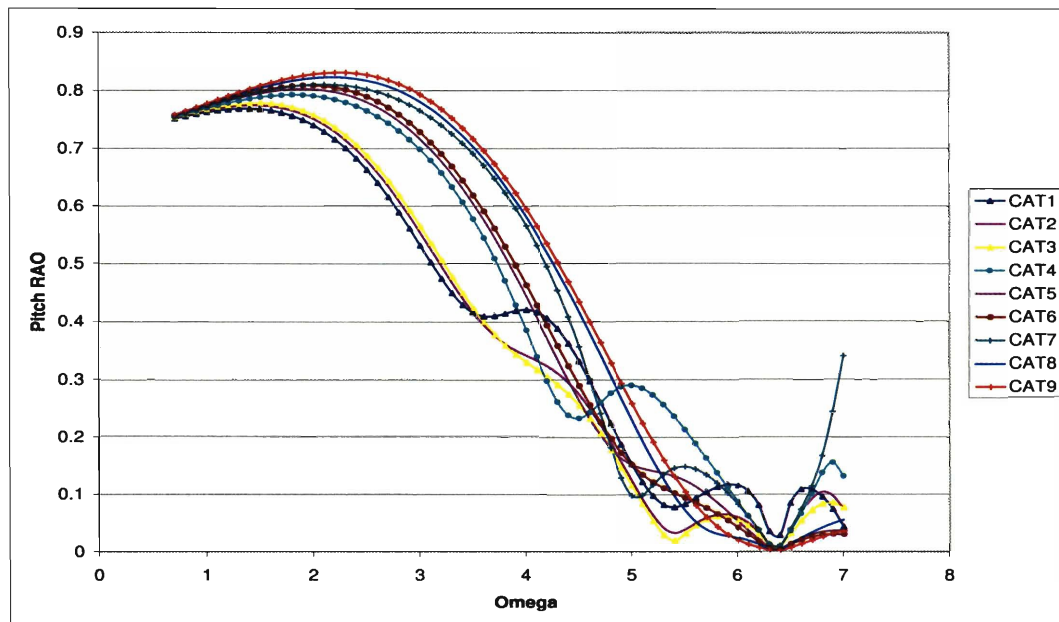


Figure C-18: Case Study Analysis of Catamaran Geometries: Pitch RAO at  $F_n = 0$  and  $\mu = 45^\circ$



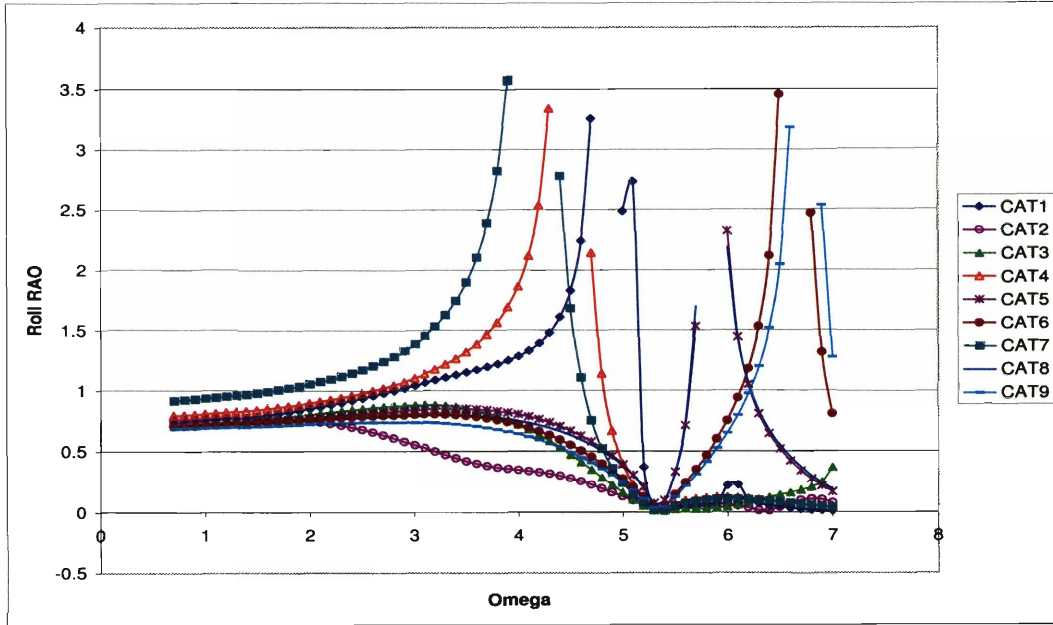


Figure C-19: Case Study Analysis of Catamaran Geometries: Roll RAO at  $F_n = 0$  and  $\mu = 45^\circ$

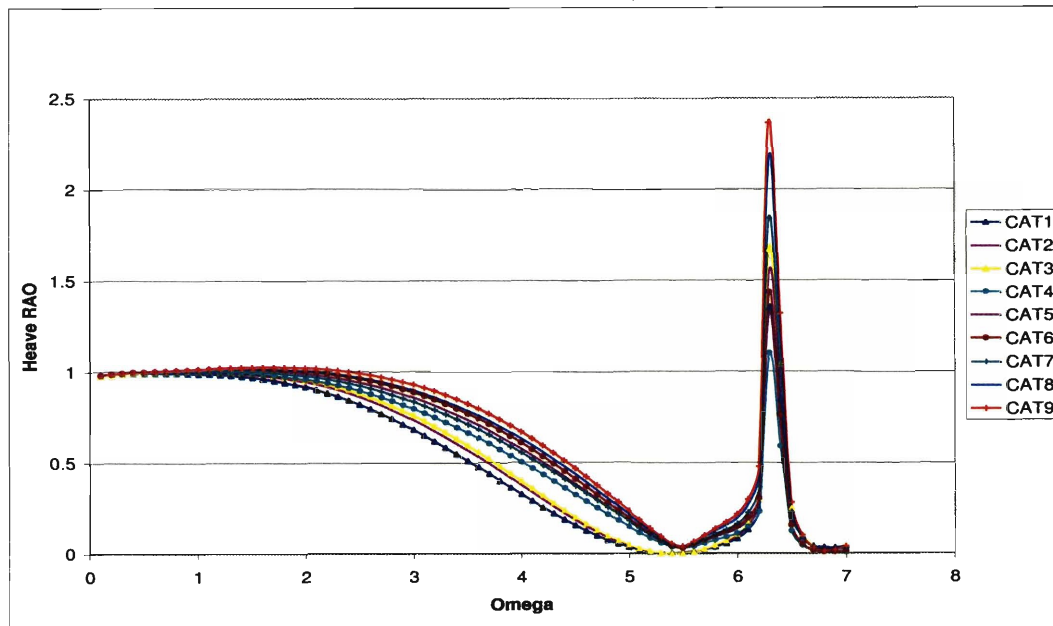


Figure C-20: Case Study Analysis of Catamaran Geometries: Heave RAO at  $F_n = 0.4$  and  $\mu = 45^\circ$

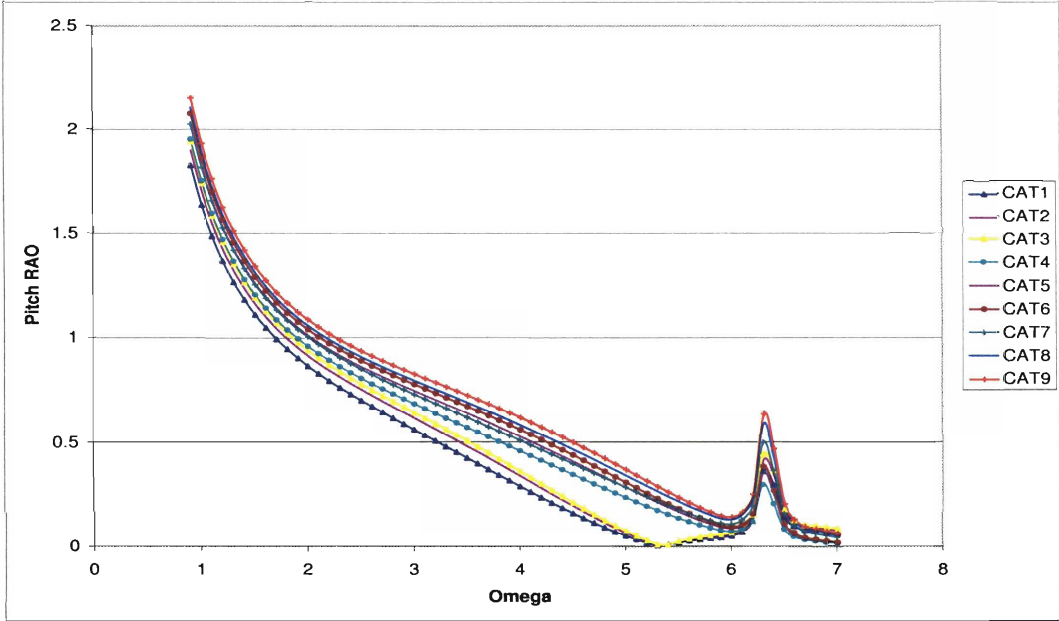


Figure C-21: Case Study Analysis of Catamaran Geometries: Pitch RAO at  $F_n = 0.4$  and  $\mu = 45^\circ$

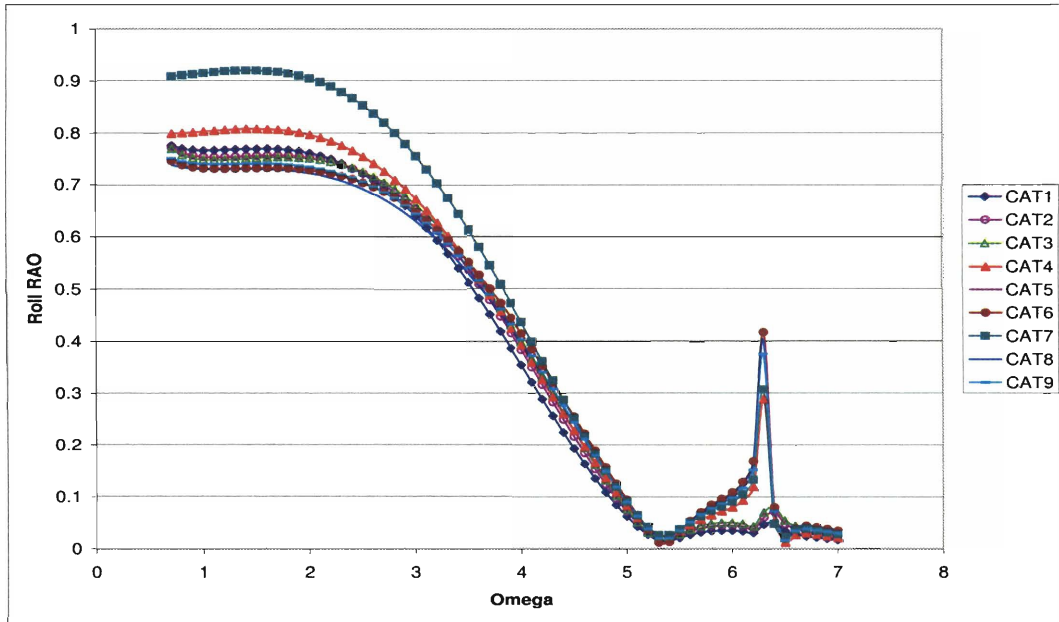


Figure C-22: Case Study Analysis of Catamaran Geometries: Roll RAO at  $F_n = 0.4$  and  $\mu = 45^\circ$

## C.2 Trimarans

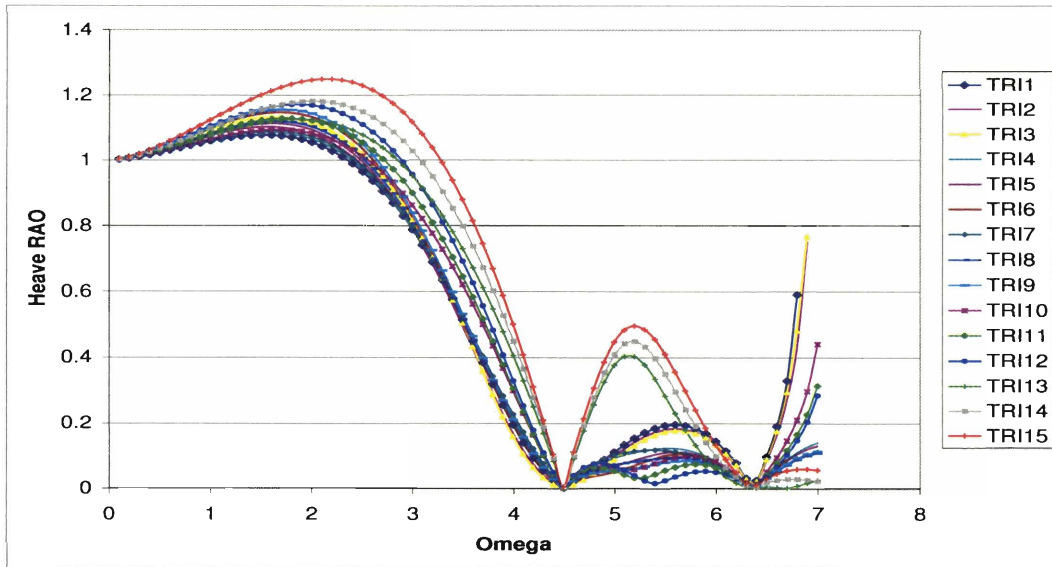


Figure C-23: Case Study Analysis of Trimaran Geometries: Heave RAO at  $F_n = 0$  and  $\mu = 180^\circ$

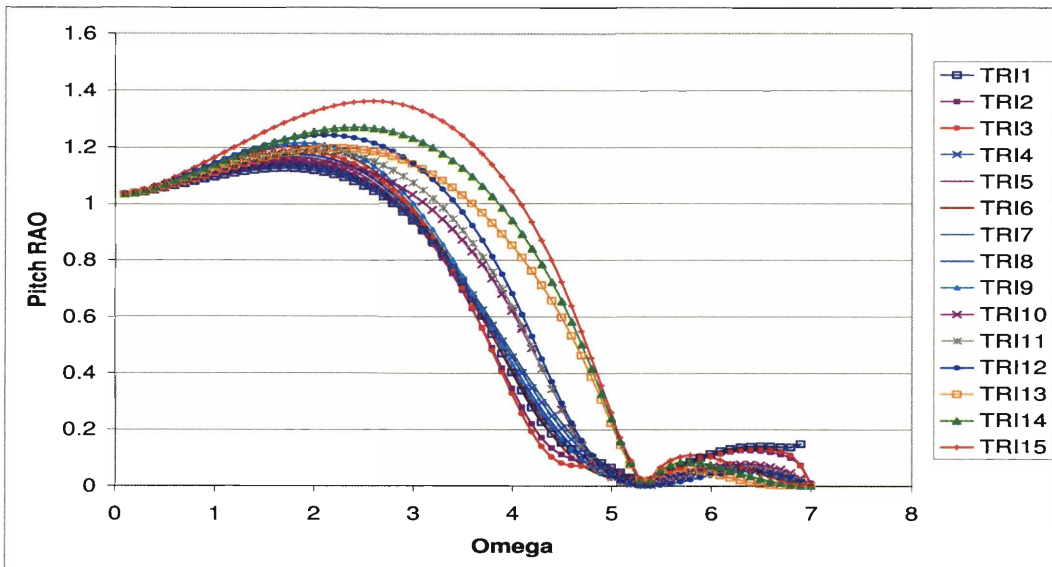


Figure C-24: Case Study Analysis of Trimaran Geometries: Pitch RAO at  $F_n = 0$  and  $\mu = 180^\circ$

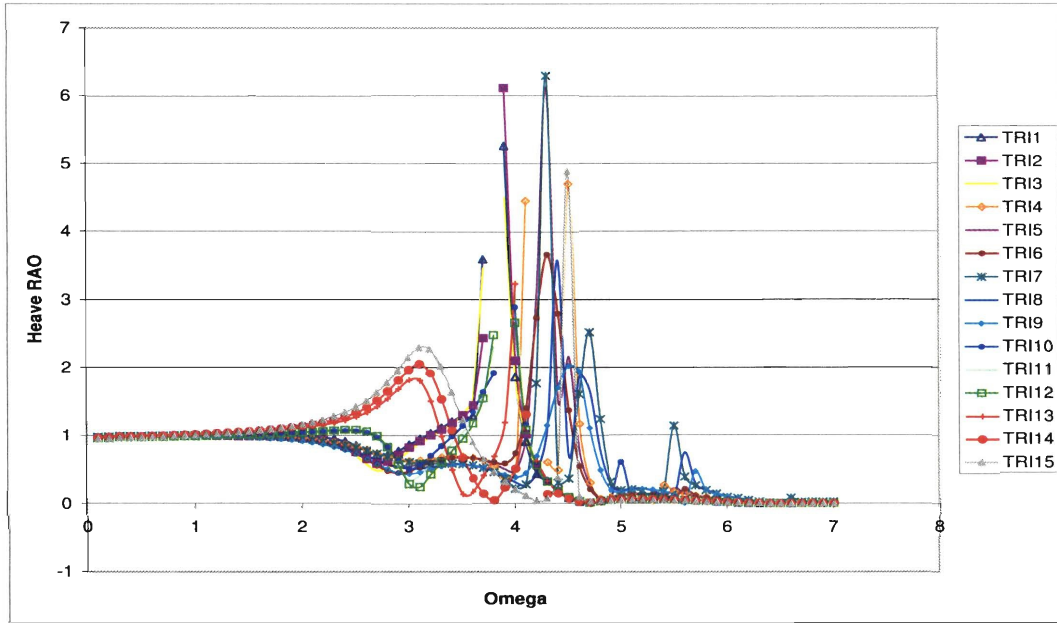


Figure C-25: Case Study Analysis of Trimaran Geometries: Heave RAO at  $F_n = 0.4$  and  $\mu = 180^\circ$

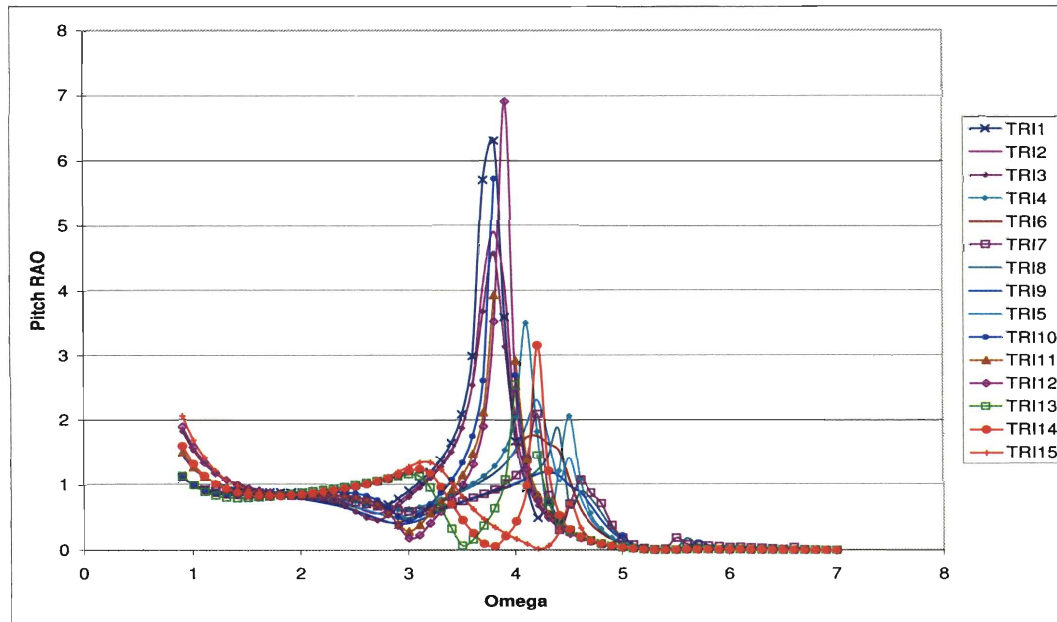


Figure C-26: Case Study Analysis of Trimaran Geometries: Heave RAO at  $F_n = 0.4$  and  $\mu = 180^\circ$

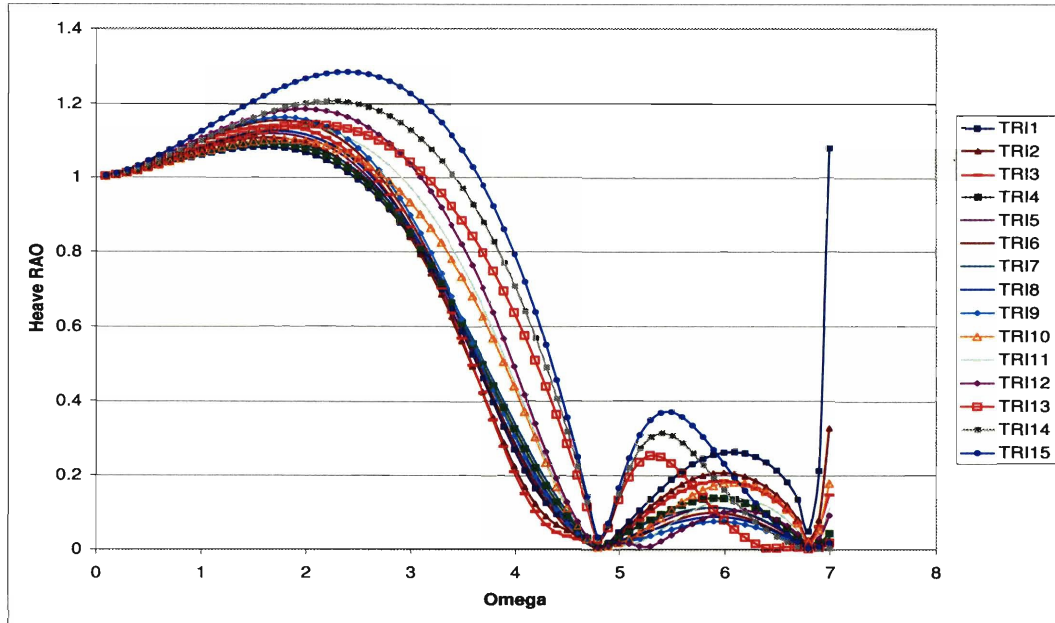


Figure C-27: Case Study Analysis of Trimaran Geometries: Heave RAO at  $F_n = 0$  and  $\mu = 150^\circ$

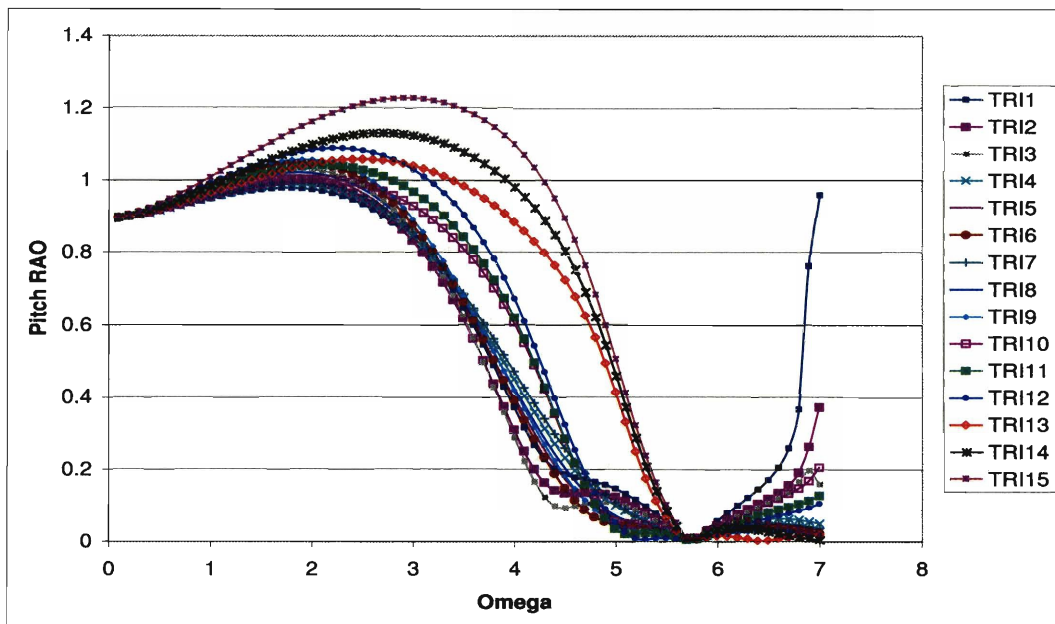


Figure C-28: Case Study Analysis of Trimaran Geometries: Pitch RAO at  $F_n = 0$  and  $\mu = 150^\circ$

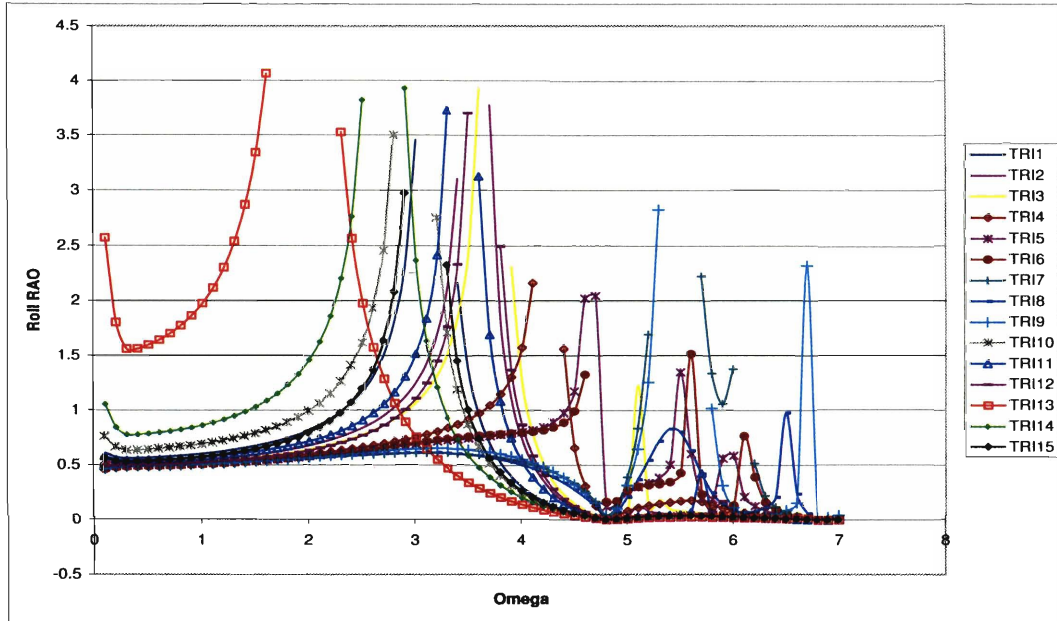


Figure C-29: Case Study Analysis of Trimaran Geometries: Roll RAO at  $F_n = 0$  and  $\mu = 150^\circ$

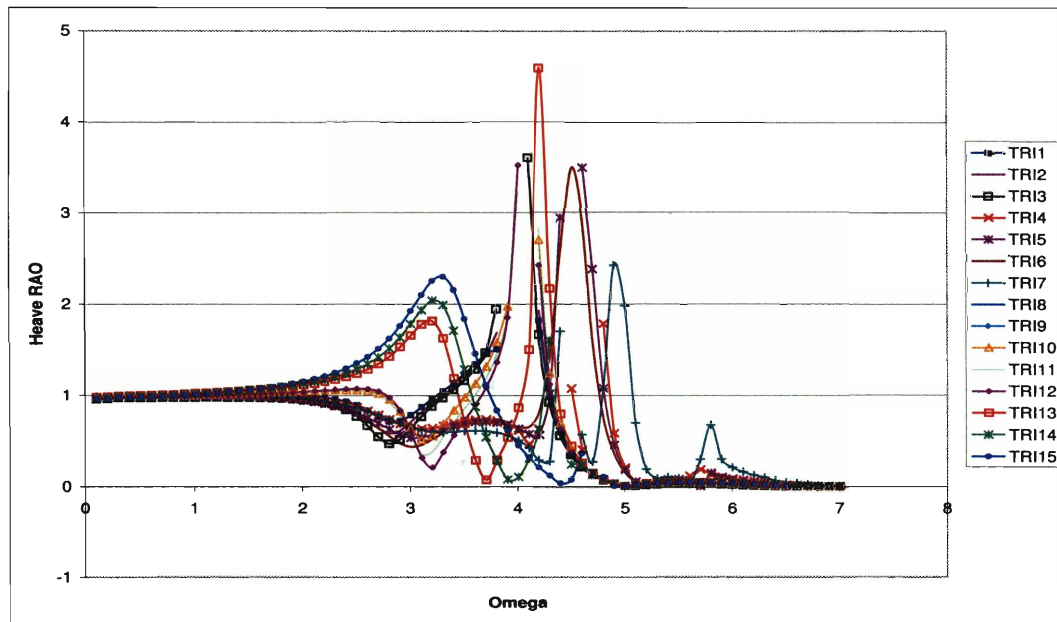


Figure C-30: Case Study Analysis of Trimaran Geometries: Heave RAO at  $F_n = 0.4$  and  $\mu = 150^\circ$

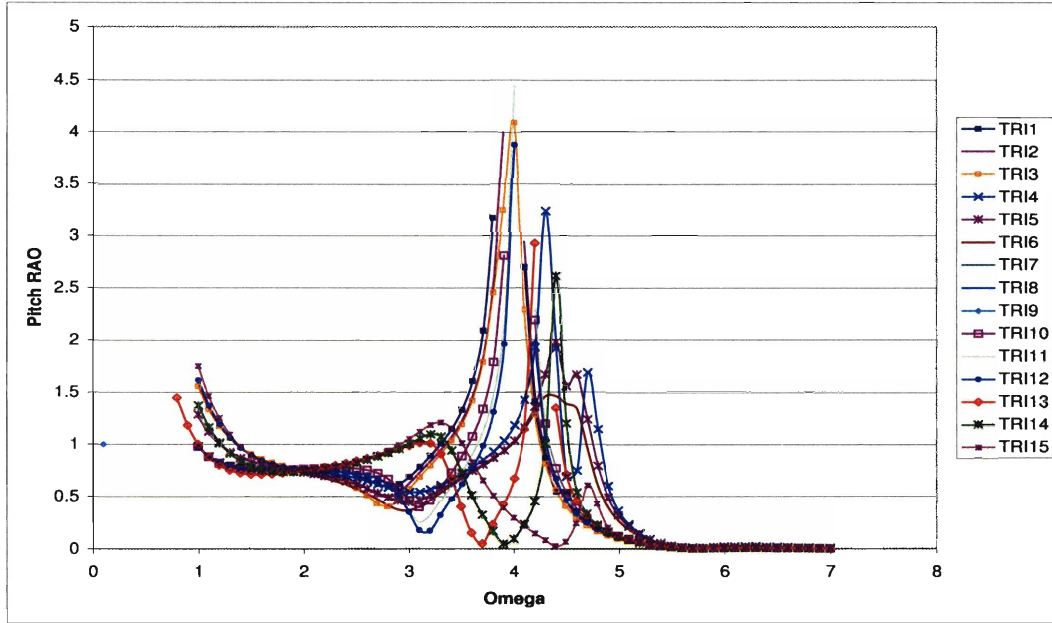


Figure C-31: Case Study Analysis of Trimaran Geometries: Pitch RAO at  $F_n = 0.4$  and  $\mu = 150^\circ$

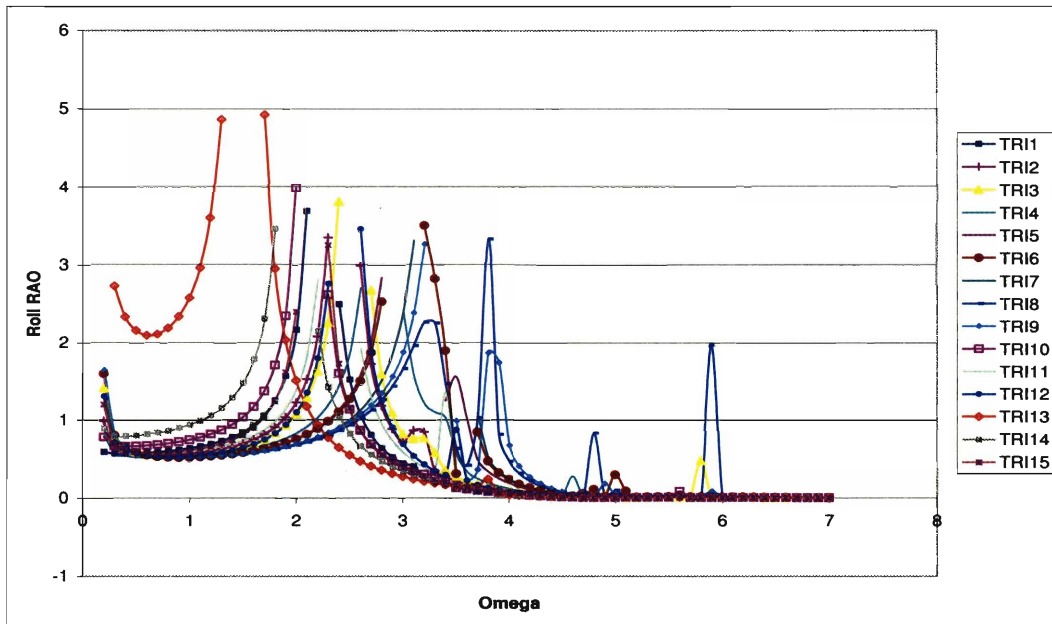


Figure C-32: Case Study Analysis of Trimaran Geometries: Roll RAO at  $F_n = 0.4$  and  $\mu = 150^\circ$

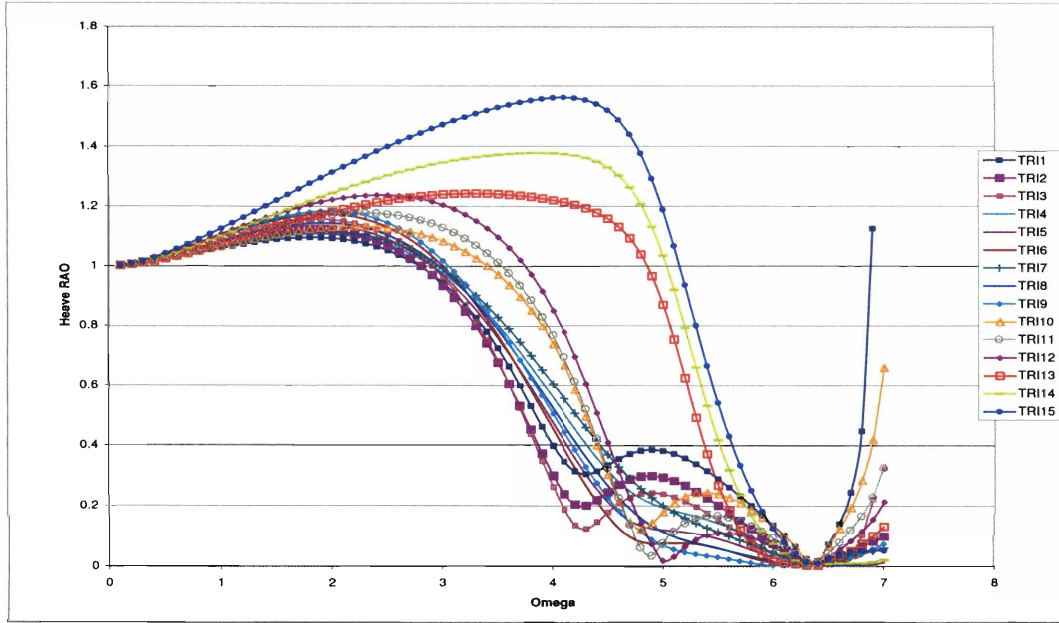


Figure C-33: Case Study Analysis of Trimaran Geometries: Heave RAO at  $F_n = 0$  and  $\mu = 120^\circ$

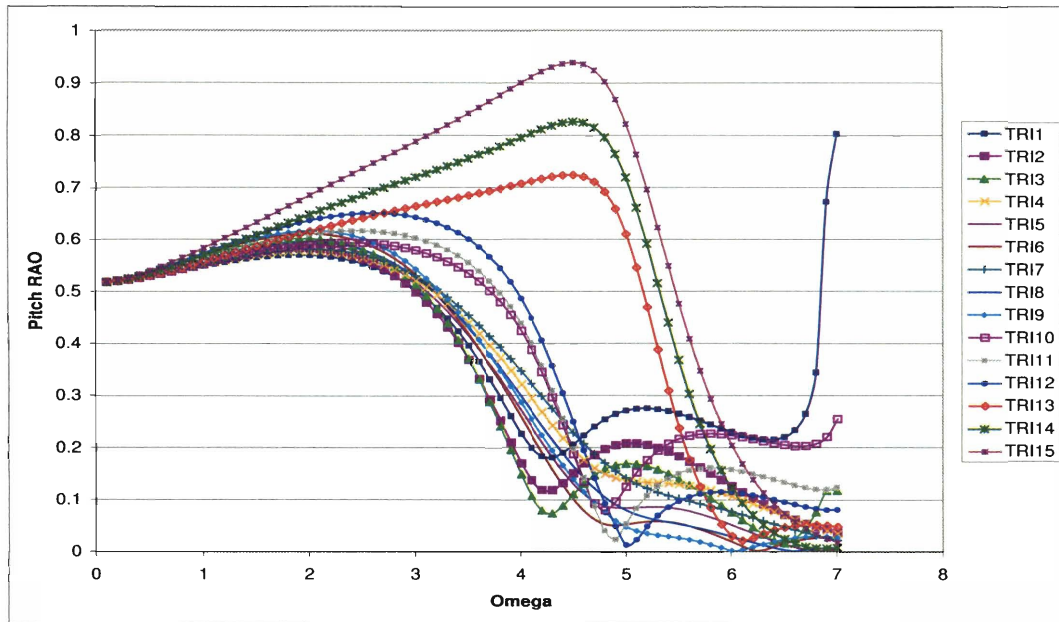


Figure C-34: Case Study Analysis of Trimaran Geometries: Pitch RAO at  $F_n = 0$  and  $\mu = 120^\circ$



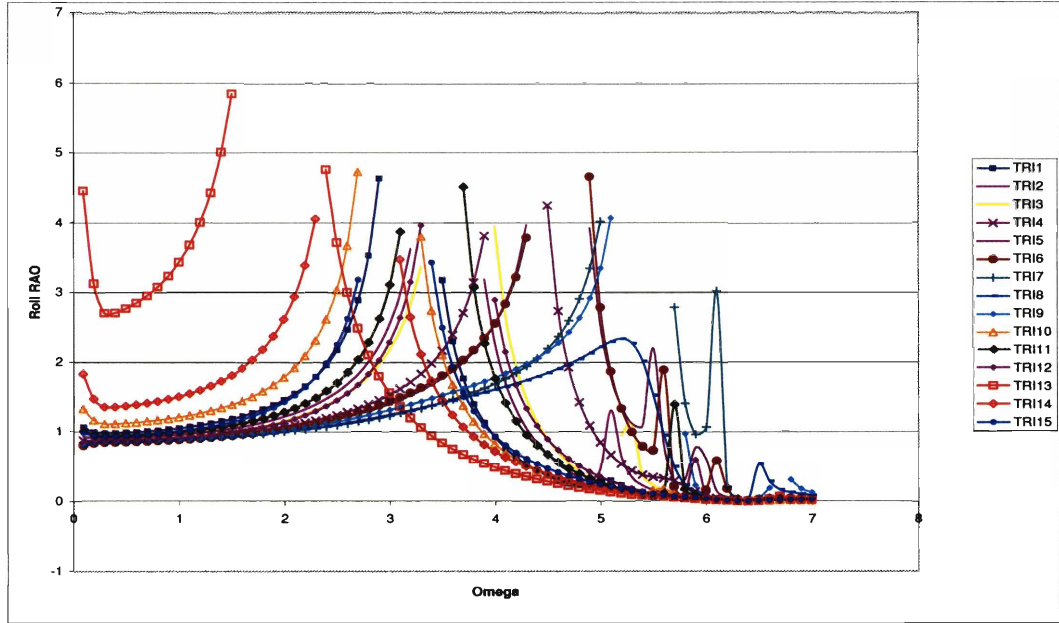


Figure C-35: Case Study Analysis of Trimaran Geometries: Roll RAO at  $F_n = 0$  and  $\mu = 120^\circ$

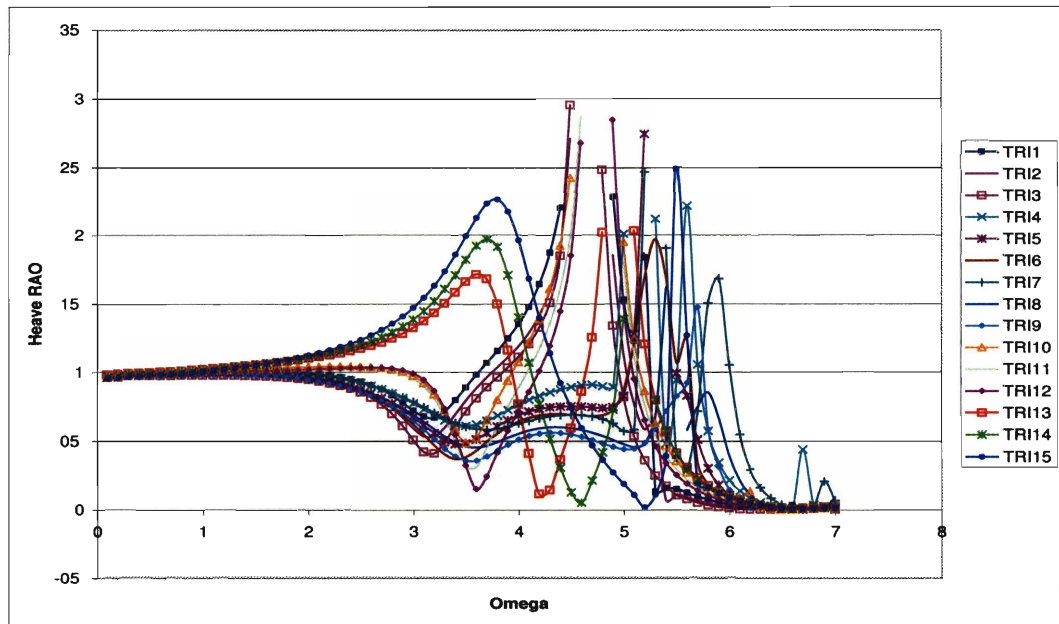


Figure C-36: Case Study Analysis of Trimaran Geometries: Heave RAO at  $F_n = 0.4$  and  $\mu = 120^\circ$

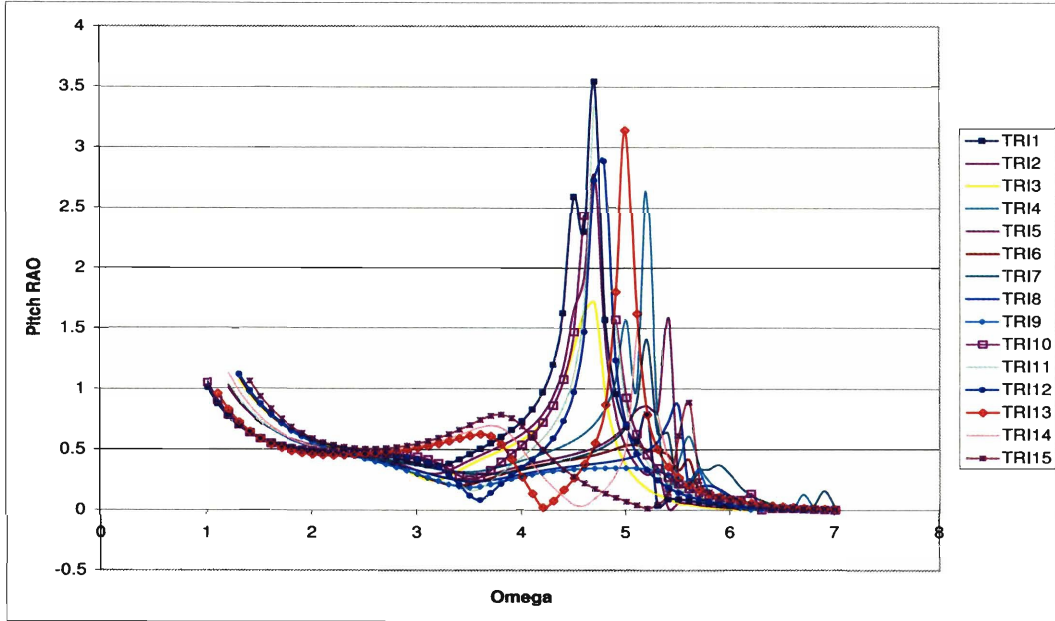


Figure C-37: Case Study Analysis of Trimaran Geometries: Pitch RAO at  $F_n = 0.4$  and  $\mu = 120^\circ$

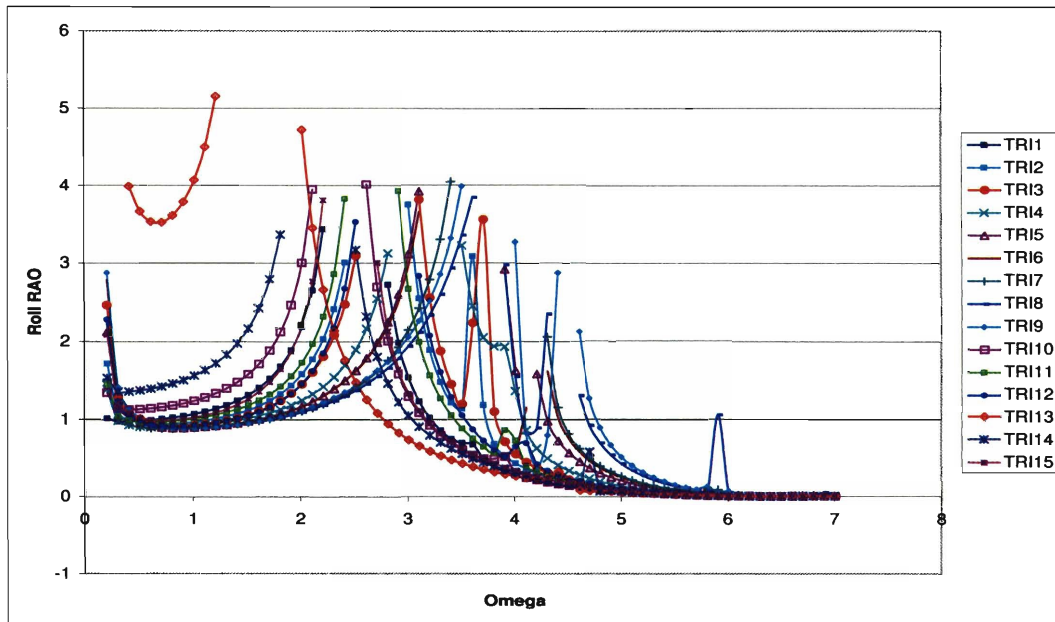


Figure C-38: Case Study Analysis of Trimaran Geometries: Roll RAO at  $F_n = 0.4$  and  $\mu = 120^\circ$

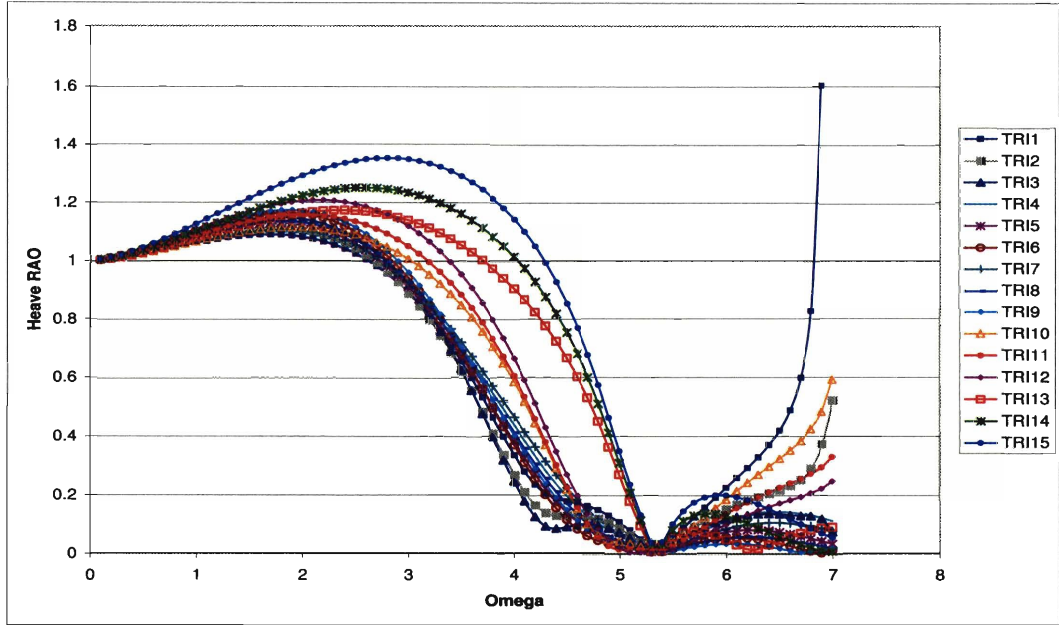


Figure C-39: Case Study Analysis of Trimaran Geometries: Heave RAO at  $F_n = 0$  and  $\mu = 45^\circ$

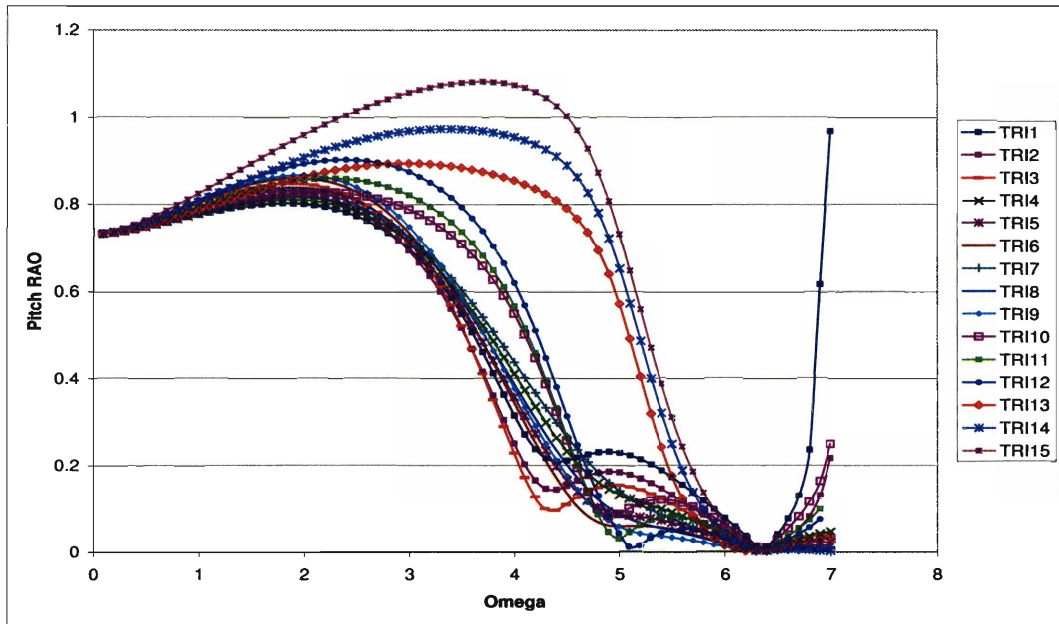


Figure C-40: Case Study Analysis of Trimaran Geometries: Pitch RAO at  $F_n = 0$  and  $\mu = 45^\circ$

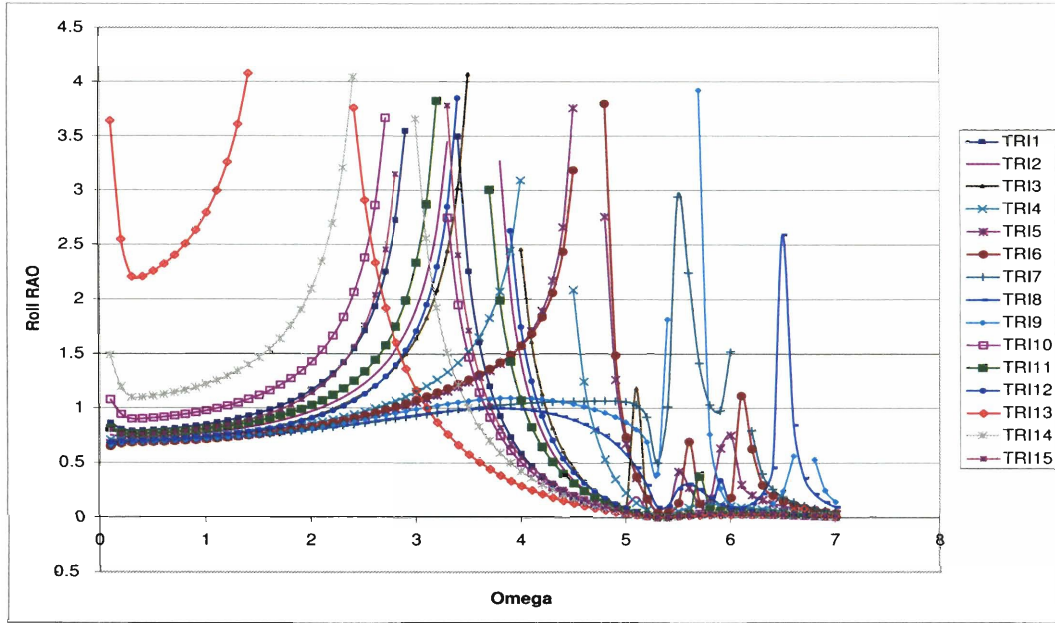


Figure C-41: Case Study Analysis of Trimaran Geometries: Roll RAO at  $F_n = 0$  and  $\mu = 45^\circ$

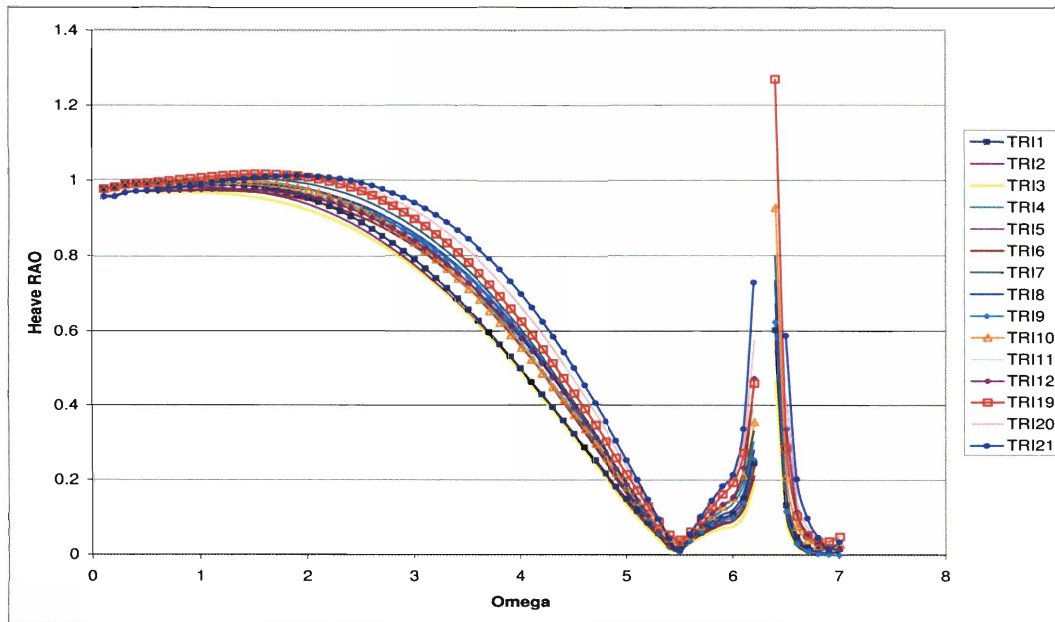


Figure C-42: Case Study Analysis of Trimaran Geometries: Heave RAO at  $F_n = 0.4$  and  $\mu = 45^\circ$

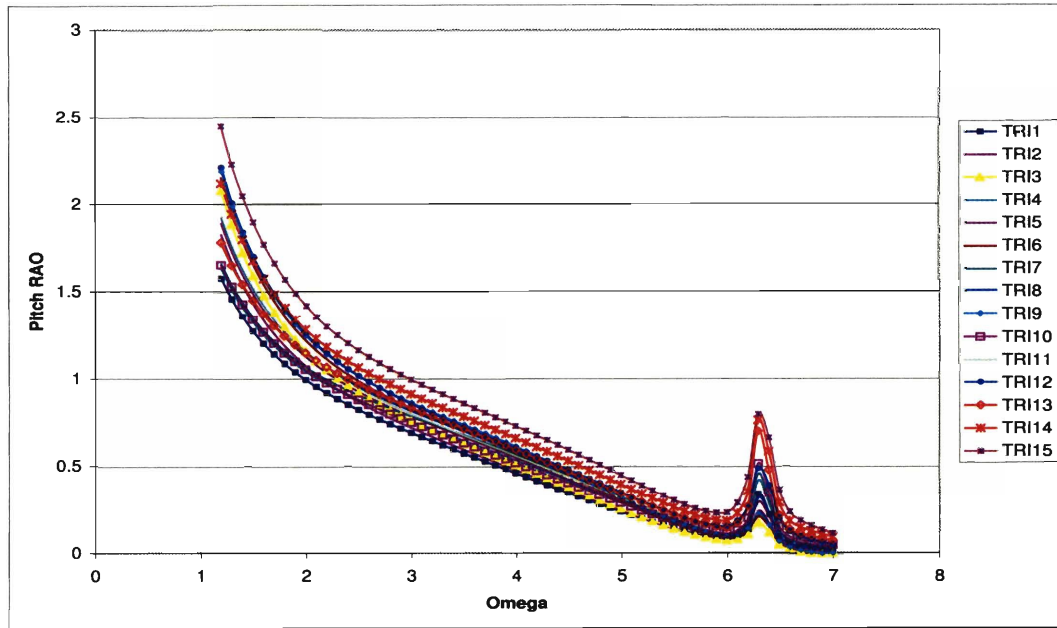


Figure C-43: Case Study Analysis of Trimaran Geometries: Pitch RAO at  $F_n = 0.4$  and  $\mu = 45^\circ$

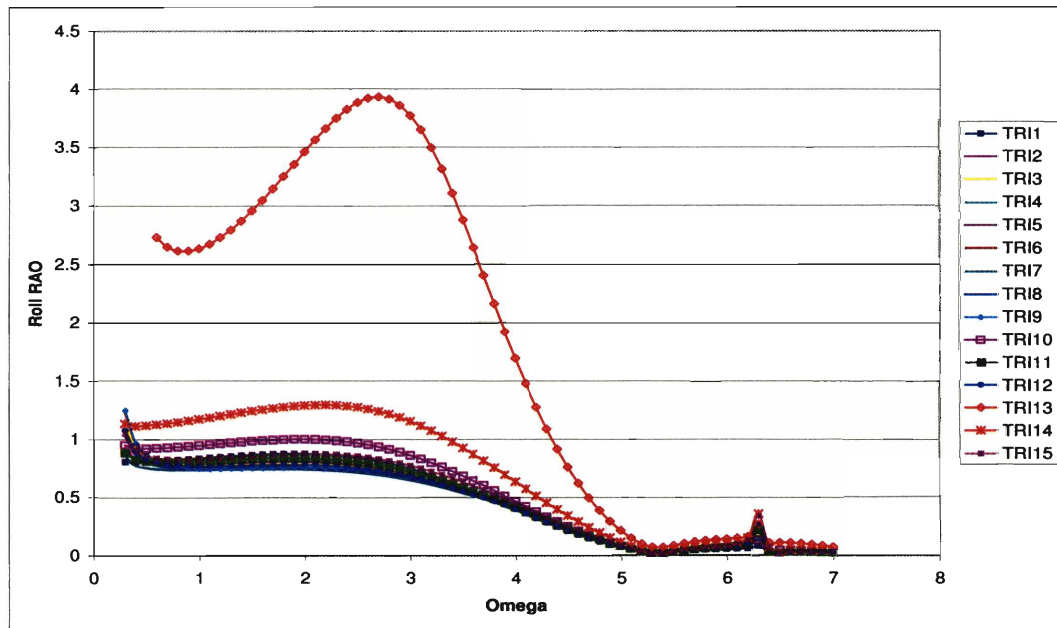


Figure C-44: Case Study Analysis of Trimaran Geometries: Roll RAO at  $F_n = 0.4$  and  $\mu = 45^\circ$

## Bibliography

- [1] D. Bailey. The npl high speed round bilge displacement hull series. *Maritime Technology Monograph, The Royal Institution of Naval Architects*, 1976.
- [2] R. Centeno, N. Fonseca, and C. Guedes Soares. Prediction of motions of catamarans accounting for viscous effects. *Int. Shipbuild. Progr.*, 47(451):303-323, 2000.
- [3] H. S. Chan. Prediction of motion and wave loads of twin-hull ships. *Marine Structures*, (6):75-102, 1993.
- [4] P. Couser. Seakeeping analysis for preliminary design. Technical report, Formation Design Systems, 2000.
- [5] M. R. Davis and D. S. Holloway. The influence of hull form on the motions of high speed vessels in head seas. *Ocean Engineering*, 30:2091-2115, 2003.
- [6] United States of America Department of Defense. Seabasing joint integrating concept. Technical Report Version 1.0, August 2005.
- [7] W. Frank. Oscillation of cylinders in or below the free surface of deep fluids. Technical Report 2375, Naval Ship Research and Development Center, Washington, DC, October 1967.
- [8] J. Gerritsma. Distribution of hydrodynamic forces along the length of a ship model in waves. Technical Report 144, Technical University of Delft, Netherlands, 1966.
- [9] J. Gerritsma and W. Beukelman. Comparison of calculated and measured heaving and pitching motions of a series 60,  $cb=0.70$  ship model in regular longitudinal waves. Technical Report 139, Ship Research Center, Delft, Netherlands, 1966.

- [10] J. Gerritsma and W. Beukelman. Analysis of the modified strip theory for the calculation of ship motions and wave bending moments. *International Shipbuilding Progress*, 14(156), 1967.
- [11] R. B. Inglis and W. G. Price. A three dimensional ship motion theory comparison between theoretical prediction and experimental data of the hydrodynamic coefficients with forward speed. *Transactions, RINA*, 124, 1981.
- [12] B. King, R.F. Beck, and Magee. Seakeeping calculations with forward speed using time-domain analysis, 1988.
- [13] B. V. Korvin-Kroukovski and W. R. Jacobs. Pitching and heaving motions of a ship in regular waves. *Transactions, Society of Naval Architects and Marine Engineers*, 65, 1957.
- [14] C. M. Lee, H. Jones, and J.W. Bedel. Added mass and damping coefficients of heaving twin cylinders in a free surface. Technical Report 3695, NSRDC Report, 1971.
- [15] E. V. Lewis. *Principles of Naval Architecture*, volume 3, Motions in Waves and Controllability. The Society of Naval Architects and Marine Engineers, Jersey City, CT, second revision edition, 1989.
- [16] S. Liapis and R.F. Beck. Seakeeping computations using time-domain analysis, 1985.
- [17] A. Mansour and K. Choo. User's manual and program listing of cat-5 for catamarans. Technical Report 73-9, Massachusetts Institute of Technology, 1973.
- [18] A. F. Molland, J. F. Wellicome, P. Temarel, J. Cic, and D. J. Taunton. Experimental investigation of the seakeeping characteristics of fast displacement

- catamarans in head and oblique seas. Technical report, The Royal Institution of Naval Architects, University of Southampton, 2001.
- [19] N. Nordenstrom, O. Faltinsen, and B. Pedersen. Prediction of wave induced motions and loads for catamarans. Technical Report OTC 1481, Offshore Technology Conference, Houston, Texas, 1971.
- [20] M. Okhusu. On the motion of multihull ships in waves. Technical Report Vol. XVIII, No. 60, Research Institute for Applied Mechanics, Japan, 1970.
- [21] K.R. Owen and M. T. Templeman. High speed sea-lift technology, total ship systems engineering directorate technology projection report. Technical report, Carderock Division NSWC, Bethesda, MD, 1998.
- [22] H. Rathje and T. E. Schellin. Viscous effects in seakeeping prediction of twin-hull ships. *Schiffstechnik Bd*, 44:44–52, 1997.
- [23] N. Salvesen, O. E. Tuck, and O. Faltinsen. Ship motions and sea loads. *Transactions, Society of Naval Architects and Marine Engineers*, (78):250–287, 1970.
- [24] P. D. Scлавounos. User manual of niirid. Technical Report Version 1.0, Department of Ocean Engineering, Massachusetts Institute of Technology, June 1985.
- [25] Second International Conference on Numerical Ship Hydrodynamics. *Computations of Three-Dimensional Ship Motions with Forward Speed*, University of California, Berkeley, 1977.
- [26] K. J. Spyrou and J. M. T. Thompson. The nonlinear dynamics of ship motions: A field overview and some recent developments. *Phil. Trans. R. Soc. Lond.*, (358):1735–1760, 2000.
- [27] M. St Denis and W. J. Pierson. On the motions of ships in confused seas. *Transactions, Society of Naval Architects and Marine Engineers*, 61, 1953.



- [28] F. Ursell. On the heaving motion of a circular cylinder in the surface of a fluid. *Quarterly Journal of Applied Mathematics*, (2):218–231, 1949.
- [29] F. Ursell. On the rolling motion of a circular cylinder in the surface of a fluid. *Quarterly Journal of Applied Mathematics*, (2):335–353, 1949.
- [30] S. Wang and R. Wahab. Heaving oscillations of twin cylinders in a free surface. *Journal of Ship Research*, pages 33–48, March 1971.
- [31] F. Zouridakis and D. Wang. High speed connector design project. Technical report, Massachusetts Institute of Technology, Department of Ocean Engineering, May 2005.